

Ecology and Development Series No. 58, 2008

Editor-in-Chief:
Paul L.G.Vlek

Editors:
Manfred Denich
Christopher Martius
Charles Rodgers
Nick van de Giesen

Lazare Tia

Modeling of vegetation dynamics and its contribution to
the water balance in semi-arid lands of West Africa

ABSTRACT

Initially considered as merely a spectator in the functioning of the Earth system, vegetation is now recognized as an important component of the global climate system through its control of energy fluxes over substantial portions of the land surface. Moreover, it has been shown that vegetation-atmosphere interactions regulate local weather and hydrological balances and regional climate. Thus, the vegetation-climate feedback is deemed essential to be included in climate change studies.

This study focuses on the estimation of the contribution of tree stands to the surface water balance by means of transpiration and actual evapotranspiration (ET_a). The study used the nature reserve of Bontioli (NRB) in southwestern Burkina Faso, from which it scaled up to larger areas within the Volta Basin. This was achieved by modeling tree density and estimating daily whole-tree water use rates.

The method of research encompasses two components: (1) estimation of climate, tree species and water-related variables, and (2) remote sensing and GIS studies. The quantification of tree water uptake was achieved by the xylem Heat-Balance method to assess sap flow rates of 17 tree species measured continuously from April 2005 to December 2006. During this period, weather data were recorded by Eddy Correlation and microclimate stations. Tree parameters were collected on the ground according to biometric standard methods in order to determine the phytosociology and the physiognomy of the vegetation cover. In addition, the LAI-SEB model, based on remotely sensed spectral vegetation indices and the surface energy balance outputs derived from the Aster image of November 2006, was developed to accurately estimate tree densities.

The results reveal that the NRB is useful for biodiversity conservation because it provides a habitat for 71 (± 2) tree species representing 19 families, typical for tree savanna (33 species), shrub savanna (39) and gallery forest (10). The LAI-SEB model produced validated large-scale maps of (1) tree density by stem count, (2) tree density by DBH estimates and (3) tree density by crown cover estimates. The reliability of the model was proven through the comparison between the mean absolute tree density (331 ± 4 stems ha⁻¹) and the mean predicted tree density (325 ± 87 stems ha⁻¹).

In the study area, the mean annual ET_a was 94 % of the rainfall in the dry year 2005 and 80 % in the wet year 2006. The mean daily whole-tree water use rates ranged from 10.1 kg day⁻¹ for *Crossopteryx febrifuga* to 492 kg day⁻¹ for *Pterocarpus erinaceus*. Those rates were influenced and regulated by weather conditions, specifically by solar energy. Moreover, the field-specific mean daily tree stand transpiration was 0.7 mm day⁻¹; transpiration rates increased from dry to rainy seasons with highs between mid-June and mid-September. The predicted tree stand transpiration map obtained by means of the LAI-SEB model shows that 62.1 % of the map surface were not contributing to transpiration, whereas 34.3 % of its surface transpired between 0 and 1 mm day⁻¹. The mean daily ET_a was 3.6 mm day⁻¹. The final analysis highlight that the contribution of large trees (DBH > 5 cm) to the water balance ranges from 9 to 20 % of rainfall, depending on the vegetation type and the weather conditions.

These results demonstrate the importance of trees in the functioning of the surface water balance and climate regulation through the maintenance of evapotranspiration in semi-arid regions, particularly during dry seasons. Consequently, to mitigate drought, water scarcity, poverty, threats to livelihood and food security one should start by preventing the destructive effects of anthropogenic activities on vegetation covers. In this context, decision-makers should advocate regional and concerted efforts to restore natural vegetation through reforestation campaigns.

Die Modellierung der Vegetationsdynamik und deren Bedeutung für die Wasserbilanz in semi-ariden Regionen Westafrikas

KURZFASSUNG

Ursprünglich wurde die Vegetation lediglich als Zuschauer beim Funktionieren der Erdeökosystemen betrachtet. Nun wird sie als wichtiger Bestandteil des globalen Klimasystems aufgrund ihrer Beeinflussung der Energieflüsse über beträchtliche Teile der Landoberfläche verstanden. Hinzu kommt, dass die Wechselwirkungen zwischen Vegetation und Atmosphäre, die das lokale Wetter und das hydrologische Gleichgewicht sowie das regionale Klima regulieren, ausreichend nachgewiesen wurden. Daher ist die Rückkopplung von Vegetation und Klima wichtig genug, um in Studien über den Klimawandel berücksichtigt zu werden.

Diese Studie legt ihren Schwerpunkt auf den Beitrag, den die Baumbestände durch ihre Transpiration und die aktuelle Evapotranspiration (ETa) zum Oberflächenwasserhaushalt haben. Sie wurde im Naturschutzgebiet von Bontioli im Südwesten von Burkina Faso durchgeführt. Die Ergebnisse werden hochskaliert auf größere Gebiete im Volta Becken. Hierzu wurde die Modellierung von Baumdichte und die Ermittlung der von den Bäumen täglich umgesetzten Wassermenge durchgeführt.

Die Methode besteht aus zwei Teilen: (1) klima-, baumarten-, und wasserbezogene Variablen sowie (2) Fernerkundung und GIS-Techniken. Die durch die Bäume aufgenommene Wassermenge wurde mit der Xylem Heat-Balance Methode ermittelt. Dazu wurde der Saftfluss von 17 Baumarten zwischen April 2005 bis Dezember 2006 durchgehend gemessen. In diesem Zeitraum wurden Wetterdaten durch Eddy-Kovarianz- und Kleinklimastationen aufgezeichnet. Baumparameter wurden am Boden auf der Grundlage von biometrischen Standardmethoden erfasst, um die Phytosoziologie und die Physiognomie der Vegetationsbedeckung zu ermitteln. Außerdem wurde das LAI-SEB-Modell auf der Grundlage von fern erkundeten Spektralvegetationsindices und Oberflächenenergiehaushalt aus dem Aster-Satellitenbild von November 2006 zur Berechnung der Baumdichte entwickelt.

Die Ergebnisse zeigen, dass das Naturschutzgebiet Bontioli ein geeigneter Pool für den Biodiversitätenschutz darstellt, da es Lebensraum für 71 (± 2) Baumarten, unterteilt in 19 Familien nach Baumsavanne (33 Arten), Strauchsavanne (39) und Galeriewald (10), bietet. Das LAI-SEB-Modell produzierte validierte, großmaßstäbliche Karten von (1) Baumdichten auf der Grundlage von Anzahl der Baumstämme, (2) Baumdichten auf der Grundlage von Stammumfang sowie (3) Baumdichten auf der Grundlage von Kronenbedeckung. Die Zuverlässigkeit des Modells wurde durch den Vergleich zwischen der mittleren absoluten Baumdichte (331 ± 4 Stämme ha^{-1}) und der mittleren errechneten Baumdichte (325 ± 87 Stämme ha^{-1}) nachgewiesen.

Die Ergebnisse zeigen außerdem, dass im Untersuchungsgebiet die mittlere jährliche ETa 94 % der Niederschlagsmengen im trockenen Jahr 2005 und 80 % im nassen Jahr 2006 betrug. Der mittlere tägliche Wasserverbrauch von ganzen Bäumen lag zwischen 10.1 kg Tag^{-1} bei *Crossopteryx febrifuga* bis $492.3 \text{ kg Tag}^{-1}$ bei *Pterocarpus erinaceus*. Diese Mengen wurden durch die Wetterbedingungen beeinflusst und reguliert, insbesondere durch den Bodenwärmefluss in Zusammenhang mit Lufttemperatur. Außerdem betrug die feldspezifische mittlere tägliche Transpiration von Baumbeständen 0.7 mm Tag^{-1} ; die Transpirationen nahmen von den Trocken- zu den Regenzeiten zu, wobei diese Zunahme zwischen Mitte Juni und Mitte September hoch war. Die durch das LAI-SEB-Modell erhaltene Karte der Transpiration der Baumbestände zeigt, dass 62.1 % der Region hinsichtlich Transpiration unproduktiv war, und dass in 34.3 % des Gebietes die Transpiration zwischen 0 und 1 mm Tag^{-1} betrug; die mittlere tägliche ETa betrug 3.6 mm Tag^{-1} . Die abschließende Analyse zeigt, dass der Beitrag der großen Bäume ($DBH > 5 \text{ cm}$) zum Wasserhaushalt zwischen 9 und 20 % des Niederschlags beträgt, abhängig von Vegetationstyp und Wetterbedingungen.

Die Ergebnisse zeigen, wie wichtig die Bäume mit ihrer Evapotranspiration für Oberflächenwasserhaushalt und Klimaregulierung in semi-ariden Gebieten sind, insbesondere während der Trockenzeit. Als Konsequenz müssen die destruktiven Auswirkungen menschlicher Aktivitäten auf die Vegetationsbedeckung verhindert werden. Nur durch Erhalt und Erweiterung der Vegetationsbedeckung können Dürren, Wasserknappheit, Armut, und Nahrungsmittelknappheit erfolgreich und nachhaltig bekämpft und werden. In diesem Zusammenhang sollten sich Entscheidungsträger für regionale und konzertierte Maßnahmen einsetzen, um die natürliche Vegetation durch Wiederaufforstung wiederherzustellen.

Modélisation de la dynamique de la végétation et de sa contribution au bilan hydrologique des régions semi-arides de l'Afrique de l'Ouest

RESUME

Initialement considérée comme un simple spectateur dans le fonctionnement du système terrestre, la végétation est maintenant reconnue comme une importante composante du système climatique global à travers son contrôle des flux d'énergie au-dessus de parties substantielles de la surface terrestre. En outre, il a été prouvé que les interactions végétation-atmosphère règlent le temps, les cycles hydrologiques locaux et le climat régional. Aussi, est-il jugé indispensable d'inclure le feedback végétation-climat dans les études portant sur le changement climatique.

Cette étude se focalise sur l'estimation de la contribution des peuplements arborescents au bilan hydrologique de surface à travers la transpiration et l'évapotranspiration actuelle (ETa). L'étude est partie de la réserve naturelle de Bontioli (RNB) au sud-ouest du Burkina Faso, puis a été étendue à l'échelle de plus vastes régions à l'intérieur du bassin versant de la Volta. Cela a été possible grâce à la modélisation de la densité des arbres et à l'estimation des taux journaliers d'utilisation de l'eau par l'arbre.

La méthode de recherche comprend deux parties : (1) les variables relatives à l'analyse du climat, à l'inventaire des espèces arborescentes et celles liées à l'eau, et (2) les études de la télédétection et du SIG. La quantification de l'utilisation de l'eau par l'arbre a été réalisée par la méthode de xylem Heat-Balance qui a permis d'obtenir les taux de flux de sève de 17 espèces arborescentes, mesurés en continu d'avril 2005 à décembre 2006. Au cours de cette même période les données météorologiques ont été enregistrées par les stations d'Eddy Corrélation et de microclimat. Les paramètres des arbres ont été collectés sur le terrain, en fonction des méthodes standard d'inventaire, dans l'optique de déterminer la phytosociologie et la physiologie du couvert végétal. En plus, le modèle LAI-SEB a été développé pour estimer avec précision les densités d'arbre par la télédétection, à partir des indices de végétation et des données du bilan d'énergie à la surface dérivés de l'image Aster de Novembre 2006.

Les résultats révèlent que la RNB est utile à la conservation de la biodiversité en ce sens qu'elle abrite 71 (± 2) espèces arborescentes regroupées en 19 familles typiques de la savane arborée (33 espèces), la savane arbustive (39) et la forêt galerie (10). Le modèle LAI-SEB a produit des cartes validées, à grande échelle de (1) la densité des arbres par comptage de pied, (2) la densité des arbres par estimation du DBH, et (3) la densité des arbres par estimation de la surface du houppier. La fiabilité du modèle a été prouvée par la comparaison entre la densité moyenne absolue des arbres (331 ± 4 pieds ha^{-1}) et la densité moyenne relative des arbres (325 ± 87 pieds ha^{-1}).

L'étude révèle que la moyenne annuelle d'ETa était de 94 % des précipitations en année sèche 2005 et 80 % en année humide 2006. Les moyennes journalières de taux d'utilisation de l'eau par l'arbre ont varié entre 10,1 kg j^{-1} pour *Crossopteryx febrifuga* et 492 kg j^{-1} pour *Pterocarpus erinaceus*. Ces taux ont été influencés et contrôlés par les facteurs météorologiques, spécialement par l'énergie solaire. En outre, la moyenne journalière de transpiration de peuplements arborescents, relative au site d'étude a été de 0,7 mm j^{-1} ; les taux de transpiration se sont accrus de la saison sèche à la saison de pluie avec des niveaux records entre la mi-juin et la mi-septembre. La carte de la transpiration relative des arbres, obtenue à partir du modèle LAI-SEB, montre que 62,1 % de sa surface n'ont pas contribué à la transpiration alors que 34,3 % de sa surface ont transpiré entre 0 et 1 mm j^{-1} . L'analyse finale fait ressortir que la contribution des grands arbres ($\text{DBH} > 5$ cm) au bilan hydrologique a varié entre 9 et 20 % des précipitations, en fonction du type de végétation et des conditions météorologiques.

Ces résultats démontrent l'importance des arbres dans le fonctionnement du bilan hydrologique de surface et le contrôle du climat à travers le maintien de l'évapotranspiration en

régions semi-arides, particulièrement pendant les saisons sèches. Par conséquent, l'on devrait commencer à prévenir les effets destructifs des activités humaines sur les couverts végétaux afin d'atténuer la sécheresse, la pénurie d'eau, la pauvreté, les menaces sur les moyens de subsistance et la sécurité alimentaire. Dans ce contexte, les décideurs devraient préconiser des efforts concertés et régionaux afin de restaurer la végétation naturelle par le biais des campagnes de reforestation.

TABLE OF CONTENTS

1	GENERAL INTRODUCTION	1
1.1	Introduction	1
1.2	Problem statement	2
1.3	Research justification	4
1.3.1	Water issues: water scarcity, hydrological cycle change.....	4
1.3.2	Understanding vegetation dynamics in the global change.....	5
1.3.3	Need of data for sustainable management of natural resources.....	5
1.3.4	Importance of the nature reserve of Bontoli.....	6
1.3.5	Strength of geomatic techniques.....	6
1.4	Research objective.....	8
1.5	Thesis structure.....	9
2	STUDY AREA.....	10
2.1	Geographical location.....	10
2.2	Physical environment	10
2.2.1	Geology.....	10
2.2.2	Geomorphology and relief.....	12
2.2.3	Pedology	14
2.2.4	Hydrography and groundwater	15
2.2.5	Rainfall.....	16
2.3	Biological environment	19
2.3.1	Vegetation type and composition	19
2.3.2	Flowering period.....	20
2.3.3	Vegetation seasonal disturbance: bushfire.....	22
2.3.4	Fauna.....	22
2.4	Human activities	23
2.5	Conclusions	24
3	GENERAL RESEARCH METHOD.....	25
3.1	Introduction	25
3.2	Sap flow measurements	25
3.2.1	Site selection	25
3.2.2	Measurement equipment installation.....	27
3.2.3	Sapwood sampling and analysis	30

3.3	Tree biometric measurements.....	32
3.3.1	Sampling method and plot size.....	32
3.3.2	Phytoecological unit derivation by GIS.....	35
3.3.3	Field-based surveys.....	35
3.4	Photogrammetry, remote sensing and GIS.....	38
3.4.1	Data acquisition.....	39
3.4.2	Land Use Land Cover Change (LULCC).....	39
3.5	Conceptual framework.....	39
3.5.1	Data description.....	39
3.5.2	Data integration and analysis.....	39
3.5.3	General data source.....	42
3.6	Summary.....	42
4	TREE SPECIES DIVERSITY AND SPATIAL PATTERNS.....	43
4.1	Introduction.....	43
4.2	Materials and methods.....	43
4.2.1	Tree species diversity estimates.....	43
4.2.2	Ecological modeling of tree spatial patterns.....	46
4.2.3	Tree community ordination.....	46
4.2.4	Mapping savanna vegetation.....	47
4.3	Results and discussion.....	50
4.3.1	Dominant tree species and biodiversity.....	50
4.3.2	Spatial patterns of trees.....	55
4.3.3	Definition of the potential phytoecological zones.....	58
4.3.4	Mapping vegetation cover.....	65
4.4	Conclusions.....	73
5	TREE DENSITY PREDICTION BY THE LAI-SEB MODEL.....	75
5.1	Introduction.....	75
5.2	Materials and methods.....	76
5.2.1	Tree density estimation using biometric data.....	76
5.2.2	LAI-based tree density estimation.....	76
5.2.3	Tree density derivation by regression analysis.....	80
5.3	Results and discussion.....	84
5.3.1	Tree density estimates based on biometric data.....	84
5.3.2	LAI-based tree density estimates.....	88
5.3.3	Tree density estimation from optical remote sensing derivatives.....	94
5.4	Conclusions.....	112

6	LAND USE AND LAND COVER CHANGE DETECTION	114
6.1	Introduction	114
6.2	Materials and methods.....	115
6.2.1	Choice of multi-temporal and multi-sensor images.....	115
6.2.2	Satellite image pre-processing.....	115
6.2.3	Mapping LULC using the SVM technique.....	115
6.2.4	Change detection method.....	116
6.3	Results and discussions	117
6.3.1	Accuracy assessment of the change detection products	117
6.3.2	Analyzing land cover change outputs.....	118
6.3.3	Interpreting the changes.....	119
6.3.4	LULC output.....	122
6.5	Conclusions	123
7	CONTRIBUTION OF TREES TO WATER BALANCE	124
7.1	Introduction	124
7.2	Materials and methods.....	124
7.2.1	Surface water balance	124
7.2.2	Sap flow measurement by xylem Heat-Balance method.....	126
7.2.3	Impacts of vegetation cover change on water balance	129
7.3	Results and discussion.....	129
7.3.1	Whole-tree water use	129
7.3.2	Tree water use and weather conditions.....	131
7.3.3	Tree stand transpiration	142
7.3.4	Tree stand contribution to surface water balance	146
7.4	Conclusions	149
8	GENERAL CONCLUSION.....	150
8.1	General summary.....	150
8.1.1	Usefulness of biodiversity conservation	150
8.1.2	The LAI-SEB model for tree density prediction	150
8.1.3	Tree stand contribution to surface water balance	151
8.1.4	LULC and climate change	152
8.2	Conclusions and recommendations	152
	REFERENCES	155
	APPENDICES	165
	ACKNOWLEDGEMENTS	174

ACRONYMS AND ABBREVIATIONS

AAV	Actual Area under Vegetation
AMR	Area-based Matching Ratio
AVV	Autorité des Aménagements des Vallées des Volta
BIOTA	Biodiversity Monitoring Transect Analysis
BRGM	Bureau de Recherches Géologiques et Minières
CA	Correspondence Analysis
CASI	Compact Airborne Spectrographic Imager
DBH	Diameter at Breast-Height
DCW	Digital Chart of the World
DLLAI	Drip Line Leaf Area
DLR	German Aerospace Center
EC	Eddy Correlation/Covariance
ECDPM	European Centre for Development Policy Management
ELADP	Ellipsoidal Leaf Angle Distribution Parameter
ESRI	Environmental Systems Research Institute
FAO	Food and Agriculture Organization
FCB	Forêt Classée de Bontioli
FPAR	Fraction of Absorbed Photosynthetically Active Radiation
GDP	Gross Domestic Product
GndCover	Ground Covered by canopy
GPS	Global Positioning System
GWP	Global Water Partnership
IFAD	International Found for Agricultural Development
IMK-IFU	Institute for Meteorology and Climate Research
IGBP	International Geosphere-Biosphere Programme
IPVI	Infrared Percentage Vegetation Index
IRDC	International Development Research Center
ISSS	International Society of Soil Science
IUCN	International Union for Conservation of Nature and Natural Resources
LAI	Leaf Area Index
LAIDev	Root mean square deviation of LAI

LIDAR	Light Detection And Ranging
LULC	Land Use Land Cover
LULCC	Land Use Land Cover Change
MAD	Multivariate Alteration Detection
Max	Maximum
MEIS	Multispectral Electro-optical Imaging Scanner
MET	Ministère de l'Environnement et du Tourisme
Min	Minimum
MLR	Multiple Linear Regression
MM	Multimedia
NDVI	Normalized Vegetation Index
NRB	Nature Reserve of Bontioli
NLR	National Aerospace Laboratory
ORSTOM	Office de la Recherche Scientifique et Technique Outre-Mer
P	Path
PC	Principal Component
PCA	Principal Component Analysis
PCR	Principal Component Regression
PLSR	Partial Least Squares Regression
R	Row
RA	Reciprocal Averaging
RADAR	Radio Detection And Ranging
RMSE	Root Mean Square Error
RMSEC/P	Root Mean Square Error of Calibration/Prediction
SAVI	Soil Adjusted Vegetation Index
SIG-BF	Système d'Information Géographique - Burkina Faso
SFL	Seasonally Fluctuation of LAI
SPOT	Système Pour l'Observation de la Terre
Stdev	Standard Deviation
SVM	Support Vector Machine
SWIR	Short Wave Infra Red
TIR	Thermal Infra Red

UNEP	United Nations Environment Programme
UNESCO	United Nations Educational, Scientific and Cultural Organization
UNU	United Nations University
UP	Umweltanalytische Produkte
VNIR	Visible Near Infra Red

SYMBOLS

ET_a	Actual evapotranspiration	(mm day ⁻¹)
T_a	Air temperature	(°C)
ΔS	Change in storage	(mm)
r	Circle crown radius	(m)
S	Crown cover surface	(m ²)
ds	Diameter at sap flow measurement height	(cm)
Q	Discharge	(mm)
b	Ellipse major radius	(m)
a	Ellipse minor radius	(m)
ET	Evapotranspiration	(mm day ⁻¹)
J	Evenness index	(-)
$E(\hat{S}_n)$	Expected number of tree species in a random sample	(-)
sf_e	Extrapolated sap flow rate	(ml min ⁻¹)
Dbh_m	Field-measured tree DBH	(cm)
G	Ground Heat Flux	(W m ⁻²)
I	Index of dispersion test	(-)
\hat{S}	Jackknife estimator of species richness	(-)
LE	Latent Heat Flux	(W m ⁻²)
λ	Latent heat of evaporation	(-)
L	Loss to deep groundwater	(mm)
S_c	Mean circle surface area	(m ²)
S_e	Mean ellipse surface area	(m ²)
t	Mean hourly air temperature	(°C)
R_n	Net radiation	(W m ⁻²)
p_i	Relative abundance of each tree species	(-)
T_{rd}	Relative tree density	(stems ha ⁻¹)
sd	Sap flow density	(ml cm ⁻² min ⁻¹)
sa	Sapwood area	(cm ²)

General introduction

sr	Sapwood radius	(cm)
Hs	Sensible Heat Flux	(W m ⁻²)
H	Shannon diversity index	(-)
D	Simpson index	(-)
T_s	Surface temperature	(°C)
ΔT_{night}	Temperature difference at night	(-)
ΔT_{actual}	Temperature difference measured	(-)
Dbh_p	Total DBH of a plot	(cm)
Th	Tree height	(m)
T_p	Tree transpiration rate at plot level	(mm day ⁻¹)
sf	Whole-tree sap flow rate	(kg day ⁻¹)
Dbh_e	Young tree DBH	(cm)
sf_e	Young tree sap flow rate	(kg day ⁻¹)

1 GENERAL INTRODUCTION

1.1 Introduction

People are becoming increasingly aware of the shrinking water resources worldwide due to global change, and since the 1960s a large number of scientists, water policy analysts and water policy makers have warned of an approaching worldwide water crisis (Hoekstra 1998). This awareness was sustained by the creation of the International Hydrological Decade (IHD) in 1965 to better understand the world water balance. Twelve years later (1977), the United Nations organised the UN Water Conference in Mar del Plata, Argentina, as the result of a global political awareness of the importance of water resources and their sustainable management.

In the late 1980s, the understanding of the global change was focused on the dynamic atmosphere-ocean interactions largely ignoring the terrestrial vegetation, which was merely considered a spectator rather than a player in the functioning of the Earth's ecosystem (Blodget 1857; Kabat et al. 2004). This situation is changing, as vegetation is now recognized as an important component of the Earth's system to be taken into account in global change research. The role of vegetation-atmosphere interactions that regulate local weather and hydrological balances and the regional climate have been fully demonstrated (Kabat et al. 2004).

The scale of water-related issues often exceeds national boundaries (Hoekstra 1998). The river basin is considered an appropriate level of research, because river basins are the natural entities for water flows (UN 1970). The arid and semi-arid lands of West Africa are found mainly in the basins of the Niger and Volta Rivers, principal source of water supply for human needs and ecosystems regulation.

The Volta Basin, some 400,000 km², with 6 riparian countries of which Ghana and Burkina Faso each cover 40 %, is the subject of an international and interdisciplinary research program conducted by the GLOWA Volta Project. The central objective is “the analysis of the physical and socio-economic determinants of the hydrologic cycle in the Volta Basin in the face of global change” (GLOWA 2000). Specific objectives relevant to 15 sub-projects are nested within the project. Sub-project A1 analyzes the long term influences of global climate change and regional land use change on the water balance in the Volta Basin, Sub-projet L1 focuses on the accurate

multisource and multitemporal land use classification of the whole basin, while Sub-project L3 seeks to characterize phenological crop and vegetation changes by means of geomatic technology (GLOWA 2002).

Burkina Faso is the subject area of the BIOTA (Biodiversity Monitoring Transect Analysis Africa) West Africa Project, which also covers Côte d'Ivoire and Benin. The goal of the project is to “identify the drivers and processes leading to biodiversity loss, develop methods for the preservation of biodiversity on various scales integrating scenarios on the effects of global change and create and propose tools that contribute to the sustainable use of biodiversity” To achieve that goal the project is organized according to ten subprojects and forms together with BIOTA East and Southern Africa and BIOTA Marocco the joint project BIOTA Africa. The major task of subproject W02 (BIOTA West) is the continuous analytical monitoring of hydrometeorological and biophysical parameters that affect local biocenosis.” (BIOTA 2007).

As a contribution to the ongoing workflows, the current research is designed in interface with both GLOWA Volta and BIOTA West Africa Projects, specifically with the relevant sub-projects mentioned herein.

1.2 Problem statement

Particular attention has been paid to arid regions during the past decades because dry lands, which include a range of terrestrial ecosystems in arid, semi-arid, and dry sub-humid zones (Lambert et al. 2005) often with striking landscapes, cover more than one-third of the Earth's land surface, i.e., approx. 49 million km² (Lambert et al. 2005; Lehouérou 1992; Wickens 1998). In these areas rainfall is less than potential evapotranspiration, runoff, etc. (Kassas 1992). The harsh climate augmented by human mismanagement often leads to human misery (Dregne 1992),

In general, all scenarios and projections on the global water demand predict that the water demand during the 21st century will be even greater than in the 20th century (Hoekstra 1998). In dry regions, the problem of water scarcity will be acute. Water demand will be confronted with a lower water supply due to climate change conditions and global warming: over the last 100 years, the surface temperature of the Earth has risen dramatically between 0.4 °C and 8.0 °C (NASA 2002). Most of the

state-of-the-art climate models predict an increase in the mean annual global surface temperature by between 1.4 and 5.8 °C by the end of 21st century (NASA 2002; Yasunari 2002a). Thus, the average rate of warming would likely be greater than any seen in the past 10,000 years (Watson 1998). This profound and progressive deterioration of the climatic and environmental conditions will lead to changes in the global hydrological cycle (Hoekstra 1998; Yasunari 2002a) threatening the water security of the more than 1.2 billion people living in arid and semi-arid lands (Wickens 1998).

An analysis of Dregne's (1992) table of world arid zones distribution, based on Budyko's (1956) Aridity Index, reveals that 52 % of Africa's land surface belong to arid (3.57 million km²) and semi-arid lands (2.95 million km²), where more than 39 % of the continent's 688 millions inhabitants live (UNEP 1997). The proportions of drylands are higher in West Africa where Burkina Faso, a country with a tropical dry climate, has 29 % of its surface shared between arid lands (10,000 km²) and semi-arid lands (70,000 km²). With a long dry season (from mid-November to mid-April) often dominated by the Harmattan¹, Burkina Faso has to cope with hot temperatures and lack of rainfall. Moreover, only 0.15 % of the surface of the country is covered by surface water. This increases the problem of water scarcity and affects the well-being of the population in terms of water demand (Sawadogo 1997).

In Burkina Faso, which ranks 202nd on the poverty scale (GDP per capita = \$ 1,400) among the 229 countries worldwide (CIA 2007), inadequate rainfall or water for irrigation for food crops creates perpetual food shortage. Indeed, the problem of drought was severe in the early 1970s and mid-1980s, largely destroying the natural vegetation (Sawadogo et al. 2001). Moreover, soils are poor in phosphate and nitrogen, shallow, dry and easy to erode. About 20 % of the population suffers from chronic food insecurity and an additional 40 % are at risk of food insecurity (IFAD 2004). The issues mentioned above raise an important two-dimensional question:

How to improve the welfare and the prospects of population in Burkina Faso as regards to water supply and food security, and at the same time contribute significantly to establish sustainable land use and mitigate climate change?

¹ The Harmattan is a hot, dry and dusty wind that blows from the Sahara toward the Atlantic Ocean. In Burkina Faso, it blows from December to February.

In the fight against food insecurity, the country has mobilized rural partners to come together. Moreover, the fight against desertification, water scarcity and climate change is a constant challenge for farmers, government agencies, NGOs and development-project planners. Therefore, to help them in their decision making processes, professionals of natural resources management and decision-makers realized the need to build computer-based Decision Support Systems (DSS) or Multiple Objective Decision Support Systems (MODSS). These systems require a lot of consolidated information and data on land use, land cover changes and natural resources dynamics (IFAD 2004). For many developing countries, DSSs are new techniques for dealing with sustainable development (Kersten et al. 2000). As a scientific contribution to the development of such DSSs, the current research aims to produce a sound scientific database on surface water balance components in relation to vegetation parameters.

1.3 Research justification

1.3.1 Water issues: water scarcity, hydrological cycle change

Water is essential for all socio-economic development and for maintaining healthy ecosystems. Therefore, water scarcity affects all social and economic sectors and threatens the sustainability of the natural resources base (UN 2006). Global change is affecting water resources basically through climate change, which will change the hydrological cycle, the balance of temperature, and rainfall (Watson et al. 1998). Hence, by 2025, the number of countries experiencing water stress in Africa will rise to 18 (McCarthy 2001). Moreover, addressing this problem is becoming complex, as efforts to provide adequate water resources for Africa are confronted with a number of challenges including population pressure, problems associated with land use such as erosion, and possible ecological consequences of land-use change on the hydrological cycle (Watson et al. 1998). A further cause for concern is that mankind's ability to predict hydrological changes is smaller than its ability to predict temperature changes (Hoekstra 1998). Currently, to counter the threats of drought and water scarcity gigantic water projects are offered as a solution (Vandana 1991).

1.3.2 Understanding vegetation dynamics in the global change

In semi-arid regions, the problems of rainfall reduction and variability, climate change, and water scarcity are worsened by the increasing disturbance of the natural relationship between vegetation and climate by human activities.

Vegetation is an important component of the global climate system (Bounoua et al. 2002; Chase et al. 2000). Through its control of energy fluxes over substantial portions of the land surface, it controls how, from the land surface, parts of the energy fluxes return as long-wave radiation to warm the atmosphere, whereas some reinject water into the atmosphere through leaves' transpiration. In turn, vegetation distribution, structure, and physiological state are largely determined by climate. Therefore, the vegetation-climate feedback needs to be included in climate change studies (Friend 2003). However, there is a concern is that even dominant vegetation types have not yet been comprehensively studied (Walter and Steffen 1996).

Therefore, the current research focuses on land use and land cover change. It aims to classify the vegetation and analyse its functional and physiological parameters in order to better understand whether and why changes in tree densities are impacting the hydrological cycle (Vlek and van de Giesen 2002), and how vegetation cover dynamics thus affect the Earth's environment (Townshend et al. 1993).

1.3.3 Need of data for sustainable management of natural resources

There is widespread agreement among experts that effective solutions to water-related and environmental problems begin and end with good information and data. Hence, good baseline data are essential for analysis of all hydrological issues and for the formulation of sound water policy (Naff 1999).

In Burkina Faso, the need for new and accurate data is becoming more acute, since decision-makers, natural resources managers and professionals are engaged in a fight against the threat of desertification and water shortage, conscious that the welfare of human societies and the quality of life is directly linked to sustainable use of the natural resources (UNU 2004).

1.3.4 Importance of the nature reserve of Bontioli

The choice of the nature reserve of Bontioli (NRB) as a small scale study area is justified by the fact that it is located in the province of Bougouriba (southwestern Burkina Faso) within the Volta Basin, which is the area of investigation of GLOWA Volta and BIOTA West Africa Projects. In the Volta Basin, severe problems of water scarcity and climate disturbance are evident. Vegetation cover is dominated by savanna and the forest landscape is sparse, degraded by bushfires and human activities.

The NRB is classified by the World Conservation Union (IUCN) in the Category IV of protected areas. Therefore, it is an area of land subject to active intervention for management purposes so as to ensure the maintenance of habitats and/or to meet the requirements of specific species (IUCN 2004). Due to its statute, the NRB contains representative species of the primary vegetation of the region, remnants of which are scattered in the surrounding cultivated areas. It thus offers a baseline ecosystem with the key species found in the basin. Moreover, an Eddy Covariance station (C. Brümmer - Virtual Institute) and a microclimatic station (J. Szarsynski - BIOTA West Africa) were installed in the nature reserve prior to the beginning of this research to provide information on the water balance of the area.

1.3.5 Strength of geomatic techniques

The use of geomatic techniques in such research dealing with modeling and scaling up land-related geographical variables cannot be ignored, as the advance of these scientific technologies provides great potential to extend environmental modeling from local to global systems (Bian 1997). These techniques actually offer the possibility of providing new data (Heirtzler 1993).

Remote sensing

Physical and biological scientists have grappled with the challenges of data requirements for a decade or more and have come to recognize the utility of satellite remote sensors as major sources of consistent, continuous data for atmospheric, ocean, and land studies at a variety of spatial and temporal scales (CIESIN 2006).

Indeed, Earth observation or remote sensing plays an important role in the monitoring of global, regional and local environmental and climatic problems (NLR

2003). Hence, many scientists today are working on links between remote sensing and more sophisticated climate models; for most of them the goal is a better understanding of climate, while others focus on prediction and control (Fleming 1998).

Moreover, historical satellite data have emerged as a key source of data for understanding and managing forests. In part, this is because historical satellite data provide information about past conditions and changes in those conditions. The relatively low cost of historical Landsat data sets is another reason for utilizing such information wherever possible. In addition, historical satellite data is potentially available over much of the globe.

Nowadays, satellite imagery is being harnessed to the task of mapping water resources, deforestation, forest biomass, etc. Its potential uses include identification of strategically important areas for assistance, monitoring forest cover change in protected or critically important areas. It is, among other uses, a common frame of reference for planning and coordination of conservation actions (Freeman and Fox 1994). Very often, remote sensing projects involve the use of the most common types of imagery with lower resolution and multispectral capabilities, ideal for studying large areas.

Geographic Information System (GIS)

Within an increasingly digital world, GIS has emerged over the last 10 years as a new and easily accessible tool for representing spatial systems (Longley and Batty 1996). Its ability to link graphical (maps) to attribute data (tables) and its power to analyze and display data in a variety of sophisticated ways that allow for quick and easy discernment of patterns in data makes a GIS such a powerful and useful tool in so many fields (Vance et al. 2000; Shamsi 2002). It is estimated that 80 % of the data used by managers and decisions makers is related geographically (Malczewski 1999).

Moreover, with the rapid development of computers, GIS can help experienced specialists by saving a great amount of time in the search for solution of spatial queries, and by providing channels of communication between the hydrological and other models, which allows them to combine such models for more sophisticated and complex analysis (Kovar and Nachtnebel 1996). Another advantage of GIS is that the integration of digital photogrammetry applications into GIS databases offers new

possibilities for the end-users, allowing data collection in a raster/vector-based GIS environment (Madani 2001).

Preparing site maps of fauna and flora or vegetation as well as land capability is done easily using GIS. Furthermore, GIS helps in monitoring and analyzing temporal and spatial changes in ecosystems that are due to both natural and man-made disturbances over time (Baskent and Misir 2002). Finally, GIS is an inter- and transdisciplinary tool that offers the possibility of integrating perspectives and making findings accessible to broader audiences (Shamsi 2002). GIS analysis can show the connection between whole-tree water use, tree density changes and local climate changes.

1.4 Research objective

The main purpose of the research reported here is to estimate the contribution of tree stands to the surface water balance by means of transpiration and actual evapotranspiration analysis, from the site scale up to a large area of the Volta Basin. This objective is based on the hypothesis that trees play an important role in the functioning and the control of the surface water balance of semi-arid regions, particularly during dry periods.

As dictated by the principal research guideline, specific objectives are defined:

- (1) To characterize savanna vegetation physiognomy and to establish phytoecological zones based on tree species diversity, tree density and spatially explicit tree patterns;
- (2) To model and scale up tree density by multivariate regression analysis using optical remotely sensed vegetation indexes and surface energy balance derivatives;
- (3) To estimate daily whole-tree water use by xylem Heat-Balance method and biometric standard methods, and scale up to tree stands transpiration flux by linear regressions;
- (4) To estimate the contribution of tree stands to the surface water balance;
- (5) To analyze the effects of vegetation cover conversion on local climate and tree-water relations for prediction purposes.

1.5 Thesis structure

The current contribution is organized in eight chapters, which can be regrouped in three parts. The first part introduces the questions of research (Chapter 1) and the field-study area (Chapter 2). Chapter 3 describes the general research method.

The second part of the thesis deals with spatially explicit tree patterns and their dynamics. It provides the basic outputs useful to address the main issue of whole-tree water relationships. Chapter 4 covers tree species diversity and spatially explicit patterns for classification purposes, and Chapter 5, a key synthesis chapter, develops a multivariate regression model (LAI-SEB model) based on remotely sensed vegetation indexes and surface energy balance derivatives to predict tree density and DBH. In the end, Chapter 6 presents data on land use and vegetation cover conversion for predictive purposes.

Finally, in Chapter 7 the principal results of the study are used to address the main research question, i.e, the contribution of trees to the surface water balance. The key results are summarized and discussed in Chapter 8, which includes the general conclusion and recommendations.

2 STUDY AREA

2.1 Geographical location

The study area is the Faunal Reserve of Bontioli also called protected area of Bontioli or “Forêt Classée de Bontioli”. It was listed as a nature reserve (25,000 ha) by the Burkinabe government according to the ministerial decree n° 3147/SEF of 29 March 1957 (MET 1994). The Faunal Reserve consists of the Total Reserve and the Partial Reserve. The research activities focus on the total reserve, because the partial reserve of Bontioli has no consistent savanna cover due to the high pressure of human activities.

The Total Reserve is located in the province of Bougouriba in southwestern Burkina Faso, between latitudes 10°70’ and 10°95’ N, and longitudes 3°02’ and 3°20’ W. With a perimeter of 83.39 km, it covers an area of 13,714 ha and lies in a rectangle measuring 17.41 km by 16.58 km (Figure 2.1). For simplification, the Total Reserve is called Nature Reserved of Bontioli (NRB).

2.2 Physical environment

2.2.1 Geology

The main geological platform of the Bougouriba valley to which the nature reserve of Bontioli belongs is from the Precambrian time. It is dominated by crystalline rocks and sedimentary layers oriented in a north-south direction. Individual massifs are underlaid by green rocks (AVV 1988).

More than 70 % of the NRB are dominated by migmatites and undifferentiated granites (Figure 2.2). In the western part, from north to south, lays a large cover of undifferentiated cuirass. From north to east, diabases, basalts and andesites dominate.

Study area

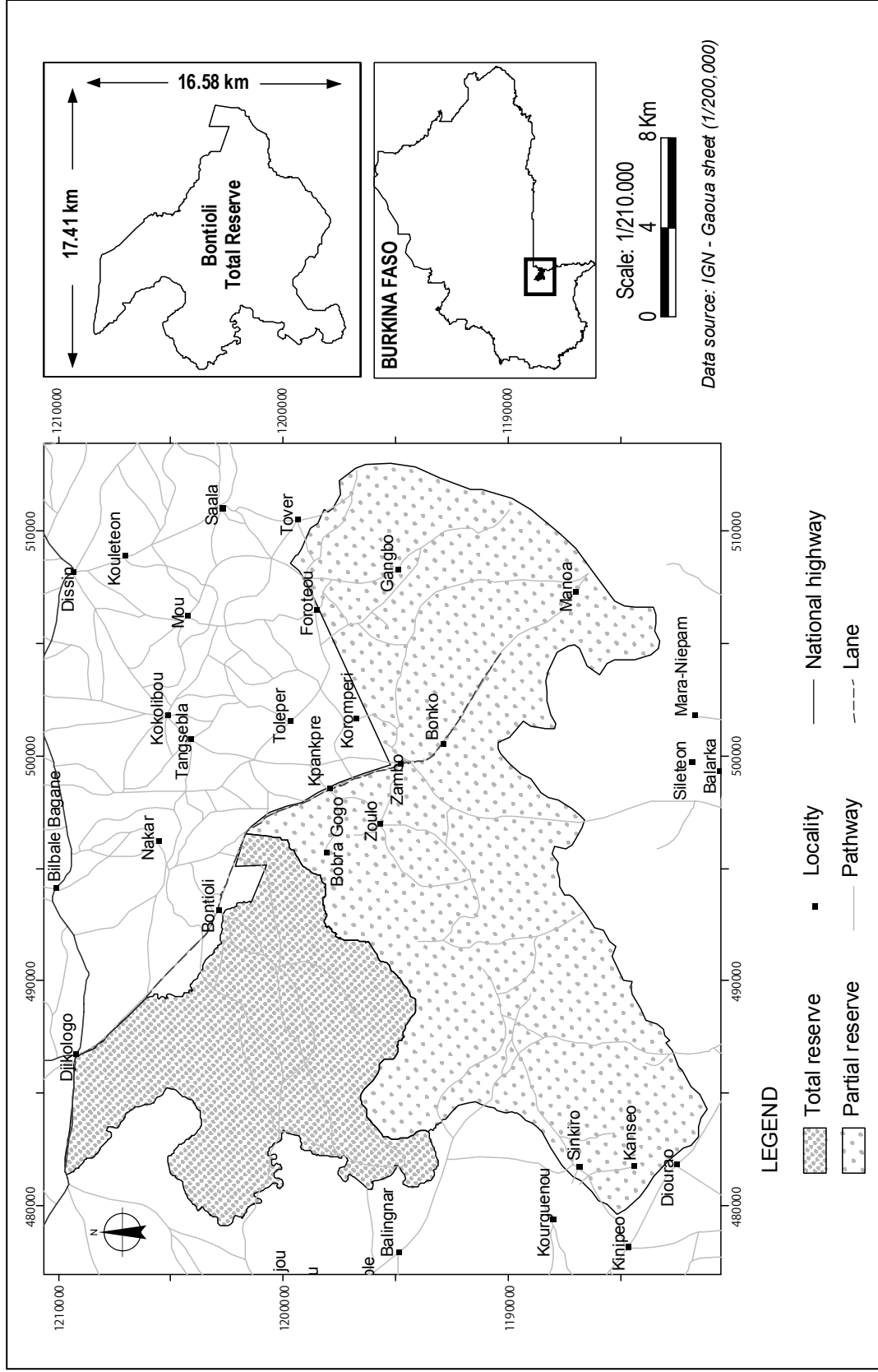


Figure 2.1: Geographical description of the Nature Reserve of Bontioli (NRB)

Study area

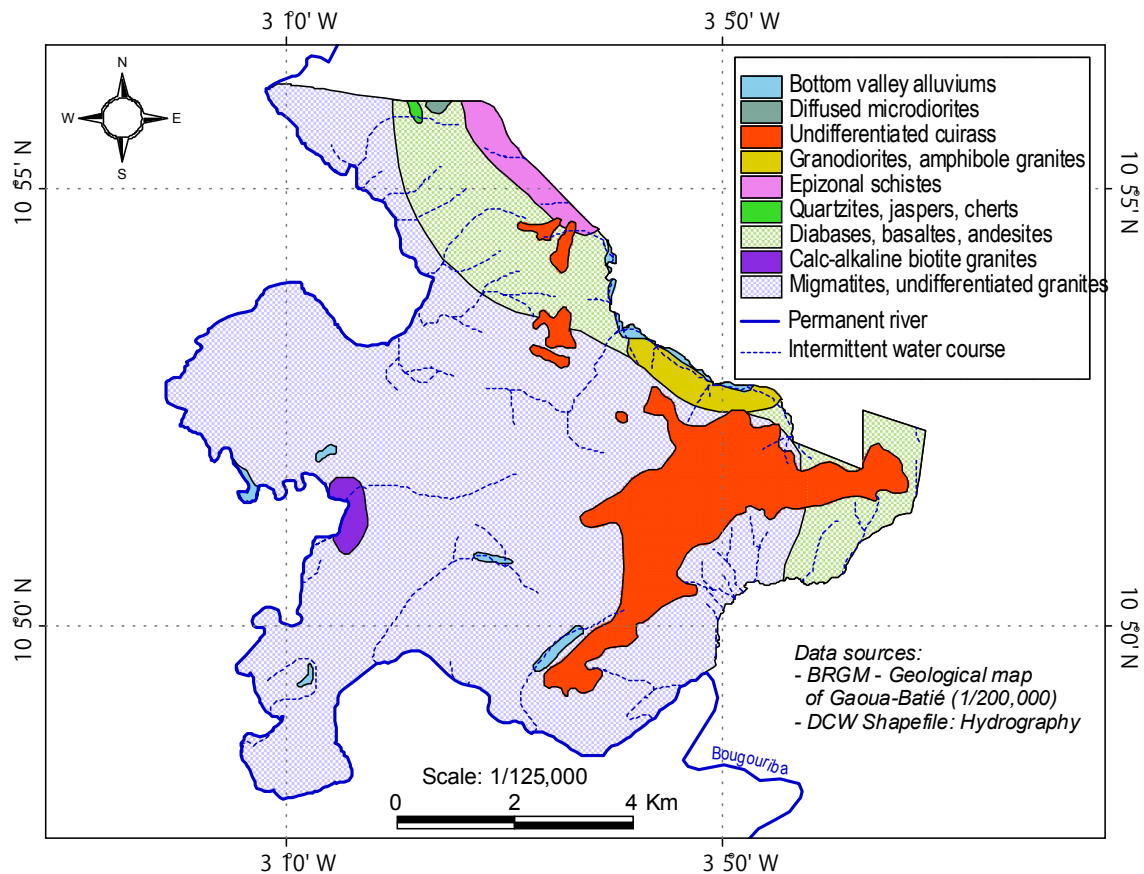


Figure 2.2: Hydrogeology of the NRB

2.2.2 Geomorphology and relief

Geomorphology

The landforms of the NRB can be divided into three geomorphological sets: low glacis, alluvial plains and bars.

- The low glacis are dominant, and their characteristics are influenced by the source rocks. The green rocks transform the glacis into laterite surfaces. In principle, on granites, schists and sandstones, the glacis have the aspect of a non-cuirass surface, but due to the phenomena of alteration and erosion, the glacis evolve to indurate landforms.
- The alluvial plains result from the dynamics of the alluvial terraces of the Bougouriba River and its main tributaries.
- The bars are developed along the Bougouriba River (AVV 1988).

In general, the cuirass layers consist of iron and aluminum and cover most of the landforms; the underground layers have also the same mineral composition (Pigeonnière et al. 2001). The underground layers account for the aspect of the relief.

Relief

The relief resulting from the geomorphological sets described above is flat with local undulations. The highest altitudes recorded by the differential GPS are around 350 m and the lowest about 240 m. The alluvial plains and the bars, mainly covering the western and southern part of the reserve, are the lowest, whereas the low and medium glacis cover the highest altitudes (Figure 2.3). The low glacis are stretched over the eastern part of the reserve, from the north to the south. In sum, the altitudes decrease from the north-east to the south-west, from the glacis to the bars.

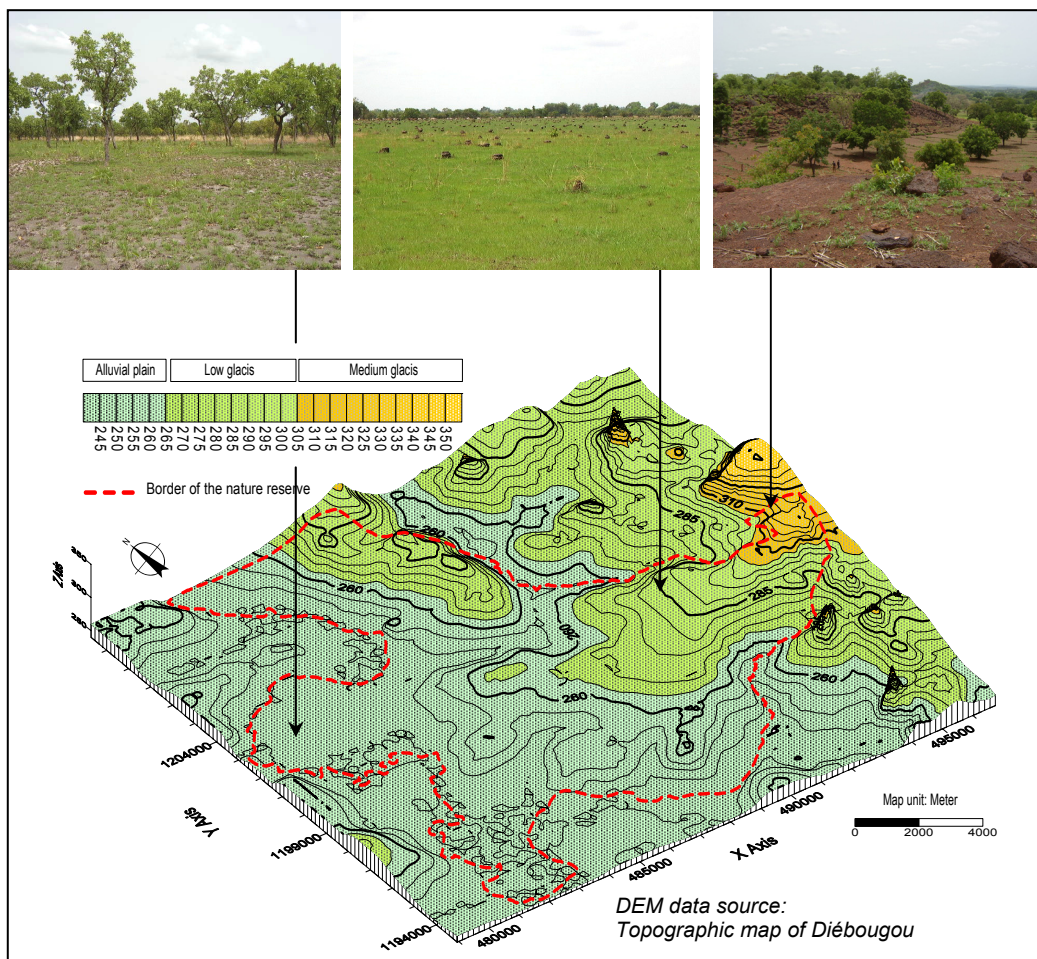


Figure 2.3: Description of the landforms by DEM. Correspondent pictures of ground-truth landforms and soils (May-June 2006)

2.2.3 Pedology

Five soil types are found in the research area (Figure 2.4), but three, i.e., depleted-indurated, reworked soils (1), pseudogley soils (2) and soils formed by erosion (3), are dominant. The different soil types are associated with clay, silt, sand and gravel layers.

In general, the silt and clay layers are present along the Bougouriba valley and in the adjacent alluvial plains, whereas gravels are found in soils formed by erosion in the low glaciais where the cuirass is omnipresent. Depleted and indurate, reworked soils are interspersed between the more well-defined soils. They are recognized by their high content of gravels and level of induration.

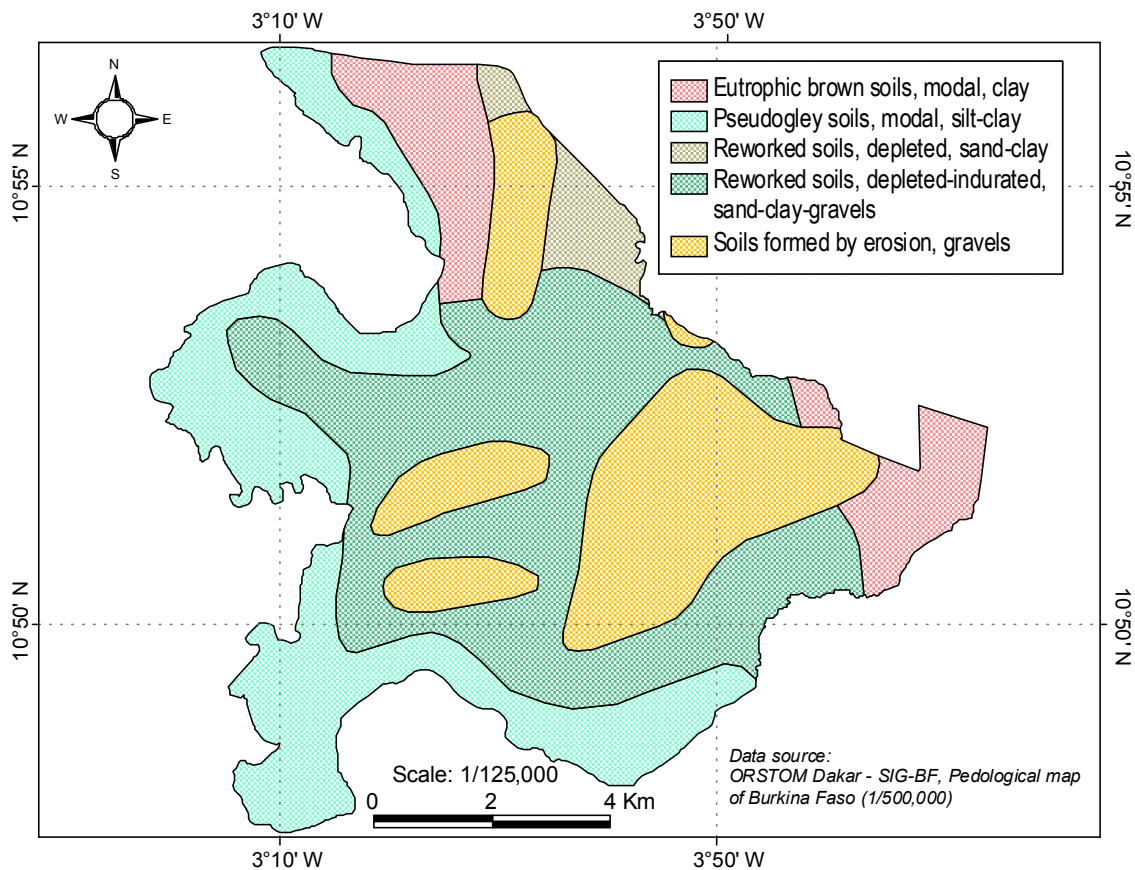


Figure 2.4: Main soil types in the NRB

According to field observations, the physiognomy and phytosociology of the vegetation vary according to the soil units and landforms. Illegal farmers who have settled in the nature reserve often cultivate sorghum, cotton, and maize on lowlands, where the rates of gravels and cuirass are relatively low. They prefer weakly developed soils on basic rocks, which are generally rich in calcium and magnesium. A large-scale

analysis reveals that the soils within the Volta Basin of Burkina Faso are not enough fertile, poor in phosphorus and nitrogen, strongly eroded and depleted (FAO 1996).

2.2.4 Hydrography and groundwater

Hydrography

The Bougouriba (Figure 2.5, insert 1) is the main river that determines the architecture of the hydrographical network. It has a regular slope of 0.2 m per km along its total length of 406 km (Moniod et al. 1977). The river is not permanent, because it records some periods of interruption in the interval between January and June, and reaches its highest flow level in September ($167 \text{ m}^3 \text{ s}^{-1}$), flooding the adjacent alluvial plains (AVV 1988).

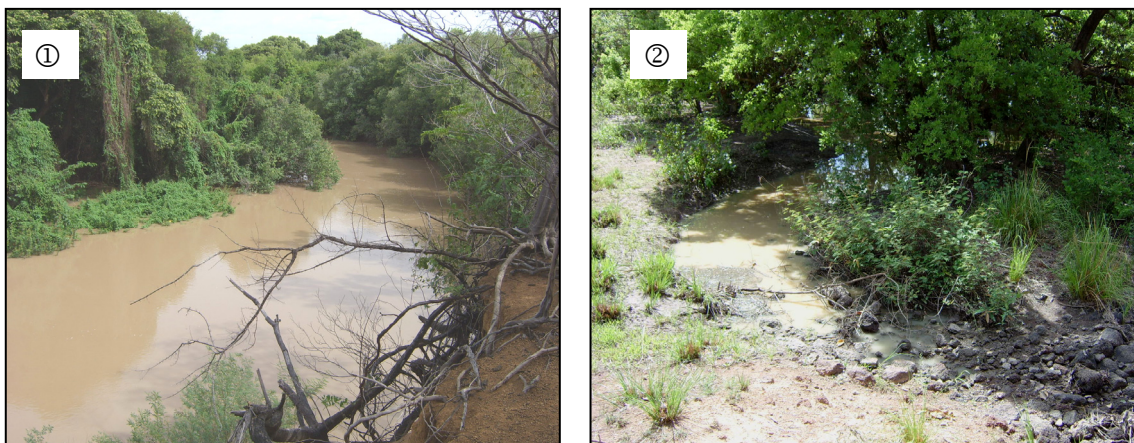


Figure 2.5: Extent of the Bougouriba river in the western NRB in June 2006 (insert 1).
Insert 2 shows an intermittent river drying up in northern NRB in June 2005

The surface of the NRB is poorly supplied with water sources. During the dry seasons, all existing intermittent streams and ponds quickly dry up under the stress of the hot climatic conditions, just after the last rainfalls. The Bougouriba itself is also affected by the dry weather to the point that its colour changes to red-brown in crucial periods of intense evaporation and erosion due to the first rainfalls of the rainy season (Figure 2.5, insert 1).

Groundwater

The extent of the aquifer depends on the nature and the depth of the underlying laterite layers and the tectonic fault. In general, water reserves are limited to the underground clay laterite layers. According to geophysical investigations, the chance to meet water underground in fractures of the area is high in the green rock substratum, in schists, along quartz veins and on granites, or in phaneric arenas (AVV 1988). An overall estimation of the renewable water resources in the country predicts a decrease by two thirds from 1990 to 2025 (GLOWA 2002).

2.2.5 Rainfall

Being located at the heart of the Sahel, Burkina Faso falls within the tropical dry climate of the Sudano-Sahelian type characterized by two seasons: one dry season and one rainy season. The length of the rainy season decreases from South to North (Pigeonnière et al. 2001).

The NRB falls completely within the South Sudan climatic zone with rainfall averaging 900 - 1,000 mm per year. In 2006, the total rainfall over the reserve was 918.6 mm (Bontoli station: 10°51'55''N, 3°04'21''W). This zone is described as follows:

- a dry season from mid-November to mid-April
- a rainy season from mid-June to mid-September
- two unpredictable transition periods: a dry period (mid-April to mid-June) and a wet period (mid-September to mid-November).

An overall analysis of three stations Dano (3°20' W, 11°53' N, 457 m), Diébougou (3°13' W, 10°56' N, 294 m) and Dissin (2°55' W, 10°55' N, 274 m) reveals a relative decrease in rainfall over 26 years (1965-1990) with a pronounced decrease between 1970 and 1975 (Figure 2.6, insert 2). Figure 2.6 (insert 1) shows that it rains less in Dano (some 25 km from NRB) compared to the two other localities closer to the NRB.

From the provincial scale up to the national level, rainfall decreased from decade to decade in the whole country (Figure 2.7). Hence before the 1970s, the NRB

Study area

was crossed by the isohyet 1,100 mm per year, whereas during the period 1960-1990, it was located between the isohyets 900 and 1,000 mm per year.

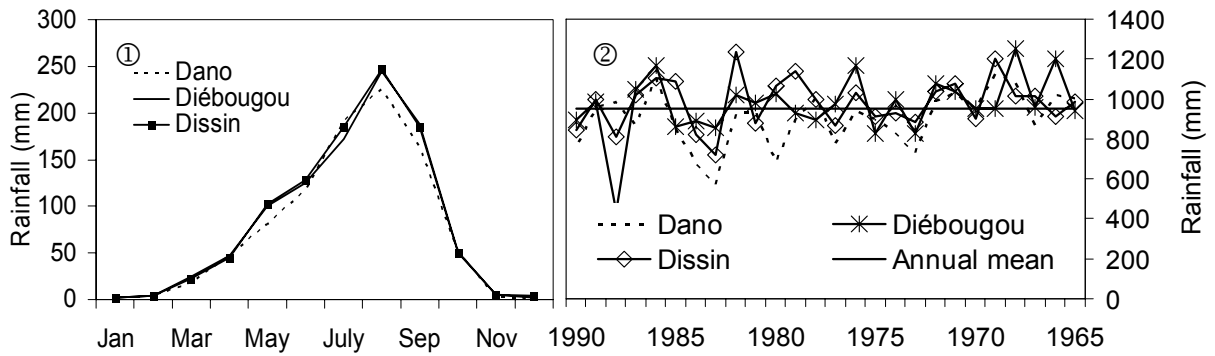


Figure 2.6: Mean rainfall from 1965 to 1990. Insert 1: Average monthly rainfall; insert 2: Average annual rainfall (Data source: FAO).

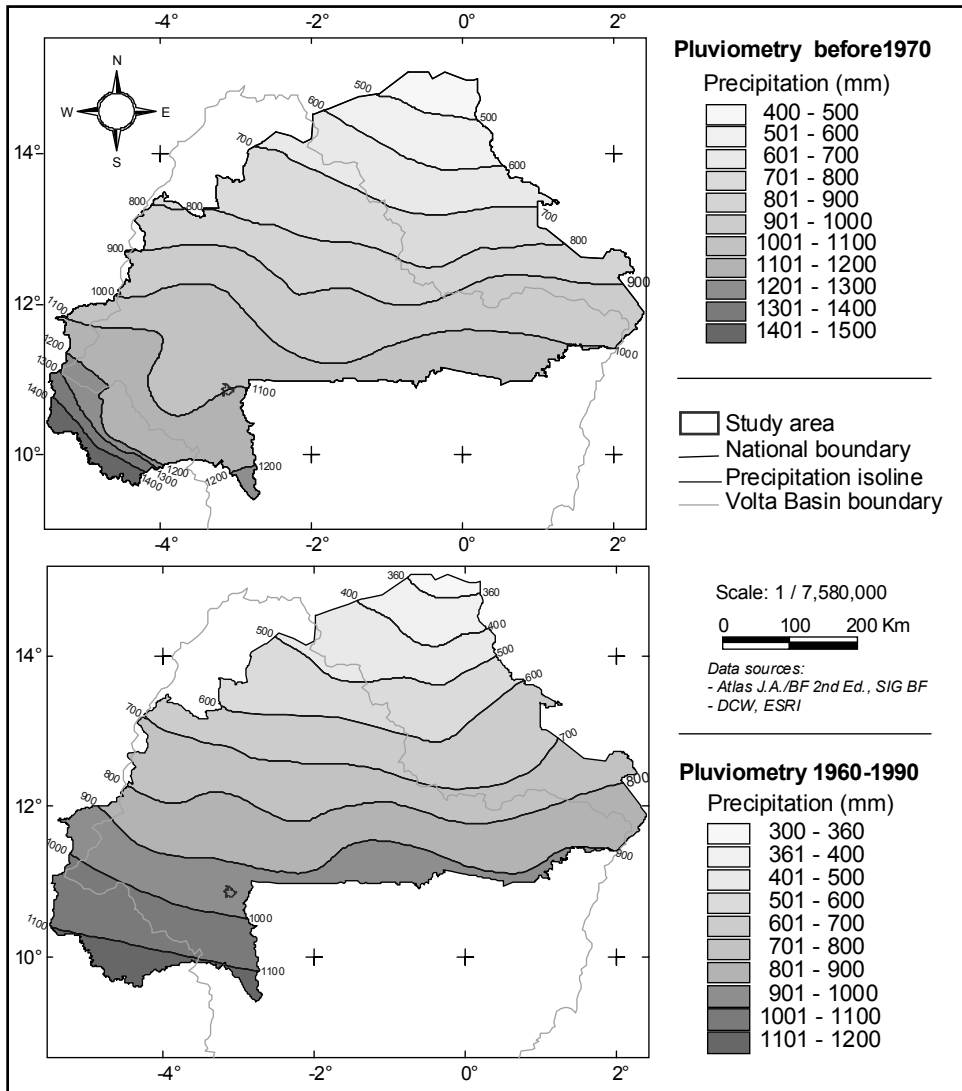


Figure 2.7: Decreasing rainfall in Burkina Faso: 1970-1990

The wind rose of the reserve (Figure 2.8) for the 3-years period 2004-2006 shows that a high proportion of wind blows in the directions NE-SW and E-W directions. The mean wind direction is NNW-SSE (154deg) 32 % of the time with 48.8 % of the wind blowing at speeds ranging from 0.5 to 2.0 m s⁻¹. Relatively high wind speeds (i.e., speed > 5.5 m s⁻¹) are almost nonexistent (0.1 %). Nineteen percent of the winds are considered calm (i.e., speed < 0.5 m s⁻¹). As a whole, the mean wind speed is 1.44 m s⁻¹; the value is lower in the rainy season (1.11 m s⁻¹) than in the dry season, when wind speeds up to 1.63 m s⁻¹ occur.

During rainy periods, wind direction switches to between S-N and E-W with an emphasis on the SE-NW direction. Relatively heavy rains (i.e., > 11 mm h⁻¹) are associated with SE-NW, ESE-WNW and E-W winds (Figure 2.9).

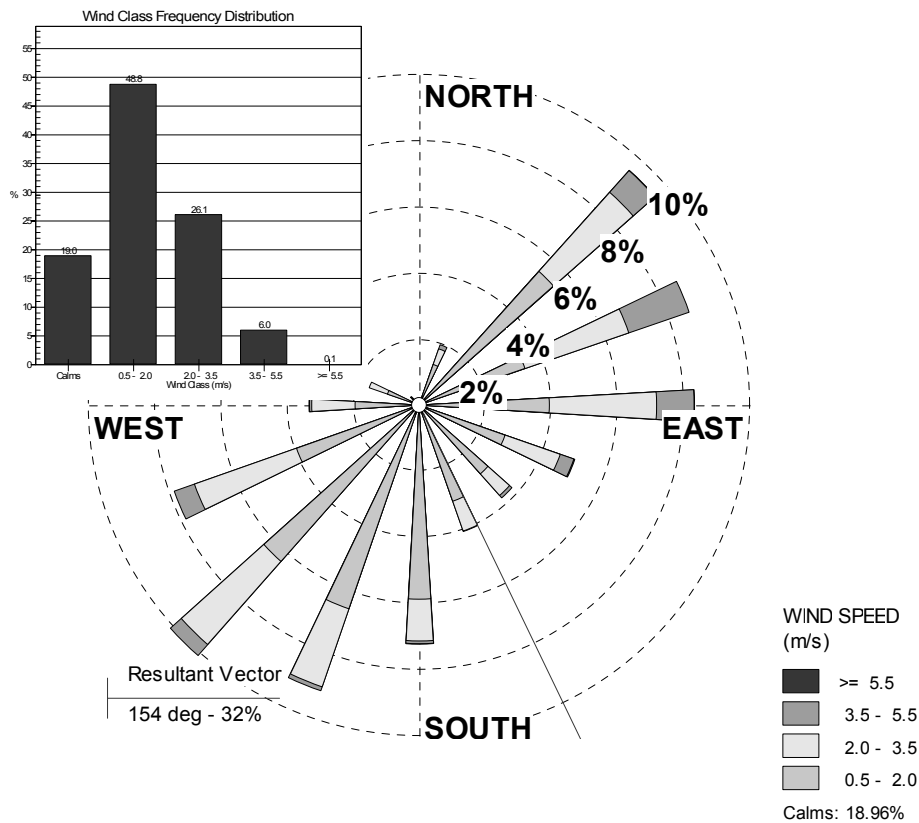


Figure 2.8: Wind rose of the NRB. Wind speed as a function of wind direction (April 2004 - Dec. 2006). Orientation: wind direction means “blowing from”. (Climate data provided by J. Szarsynski – BIOTA West)

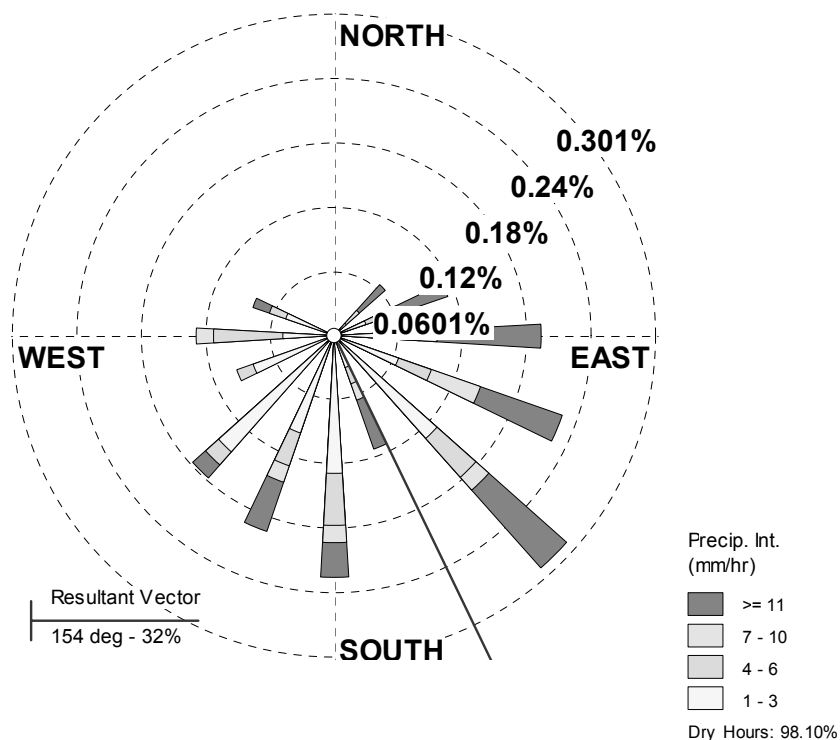


Figure 2.9: Rain rose of the NRB. Rainfall intensity as a function of wind direction (April 2004-Dec. 2006). Orientation: wind direction means “blowing from”. (Climate data provided by J. Szarsynski – BIOTA West)

2.2.6 Net radiation, air temperature and relative humidity

The mean net radiation over the last past three years (2004 - 2006) was 97.2 W m^{-2} with maxima of about $1,100 \text{ W m}^{-2}$. The mean air temperature for the same period was $27.1 \text{ }^{\circ}\text{C}$ with maximum temperatures reaching $40 \text{ }^{\circ}\text{C}$ in the dry season (March-April) and minima of about $20 \text{ }^{\circ}\text{C}$ in December, the period of the Harmattan. The rainy season was cooler with $25.8 \text{ }^{\circ}\text{C}$, while the dry season scored the highest mean air temperature of $30.9 \text{ }^{\circ}\text{C}$.

Mean relative humidity was 58.7% with seasonal variations; in the dry season it was 20.9% which increased to 79% in the rainy season when maxima of 95% were recorded. Minima of 4% were observed in dry season.

2.3 Biological environment

2.3.1 Vegetation type and composition

According to the classification of the vegetation zones established by Pigeonnière (2001), the NRB belongs to the Sudano-Guinea savanna typical for the southwest of the country. This area is characterized by abundant tree species such as *Burkea africana*,

Isoberlinia doka, *Isoberlinia dalzielii*, *Detarium microcarpum*, *Uapaca togoensis*, *Parinari polyandra*, etc. Among shrub and tree savannas, some gallery forests grow along riverbeds.

The NRB is dominated by tree and shrub savanna woodlands, where the most dominant tree species are broadly *Burkea africana*, *Pterocarpus erinaceus*, *Crossopteryx febrifuga*, *Combretum spp* (Figure 2.10). Trees are both evergreen and deciduous. In comparison with the surroundings environment, vegetation cover is still important to the extent that the woody potentiality varies from medium (north, southeast) to high (west, center and southwest).

2.3.2 Flowering period

Guinko (1984) distinguishes four main flowering periods according to season: (1) a high flowering (rainy season), (2) a medium flowering (beginning of the dry season), (3) a low flowering (dry season), (4) an important flowering period for trees (end of dry season).

After the first rainfalls of the rainy season, the grassland reappears and tree-crown covers are rich in leaves. The optimal period for the high flowering phase is September-October, when it is easy to distinguish the vegetation physiognomy and describe tree species. From the beginning of the dry season and later, after the bushfires, most of the trees look dead, are leafless and covered by fire marks. Some species like *Bombax constatum*, *Stereospermum kunthianum*, *Combretum glutinosum*, *Ceiba pentandra* flower in November-December. Other species like *Lonchocarpus laxiflorus*, *Afzelia africana*, etc. continue to flower in January - March.

At the end of the dry season (April - May) most of the trees, particularly *Lanea microcarpa*, *Annona senegalensis*, *Combretum nigricans*, *Pseudocedrela kostchyi*, are covered with leaves and flowers.

Study area

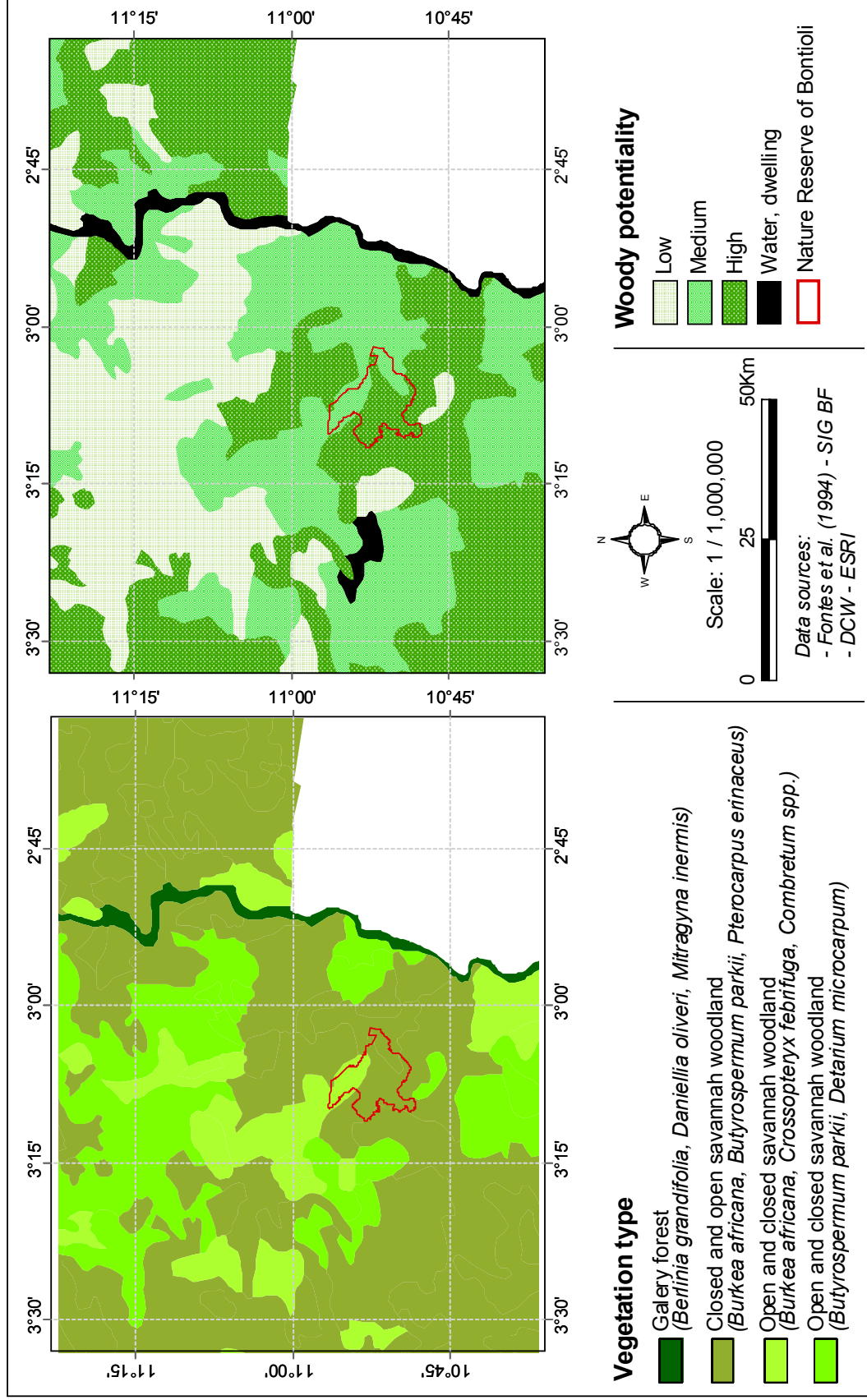


Figure 2.10: Main vegetation types and woody potentiality of the NRB and its surroundings

2.3.3 Vegetation seasonal disturbance: bushfire

Though bushfires are officially forbidden, they occur every year in November-December or later. Observations in the NRB showed that bushfires seriously affect trees by atrophying them and burning their branches and buds. For their own protection, some trees have barks that are thick and rough. During our surveys through the NRB, the bushfire marks were omnipresent. The whole reserve is affected and parts of its landscape often look like a chimney. This situation sometimes makes it difficult to distinguish the different savanna types. In more disturbed areas, the height and density of trees are almost the same, though the area is bound to be classified as a different savanna type than that observed.

2.3.4 Fauna

The landscapes of the reserve are shared by wild and domestic animals. Few wild animals, namely *Erythrocebus patas*, *Kobus Kob*, *Hippotragus equinus*, *Lepus capensis*, *Cephalophus*, communities of birds (*Numida*, *Columba*, *Streptopelia*, *Necrosyrtes*, *Aquila*, *Terathopius*, etc.) and snakes were observed during the field campaigns. Elephant tracks were observed along the Bougouriba River in the alluvial plains extending from north to west (Figure 2.11).

AVV (1988) went into details about the analysis of the fauna dynamics. In the 1970s, some hippopotamus, buffalos and other species of monkeys and antelopes existed, but now they have all vanished due to the pressure of intensive poaching (AVV 1988). On the other hand, large herds of cattle, goat and sheep were omnipresent in the park. In the center of the reserve, a few donkeys and dogs often roamed.

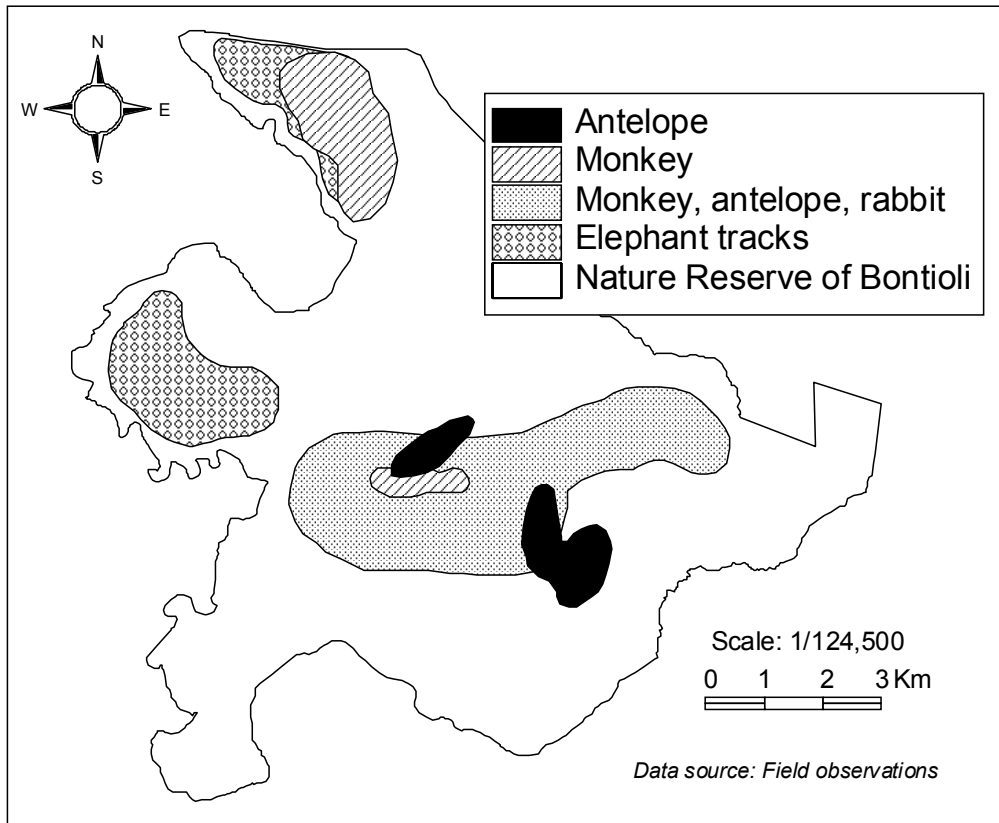


Figure 2.11: Non-exhaustive observation-based map of wild animal location in the NRB

2.4 Human activities

Despite its statute of a protected area, the NRB is constantly being exploited by riparian populations and nomad Peule herders. Illegal human activities in the NRB include: farming, livestock farming, firewood cutting (Figure 2.12). The increasing population demands for food, the reduction of fertile soils and the poor monitoring within the “Forêt classée de Bontioli” offers farmers opportunities to settle in the reserve. They often cultivate millet, red and white sorghum, maize, rice and cotton

Though the NRB is a protected area, herders let cattle, sheep and goat roam in the reserve, because water from the Bougouriba River is available, the grasslands are not entirely destroyed by bushfires. Moreover, in the reserve, herders escape conflicts with farmers over the damages caused by their animals.



Figure 2.12: Farmers in action in the NRB. Women carrying firewood and cattle roaming in a freshly cleared farm (northern NRB)

2.5 Conclusions

As a whole, the natural environment of the NRB is favourable for the development of the savanna vegetation characteristic of the South Sudan climatic zones with annual rainfall of around 950 mm. The listing of area as nature reserve in March 1957 would have been sufficient for the regeneration of the whole reserve with most of its wild animals if human pressure had not been so intense. Though all the main tree species characteristic of the tree and shrub savanna woodlands exist, the NRB is threatened yearly by the harsh bushfires and farmers need for expansion.

3 GENERAL RESEARCH METHOD

3.1 Introduction

The method aimed at quantifying accurately the whole-tree water use by sap flow techniques, and by determining the phytosociology and physiognomy of the savanna landscapes in relation to the phytoecology of the natural milieu. The two data sets were coupled with remote sensing and GIS techniques in order to upscale the contribution of the trees to the surface water balance over a large area within the Volta Basin. The field studies were conducted at the reserve scale (April-June, September-October 2005 and April-June 2006) and the results were scale up to the satellite scene coverage and sub-basin scales.

This chapter focuses on the field measurement methods. The surface water balance components analysis, i.e., the calculation of tree stands transpiration rates and the upscaling process, are explained in chapters 5 and 7.

3.2 Sap flow measurements

The sap flow measurement equipment (UP GmbH) consisted of two measurement systems: a fixed system (provided by J. Szarzynski - BIOTA West) and a mobile system (Prosalog, Small Edition). Both systems have the same principle of measurement with the difference that the first carries a maximum of 12 sensors and works with solar panels and the second works with 3 to 5 sensors and uses a small 12 Volt-DC battery.

3.2.1 Site selection

As a preliminary step to site selection and installation of the sap flow equipment, airborne surveys (Figure 3.1) followed by ground investigations were undertaken to study the physiognomy and the phytosociology of the vegetation units, and obtain an overview of the dominant tree species per vegetation type and land unit.

The type of aircraft used was suitable for low altitude flights and allowed taking high resolution images with the Agricultural Camera Tetracam. However, even with the slowest flight speed, gaps in the series of images over the NRB could not be avoided. That limited the possibility of assembling the images into a mosaic, and they

thus had to be analysed individually. Processing the 3-band images (red, green and blue bands) produced a spectrum of vegetation indexes, i.e., SAVI, NDVI and IPVI.

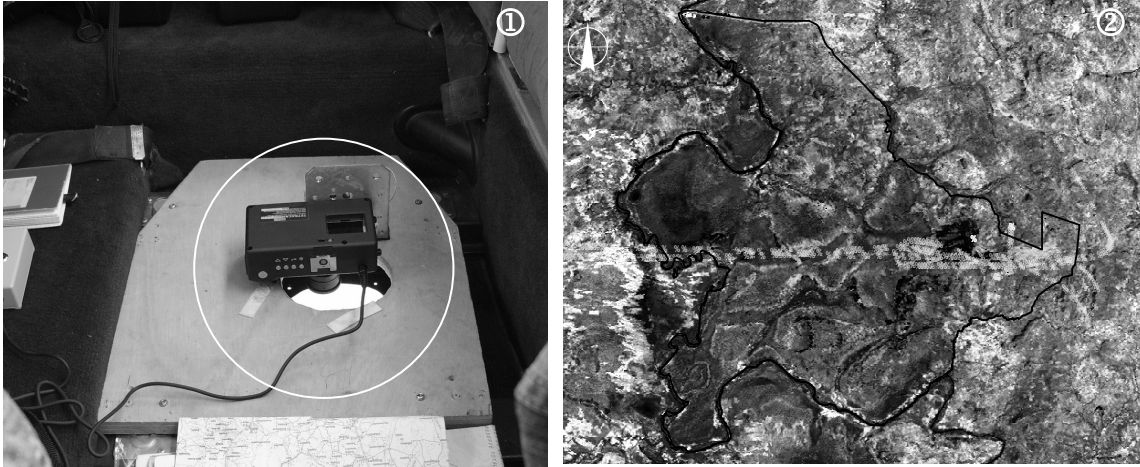


Figure 3.1: Airborne survey over the study area. Insert 1: Agricultural Camera Tetracam on board (in circle) capturing high resolution images; insert 2: satellite image showing flight path over study area (in white).

The information derived from the surveys were overlaid on the satellite image Landsat 7 ETM+, scene 152/56, bands 457, 28 Oct. 2002 (Provided by the University of Maryland) for the final site selection decision (Figure 3.1). Priority for sap flow measurement with the fixed system installation was given to sites not farther than 2 km from the micrometeorological and Eddy Covariance stations (Figure 3.2) in view of coupling the climatic data for later sap flow data analysis.

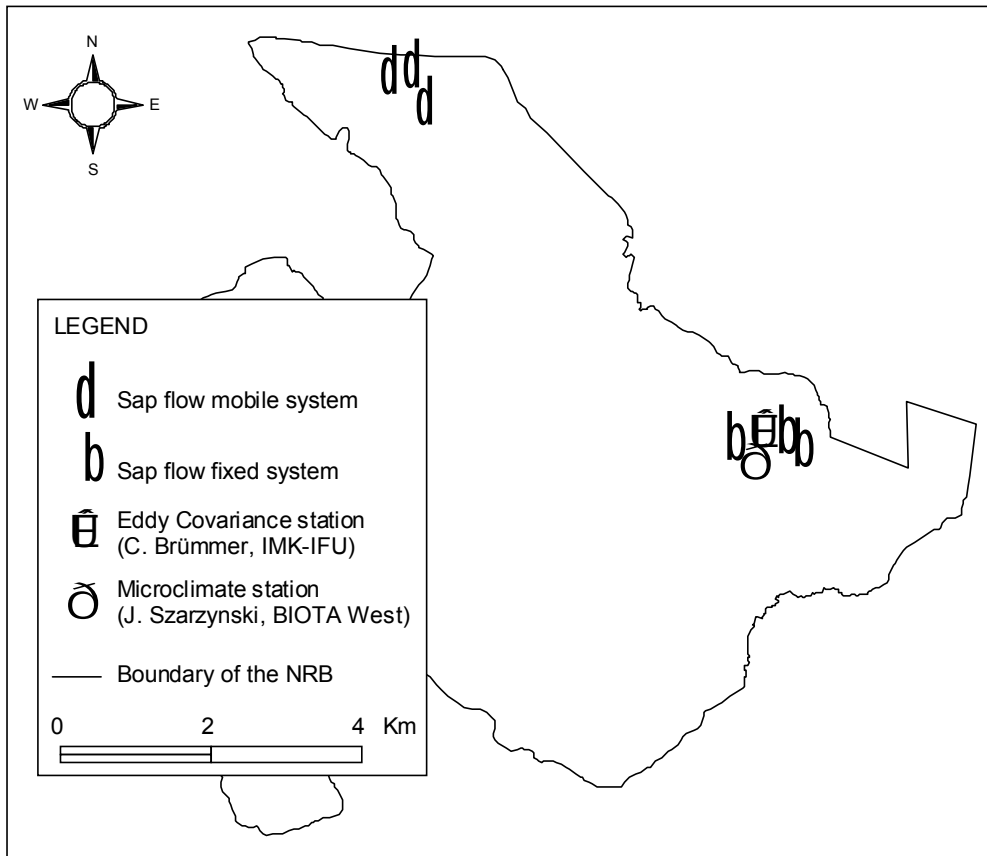


Figure 3.2: Sap flow measurement sites in the NRB.

3.2.2 Measurement equipment installation

Equipment installation

The sap flow measurement equipment was installed in four steps (Figure 3.4). Two fixed systems were installed for long-time series measurements with solar panels and strong accumulative dry batteries for long-time functioning autonomy (Figure 3.3). The objective was to cover the different seasons within a one-year period so as to analyze the variation of tree species water uptake.

Additional sap flow measurements were done in parallel with a mobile system to study the trend in the water uptake of the other dominant tree species. The advantage of such a flexible system that the measurement site can be changed to a new one, covering the maximum number of tree species. But, this system requires more monitoring time since the battery needs to be replaced every two to four days, the memory card (MM card, 64 mb) is overloaded after 15 days. During continuous measurements, tree-level sap flow was logged every 20 sec and saved to the datalogger as 10-min averages.

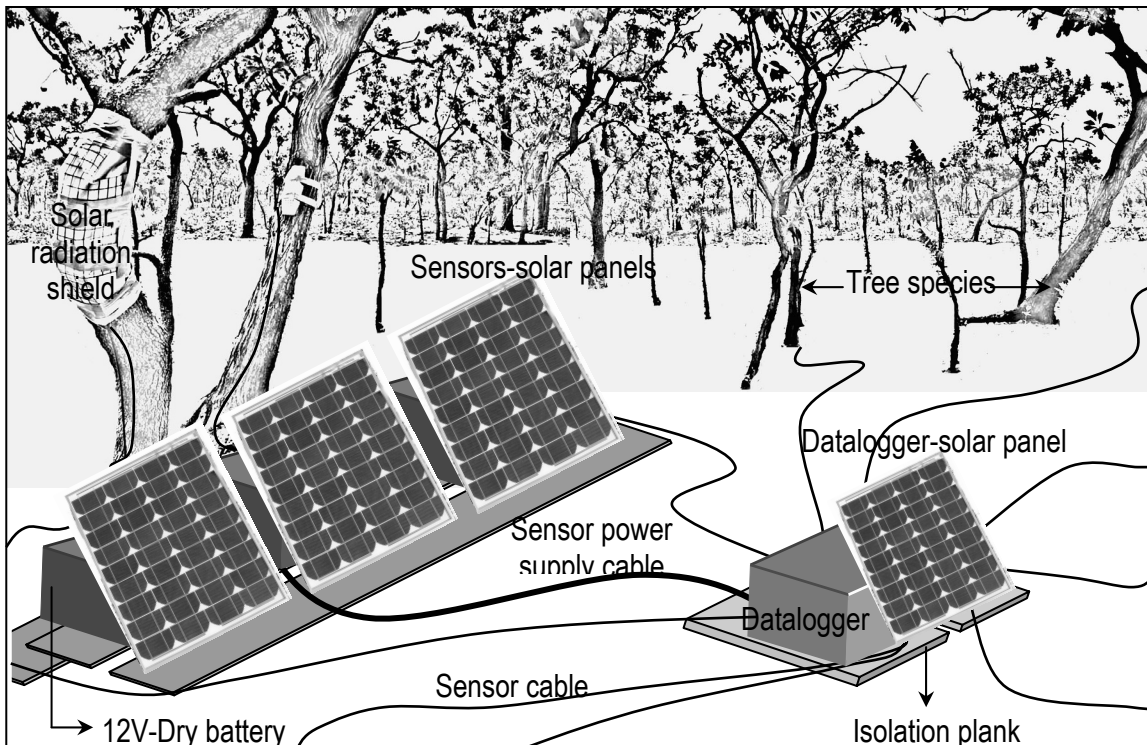


Figure 3.3: Set-up of fixed system for sap flow measurement

Principle of sap flow measurement

In step 2 of the sap flow equipment installation (Figure 3.4), two needles of a sensor are inserted in holes of 2.1 mm into tree sapwood at breast-height, one above the other, at the north side of the tree to avoid the thermal effects of sunshine. The upper needle (yellow) is heated by a constant current of 84 mA provided by the batteries in connection with solar panels.

This results in a temperature difference between both needles, which depends on the sap velocity. High flux transports the heat upwards and shows a low signal, whereas low flux causes the highest temperature difference (UP 2001). The data sets retrieved from the dataloggers for the relevant sapwood areas are coupled to calculate whole-tree water use.

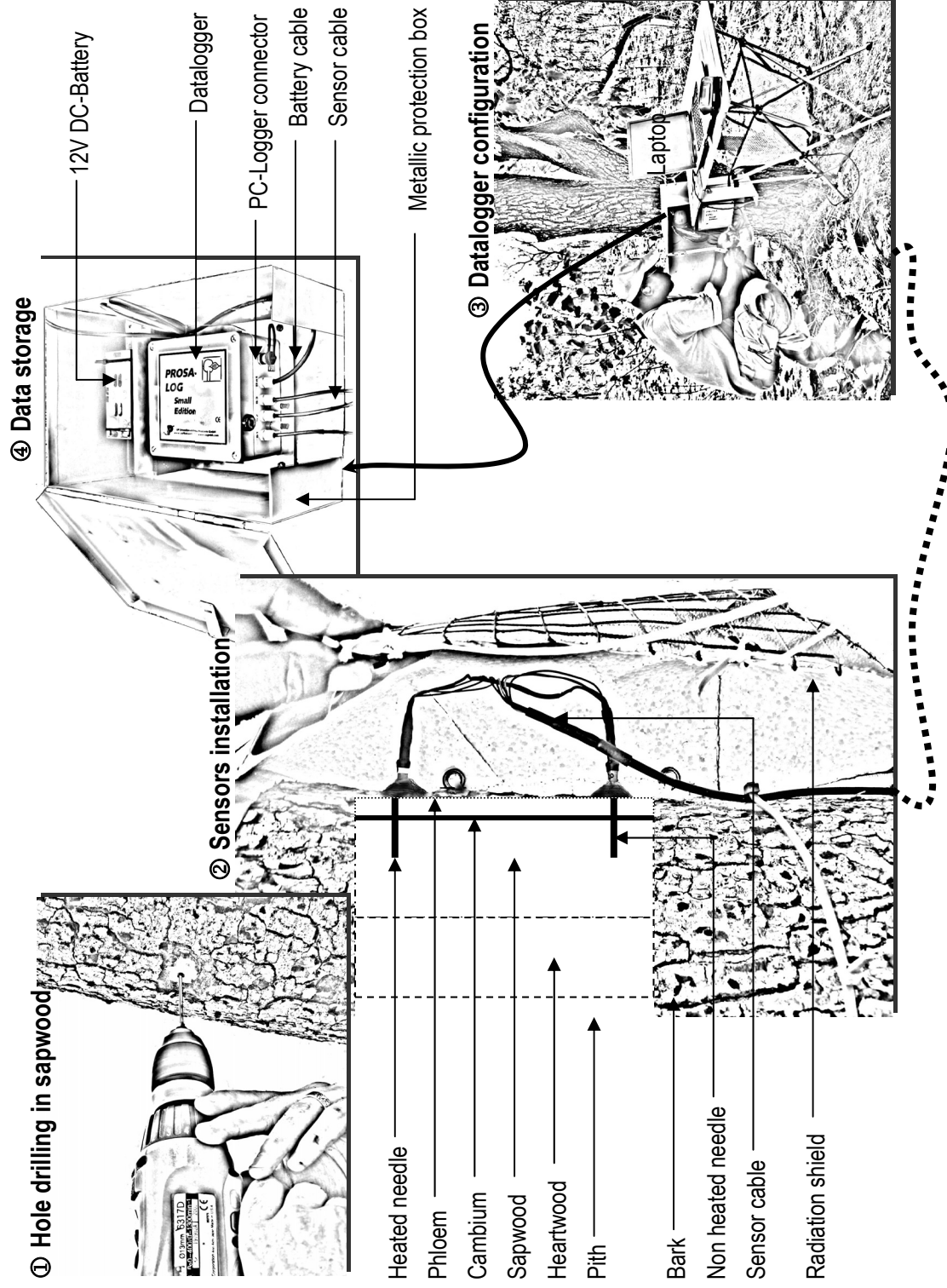


Figure 3.4: Set-up of mobile system for sap flow measurement

3.2.3 Sapwood sampling and analysis

Sapwood sampling

For accurate tree sap flow calculation, the sapwood was sampled close to the sensor, in the zone between the two needles. The sapwood sampling drill (Suunto) was inserted into the tree perpendicularly to the trunk so as to transversally cut the capillaries of the sapwood (Figure 3.5). First visual measurements of the sapwood radius were done in the field based on the wet parts of the sapwood samples, and then the samples were conserved in alcohol (ethanol, 70 %). The field measurements were supplemented in the laboratory with microscopic analysis.

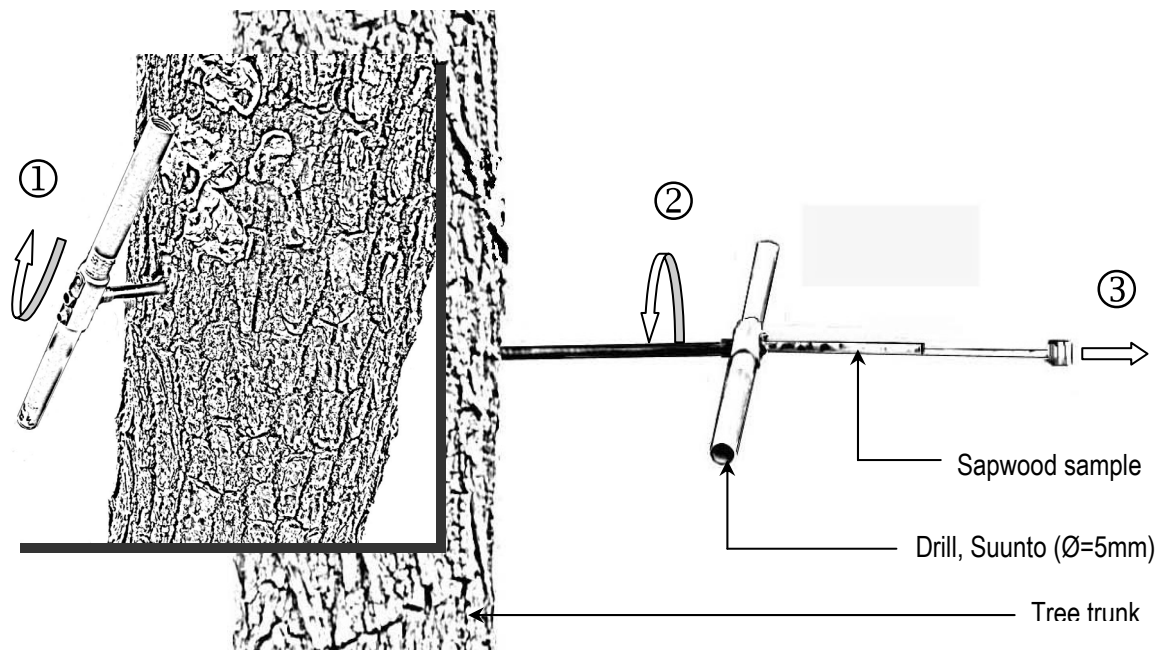


Figure 3.5: Sapwood sampling

Principle of sapwood area determination

The sapwood samples were dried in an electric oven at 61 °C for 2-3 days. Then they were analyzed using a microscope (Figure 3.6). The total length of each sample was measured before and after drying in the oven in order to determine the shrinkage rate. That rate was used at the end of the measurement to derive the actual sapwood area. The principle of the determination of the sapwood area is based on the presence of

capillaries along the sample; the sapwood area starts with capillaries and ends when the capillaries gloss over and can no longer be observed. The size of the capillaries varied from one sample to another with differences in tree characteristics and age: some capillaries were easy to observe while others were more difficult.

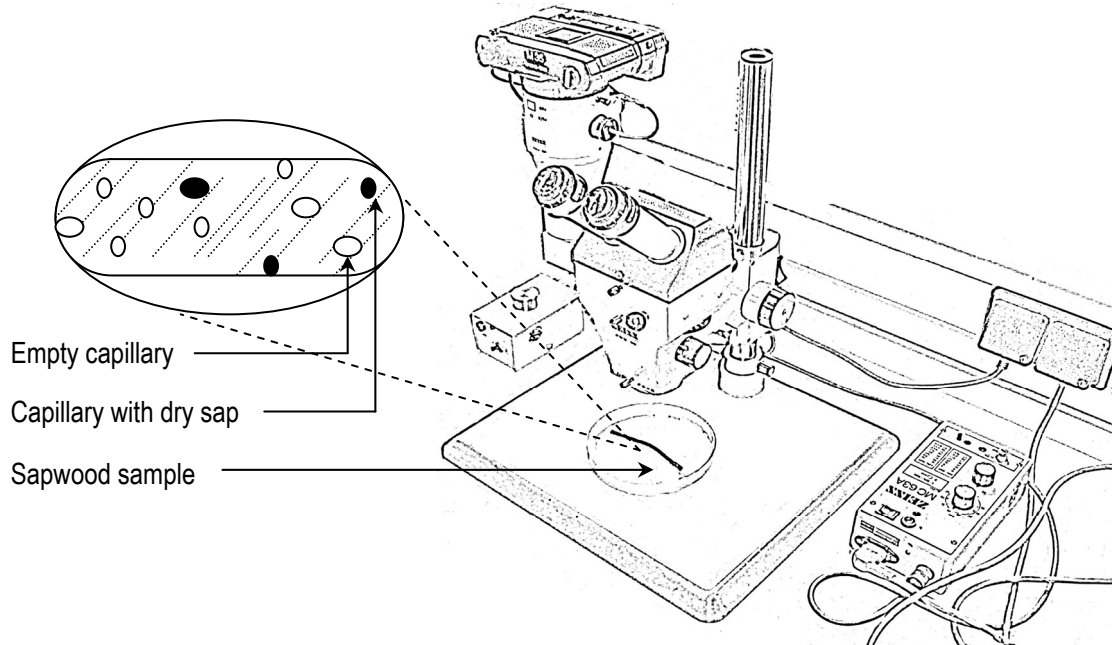


Figure 3.6: Principle of determination of sapwood area. Use of ZEISS microscope

In fact, the sapwood area, i.e., the water-transporting area (cm^2), cannot be directly determined from direct visual observation. The sapwood radius can be measured using the microscope and a measurement tool. Assuming the tree trunk to be a perfect circle, the sapwood area (sa) is derived from the sapwood radius (sr) and the trunk diameter at sap flow measurement height (ds) as follows:

$$sa = \left[\left(\frac{ds}{2} \right)^2 \times \pi \right] - \left[\left(\frac{ds}{2} - sr \right)^2 \times \pi \right] \quad (3.1)$$

Calculation of sap flow

Once the sapwood area of the wood is known, the calculation of the sap flow (sf) of an individual tree species is done according to the equations as follows (Granier 1987):

$$sf = sd \times sa \text{ (ml} \cdot \text{min}^{-1}\text{)} \quad (3.2)$$

$$sd = 0.714 \times \left(\frac{\Delta T_{night}}{\Delta T_{actual}} - 1 \right)^{1.231} \text{ (ml} \cdot \text{cm}^{-2} \cdot \text{min}^{-1}\text{)} \quad (3.3)$$

where ΔT_{night} = Temperature difference at night (minimum value of the dataset)
 ΔT_{actual} = Temperature difference measured
 sa = Sapwood area (cm²)
 sd = Sap flow density

The calculation of sap flow was done for all tree species of the measurement sites. Thus, the quantification of the overall savanna water release was processed based on tree density in an upscaling process.

3.3 Tree biometric measurements

The tree biometric method consists of measuring diameter, height and crown parameters of standing trees with appropriate tools. That method encompasses a sampling technique, GIS processing, and intensive field surveys.

3.3.1 Sampling method and plot size

Systematic sampling

The systematic sampling method was used because of its simplicity of application in the field (Krebs 1989). It has other advantages such as the easy location of the plots, the regular distribution of the plots over the whole vegetation cover providing more information, and the possibility to map the spatial distribution of the characters estimated (Rondeux 1999). Based on the systematic sampling method, the surface of the NRB was divided into regular square grid units at 1 km intervals, leading to 142 plots to investigate (Figure 3.7).

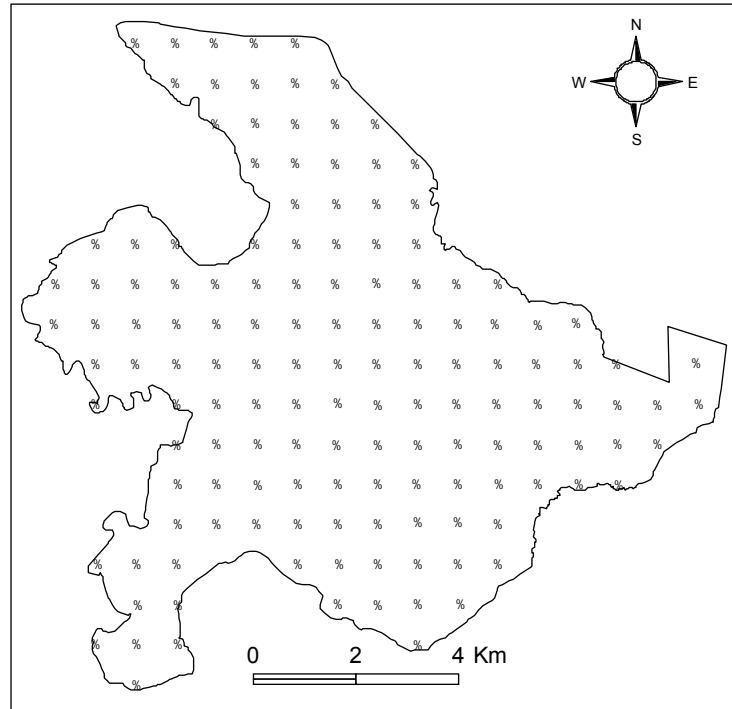


Figure 3.7: Systematic sampling. Regular square grid at 1 km intervals

Plot size

As usual in West African savanna regions and according to common surveys in similar geographic zones of our field research, the minimum surface required to establish a plot is 900 m². In very dense savanna areas, this surface can be reduced to 400 m². For the choice of the final plot size, three different sizes were tested: 400 m², 900 m² and 2,500 m².

Plots of 400 m² underestimated tree density and did not always take into account representative vegetation units, whereas plots of 2,500 m² overestimated vegetation units and were time consuming. With such large plots, work time would be doubled and mapping trees for spatial distribution could be tricky due to the insufficiency of data. Finally, the plot size adopted was a square of 30 m x 30 m (900 m²). All the measurements were done within that square.

After collecting data on the variables of analysis, 10 m-square was delimited randomly inside the main plot to name and count the saplings and seedlings (Figure 3.8). The purpose of that sub-plot was to collect data useful for the analysis of the regeneration dynamics of the reserve. Knowing the regeneration time of each tree species is a reference clue to predict tree density dynamics.

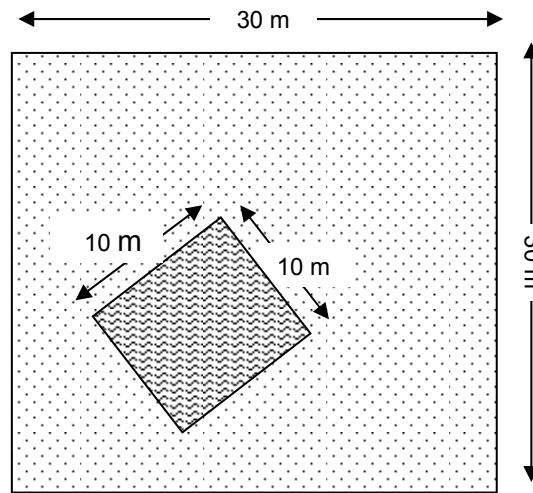


Figure 3.8: Delimitation of plot and sub-plot

Oriented-plot survey strategy

Aware of the monotony of the landforms and the slight variation of the phytosociology of the vegetation cover, and with a view to save time by avoiding redundancy in the surveys and by reducing field expenses (fuel, workforce expenses), the oriented-plot method was adopted based on the systematic sampling. This method consists of one survey from a predefined plot (chosen grid) and attribution of the results of that survey to the neighbour grids that have the same characteristics of landform and phytosociology. Therefore, the oriented plots were defined beforehand on the basis of remotely sensed images analysis and field knowledge (Figure 3.9).

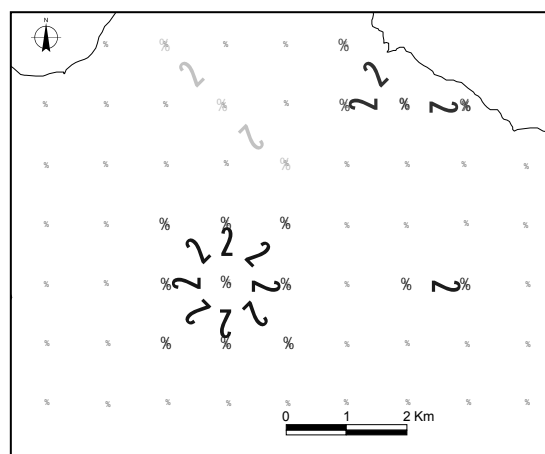


Figure 3.9: Different possibilities for neighbourhood parameters attribution. Arrows show attribution of parameters of the measured plot to similar neighbors.

3.3.2 Phytoecological unit derivation by GIS

In view of later upscaling processing, GIS techniques were used to derive first step phytoecological units by overlaying four layers of information such as layers of geology, pedology, landform and savanna physiognomy. Details on the different steps are given in the next chapters. Representative grids were chosen in each phytoecological unit for field surveys.

3.3.3 Field-based surveys

Measurement technique

The field survey was based on dendrometry and dendrology measurement techniques. To increase the accuracy of measurements, state-of-the-art measurement tools and devices such as long and short-distance laser meters, clinometer (Suunto), and GPS were used to collect individual tree physical parameters on the ground (Figure 3.10).

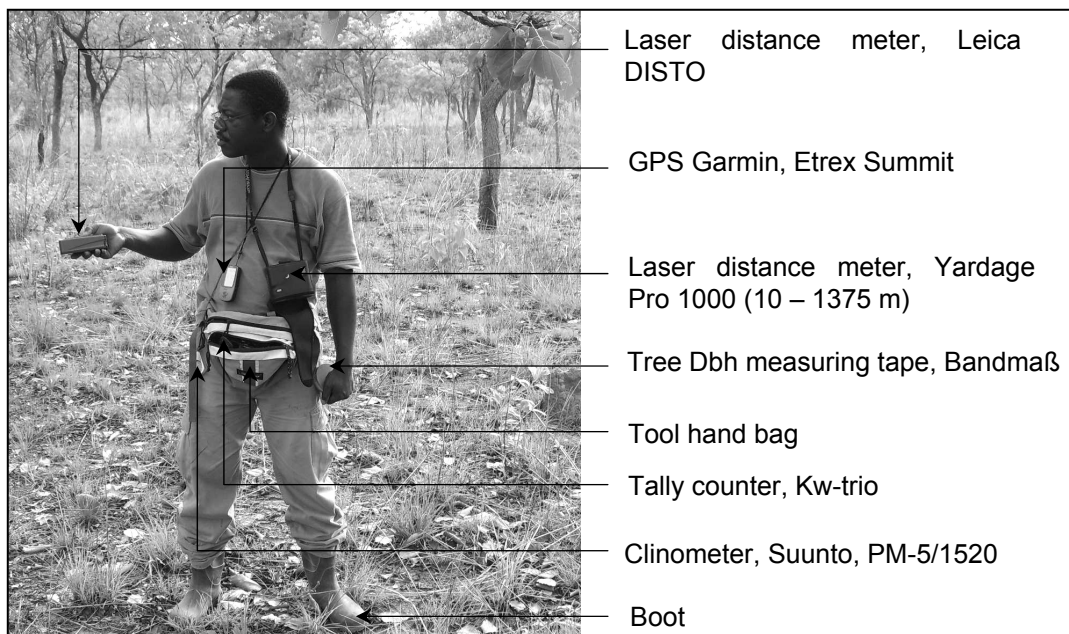


Figure 3.10: Tree biometric measurement. Use of state-of-the-art high accuracy tools

Field measurement devices such clinometer (Suunto, PM-5/1520), tree diameter at breast-height (DBH) measuring tape and the short distance meter (Leica DISTO) were always used by the same technician to avoid or reduce bias in final data. The plots were delimited by representative vegetation units in the surroundings of GPS indication.

Variables of analysis

The variables of analysis were: tree species (scientific name), geographical position of tree, DBH, tree height, crown radius, crown height (Appendix 2), savanna physiognomy, soil type and land unit.

Tree species scientific name

The scientific names of the tree species were abbreviated to facilitate use in the field and enable easy GIS processings. The abbreviation was done by choosing the first letter of the first part of the name and the first letter of the second part of the name; the second or third letter of the second name was chosen in case the abbreviation looked similar to another one.

Eg: *Combretum fragrans* = Cf

Crossopteryx febrifuga = Ce

Diameter at breast-height (DBH)

The diameter is the distance between two opposite tangents, parallel to the trunk of the tree (Rondeux 1999). By convention, the DBH is measured at breast-height, i.e., at 1.3 m above the ground surface. Several devices such as Electronic Compass, POLLANSCHÜTZ Compass, Dendrometer BARR and STROUD can be used. In this research, the DBH was measured using measuring tape, and trees with DBH smaller than 5 cm were not taken into account, as they were considered part of the regeneration stand.

Tree height

In dendrometry, several definitions exist for tree height. In the field, tree height was measured with a clinometer (Suunto) considering the distance between the ground surface and the top of the tree. Only trees with minimum height of 1.30 m were taken into account in tree census; individuals under that threshold were considered to be part of the regeneration stand (saplings and seedlings).

Crown radius, crown cover

The crown cover or crown surface is the part of the tree seen on aerial photographs.

Hence, crown covers are variables useful for tree density calculation and mapping. As horizontal projections of crown cover are rarely a circle, four crown radius were diametrically measured with the distance meter (Leica DISTO) considering the longest and shortest sizes of the crown.

Given the varying geometry of crown covers in nature, the calculation of crown surface area was done according to formulas of circle (radius = r_1, r_2, r_3, r_4) and ellipsoid (minor radius = a_1, a_2 and major radius = b_1, b_2) surface areas. Since mean circle surface area (S_c) overestimates the crown cover surface area and mean ellipse surface area (S_e) underestimates it, the final crown cover surface was calculated as follows:

$$S = \frac{\text{Mean Circle Surface Area} + \text{Mean Ellipse Surface Area}}{2} = \frac{S_c + S_e}{2} \quad (3.4)$$

$$\text{with } S_c = \left(\pi \sum_{i=1}^n r_i^2 \right) / n \quad (3.5)$$

$$\text{and } S_e = \left(\pi \sum_{i=1}^n ab \right) / n \quad (3.6)$$

$$\text{Combining equations (3.4) and (3.5), } S = \frac{\left(\pi \sum_{i=1}^n r_i^2 \right) + \left(\pi \sum_{i=1}^n ab \right)}{2n} \quad (3.7)$$

$$\text{In detail, } S = \frac{(\pi r_1^2 + \pi r_2^2 + \pi r_3^2 + \pi r_4^2) + (\pi a_1 b_1 + \pi a_1 b_2 + \pi a_2 b_1 + \pi a_2 b_2)}{8} \quad (3.8)$$

where n = Number of radius
 r = Crown radius (circle)
 a = Crown major radius (ellipse)
 b = Crown minor radius (ellipse)

Crown height

From existing conventions, the crown height is defined as the distance between the lowest level of foliage and the top of the tree. This was measured with a clinometer (Suunto).

Savanna physiognomy

In the field, two important criteria were chosen to define the type of savanna: tree height and soil type. A third criterion was mentioned in case of difficulties in differentiating the savanna type, i.e., the species composition (phytosociology). Some tree species such as *Terminalia macroptera*, *Pseudoceudrela kotschii*, *Combretum fragrans* grow on wet phytocological units, whereas *Terminalia laxiflora*, *Combretum glutinosum*, *Pterocarpus erinaceus* prefer dry lands. Thus, two savanna types were defined: (1) tree savanna, and (2) shrub savanna woodlands.

- (1) Tree savanna woodland: soil type = clay, sandy clay and sub-classes; tree height > 6 m
- (2) Shrub savanna woodland: soil type = cuirass and sub-classes; tree height = 1.30-6 m.

The characterization of high, medium and low tree densities, and the correlation of tree species with the types of savanna were processed according to existing ecological methods and models.

Soil types, landforms

Field surveys were conducted according to the oriented plot survey method on each landform (mainly glacia and alluvial plain) and each soil type (mainly clay, sandy clay and indurated soil) (Refer to figures 2.4 and 2.5). Oriented grids were chosen by GIS techniques. Information on pedology and geomorphology are based on existing maps and shapefiles.

3.4 Photogrammetry, remote sensing and GIS

Several data sets were combined and processed to capture the spatial dynamics of tree species and estimate whole-tree water use rates (Figure 3.11).

3.4.1 Data acquisition

Two data sets covering the dry and rainy seasons were used: aerial photographs (IGB/JICA – 1/20,000 scale) and satellite images (Landsat and Aster). The first data set was used to assess spatial distribution, and the second was used for classification purpose and for change detection. Additional data, such as maps of geology, pedology and vegetation, were acquired and transformed into shapefiles. (Data source: see section 3.5.3)

3.4.2 Land Use Land Cover Change (LULCC)

LULCC outputs were useful for the description of the dynamics of the study area and its components. In a first step, a LULCC classification map was processed in order to help chose site selection for measurements. The map was validated during field surveys.

3.5 Conceptual framework

The first step in the research was the general data acquisition during the first field campaign, the second step dealt with the second fieldwork and first data processing, and the last step the final processing and scientific results (Figure 3.11)

3.5.1 Data description

The three categories of data (remotely sensed imagery, land/landform and ecosystem/water) were transformed into statistics and vector files. Satellite image and DEM georeferenced data remained in raster format for further analysis (Figure 3.12). The shapefiles were georeferenced according to the projection system WGS 84/UTM 30N. The vector file of the NRB boundary derived from the topographical map Diébougou 1/50,000 (Gaoua 4d NC-30-XV) was adjusted to the satellite image Landsat 7 ETM+, slightly modifying the original boundary.

3.5.2 Data integration and analysis

The base map of the nature reserve was the same for all spatial processing of the NRB so that all information layers overlaid perfectly in the GIS. Data were stored in a global database with interconnection links. The database was computed according to geostatistical and geospatial approaches for the modeling of tree density, tree species

richness and spatial patterns, and contribution of tree stands to the surface water balance.

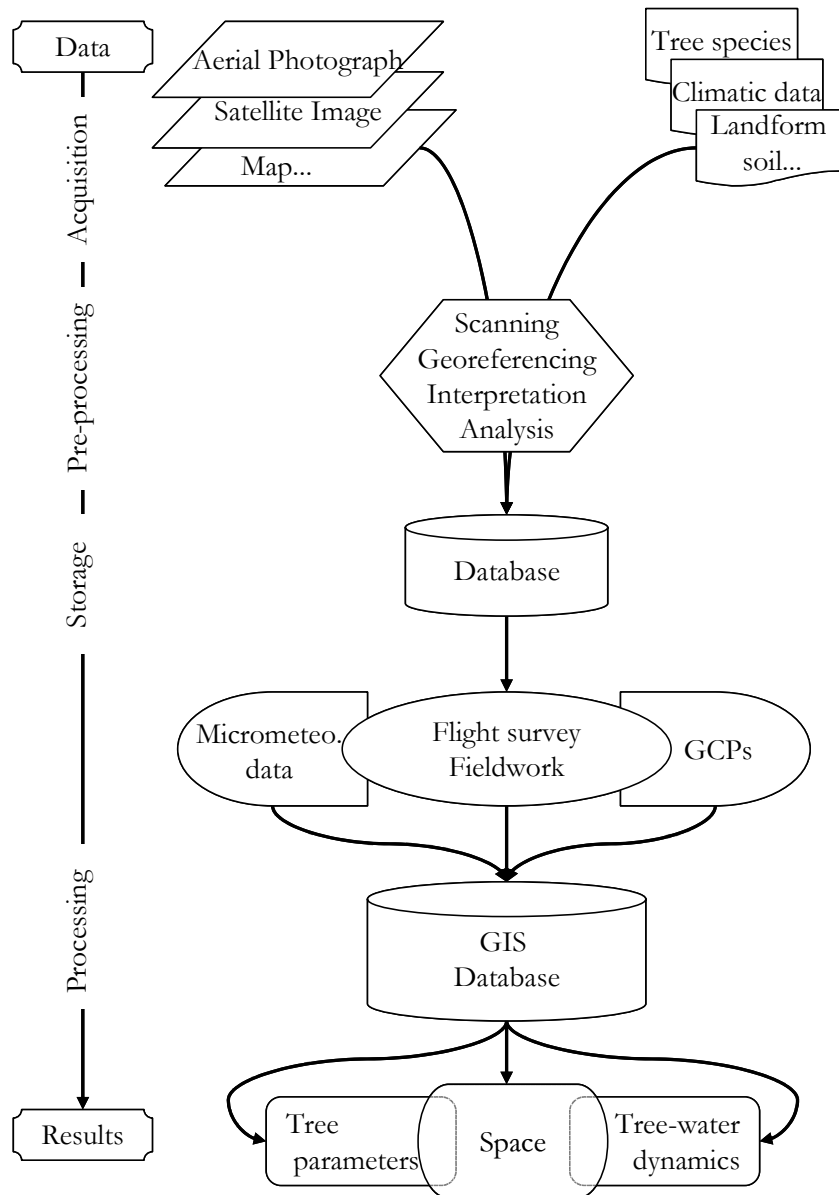


Figure 3.11: Combining remote sensing, GIS techniques and field data for multivariate analysis

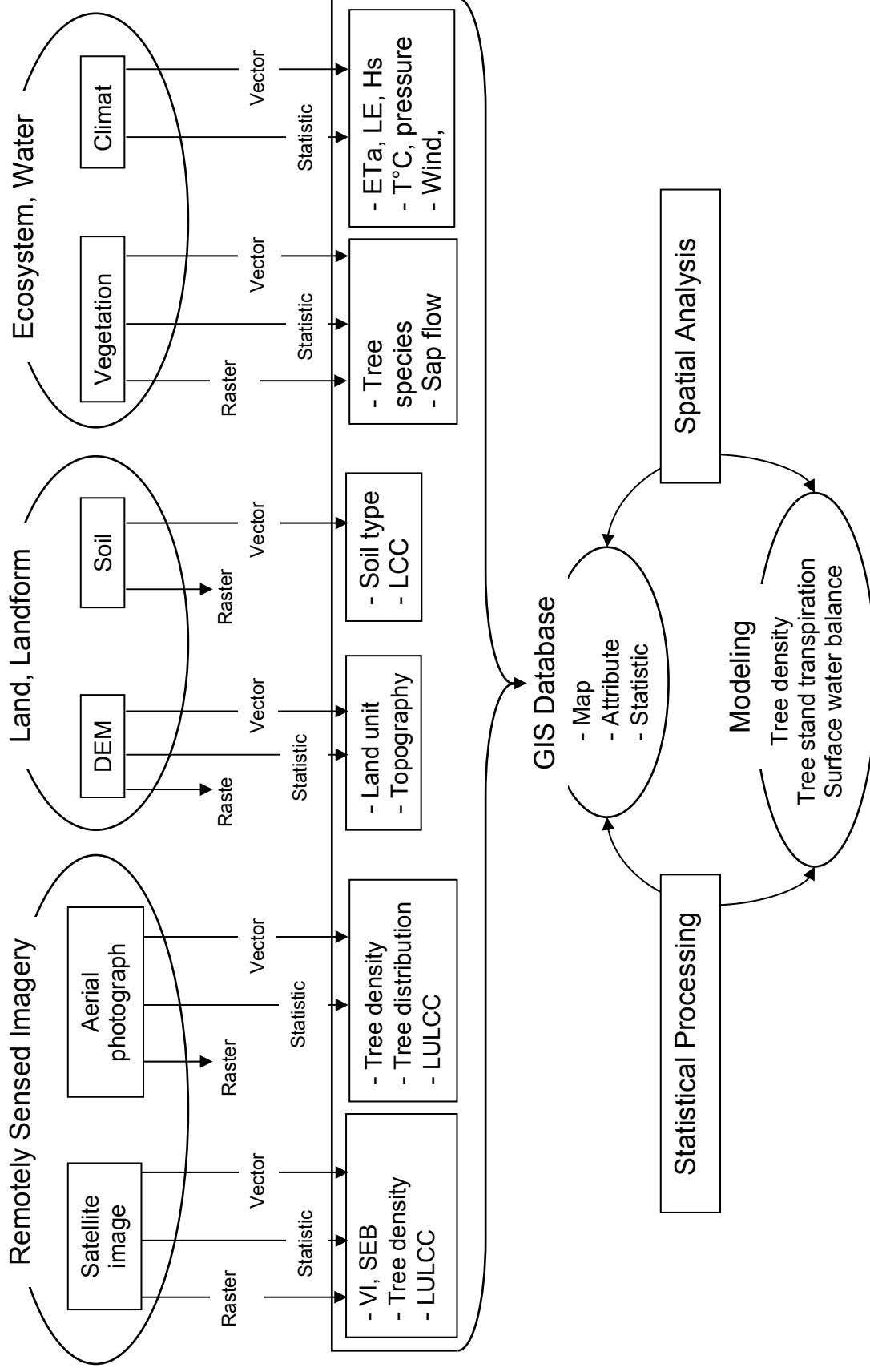


Figure 3.12: Conceptual framework of the modelling of tree stand transpiration

3.5.3 General data source

In addition to the field measurement data, data from other sources were used. These comprise satellite images, sap flux and meteorological data (Table 1).

Table 3.1: Additional data used in the study

Data source	Parameter	Provided by
Global Land Cover Facility (GLCF) –	Landsat-5 TM scene 196/52, Oct. 1986, L1G, USGS	University of Maryland
NASA Landsat Program	Landsat-7 ETM+ scene 196/52, Oct. 1999 and 2002, Nov. 2000, L1G, USGS	
USGS - EROS	Aster_L1B_00311242006104945_20061221134014_14047, Nov. 2006, L1B, USGS	Mr M. Schramm from the University of Wuerzburg/DLR/Biota West Africa Project
Bontoli Eddy Covariance station	Latent heat flux (LE), sensible heat flux (Hs)	Mr C. Brümmer from IMK-IFU, Virtual Institute
Bontoli microclimate station	Air pressure, air temperature, net radiation, rainfall, relative humidity, soil heat flux, soil temperature, wind speed/direction	Dr. J. Szarsynski from the Glowa Volta and Biota West projects

3.6 Summary

The general research method encompasses two components: on the one hand climate, tree species and water-related variables, on the other the geomatic approach (remote sensing, GIS, photogrammetry). With the first component, the contribution of tree species to the surface water balance at site-scale are estimated, with the second component the results of the first component are upscaled.

4 TREE SPECIES DIVERSITY AND SPATIAL PATTERNS

4.1 Introduction

Through its control of energy fluxes over substantial portions of the land surface, vegetation is an important component of the global climate system (Bounoua et al. 2002). In semi-arid regions, issues of rainfall reduction and variability, climate change, and water scarcity are aggravated by the increasing disturbance of the natural relationship between vegetation and climate. Even the role of disturbing dominant vegetation types has not yet been sufficiently studied (Walter and Steffen 1996). The current chapter focuses on the spatial distribution of the savanna physiognomy and phytosociology in relation to environmental factors such as soil types and land units, in order to establish an accurate classification map with phytoecological zones of the vegetation landscapes.

4.2 Materials and methods

4.2.1 Tree species diversity estimates

Species richness and evenness were used to measure tree species diversity by means of the Shannon (1948) and Simpson (1949) functions. The Shannon-index, H' , also called the Shannon-Wiener index or the Shannon-Weaver-index, is a widely used measure of biological diversity (Chao and Shen 2003), because it has the advantage of taking into account species richness and the evenness. The Shannon-index of diversity is defined by:

$$H' = - \sum_{i=1}^s p_i \log p_i \quad (4.1)$$

where $p_i = \frac{n_i}{N}$ = Relative abundance of each species

n_i = Number of individuals in each species

N = Total number of all individuals

S = Number of species (i.e., species richness)

Simpson (1949) showed that for the probability that two individuals chosen at random and independently from the population will be found to belong to the same group, the unbiased estimator is defined by his index (D) as follows:

$$D = \frac{\sum n_i(n_i - 1)}{N(N - 1)} \quad (4.2)$$

where N and n_i = as defined above

Species richness

With a total area of 13,714 ha savanna vegetation, it was impossible to enumerate all tree species of the research site. Species richness was estimated using the Jackknife and Rarefaction estimates for 54 plot samples of 30 m x 30 m.

Jackknife model

The Jackknife estimate method (Quenouille 1949; Tukey 1958) is based on a presence-absence table of unique species. As defined by Krebs (1989), a unique species is a species that occurs in one and only one plot. Unique species are spatially rare species and are not necessarily numerically rare, since they could be highly clumped. The Jackknife estimate function (\hat{S}) is:

$$\hat{S} = s + \left(\frac{r-1}{r} \right)^k \quad (4.3)$$

where s = Observed total number of species present in r plots

r = Total number of plots sampled

k = Number of unique species

For more information about the variance and the confidence limit of equation 4.3, refer to Appendix 1.

Rarefaction model

The rarefaction method (Sanders 1968) is a statistical estimate of the number of species expected in a random sample of individuals taken from a collection (Krebs 1989). This method was proposed by Sanders (1968) for standardizing all samples to a common size. Several years later, Hulbert (1971) and Simberloff (1972) proposed a corrected algorithm derived from the model of Sanders (1968) to estimate species richness.

The Analytic Rarefaction 1.3 software design by Holland (2003) and based on these models are used to compute the expected number of species. The software is available at <http://www.uga.edu/~strata/software/Software.html> and was applied to the datasets obtained from the 54 subplots.

Evenness

According to Krebs (1989), evenness measures attempt to quantify the unequal representation of species against a hypothetical community in which all species are equally common. Hence, evenness refers to how the species abundance is distributed among species (Ludwig and Reynolds 1988). The most commonly used index of evenness is based on the Shannon-Wiener index:

$$J = \frac{H'}{H_{\max}} \quad (4.4)$$

where J' = Evenness measure (range 0 - 1)

H' = Shannon-index of diversity (Equation 4.1)

H_{\max} = Maximum possible value of Shannon-index; $H_{\max} = \log S$

Combining equations (4.1) and (4.4), the evenness index is finally defined by:

$$J = \frac{-\sum_{i=1}^s p_i \log p_i}{\log S} \quad (4.5)$$

Analyzing the evenness index, Ludwig and Reynolds (1988) concluded that when all species in a sample are equally abundant, the evenness index should be

maximum and decrease toward zero, as the relative abundance of the species diverges away from evenness. This was also calculated for the 54 datasets.

4.2.2 Ecological modeling of tree spatial patterns

The spatial pattern of plant distribution is an important characteristic of ecological communities (Ludwig and Reynolds 1988). Though it is still quite impossible to classify degrees of spatial distribution of tree species (Krebs 1989), it is easy to statistically determine their spatial patterns (i.e., aggregated or clumped, uniform and random). Krebs (1989) proposed two main statistical distribution methods for this purpose: the Poisson distribution and the negative binomial distribution.

At first, the Poisson distribution was used to estimate tree spatial patterns. When the Poisson model did not fit to the representation of the tree species distribution i.e., when the species were not randomly distributed, the negative binomial model was considered for estimation of spatial patterns (i.e., aggregated). In sum, the Poisson distribution is the appropriate model for describing data when randomness prevails, whereas the negative binomial model works with aggregated patterns.

Given the three spatial patterns, Ludwig and Reynolds (1988) define the relevant variance-to-mean relationships and the statistical related-models as follows:

- Random pattern: $\sigma^2 = \mu$ (Poisson distribution)
- Clumped pattern: $\sigma^2 > \mu$ (Negative binomial distribution)
- Uniform pattern: $\sigma^2 < \mu$ (Positive binomial distribution)

where σ^2 is the variance and μ is the mean.

The parameters used for these methods were proportion of individuals in a plot, total number of plots, number of plots containing zero individual

4.2.3 Tree community ordination

The term ordination derives from early attempts to order a group of objects. It is a term used to describe a set of techniques (Ludwig and Reynolds 1988) with the usual objective of helping to generate hypotheses about the relationship between the species

composition at a site and the underlying environmental gradients (Digby and Kempton 1987). According to Orloci (1978), and Ludwig and Reynolds (1988), one of the major goals of ordination is to simplify and condense massive data sets in the hope that ecological relationships will emerge. The ordination method is used to summarize the variation in a biotic community, particularly stressing the continuity of change in community composition (Lepš and Šmilauer 2003).

The software CANOCO (Microcomputer Power, NY) was used to achieve the analysis of tree community ecology, as it is the most popular tool for constrained and unconstrained ordination in ecological applications (ter Braak and Šmilauer 2002). The theoretical methods are developed in its reference manual. The software contains both linear and unimodal methods of ordination: the linear method is Principal Component Analysis (PCA), the unimodal methods are Correspondence Analysis (CA) or Reciprocal Averaging (RA) and Detrended Correspondence Analysis (DCA).

Clarifying the difference between the two methods, Dolédec and Chessel (1991) point out that PCA makes the abundant species become more important, whereas CA does the same with rare species. Hence, they conclude that the use of PCA or CA is a scientific choice based on the ecological objectives. For example, for the same sampling units, if the species abundance changes are of interest, then PCA must be used, otherwise CA is preferable. In case there are different sampling methods to collect data, CA is the only way to make an ordination of data.

The software CAP (PISCES, UK) was used for the analysis of the relationships between tree community and the environmental factors (i.e., soil and vegetation types). Similarity and association analysis were achieved using respectively the methods of Kukzynski and Chi-Square. Both methods are explained in the instruction manual of CAP (PISCES 2001). In sum, each of the method remains valuable when used within the range of its intended limits. For details, refer to PISCES (2001) and ter Braak and Šmilauer (2002). Ordination was performed on three parameters of the sample plot dataset: tree species, soil and vegetation types.

4.2.4 Mapping savanna vegetation

Remote sensing (RS) and GIS are complementary techniques used to address the classification and the mapping of the vegetation covers of the NRB. The task of RS

consisted of transforming and converting the satellite images into shapefiles with related attribute tables that were overlaid and processed in a GIS to obtain the final vegetation map (Figure 4.1).

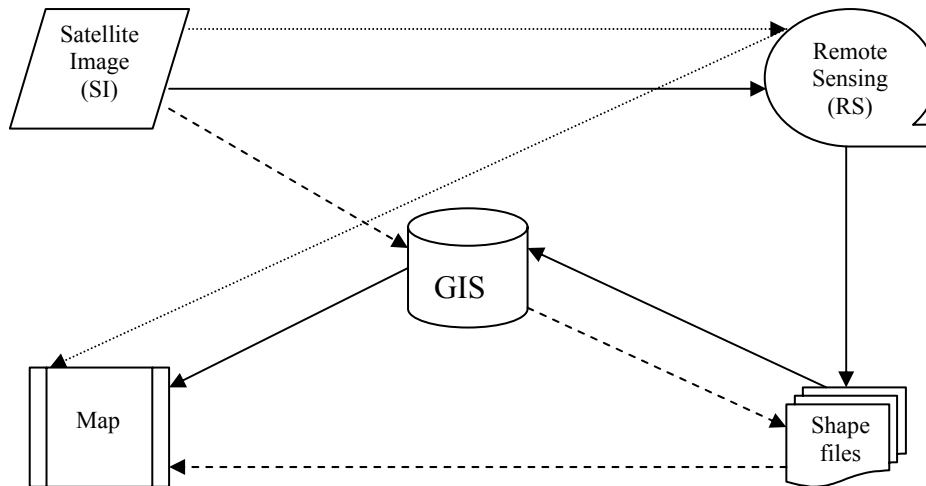


Figure 4.1: Possibilities of vegetation cover mapping. With the development of integrative softwares, the classical scheme SI-RS-GIS-Shapefiles-Map is no longer unique. Other possibilities exist: SI-RS-Map and SI-GIS-Shapefiles-Map. The arrows indicate the mapping possibilities.

Satellite images processing

The orthorectified Aster and Landsat images (coverage: path 196 - row 52) were used to derive information on the vegetation coverage of the study area. The image processing steps were summed up to geometric corrections, enhancement, transformation, classification, and interpretation.

Geometric correction

The methods of image-to-image and image-to-map geo-correction were used to process the digital imagery before the fieldwork. This first step was helpful to determine broadly the main classes of vegetation coverage. After the first fieldwork, the image to ground geo-correction method was used to provide higher precision to the geo-corrected digital image.

Transformation

As the raw image is not enhanced, enhancement is used to improve the spatial and

spectral quality of the satellite image. Two channels (Infrared 3 and Near infrared 4) were used for image transformation to compute and enhance information layers on land cover. From these channels, NDVI (Rouse et al. 1974; Tucker 1979) was computed as follows:

$$NDVI = \frac{NIR - IR}{NIR + IR} \quad (4.6)$$

where $NDVI$ = Normalized Difference Vegetation Index

NIR = Near Infrared, and IR = Infrared

Supervised classification

In remote sensing, classification is the process of sorting pixels into a finite number of individual classes, or categories, of data based on the data file values. If a pixel satisfies a certain set of criteria, then the pixel is assigned to the class that corresponds to those criteria (Erdas 1999). The process of classification was done in two steps: (1) recognition of categories of real-world objects, and (2) labeling of the pixels (Mather 1999). The supervised classification required field-based knowledge. It was processed using the software Erdas Imagine as follows:

- (1) *Training samples*: They were located by visual recognition of land units and vegetation patterns. Samples were digitized according to the methods of polygon and seed tool as detailed in the software Erdas Imagine.
- (2) *Signature evaluation*: Each training sample was scrutinized in a signature editor; the histogram of each band should have a unimodal distribution, which was sign of a good classification.
- (3) *Image classification*: The parametric method was used, precisely the Maximum Likelihood method, which uses the training data sets to estimate the means and the variances of the classes used to estimate probabilities. As such, this method was effective in image classification.
- (4) *Accuracy assessment*: Accuracy assessment determines the quality of the information derived from remotely sensed data. Therefore, the purpose of

quantitative accuracy assessment is to identify and measure the degree of error in the final thematic maps (Congalton and Green 1999). In addition to computing an error matrix to represent effectively the map accuracy, Conditional Kappa was computed to analyze the agreement for individual classes within the matrix.

Mapping spatial distribution of trees

Once the difference classes of vegetation cover were obtained, the outputs were compiled in a GIS database and linked to attribute tables. The software ArcGIS (ESRI, NY) was used to design the final maps according to spatial and statistical requests. Five shapefile layers were taken into account to map phytoecological zones of the protected area. They are:

- Pedological map shapefile (Figure 2.4, Chapter 2, section 2.2.3)
- Geographical coordinates of individual tree relevant to each phytoecological zone
- Buffer zone (25 m) around the Bougouriba river, from north to south to determine the gallery forest class
- Boundary layer of the protected area of Bontioli
- Savanna vegetation classification map shapefile

4.3 Results and discussion

4.3.1 Dominant tree species and biodiversity

Major tree species and families

Considering a 95 % confidence interval, the NRB has approximately 71 ± 2 tree species (i.e., the range between 69 and 73 species) listed in the Table 4.1 according to the degree of abundance.

The tree community is spatially organized according to three main vegetation types, namely tree savanna, shrub savanna and gallery forest. That result confirms the physiognomic classification of Pigeonnière (2001). But the phytosociological classification of the reserve should retain as major tree species *Terminalia macroptera* (11.7 %), *Detarium microcarpum* (9 %), *Vitellaria paradoxa* (8.9 %), *Entada africana* (6.7 %) instead of *Burkea africana*, *Pterocarpus erinaceus*, *crossopteryx febrifuga*, *Combretum spp*, as the author mentions.

However a good classification of the major tree species was obtained by considering the physiognomy of the savanna vegetation. In this analysis, tree species considered minor for the whole nature reserve are seen to be major species in their appropriate environmental conditions. This is the case for *Isoberlinea doka* in wood savanna. For details, refer to Table 4.2 and Appendix 3.

The tree species belong to 19 families; the 10 major families are Combretaceae (35 %), Cesalpiniaceae (17 %), Mimosaceae (12 %), Sapotaceae (9 %), Fabaceae or Papilionaceae (7 %), Rubiaceae (6 %), Anacardiaceae (5 %), Meliaceae (4 %), Bombacaceae (1 %) and Ebenaceae (1 %) (Refer to Appendix 4 for details). The NRB is dominated by Combretaceae, which are present in all vegetation types.

Table 4.1: Classification of tree species according to abundance. On average, $6 (\pm 2)$ species per 900 m²; variance, $s^2 = 46.17$. Sap flow measurement species are marked with an asterisk. Count = number of individuals, (%) = percentage of tree species

Species name	Count	%	Species name	Count	%
<i>Terminalia macroptera</i> *	184	11.7	<i>Burkea africana</i> *	10	0.6
<i>Detarium microcarpum</i> *	141	9.0	<i>Terminalia avicennioides</i>	10	0.6
<i>Vitellaria paradoxa</i> *	140	8.9	<i>Vitex doniana</i>	10	0.6
<i>Entada africana</i> *	106	6.7	<i>Hexalobus monopetalus</i>	9	0.6
<i>Crossopteryx febrifuga</i> *	84	5.3	<i>Khaya senegalensis</i>	8	0.5
<i>Terminalia laxiflora</i> *	79	5.0	<i>Combretum nigricans</i>	7	0.4
<i>Combretum glutinosum</i> *	68	4.3	<i>Gardenia erubescens</i>	4	0.3
<i>Daniellia oliveri</i> *	55	3.5	<i>Syzygium guineense</i>	4	0.3
<i>Pseudocedrela kotschyi</i> *	54	3.4	<i>Xeroderris stuhlmannii</i>	4	0.3
<i>Pterocarpus santalinoides</i>	54	3.4	<i>Bridelia scleroneura</i>	3	0.2
<i>Combretum fragrans</i> *	50	3.2	<i>Gardenia ternifolia</i>	3	0.2
<i>Piliostigma thonningii</i>	46	2.9	<i>Lannea velutina</i>	3	0.2
<i>Pericopsis laxiflora</i>	41	2.6	<i>Acacia macrostachya</i>	2	0.1
<i>Acacia dudgeoni</i> *	40	2.5	<i>Garcinia livingstonei</i>	2	0.1
<i>Combretum collinum</i> *	40	2.5	<i>Maytenus senegalensis</i>	2	0.1
<i>Pterocarpus erinaceus</i> *	39	2.5	<i>Strychnos innocua</i>	2	0.1
<i>Lannea acida</i>	35	2.2	<i>Ximenia americana</i>	2	0.1
<i>Lannea microcarpa</i> *	35	2.2	<i>Cola laurifolia</i>	1	0.1

Tree species diversity and spatial patterns

Table 4.1 (Continued)

Species name	Count	%	Species name	Count	%
<i>Combretum molle</i>	31	2.0	<i>Cassia sieberiana</i>	1	0.1
<i>Bombax costatum</i>	23	1.5	<i>Feretia apodanthera</i>	1	0.1
<i>Diospyros mespiliformis</i>	22	1.4	<i>Grewia bicolor</i>	1	0.1
<i>Anogeissus leiocarpus*</i>	20	1.3	<i>Hymenocardia acida</i>	1	0.1
<i>Acacia sieberiana</i>	19	1.2	<i>Keetia cornelia</i>	1	0.1
<i>Lonchocarpus laxiflorus</i>	18	1.2	<i>Paullinia pinnata</i>	1	0.1
<i>Isoberlinea doka</i>	16	1.0	<i>Sarcocephalus latifolius</i>	1	0.1
<i>Terminalia Glaucescens</i>	14	0.9	<i>Saba senegalensis</i>	1	0.1
<i>Parkia biglobosa*</i>	11	0.7	<i>Tamarindus indica</i>	1	0.1
<i>Stereospermum kunthianum</i>	11	0.7	<i>Vitex chrysocarpa</i>	1	0.1

Table 4.2: Major tree species distribution as a function of vegetation type in the NRB.
Count = number of individual, (%) = percentage of tree species

Shrub savanna		Wood savanna		Tree savanna	
Species = 39	%	Species = 28	%	Species = 33	%
Count = 774		Count = 187		Count = 583	
<i>D. microcarpum</i>	11.5	<i>P. santalinoides</i>	18.5	<i>T. macroptera</i>	30.4
<i>Vitellaria paradoxa</i>	9.9	<i>Pericopsis laxiflora</i>	10.9	<i>Vitellaria paradoxa</i>	10.1
<i>Entada africana</i>	8.9	<i>Combretum glutinosum</i>	8.7	<i>P. kotschyi</i>	9.0
<i>C. glutinosum</i>	6.7	<i>Piliostigma thonningii</i>	7.1	<i>Combretum fragrans</i>	6.0
<i>T. laxiflora</i>	6.0	<i>Isoberlinea doka</i>	4.4	<i>C. febrifuga</i>	4.7
Sparse forest		Gallery forest			
Species = 13	%	Species = 10	%		
Count = 46		Count = 19			
<i>Daniellia oliveri</i>	34.8	<i>Syzygium guineense</i>	36.4		
<i>Terminalia laxiflora</i>	21.7	<i>Cola laurifolia</i>	9.1		
<i>Isoberlinea doka</i>	8.7	<i>Garcinia livingstonei</i>	9.1		
<i>Bridelia scleroneura</i>	6.5	<i>Keetia cornelia</i>	9.1		
<i>P.erinaceus</i>	6.5	<i>Lannea acida</i>	9.1		

Species richness and biodiversity

The index of diversity (e.g., $H' = 1.5$) and the Shannon-Wiener index of evenness ($J = 0.8$) indicate an overall acceptable level of species diversity in the NRB. This is despite the geographical location of the reserve in a semi-arid area, under harsh environmental conditions, constant anthropogenic disturbances and frequent bushfires. In the NRB, the

main tree species of the primary vegetation of the phytogeographical zone are still to be found.

The species diversity varies spatially according to the vegetation type, the land unit and the soil type. Highest number of tree species are found in shrub savanna, on cuirass soils, on the alluvial plain and low glacis, whereas few tree species grow in gallery forests along the Bougouriba river, on litter soil and on medium glacis (Tables 4.3 and 4.4)

Table 4.3: Distribution of Shannon-Wiener index of evenness (J) as a function of environmental factors in the NRB.

Vegetation type	J	Land unit	J	Soil type	J
Shrub savanna	0.9	Alluvial plain	0.7	Cuirass soil group	0.9
Tree savanna	0.7	Low glacis	0.9	Clay soil group	0.7
Wood savanna	0.9	Medium glacis	1.0	Reworked soil group	0.8
Sparse forest	0.8	Tabulary mound	0.8	Litter	0.9
Galery forest	0.9				

Table 4.4: Distribution of tree species richness in the NRB as a function of environmental factors. Use of three estimates models: Rarefaction, Jackknife and modified Jackknife. 95 % confidence interval margin errors are in brackets.

Vegetation type	Number of tree	Number of Tree species	Expected number of tree species		
			Rarefaction model	Jackknife model	Modified Jackknife
Shrub savanna	774	39	53 (± 4)	43 (± 10)	48 (± 5)
Tree savanna	583	33	50 (± 5)	32 (± 13)	38 (± 7)
Wood savanna	187	28	38 (± 5)	26 (± 12)	32 (± 6)
Sparse forest	46	13	22 (± 5)	13 (± 13)	19 (± 6)
Galery forest	19	10	13 (± 3)	9 (± 12)	15 (± 6)
Soil Type					
Cuirass soil group	591	41	50 (± 5)	42 (± 11)	47 (± 5)
Clay soil group	678	36	52 (± 5)	37 (± 15)	44 (± 8)
Reworked soil group	301	30	43 (± 5)	30 (± 4)	32 (± 2)
Litter	39	13	20 (± 4)	13 (± 9)	18 (± 5)

Table 4.4 (Continued)

Vegetation type	Number of tree	Number of Tree species	Expected number of tree species		
			Rarefaction model	Jackknife model	Modified Jackknife
Land unit					
Alluvial plain	731	42	53 (\pm 4)	43 (\pm 15)	50 (\pm 7)
Low glacia	791	43	54 (\pm 4)	44 (\pm 13)	50 (\pm 5)
Medium glacia	20	7	14 (\pm 3)	7 (\pm 5)	10 (\pm 3)
Tabulary mound	67	12	26 (\pm 5)	12 (\pm 8)	16 (\pm 4)
Total number at reserve scale	1609	62	62 (\pm 1)	69 (\pm 4)	71 (\pm 2)

Dynamics of the vegetation phytosociology

The actual hierarchical classification of the NRB tree species (section 4.3.1) does not entirely reflect the composition of the initial primary vegetation of the area. The main tree species still exist but not always in the initial proportions. The anthropogenic disturbances seriously affect the phytosociology (i.e., the species composition) of the reserve. Thus, commercial and food tree species such as *Vitellaria paradoxa* (Karité, sheanut tree), *Parkia biglobosa* (Néré), *Lannea microcarpa* (Raisin, local grapes), *Lannea velutina*, and *Detarium microcarpum* are the favorites of the discriminative destruction of the vegetation cover by farmers. Other species such as *Terminalia laxiflora* and *Acacia dudgeoni* escape from clearance, respectively, because of their medicinal and soil-nutrients enrichment properties. Arbonnier (2002) argues that most of the *Terminalia spp* are used by local people to treat diseases such as haemorrhoids, dysentery, and gonorrhoea. Moreover, some of the trees such as *Crossopteryx febrifuga*, *Daniellia oliveri*, *Combretum fragrans*, *Parkia biglobosa*, *Terminalia spp* have developed a natural resistance to bushfires by developing thick and rugged trunks. It appears to be an ideal condition to survive in such disturbed and rough environmental conditions (Figure 4.2).

The hope of regeneration of the vegetation cover and biodiversity conservation in the NRB is based on the dynamics of the seedlings and the saplings. The surveys conducted through the nature reserve revealed that saplings and seedlings were abundantly present. These are, however, are vulnerable to bushfires and livestock farming. Notwithstanding its status as protected area and world heritage, the NRB still

suffers from human encroachment, and its landscapes are highly impacted despite official surveillance.

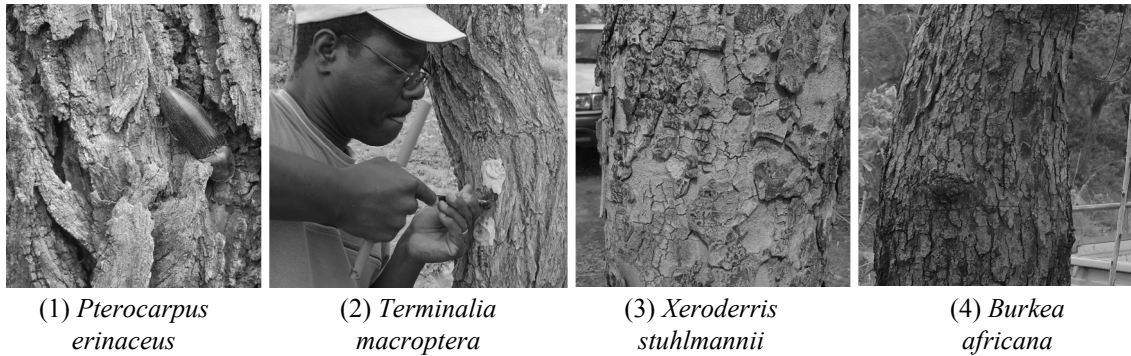


Figure 4.2: Resistant tree trunks. Thick barks show evidence of bushfire marks.

4.3.2 Spatial patterns of trees

Analysis of the probability distribution

Poisson distribution

The results of the different tests for goodness-of-fit converge to the same conclusion. The Poisson expected frequency distribution does not fit to the observed frequency distribution (Figure 4.3). Therefore, the null hypothesis that the spatial pattern of trees is a random one is rejected.

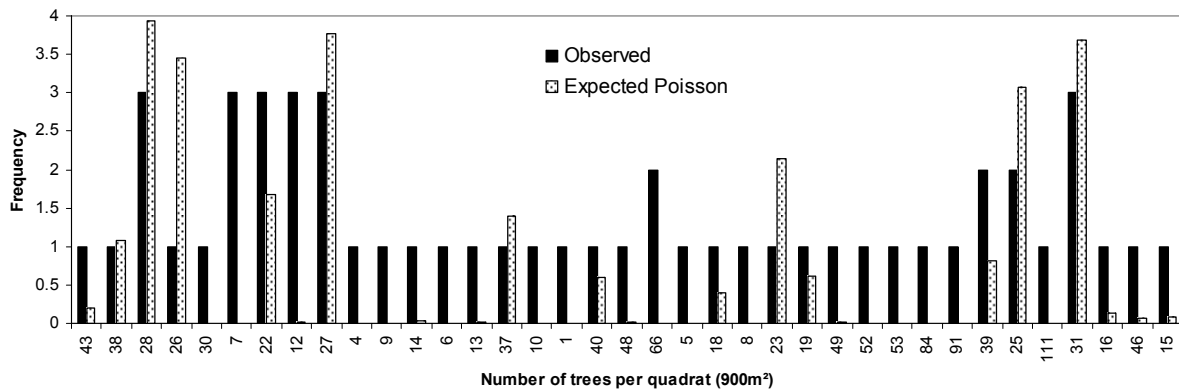


Figure 4.3: Tree species distribution per quadrat. Comparison between observed frequency and Poisson expected frequency distributions. Observed mean $\bar{x} = 29.3$ trees per 900 m²; observed variance $s^2 = 505.4$.

The results of the tests of dispersion and chi-square goodness-of-fit are as follows:

Index of dispersion test

- 1st case: Index of dispersion $I = 17.2$ (Equation a4, Appendix 1). $x^2 = 913.2$; $x_{0.975}^2 = 32.4$ and $x_{0.025}^2 = 71.4$. The null hypothesis is rejected because x^2 is superior to $x_{0.975}^2$ and $x_{0.025}^2$.

- 2nd case: Using the equation a6 (Appendix 1) of Wilson and Hilferty (1931)

$\left(\frac{x^2}{n}\right)^{1/3} - \left(1 - \frac{2}{9n}\right) = -0.15$ and $1.65\sqrt{\frac{2}{9n}} = 0.11$. The null hypothesis is rejected because

$\left(\frac{x^2}{n}\right)^{1/3} - \left(1 - \frac{2}{9n}\right)$ is inferior to $1.65\sqrt{\frac{2}{9n}}$.

Chi-square goodness-of-fit

Computed $X^2 = 2.4 * 10^{28}$ and Observed $X^2 = 32.4$

The null hypothesis is rejected because the observed chi-square is smaller than the computed one.

Negative binomial distribution

The negative binomial distribution is assumed because the Poisson expected frequency distribution does not fit to the observed frequency distribution as mentioned above.

- Initial estimate of \hat{k} , using equation a11 (Appendix 1) = 1.8

- Estimate of \hat{k} after iteration, using equation a10 (Appendix 1) = 1.3

The final value of \hat{k} (1.3) reveals that the savanna trees are spatially aggregated according to large clumps.

4.3.3 Definition of the potential phytocological zones

Tree species and environmental factors

A first-step analysis of the tables 4.1, 4.2, 4.4 and Appendix 3 shows correlations between tree species and environmental factors such as savanna physiognomy (i.e., vegetation types), land units, and soil types. Hence, some species such as *Terminalia macroptera*, *Pseudocedrela kotschyi*, *Combretum fragrans*, and *Crossopteryx febrifuga* grow in the tree savanna area, on clay soils and on alluvial plains, whereas tree species such as *Terminalia laxiflora*, *Combretum glutinosum*, and *Combretum collinum* grow exclusively in shrub savanna areas, on cuirass soils, and on medium and low glaxis. Other categories of tree species such as *Vitellaria paradoxa*, *Daniellia oliveri*, and *Entada africana* are mixed and can be found in several vegetation types.

The analysis (summarized in Table 4.5) confirms the final conclusion that there is a good correlation between the tree species and the appropriate savanna physiognomy ($r = 0.78$, $p < 0.01$). This is also the case between tree species and soil type ($r = 0.69$, $p < 0.01$), and between savanna physiognomy and soil types ($r = 0.78$, $p < 0.01$).

Table 4.5: Summary of correlations between savanna tree species and environmental factors. Total number of trees $N = 1609$, total number of tree species $n = 62$

Nominal by nominal - Association		Nominal by nominal - Contingency coefficient	
		Symmetric measures	
		Value	Approx. Sig.
Tree species	Vegetation type	0.78	0.00
	Soil type	0.69	0.00
	Land unit	0.64	0.00
Soil type	Vegetation type	0.78	0.00
	Land unit	0.61	0.00

Confirmation of the relationships tree species-environmental factors

The analysis of the relationships between tree species and the environmental factors by the ordination methods PCA and CA confirms the good relationships between tree community and environmental factors, i.e., soil and vegetation types (Table 4.5).

Most of the species vectors are tightly grouped in three parts of the plot corresponding to the soil types (Figure 4.5). Soil 1 is strongly correlated with *Terminalia laxiflora*, and *Pterocarpus erinaceus*, and Soil 2 with *Combretum fragrans*

and *Terminalia macroptera*. Soils 3 and 4 are very close, sharing common species such as *Lonchocarpus laxiflorus*, and *Bridelia scleroneura*, whereas soils 1 and 2 are very far from each other due to the significant differences in their species composition. Species such as *Entada africana*, *Vitelaria paradoxa*, and *Crossopteryx febrifuga* are associated with both soils 1 and 2.

The same observation can be made for the vegetation types. Most of the species vectors are tightly grouped in the center and the right of the ordination plot, whereas two sparse groups are observed in the top and the bottom of the plot. The center group represents species strongly associated with shrub savanna, and the right group stands for species strongly associated with tree savanna (Figure 4.6).

The longest gradient values for PCA are larger than 4 (Figure 4.5 and 4.6 (insert 1)), indicating that the linear method is not appropriate, i.e., the data are too heterogeneous and too many tree species deviate from the assumed model of linear response (Lepš and Šmilauer 2003).

This is why the unimodal method is used (Figures 4.5 and 4.6, inserts 2). “The most used method is CA. However, it is often used in the form of canonical correspondence analysis (CCA) where the axes of the ordination are constrained to maximize their relationship with a nominated set of environmental variables” (Austin 2005, p.74).

PCA Axis 2

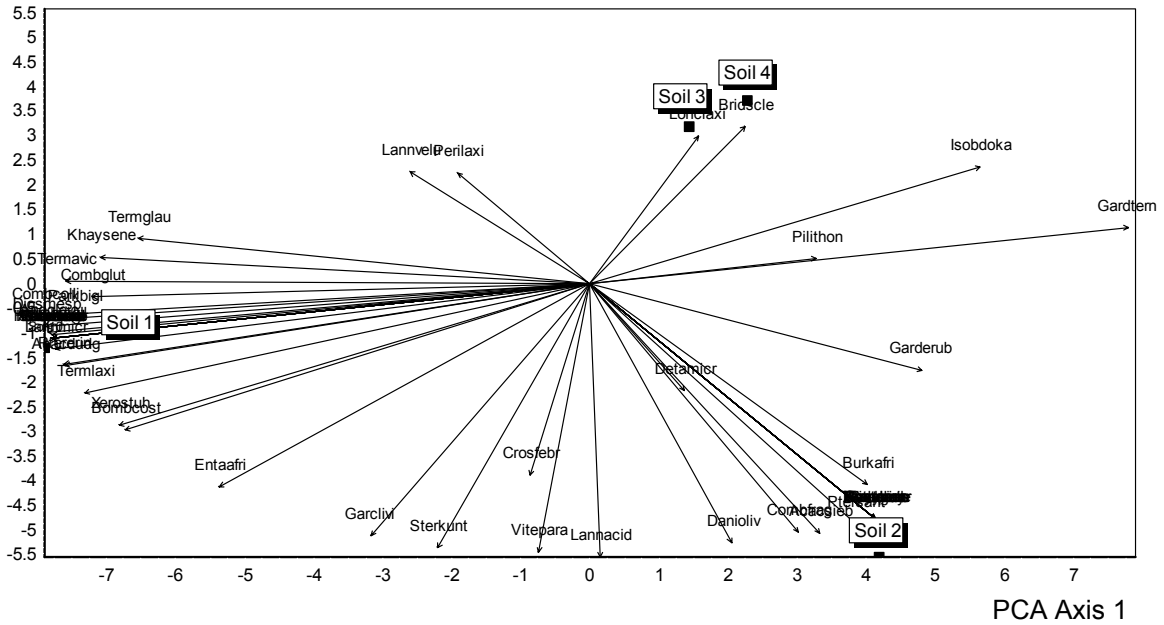


Figure 4.5: Principal Component Analysis (PCA) (insert 1) and Reciprocal Averaging (RA) or Correspondence Analysis (CA) (insert 2) of tree species as a function of soil types (boxes), illustrating the correlation between tree species and environmental factors (soil). The species are represented by the first four letters of the genus and species name.

RA Axis 2

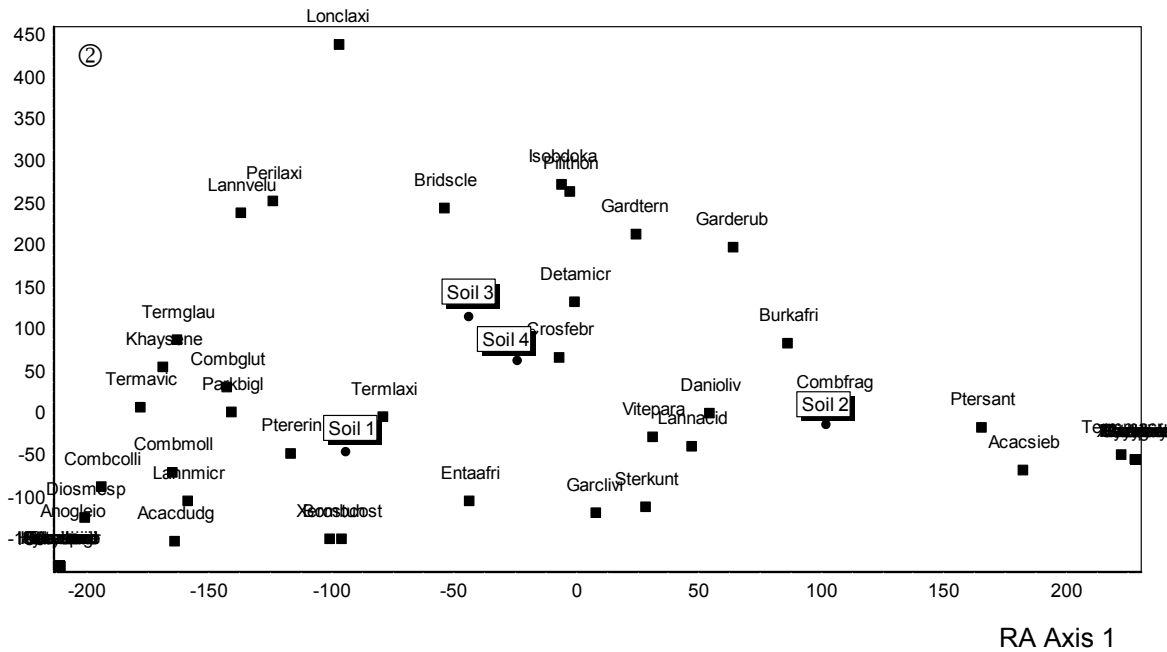


Figure 4.5: (Continued)

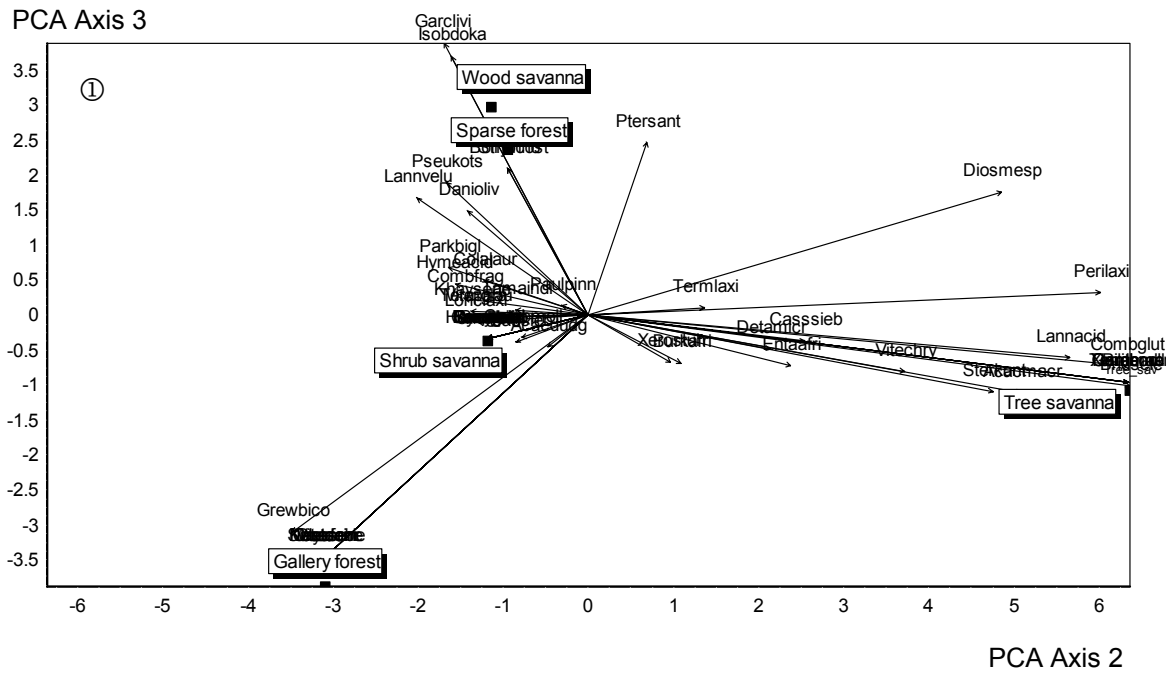


Figure 4.6: Principal Component Analysis (PCA) (insert 1) and Reciprocal Averaging (RA) or Correspondence Analysis (CA) (insert 2) of tree species as a function of vegetation types (boxes), illustrating the correlation between tree species and environmental factors (vegetation). The species are represented by the first four letters of the genus and species name. Refer to appendix 3 for details on tree species.

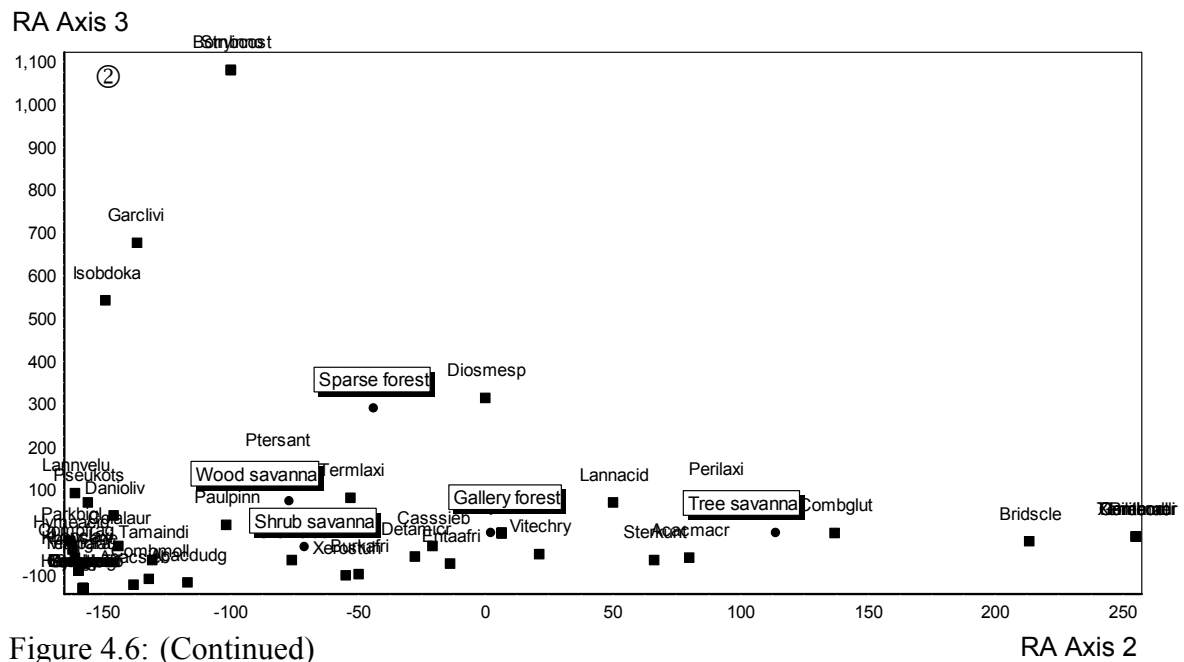


Figure 4.6: (Continued)

Delimitation of phytoecological zones

Based on the results mentioned above, five phytoecological zones can be delimited in the NRB (Table 4.6). Due to some classification and mapping constraints linked to the pixel size of the satellite images and the scale of the pedological base map (1/500,000), some of the phytoecological zones were combined with similar and dominant phytoecological zones for the final mapping.

Similarity and association analysis

The phytoecological zones are established to scaled up vegetation physiological and functional parameters in relation with tree water release estimates, from individual tree scale to province and river basin scales. Moreover, the Landsat 7 ETM+ scene P196/R052 of October 2002, used for the classification of the vegetation landscape, has a resolution of 28.5 m by 28.5 m, and the pedological map used as the underlying layer to perform the late upscaling has a scale of 1/500,000. Thus, the decision was taken to merge less representative phytoecological zones into major ones. This process of merging phytoecological clusters is done by means of association of similar clusters in relation with tree species composition. Hence, three final phytoecological zones were establish according to two main soil types (Tables 4.6 and 4.7) and three vegetation types (Tables 4.6 and 4.8) as follows:

Table 4.6: Description of the phytoecological zones. Cross tabulation of tree species name and environmental factors. Five major tree species as defined in table 4.2; land units defined by figure 2.3 (Chap. 2, sect. 2.2.2) and soil types defined by figure 2.4 (Chap. 2, sect. 2.2.3)

	Major tree species	Vegetation type	Soil type	Land unit
Phytoecological zones	1 <i>Detarium microcarpum</i> <i>Vitellaria paradoxa</i> <i>Entada Africana</i> <i>Combretum glutinosum</i> <i>Terminalia laxiflora</i>	Shrub savanna (veg 1)	① Reworked, cuirass, sand-clay-gravel soil ③ Soil formed by erosion	Low glacis Medium glacis
	2 <i>Pterocarpus santalinoides</i> <i>Pericopsis laxiflora</i> <i>Combretum glutinosum</i> <i>Piliostigma thonningii</i> <i>Isobertia doka</i>	Wood savanna (veg 3)	① Reworked, cuirass, sand-clay-gravel soil ② Pseudogley soil, silt-clay soil ③ Soil formed by erosion	Low glacis Alluvial plain

Table 4.6: (Continued)

	Major tree species	Vegetation type	Soil type	Land unit
Phytocological zones	3 <i>Terminalia macroptera</i> <i>Vitellaria paradoxa</i> <i>Pseudocedrela kotschyi</i> <i>Combretum fragrans</i> <i>Crossopteryx febrifuga</i>	Tree savanna (veg 2)	② Pseudogley soil, silt-clay soil	Alluvial plain
	4 <i>Daniellia oliveri</i> <i>Terminalia laxiflora</i> <i>Isobertia doka</i> <i>Bridelia scleroneura</i> <i>Pterocarpus erinaceus</i>	Sparse forest (veg 4)	① Reworked, cuirass, sand-clay-gravel soil ② Pseudogley soil, silt-clay soil	Alluvial plain Low glacia
	5 <i>Syzygium guineense</i> <i>Cola laurifolia</i> <i>Garcinia livingstonei</i> <i>Keetia cornelia</i> <i>Lannea acida</i>	Gallery forest (veg 5)	② Pseudogley soil, silt-clay soil	Alluvial plain

Association analysis

The association between tree species of soils 3 and 4 is strong. It is also possible to associate soils 1 and 3, though the contingency coefficient is half the first. However, there is no possibility of association with soil 2 (Table 4.7).

In consideration of the association between vegetation types (veg), veg 1, veg 3 and veg 4 were combined in one cluster, and three vegetation clusters, i.e., veg 1, veg 2 and veg 5 were formed. (Table 5.8). Then, the vegetation types 1, 2 and 5 were associated to soil types 1 and 2 in relation to the tree species composition (Table 5.10).

Table 4.7: Association of soil types as a function of tree species composition. First step: Analysis of possibilities of association between soil types; Soils 3 and 4 merged with soil 1. Second step: verification of the associations established in the first step. Numbers are contingency coefficients. High coefficients (3.8 and 6.7) show high possibility of association of soil types.

First step				Second step		
	Soil 1	Soil 2	Soil 3	Soil 4	Soil 2	Merging Soils 1, 3, 4
Soil 1	-	-	-	-		
Soil 2	-2.3	-	-	-		
Soil 3	3.8	1.1	-	-		
Soil 4	-0.1	1.3	6.7	-		
					Soil 2	Merging Soils 1, 3, 4
					-	-
					Merging Soils 1, 3, 4	-4.0

Table 4.8: Association of vegetation types (Veg) as a function of tree species composition. First step: Analysis of possibilities of association between vegetation types by chi-square method; Veg 3 and veg 4 are merged with veg 1. Second step: verification of the associations established in the first step. Numbers are contingency coefficients. High coefficients (7.3 and 8) show high possibility of association of vegetation types.

	Veg 1	Veg 2	Veg 3	Veg 4	Veg 5		Veg 2	Veg 5	Merging Veg 1, 3, 4
Veg 1	-	-	-	-	-	Veg 2	-	-	-
Veg 2	1.5	-	-	-	-	Veg 5	-3.7	-	-
Veg 3	7.3	1.8	-	-	-	Merging Veg 1, 3, 4	0	-14.3	-
Veg 4	0	0	8.0	-	-				
Veg 5	-8.4	-3.7	-2.9	-0.1	-				

Similarity analysis

The similarity analysis (Table 4.9) confirms the relationships established between tree communities and the environmental factors (i.e., soil types and savanna physiognomy). Moreover, the similarity analysis enhances the relationship between the two main vegetation types, i.e., tree savanna and shrub savanna. Hence, both savanna vegetation categories share some common tree species (contingency coefficient = 0.4).

Similarly, and as a confirmation of the relationship between vegetation types, the soil types 1 and 2, relevant to the main vegetation units mentioned above, share some common tree species, proving that the soil clusters adhere to the vegetation clusters.

Table 4.9: Non-similarity between the final clusters of vegetation and soil. Confirmation of significant difference between tree species composition units in relation to environmental factors. Numbers are contingency coefficients.

	Soil 11	Merging Soils 10, 12, 13		Veg 2	Veg 5	Merging Veg 1, 3, 4
Soil 11	-	-	Veg 2	-	-	-
Merging Soils 10, 12, 13	0.4	-	Veg 5	0.1	-	-
			Merging Veg 1, 3, 4	0.4	0.1	-

Summary description of the final phytoecological zones

The summarized phytoecological zones described in table 4.10 are used as legend for the phytoecological map derived from the Landsat 7 ETM+ image classification.

Table 4.10: Final phytocological zones of the NRB

		Major tree species	Vegetation type	Soil type	Land unit
Phytocological zones	A	<u>Count = 957 Species = 45</u> <i>Detarium microcarpum</i> (10.0 %) <i>Vitellaria paradoxa</i> (8.3 %) <i>Entada Africana</i> (7.2 %) <i>Combretum glutinosum</i> (6.8 %) <i>Terminalia laxiflora</i> (6.3 %)	Shrub savanna (veg 1)	Soil 1 = Reworked, cuirass, sand-clay-gravel soil Soil 2 = Pseudogley soil, silt-clay soil Soil 3 = Soil formed by erosion	Glacis
	B	<u>Count = 583 Species = 33</u> <i>Terminalia macroptera</i> (30.4 %) <i>Vitellaria paradoxa</i> (10.1 %) <i>Pseudocedrela kotschyi</i> (9.0 %) <i>Combretum fragrans</i> (6.0 %) <i>Crossopteryx febrifuga</i> (4.7 %)	Tree savanna (veg 2)	Soil 2 = Pseudogley soil, silt-clay soil	Alluvial plain
	C	<u>Count = 19 Species = 10</u> <i>Syzygium guineense</i> (36.4 %) <i>Cola laurifolia</i> (9.1 %) <i>Garcinia livingstonei</i> (9.1 %) <i>Keetia cornelia</i> (9.1 %) <i>Lannea acida</i> (9.1 %)	Gallery Forest (veg 5)	Soil 2 = Pseudogley soil, silt-clay soil	Alluvial plain

4.3.4 Mapping vegetation cover

Accurate classification

Spatial distribution of NDVI values

As bare cuirass and bare soil reflect similar levels of near-infrared and red, they have NDVI values near zero. Water and flooding areas have negative NDVI values, as they reflect more visible energy than infrared energy. Inversely, tree savanna and shrub savanna, which reflect more infrared energy than visible energy, have positive NDVI values. Maximum NDVI values (0.50) were recorded in the tree savanna areas in west of the reserve (Figure 4.7). The NDVI image was used as baseline for supervised classification of the savanna landscapes.

Spectral signature of land cover patterns

Figure 4.8 shows that the savanna land cover classification is based on clearly separated classes as the relevant histograms are unimodal (sign of a good classification). Exceptions are the tree savanna and bare cuirass histograms, which can be considered,

to some extent, as bimodal. That results from the combination of two classes of each category of landscape into one, i.e. the dry “*Tree savanna*” class is merged with the “*Seasonal flooding tree savanna*” class. The dry “*Bare cuirass soil*” class is merged with the “*Seasonal flooding cuirass soil*” class. The intent of merging these classes is to obtain a savanna land cover classification map (Figure 4.9) valid for both rainy and dry seasons.

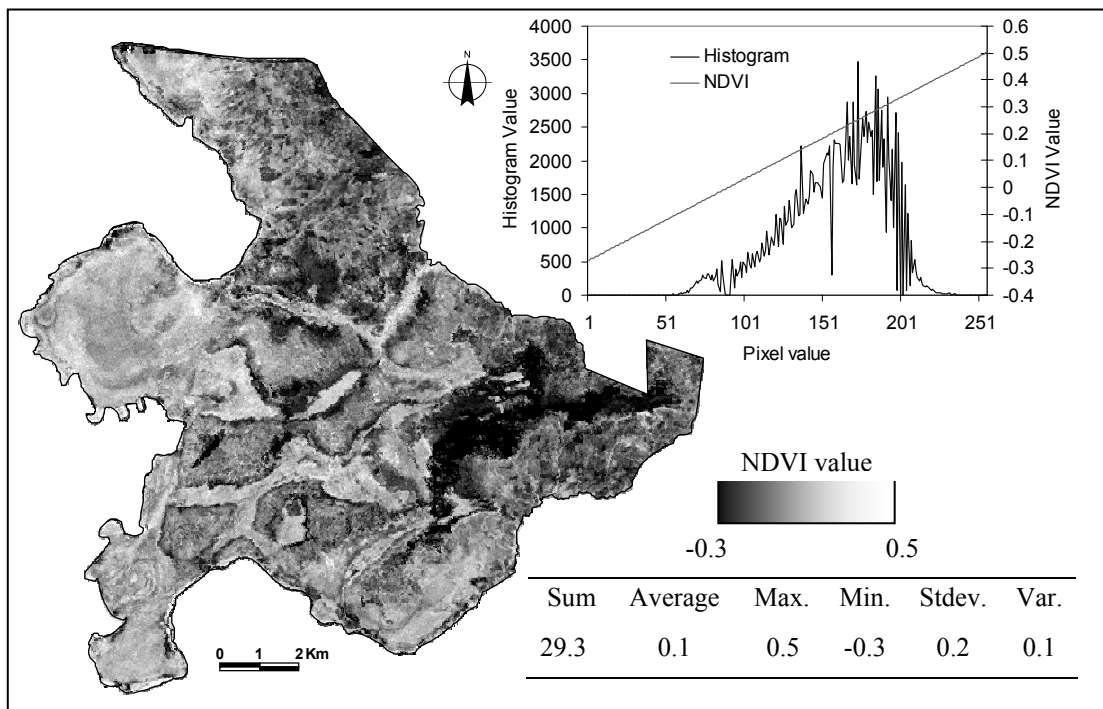


Figure 4.7: NDVI band and statistics. Data source: Landsat 7 ETM+, 196/52, Oct. 2002 (Provided by the University of Maryland)

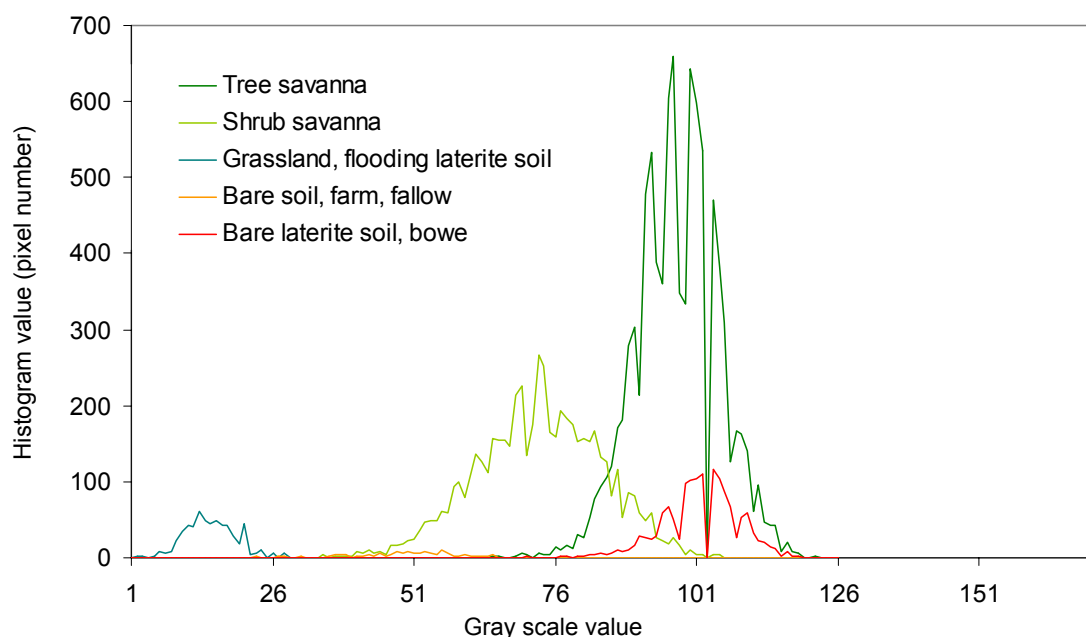


Figure 4.8: Land use land cover class signatures. Use of the NDVI image in the signature editor of Erdas Imagine (Leica Geosystems, USA). The “*Bare laterite soil, bowe*” class includes cuirass soil.

Classification accuracy assessment report

The final map resulting from the supervised classification (Figure 4.9) has an overall classification accuracy level of 98.8 % (Table 4.12), which is highly acceptable compared to the universally acceptable overall accuracy level of 85 % (Congalton and Green 1999). Detailed analysis of the error matrix (Table 4.11) confirms the overall accuracy to the extent that only the two classes “*Tree savanna*” and “*Bare soil, farm, fallow*” show a few errors of inclusion (i.e., commission errors) in the classification. Moreover, all the vegetation patterns identified on the map reflect the ground-truth, as the smallest user’s accuracy is 88.89 %, related to the class of “*Bare soil, farm, fallow*” (Table 4.12).

Analyzing the conditional kappa for each category confirms that the remotely sensed classification is correlated with the reference field data for each vegetation class (Table 4.13), as all Kappa values are greater than 0.8, i.e., 80 % (Congalton and Green 1999).

Table 4.11: Error matrix of the land cover classification. Number 1, 2, 3, 4, 5, and 6 are defined in Table 4.12

		Ground data						Total
		1	2	3	4	5	6	
Classified data	1	37	0	0	0	0	0	38
	2	0	21	0	0	0	0	21
	3	0	0	8	0	0	0	8
	4	0	0	0	4	0	0	4
	5	0	0	0	0	32	0	32
	6	0	0	0	0	0	16	18
Total		37	21	8	4	32	16	121

Table 4.12: Overall classification accuracy (98.8 %)

Class name	Reference totals	Classified totals	Number correct	Producer accuracy	User accuracy
1 = Tree savanna	37	38	37	100 %	97.4 %
2 = Shrub savanna	21	21	21	100 %	100 %
3 = Bare cuirass soil, bowal	8	8	8	100 %	100 %
4 = Grassland, seasonal flooding cuirass soil	4	4	4	100 %	100 %
5 = Seasonal flooding tree savanna	32	32	32	100 %	100 %
6 = Bare soil, farm, fallow	16	18	16	100 %	88.9 %
Totals	118	121	118		

Table 4.13: Conditional Kappa value for each category. Overall Kappa statistics = 0.98

Classified data	Kappa
Unclassified	1
Tree savanna	0.97
Shrub savanna	1
Bare cuirass soil, bowal	1
Grassland, seasonal flooding cuirass soil	1
Seasonal flooding tree savanna	1
Bare soil, farm, fallow	0.88

Tree species diversity and spatial patterns

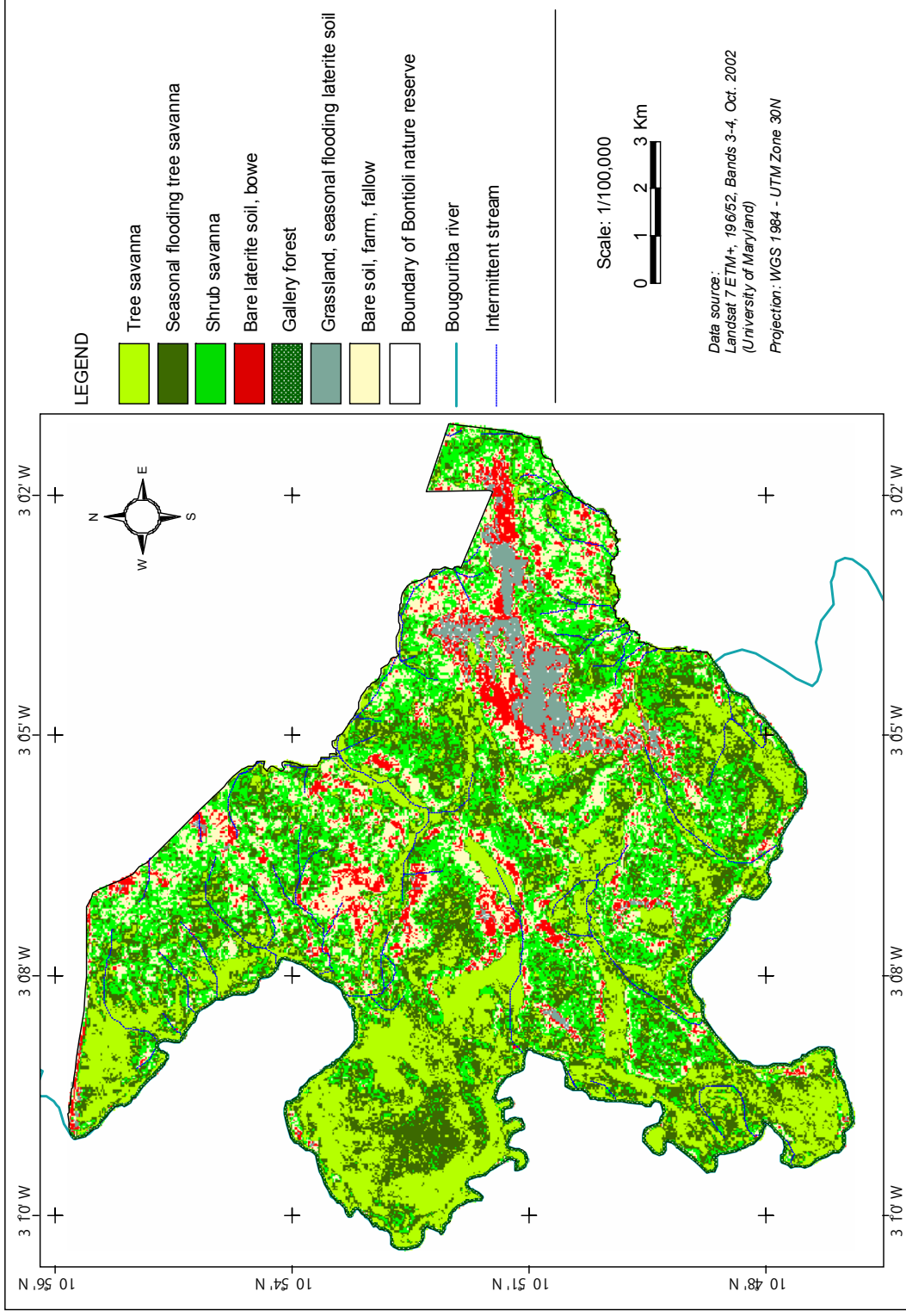


Figure 4.9: Vegetation classification map (NRB). Accuracy assesement = 98.83 %

Analysis of the phytoecological zones

Actual Area under Vegetation (AAV)

Comparing the three phytoecological zones of the NRB, the “*Shrub savanna*” (zone A) covers the largest area of the reserve (5894 ha; 43 %). The second important zone is the “*Tree savanna*” (zone B) with almost the same surface (5304 ha; 38.7 %). The “*Gallery forest*” (zone C), which is the less representative zone of the reserve (less than 1 %), follows closely the course of the Bougouriba river, from the north to the south of the reserve (Figure 4.10).

A strict analysis of the nature reserve in terms of Actual Area under Vegetation (AAV) reveals that zone A is less covered by vegetation compared to zone B (Table 4.14 ; Figures 4.7), as its *AAV* is 61.6 % as opposed to 97.7 % for zone B. The overall AAV of the NRB is 82.6 %, which indicates a high vegetation cover compared to degraded semi-arid lands.

In the evaluation of the contribution of the vegetation cover to the water balance, the AAV is very important, given that it is the proportion of land surface in a given vegetation class actually covered by vegetation. It is calculated by subtracting the non-vegetated area from the total area of the vegetation class, divided by the total area of the vegetation class. The straightforward formula of AAV for vegetation $Class_x$ is as follows:

$$AAV = \frac{Class_x \text{ total vegetation area} - Class_x \text{ non-vegetation area}}{Class_x \text{ total vegetation area}} \quad (4.22)$$

Example of AAV applied to the zone A (Table 5.14):

$$AAV_{ZoneA} = \frac{Zone A \text{ area} - Non-vegetation \text{ area}}{Zone A \text{ area}} \quad (4.23)$$

$$AAV_{ZoneA} = \frac{5894.15 - 2265.16}{5894.15} = 61.57 \% \quad (4.24)$$

Tree species diversity and spatial patterns

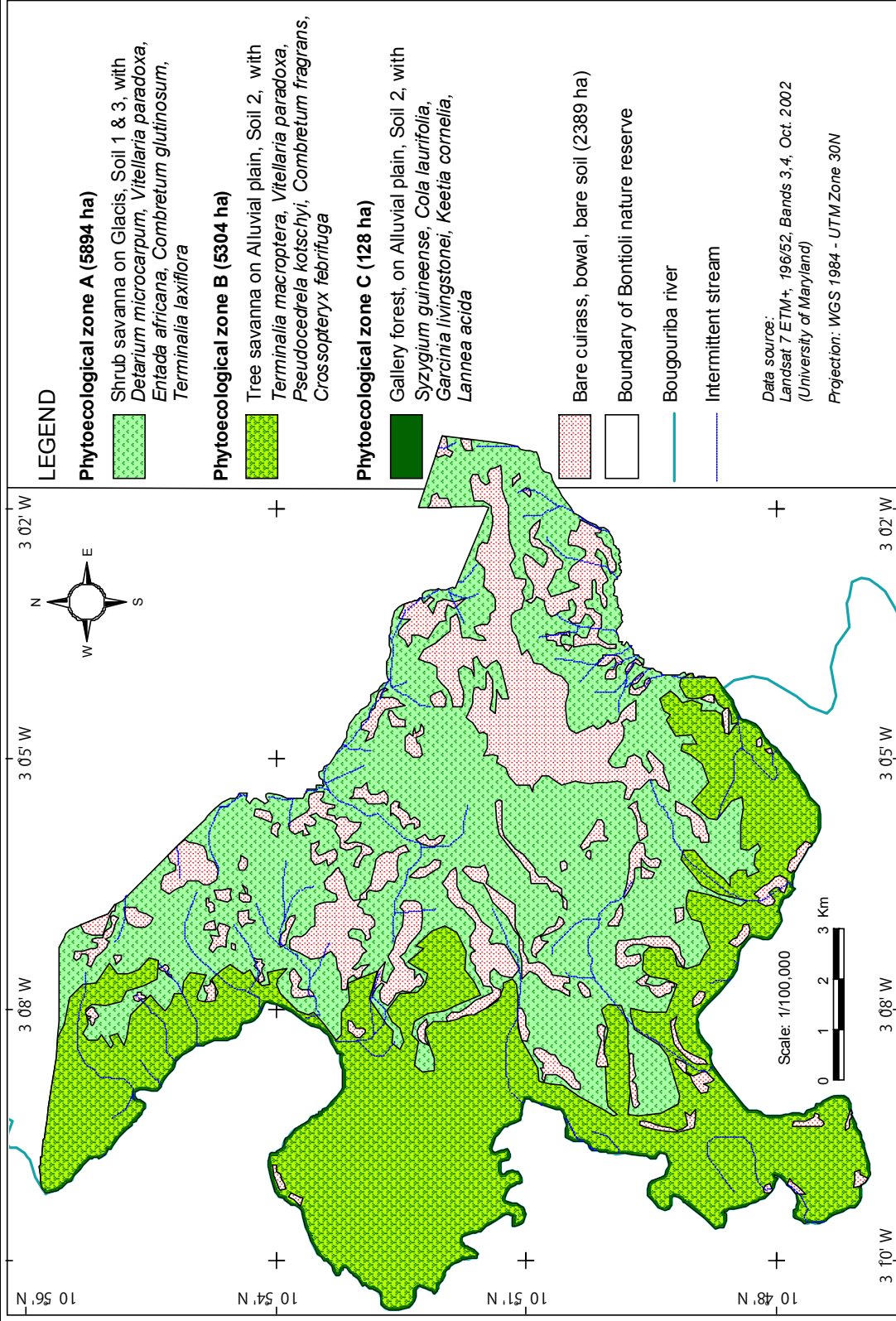


Figure 4.10: Phytoecological zones of NRB. The different zones are described in detail in Table 4.10

The “*Bare cuirass, bowal, bare soil*” class responsible for the shrinkage of the AAV of the zone A covers only 2.3 % of the zone B. Hence, this first-step analysis of the vegetation covers of the NRB leads to foresee a high contribution of zone B to tree water release to the atmosphere. Verification of this assumption will be done in the next chapters.

Table 4.14: Spatial distribution of the phytoecological zones as a function of AAV. The non-vegetated areas are bare cuirass and bare soils. AAV = Actual Area under Vegetation

Phytoecological zone	Total area (ha)	Percent with regard to the NRB (%)	Non-vegetation area (ha)	AAV (%)
Zone A	5894.2	43.0	2265.2	61.6
Zone B	5304.1	38.7	123.4	97.8
Zone C	127.5	0.9	0.0	100.0
Non-vegetation area	2388.6	17.4	-	0.0
NRB	13714.3	100	2388.6	82.6

Area-based Matching Ratio (AMR)

Even though the overall vegetation classification accuracy level was 98.8 % and a strong correlation was established between vegetation and soil layers, it can be assumed that both layers do not overlay perfectly in a GIS. Therefore, the Area-based Matching Ratio (AMR) was computed to determine the degree of matching between vegetation and soil layers.

AMR is the ratio of the resulting area of intersection (i.e., intersection between vegetation and soil surface areas) and the total soil surface area. The main purpose of this ratio is to assess the accuracy of the scaling up or extrapolation process of tree water use based on the phytoecological zones defined above. Here are possible values and interpretations of AMR:

- AMR = 1 → Perfect matching
- AMR close to 1 → High matching
- AMR close to 0 → Poor matching

In the case of the NRB, AMR is 0.8, which indicates a high degree of matching. Therefore, the scaling up of vegetation parameters based on soil information will be reliable.

4.4 Conclusions

The Nature Reserve of Bontioli provides a habitat for 71 (± 2) tree species within 19 families. The species are spatially aggregated but randomly distributed within each clump. Tree species richness, index of diversity ($H' = 1.5$) and index of evenness ($J = 0.8$) of Shannon-Wiener attest a good level of biodiversity conservation despite harsh environmental conditions and constant anthropogenic disturbance. In the NRB, the main tree species of the primary vegetation of the phytogeographical zone are still to be found.

The tree community is organized according to three main vegetation types, i.e., tree and shrub savannas, and gallery forest, detailed in an accurate classification map (i.e., overall accuracy = 98.8 %). This result confirms the physiognomic classification of Pigeonnière (2001). But the phytosociological classification of the reserve should retain as major tree species *Terminalia macroptera* (11.7 %), *Detarium microcarpum* (9 %), *Vitellaria paradoxa* (9 %), *Entada africana* (6.7 %) instead of *Burkea africana*, *Pterocarpus erinaceus*, *crossopteryx febrifuga*, *Combretum spp* as the author mentions.

The analysis of relationships between savanna physiognomy, phytosociology, soil and land units leads to a detailed map of phytoecological zones of the NRB (i.e., zones A, B and C). The overall Actual Area under Vegetation (AAV) of the NRB is 82.6 %, which indicates a high vegetation cover rate compared to degraded semi-arid lands. Moreover, the Area-based Matching Ratio (AMR) of 0.8 is an indicator of reliable accuracy assessment of scaling up or extrapolation results.

Finally, the maps of vegetation classification and phytoecological zones can be used as baseline for accurately scaling up of vegetation water release in the atmosphere from whole-plant tree water use (i.e., from reserve scale to regional scale). They can also be used in multi-agent research in where of small-scale classification maps are required. At a broader level, the results contribute to the understanding of vegetation

dynamics based on global change and can help to answer questions of how vegetation cover dynamics affect the Earth's environment.

5 TREE DENSITY PREDICTION BY THE LAI-SEB MODEL

5.1 Introduction

Given that ecological estimations are frequently subject to bias and uncertainty, the most certain way to determine tree density accurately is to count the number of tree stems per unit area (Sala et al. 2000; West 2004). The primary requirement for that accurate tree density estimate is field-based tree biometric measurements, because field data are considered verifiable (McCloy 1995; 2005). But estimations by ground measurements are often expensive, difficult and time consuming for large-area investigations. (McCloy 1995; Kim et al. 2006).

Alternatively, optical remote sensing using wavelengths ranging from the visible to the thermal infrared spectra (0.4-1.4 μm) appear to be a solution as long as statistical models based on correlation relationships between land-surface data and remotely sensed products are available for effective predictions based on field-scale data (Liang 2004). Furthermore, remote sensing is efficient in land-surface data acquisition (Konecny 2002; McCloy 2005).

Several authors have used different strategies to estimate tree density, but the results are not always reliable because they are site-specific. Thus, after reviewing most of the recent models, Huang et al. (2001) deemed tree density prediction based on linear spectral mixture analysis or linear regression techniques very complex and highly variable. Other methods, such as physically based models and fuzzy logics, are considered premature for use at large scale. However, some authors came to a common agreement that a set of linear regression may suit tree density estimation. That is also the view of Liang (2004), who claims that a realistic model could potentially be very complex with large number of variables. Huang et al. (2001) proposed analysis based on empirical relationships between tree canopy density and Landsat data using linear regression and regression tree techniques.

This chapter deals with the prediction of tree density at a spatial resolution of 30m by means of optical remote sensing imagery, through the development of an appropriate cross-validated multivariate regression model - the LAI-SEB model - which is applied to large areas within the Volta Basin (West Africa). The model will also be

used to estimate and scale up whole-tree water use, and estimate the contribution of the vegetation to the water balance.

5.2 Materials and methods

5.2.1 Tree density estimation using biometric data

Simple abundance estimates were based on ratios between quadrat area (900 m²) and tree stem frequency/crown cover/DBH. The results are compiled in a GIS-Database for mapping and validation for further processing. The calculation method of crown cover area is detailed in Chapter 3 of general research method (section 3.3) as is the tree biometric measurement method used in the field.

5.2.2 LAI-based tree density estimation

LAI determination by means of hemispherical canopy photography

Hemispherical canopy photography is a technique for studying plant canopies via photographs acquired through a hemispherical (fish-eye) lens from beneath the canopy (oriented towards the zenith) or placed above the canopy looking downward (Jonckheere et al. 2004). Photographs provided by a digital camera with a fish-eye lens have a 180 ° field angle of view, similar to a projection of a hemisphere on a plane (Rich 1990).

In the field, the digital camera Nikon - Coolpix 4500 with a fish-eye lens was used to take hemispherical photographs. The camera was mounted horizontally on a tripod at heights ranging between 0.50 m and 2 m according to the height of the trees. The back side of the camera (LCD side) was always made north-facing (Figure 5.1). Hemispherical photographs were taken during the day so as to avoid over or under-exposition of the photographs to direct sun radiation (i.e. between intervals of 8:30 - 11:00 hrs, 14:30 - 17:00 hrs). Conscious of the large view of the fish-eye, all instruments or any kind of objects and persons were hidden or cleared before taking images so that the resulting images show nothing but canopy.

The processing of the hemispherical photographs (Figure 5.2) for canopy structure characterization and LAI (Leaf Area Index) determination was done by means of the software HemiView Canopy Analysis 2.1 (Delta-T Devices Ltd).

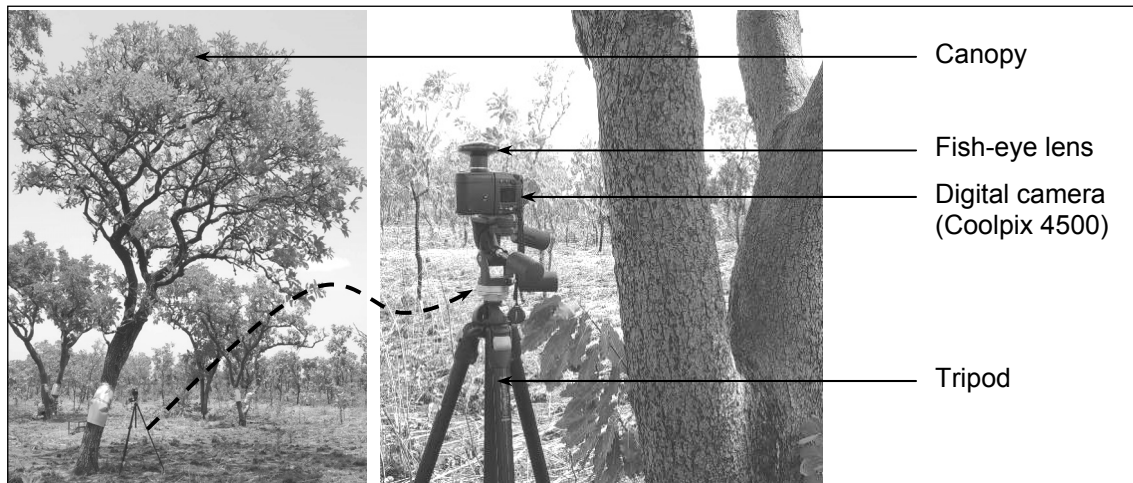


Figure 5.1: Taking upward hemispherical canopy photographs. Use of a digital camera (Nikon–Coolpix 4500) with a fish-eye lens and a tripod under high trees (> 6 m)

In practice, HemiView is used to measure the gap fractions and any ignored areas from the photograph. These values are then used as the basis for a best-fit calculation. The aim is to find the Leaf Area Density (LD) and the Ellipsoidal Leaf Angle Distribution Parameter (ELADP) which, when combined with the geometry model, give the best fit to the measured gap fraction values.



Figure 5.2: Hemispherical photograph of a *Combretum collinum* canopy ($10^{\circ}51'52''\text{N}$; $3^{\circ}04'04''\text{W}$) taken at 5:17 pm. The image shows the horizons at the edges and the zenith in the center.

LAI estimation by LAI-2000 techniques

The LAI-2000 Plant Canopy Analyzer is an electronic instrument used in the field to measure, record and compute instantaneously the amount of foliage (i.e., leaf area index or LAI) and foliage orientation (i.e., mean foliage tilt angle or MTA) in a vegetation canopy (Figure 5.3). The LAI-2000 uses a fish-eye lens projecting its nearly hemispheric view ($\pm 148^\circ$) onto five detectors arranged in concentric rings of 7, 23, 38, 53 and 68 $^\circ$, which are sensitive to radiation below 490nm. Each ring responds over a different range of zenith angles. The radiation is therefore azimuthally integrated (Li-cor 1992).

The LAI-2000 instrument measures the fraction of diffuse incident radiation (or transmittance $P(\theta_v)$) that passes through a plant canopy for a given view zenith angle (θ_v), assuming that the foliage is azimuthally randomly oriented. $P(\theta_v)$ is the ratio between the below-canopy and the above-canopy measurement. LAI-2000 computations are based on three assumptions: (1) Black foliage (under 490 nm), (2) foliage elements are small compared to the area of view of each ring detector, and (3) foliage is azimuthally randomly oriented. The model works even though no real canopy conforms exactly to these assumptions (Weiss 2001).

Table 5.1: LAI-2000 data as viewed on the control unit display or as output standard file format in the computer

FILE	DATE	TIME	VEG_TYPE	PLOT1	LAI	SEL	DIFN	MTA	SEM	SMP
1	08 MAY	09:23.35	SHRUB_SAV	A1	1.1	0.27	0.383	43	16	4
<hr/>										
ANGLES	7.000	23	38	53	68					
CNTCT#	0.613	0.854	1.140	0.584	0.274					
STDDEV	0.533	0.735	0.584	0.209	0.097					
DISTS	1.008	1.087	1.270	1.662	2.670					
GAPS	0.540	0.396	0.236	0.380	0.482					
<hr/>										
A1	09:23:47	319.50	326.10	473.70	274.40	155.60				
B2	09:24:05	110.70	107.90	78.41	81.87	66.44				
B3	09:24:18	291.30	263.20	219.30	170.80	114.70				
B4	09:24:27	295.60	259.60	229.60	119.60	71.62				
B5	09:24:38	92.47	37.62	39.27	70.14	57.74				

On the ground, measurements were taken according to one sensor mode, i.e., one reading above-canopy or in an open area (e.g., A1 in table 5.1) followed by four

readings below-canopy (e.g., B2 to B5 in Table 5.1) using the same LAI-2000 optical sensor. The process was repeated by the same person for each measurement irrespective of sky conditions. A mobile shield was used to minimize direct exposure of the optical sensor to sun radiation (Figure 5.3). In addition, pictures of each point of measurement were taken with a digital camera Digimax A6.



Figure 5.3: LAI measurements in rainy (1) and dry (2) seasons, 2005-2006

Measurements were taken every 25 m in long transects, and every 50 m in short transects, at regular intervals (Figure 5.4) designed according to the Valeri method (Baret et al. no date). Refer to the Valeri web site for more detail (www.avignon.inra.fr/valeri/). Final LAI data files were downloaded from the device to a computer using a RS-232 cable and LAI-2000 DOS software.

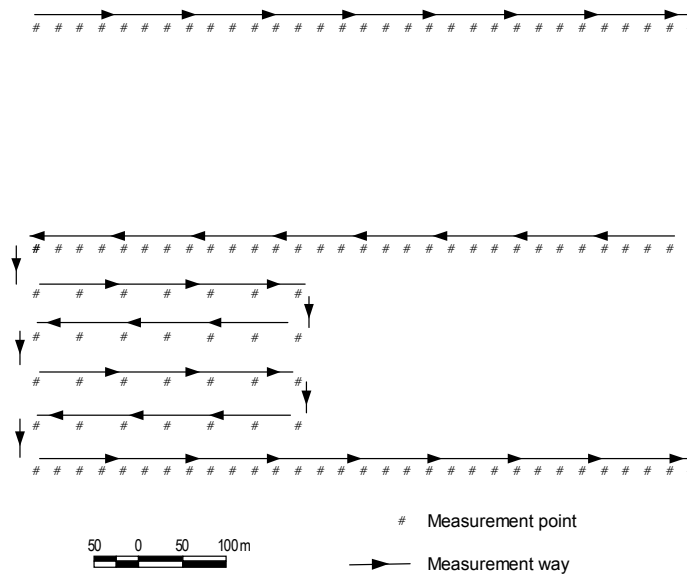


Figure 5.4: LAI-2000 measurement transects

5.2.3 Tree density derivation by regression analysis

For an automatic computation of vegetation index and surface energy balance products, the Atcor model, developed by Geosystems (2006), was used. It is a fast atmospheric correction algorithm for imagery from medium and high spatial resolution satellite sensors such as Landsat TM, Spot, Aster, Ikonos or QuickBird. The Atcor was used according to the tropical atmosphere parameters (For more details, refer to the relevant user manual).

Importance of atmospheric correction

Information retrieved from satellite images can be highly biased due to atmospheric influence which modifies the spectral information and degrades the spatial resolution of sensors. Therefore, atmospheric correction is considered to be an essential step in the processing of satellite images because it improves data analysis in many ways (Geosystems 2006):

- The influence of the atmosphere and the solar illumination is removed or at least significantly reduced;
- The multi-temporal and multi-sensor scenes with similar spectral bands recorded under different atmospheric conditions can be better compared, cleared of atmospheric influences (haze, cloud, aerosol, etc.);
- The ground reflectance data retrieved from satellite imagery can be compared to Eddy Covariance and microclimatological station measurements for verification and validation: the FPAR, LAI, Albedo, net radiation, sensible and latent heat flux values are respectively 0, 0, 25 %, 560 W m⁻², 3 W m⁻² and 332 W m⁻² for the computed remotely sensed imagery products, and 0.11, 0, 16 %, 435.5 W m⁻², 36.87 W m⁻² and 290.78 W m⁻² for the measurement stations. The validation is only based on these points, because the second microclimate station (BIOTA West Project) was installed in Dano town (some 25 km from the study area).

Computing vegetation index products

Soil-Adjusted Vegetation Index (SAVI)

The SAVI was chosen among other vegetation indices because, first, the area of investigation was dominated in places by extensive bare cuirass and bare soil surfaces (38.4 % of the shrub savanna zone; Chapter 4, section 4.3.4), and second, SAVI is suitable for defining the Leaf Area Index (LAI), the Fraction of Absorbed Photosynthetically Active Radiation (FPAR) and the surface energy fluxes (Choudhury 1994). The SAVI is defined as follows (Huete 1988):

$$SAVI = \frac{1.5 \times (NIR - R)}{0.5 + (NIR + R)} \quad (5.1)$$

where R and NIR are respectively Red and Near-Infrared band values.

Leaf Area Index (LAI)

By comparison with LAI derived from the LAI-2000-based measurements, the LAI was computed using remotely sensed imagery values and the empirical relation between vegetation index and LAI as follows (Asrar et al. 1984; Baret and Guyot 1991):

$$LAI = -\left(\frac{1}{a_2}\right) \times \ln\left(\frac{a_0 - SAVI}{a_1}\right) \quad (5.2)$$

LAI was computed using the following parameters: $a_0 = 0.72$, $a_1 = 0.61$ and $a_2 = 0.65$ (Geosystems 2006). Air temperature was calibrated according to the day (17 Nov. 2006) and time (10:40 hrs) of Aster satellite data acquisition: 33.2 °C was chosen referring to the *in-situ* microclimatological station data.

Fraction of Absorbed Photosynthetically Active Radiation (FPAR)

FPAR was computed according to LAI values as follows (Asrar et al. 1984):

$$FPAR = C \times [1 - A \times \exp(-B \times LAI)] \quad (5.3)$$

with the parameter values C=1, A=1 and B=0.4

Derivation of surface energy balance products by spectral analysis

Surface Albedo

Three bands in the green, Red, and Near-Infrared were used to calculate surface Albedo component as follows (Geosystems 2006):

$$Albedo = \left[\int_{0.3\mu m}^{2.5\mu m} \rho(\lambda) d\lambda \right] / \left[\int_{0.3\mu m}^{2.5\mu m} d\lambda \right] \quad (5.4)$$

Where $\rho(\lambda)$ is the wavelength band.

Detailed information about assumptions and extrapolation processes are developed in the Atcor user manual (Geosystems 2006).

Ground heat flux (G)

G is calculated according to SAVI and NDVI. It is defined as (Choudhury 1994):

$$G = \frac{R_n \times 0.4 \times (SAVI_m - SAVI)}{SAVI_m} \quad (5.5)$$

where $SAVI_m = 0.814$ is full vegetation cover, and $R_n =$ Net radiation.

Latent heat flux (LE)

$$LE = R_n - G - B(T_s - T_a)^n \quad (5.6)$$

Where $T_s, T_a =$ Respectively surface and air temperatures

$G =$ Ground heat flux

$R_n =$ Net radiation

$$B = 286 \times (0.0109 + 0.051 \times NDVI) \quad (5.7)$$

$$n = 1.067 - 0.372 \times NDVI \quad (5.8)$$

The computation of *other surface energy balance components* such as *Net radiation*, *Absorbed solar radiation flux*, and *Sensible heat flux (H)* are detailed in the Atcor user manual (Geosystems 2006).

Estimation of tree density by the LAI-SEB model

Nature is multivariate (Esbensen 2002), thus, a best estimation of tree stems as a function of land unit, from small to large-region scale, can be obtained by multivariate data analysis. One of the most important objectives of that method is to make use of the intrinsic variable correlations in a given data set to separate data structure from noise. This is achieved through data description, discrimination and classification, regression, and prediction.

The Partial Least Squares Regression (PLSR) (Wold 1966) was used to predict tree density because it works well compared to Principal Component Regression (PCR) and Multiple Linear Regression (MLR). PLSR deals with highly collinear predictors variables (Van Huffel 1997). It has the possibilities to easily detect erroneous measurements (Esbensen 2002). For more details on PLSR, refer to Hill and Lewicki (2006). The regression itself goes through two steps: calibration and validation (or prediction).

Multivariate calibration

The multivariate calibration is based on two matrices: the *X*-matrix of independent variables and the *Y*-matrix of dependent variables (Table 5.2). The scenario of prediction was executed once the different variables were determined. The scenario consisted of using the *X*-variables to predict the *Y*-variables at the right hand side, namely tree density by stem count or crown cover/DBH.

Table 5.2: Multivariate calibration scenario predicting Y from X.

X-Matrix (Independent variables)	Y-Matrix (Dependent variables)
LAI, SAVI, FPAR, Latent heat flux (LE),	Tree density,
Surface Albedo, Net radiation, Sensible heat flux (H),	Tree crown cover
Absorbed solar radiation flux, Ground heat flux (G)	Tree DBH

Multivariate prediction

The prediction consisted of, first, establishing a multivariate regression model between dependent and independent variables on a fine scale, and second, using the regression model on new *X*-data sets to predict new *Y*-data at a large scale.

The software The Unscrambler (CAMO Software Inc., NJ) was used to compute the regression model. It has the capability to validate the computed tree density regression model using the cross-validation for accuracy estimation. When performing the cross-validation, first, “the data set is randomly divided into k mutually exclusive and exhaustive partitions (or folds), where k is a user-defined parameter. Each partition should have approximately the same number of data instances. Then the algorithm is run k times. In the i -th run, $i = 1, \dots, k$, the i -th fold is used as the test set and the other $k - 1$ folds are temporarily merged and used as the training set for that run” (Freitas 2002, p. 20). The cross-validation approach is, in most favorable situations, almost as good as test set validation (Esbensen 2002). It helped to optimize the prediction ability by minimizing the prediction error, also called RMSEP (Root Mean Square Error of Prediction).

5.3 Results and discussion

5.3.1 Tree density estimates based on biometric data

Absolute tree density estimates

The mean tree density estimate in field plots was $331 (\pm 4)$ stems ha^{-1} , the standard deviation 250, minimum 11, and maximum 1233 stems ha^{-1} . The detailed analysis of tree density according to environmental factors reveals that the high density was recorded in tree savanna, on clay soils of alluvial plains (Table 5.3 and Figure 5.5). This can be explained by the proximity of the Bougouriba river to that part of the NRB,

where the clay soils remain wet during the dry season due to their water retention properties. Moreover, in the southwest of the NRB (10°49'22''N; 03°09'40''W), tree density is particularly high because of the incursion in the reserve of an important intermittent branch of the Bougouriba River. These results are very close to the description of Fontès and Guinko (1995), who mapped vegetation cover and land use in Burkina Faso. They stated that the South-Soudanian zone (area of the NRB) was characterized by high vegetation density.

As a whole, there are no strong disparities in tree densities between tree and shrub savannas (Figure 5.5). However, an association of particular environmental conditions, namely litter soils on even landforms with wet courses of intermittent rivers can promote the development of isolated high density spots throughout the landscapes.

Table 5.3: Absolute tree density (stems ha⁻¹) distribution as a function of environmental factors. The estimation of the average tree density is based on the number of trees per plot (900 m²)

Environmental factors	Tree count	Total plot	Average density	Max.	Min.
Vegetation type					
Shrub savanna	749	24	347	1011	11
Tree savanna	608	22	307	1233	78
Wood savanna	187	5	416	544	278
Sparse forest	46	2	256	433	78
Gallery forest	19	1	211	211	211
Total / Average	1609	54	307	687	131
Land unit					
Alluvial plain	730	26	312	1233	56
Low glacis	792	22	400	1011	11
Glacis medium	20	2	111	156	67
Tabular mound	67	4	186	344	78
Total / Average	1609	54	252	686	53
Soil type					
Cuirass soil	591	19	346	933	11
Clay soil	678	26	290	1233	56
Reworked soil	301	8	418	1011	89
Litter soil	39	1	433	433	433
Total / Average	1609	54	372	903	147

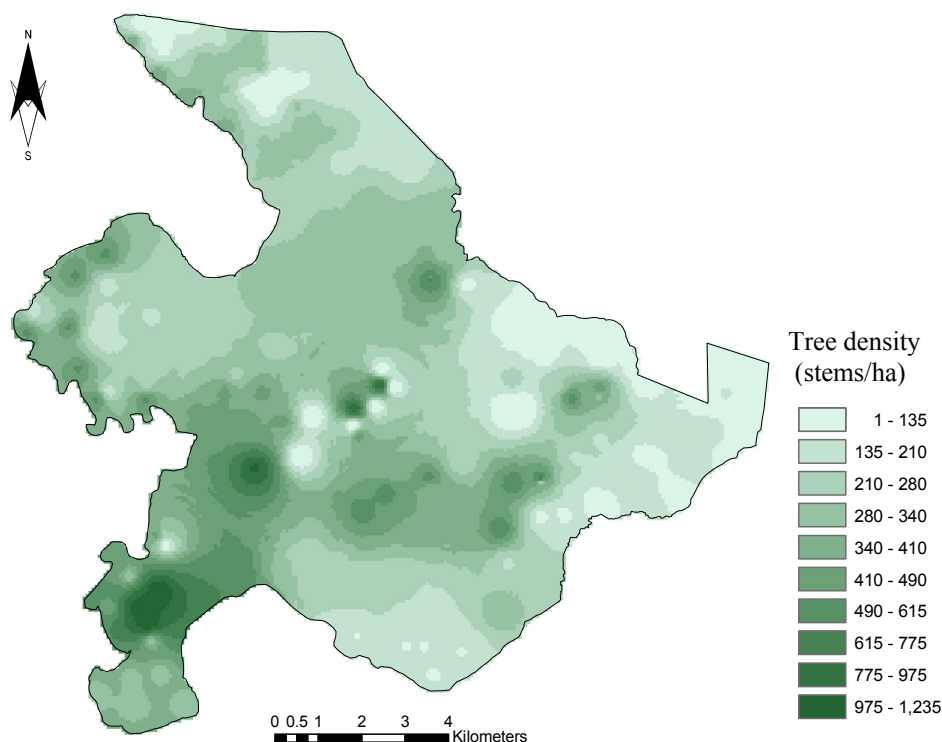


Figure 5.5: Derivation of tree density site-scale map applying the Inverse Distance Weight (IDW) interpolation model to absolute tree density point representation.

Tree density estimates by crown cover, DBH and tree height

In general, dominant tree heights (42.2 %) ranged from 3.50 - 6.55 m. Only 2.75 % of the trees were between 16 m and 22 m, and 5.86 % between 11 m and 16 m (Figure 5.6). These results confirm those of Fontès and Guinko (1995). The low occurrence of high trees is mainly due to anthropogenic disturbances, such as annual bushfires and woodcutting for farming needs. Human activities are omnipresent throughout the NRB. Exceptionally, large trees observed in low tree density areas (Figure 5.6) were commercial species such as *Vitellaria paradoxa* or sheanut tree (Karité), and *Parkia biglobosa* (Néré), which were protected by farmers for their economic value. Bagayoko (2006) made the same observation in eastern Burkina Faso on intensively used agricultural lands where *Vitellaria paradoxa* were dominant (17 stems ha⁻¹). Other large tree species like *Daniellia oliveri*, *Burkea africana*, and *Kaya senegalensis* grow in areas out of reach of bushfires and human needs.

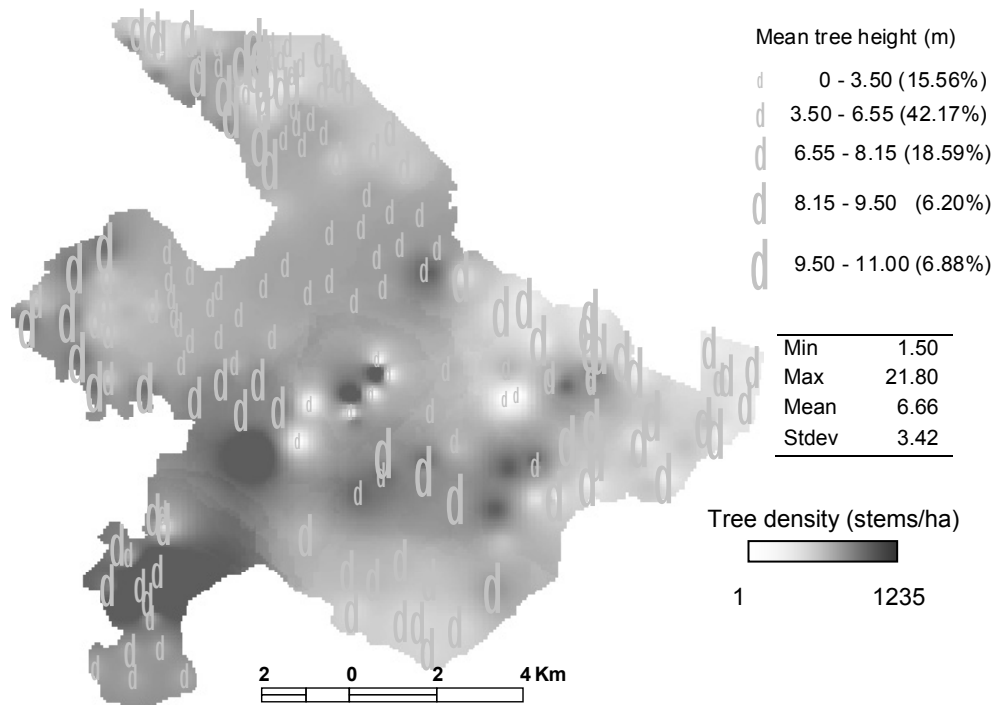


Figure 5.6: Spatial distribution of mean tree height in relation to tree density

The analysis of tree biometric parameters shows that tree height and tree crown height are highly correlated ($r = 0.81$), as is the case for tree height and tree DBH ($r = 0.71$): tall trees have high crown height and large DBH. Moreover, there are very good correlations between tree density and total DBH ($r = 0.91$), and between crown cover and total DBH ($r = 0.78$). But the correlation between tree density and crown cover ($r = 0.56$) is lower (Figure 5.7). Poor correlations were found between tree height and crown cover ($r = 0.19$), and between crown height and crown cover ($r = 0.15$).

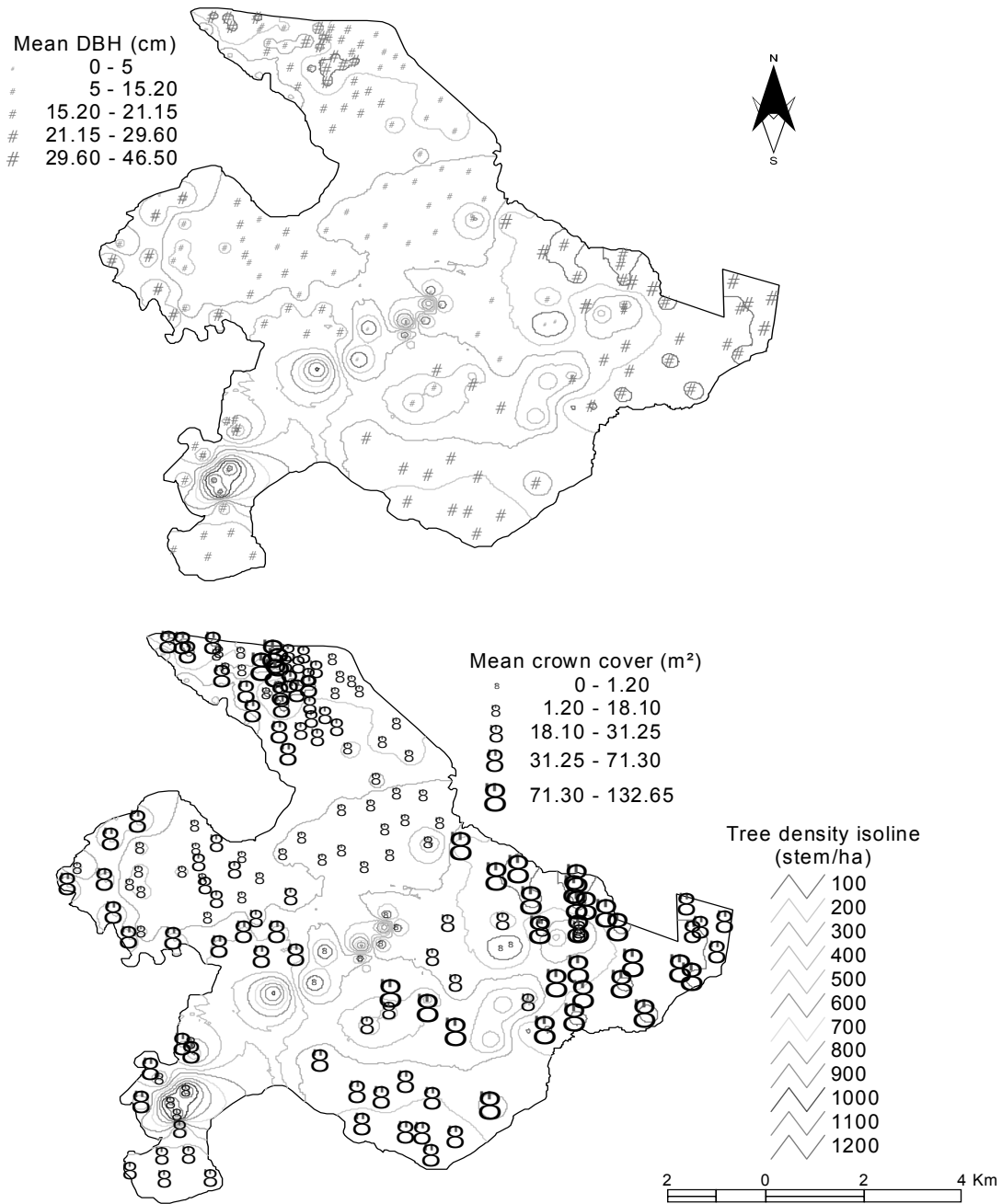


Figure 5.7: Spatial distribution of mean tree crown cover and DBH in relation to tree density

5.3.2 LAI-based tree density estimates

Analyzing vegetation cover dynamics using LAI-2000 data

LAI data recorded in the field by means of the LAI-2000 technique permit an assessment of the seasonal variation of vegetation cover density in the dry and rainy seasons. In the rainy season, vegetation covers look dense viewed from above, with

mean LAI values of 3.10 and 2.59 in shrub and tree savannas, respectively. LAI values are higher in shrub savanna (Max. = 5.69), where covers of dominant high grass (~3 m high) compete with shrubs. In the tree savanna where grass covers are less dense, LAI values reflect both tree canopy and grass covers (Max. = 2.59).

Therefore, from the rainy to dry seasons, vegetation cover density decreases drastically in shrub savanna due to the drying up of the grass cover. In contrary, in tree savanna, where LAI values are mainly influenced by tree canopy covers, the downward trend of canopy density is slower and less drastic. While grass covers dry out very quickly, tree leaves fall progressively so that, from one flowering period to the next, the protected area is still verdant in places. However, in case of bushfires, the process is extremely different with vegetation covers being quickly reduced to ashes.

The Seasonal Fluctuation of LAI (SFL), which is the difference between the LAI value in the rainy season and that in the dry season, is an approach to quantify the decrease or increase in vegetation cover density from one season to another. Thus, values of SFL higher than LAI values in the dry season reveal that the grasslands in the shrub savanna landscape changed completely in the dry season, passing from verdant to dry (Figure 5.8). In contrast, SFL values lower than the LAI values in the dry season show that the tree savanna landscapes are subject to relatively small changes from rainy to dry season compared to shrub savanna landscapes (Figure 5.9).

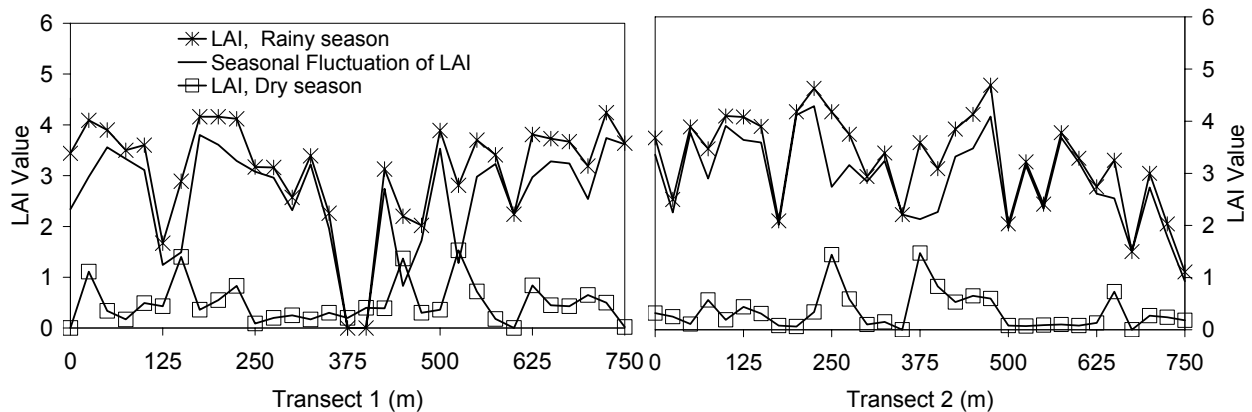


Figure 5.8: Seasonal variation of LAI in shrub savanna (eastern NRB). Measurements were done in rainy season (28 September 2005) and dry season (8 May 2006). LAI in rainy season: Min-Max = 0-5.69, Mean = 3.10, Stdev. = 1.02; LAI in dry season: Min-Max = 0-2.74, Mean = 0.57, Stdev. = 1.27.

Tree density prediction by the LAI-SEB model

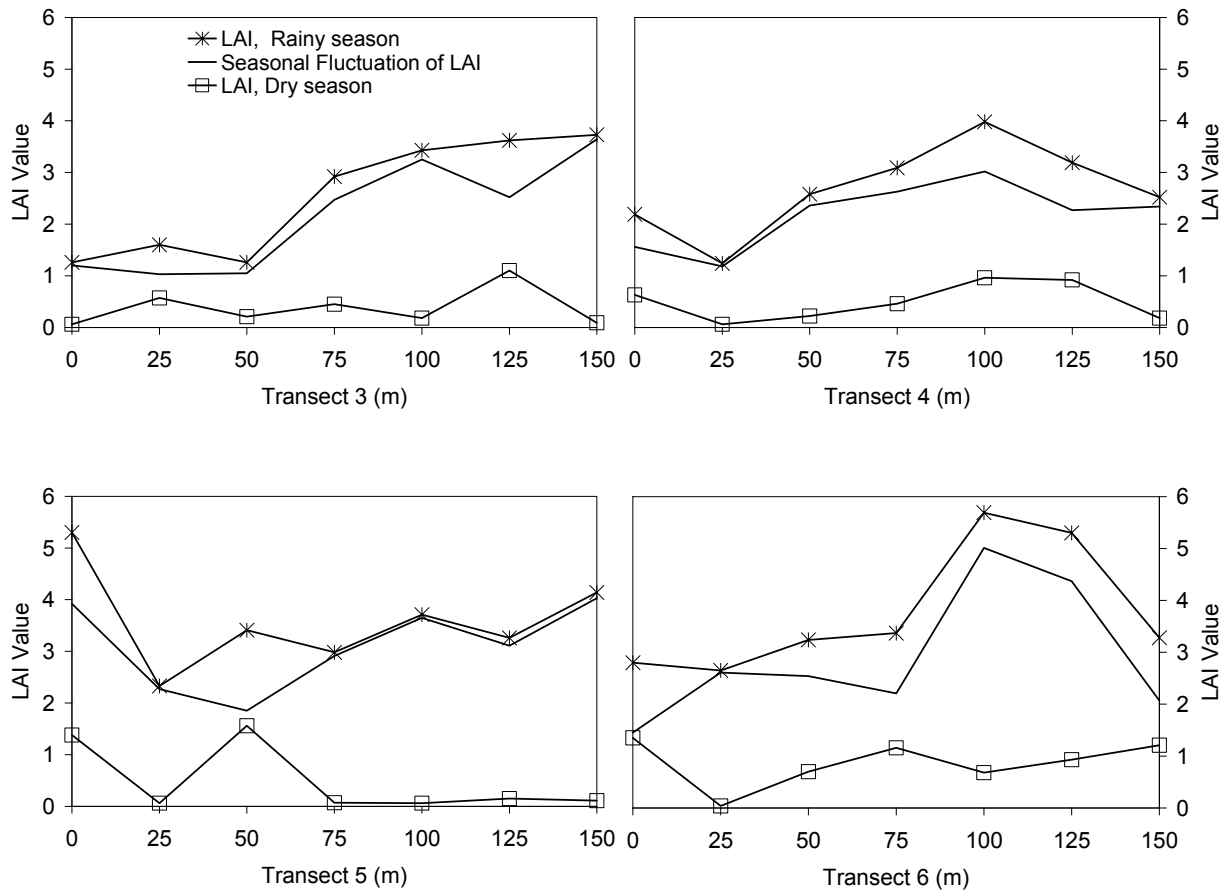


Figure 5.8: (Continued)

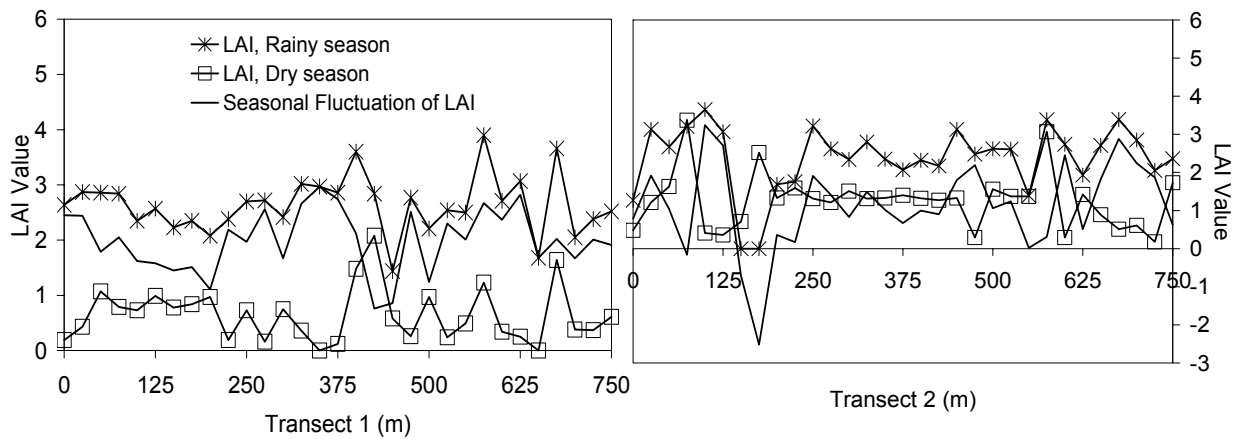


Figure 5.9: Seasonal variation of LAI in tree savanna (northern NRB). Measurements were done in rainy season (26 September 2005) and dry season (26 April 2006). LAI in rainy season: Min-Max = 0-3.90, Mean = 2.59, Stdev. = 0.73; LAI in dry season: Min-Max = 0-3.37, Mean = 1.05, Stdev. = 0.72.

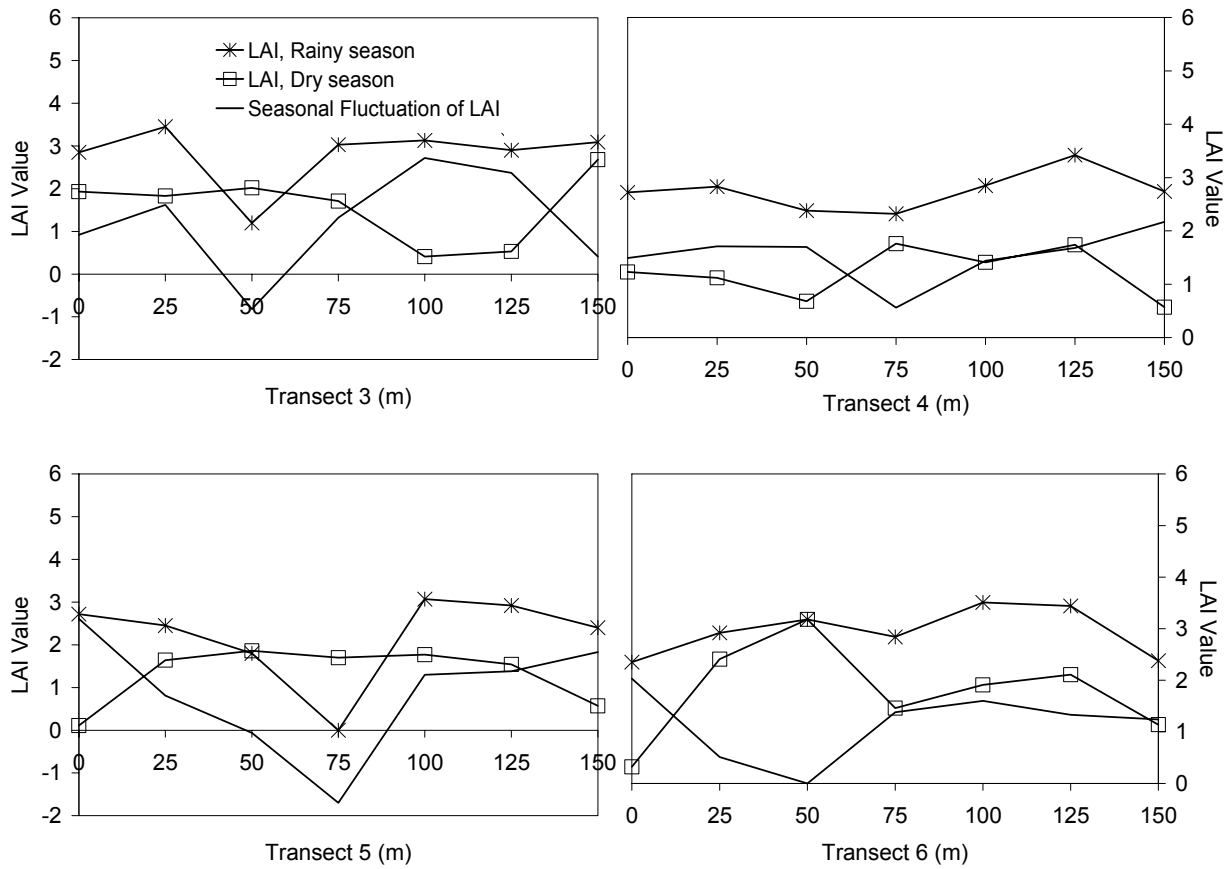


Figure 5.9: (Continued)

Tree canopy density estimation with hemispherical photography

The confirmation of the overall vegetation cover density and dynamics is done by the analysis of individual tree canopy cover. The mean LAI of mixed tree canopy cover is $0.85 (\pm 1.32)$, maximum $1.57 (\pm 1.32)$ and minimum $0.49 (\pm 0.91)$. As such, the LAI values derived from mixed tree canopy covers (Figure 5.10) are much closer to the LAI-2000 data recorded in similar environmental and seasonal conditions (section 5.3.2).

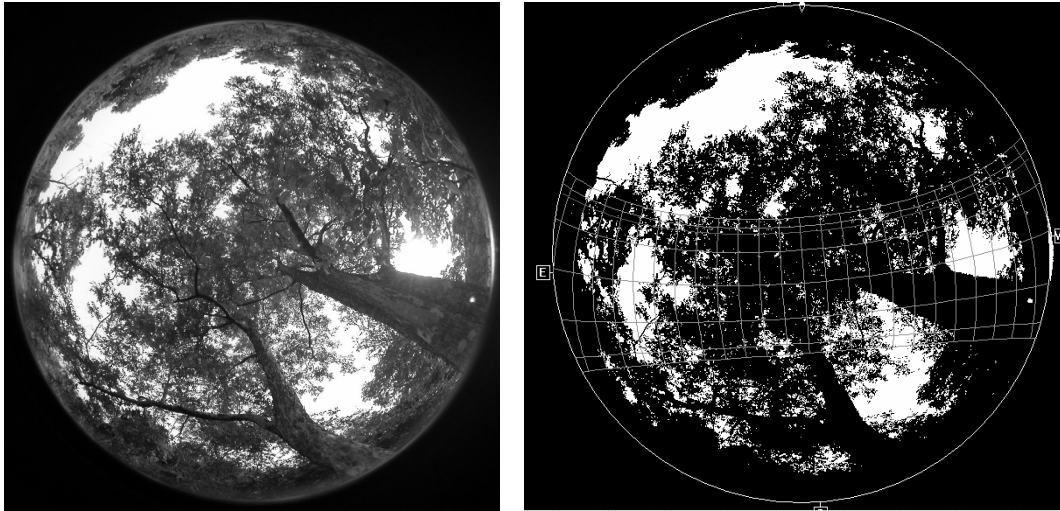


Figure 5.10: Characterization of canopy structure and LAI determination from hemispherical photograph (Hemiview). Left: tree species *Anogeisus leiocarpus* image in original colour. Right: the same image in classified form with sun path range (in green).

All ELADP values are greater than 1, meaning that tree canopy leaves and branches are predominantly horizontal (Table 5.4). This leads to reduction in the gap fractions within canopy covers and increases the surface of exposure of tree leaves to solar radiation. The predominance of horizontality in canopy characterization is confirmed by the good correlation between the overall fraction of ground covered by the canopy (*GndCover*) and the crown volume ($r = 0.72$, $p < 0.01$), i.e., the larger the tree crown volume, the larger its canopy ground coverage, and the more horizontal its canopy. On the other hand, the larger the tree crown volume, the higher is its LAI value ($r = 0.74$, $p < 0.01$). Finally, the larger the tree canopy surface, the higher its LAI value ($r = 0.93$, $p < 0.01$).

Tree density prediction by the LAI-SEB model

Table 5.4: Characterization of tree canopy leave area in sap flow measurement sites. The mixed tree canopy cover outputs are estimated from hemispherical photographs whereas the single tree canopy cover attributes are computed using tree biometric field data.

Sap flow site	Tree species name	Mixed tree canopy cover				Single tree canopy cover		
		LAI	LAIDev	Gnd Cover	ELADP	Crown volume	DLLAI	Leaf Area
Shrub savanna								
Site 1	<i>Detarium microcarpum</i>	0.70	1.20	0.46	3.65	307.63	8.15	751.99
	<i>Pterocarpus erinaceus</i>	0.74	1.28	0.46	2.90	1219.12	13.04	2980.09
	<i>Terminalia laxiflora 1</i>	0.96	2.26	0.59	6.22	176.89	8.15	432.41
	<i>Terminalia laxiflora 2</i>	0.81	1.03	0.51	4.02	296.38	8.15	724.49
	<i>Terminalia laxiflora 3</i>	0.50	0.83	0.36	4.04	273.45	8.15	668.43
	<i>Vitellaria paradoxa</i>	0.69	0.92	0.43	2.78	64.34	4.89	157.28
Site 2	<i>Burkea africana</i>	1.21	2.02	0.66	4.50	813.71	11.41	1989.08
	<i>Lannea microcarpa</i>	1.57	1.32	0.78	7.92	65.68	6.52	160.55
	<i>Anogeissus leiocarpus</i>	1.32	1.39	0.70	4.83	2586.54	22.49	6322.70
	<i>Daniellia oliveri</i>	1.17	1.42	0.63	3.48	583.73	11.41	1426.91
	<i>Pterocarpus erinaceus</i>	1.44	2.39	0.72	4.24	2148.33	18.25	5251.50
Site 3	<i>Entada africana</i>	0.88	1.44	0.46	1.84	159.41	8.96	389.66
	<i>Combretum glutinosum</i>	0.90	1.90	0.56	4.43	57.73	5.38	141.11
	<i>Acacia dudgeoni</i>	0.60	2.05	0.33	1.69	20.15	3.10	49.24
	<i>Pterocarpus erinaceus</i>	0.80	0.81	0.37	1.27	35.87	3.56	87.67
	<i>Parkia biglobosa</i>	1.01	1.58	0.58	3.44	34.84	2.93	85.16
	<i>Anogeissus leiocarpus</i>	0.86	1.54	0.37	1.13	86.15	6.19	210.58
	<i>Lannea microcarpa</i>	1.17	0.79	0.51	1.43	36.99	3.42	90.42
	<i>Combretum collinum 1</i>	1.19	1.45	0.64	3.48	24.96	5.21	61.02
	<i>Combretum collinum 2</i>	0.92	1.28	0.54	3.34	19.48	2.44	47.61
	<i>Lanea acida</i>	0.77	0.53	0.34	1.15	76.01	4.07	185.79
Tree savanna								
Site 4	<i>Pseudocedrela kotschy</i>	0.49	0.91	0.32	2.66	538.40	11.41	1316.09
	<i>Combretum fragrans</i>	0.56	1.21	0.38	3.55	18.65	3.26	45.59
	<i>Terminalia macroptera</i>	0.51	0.97	0.34	2.64	129.51	4.89	316.57
Site 5	<i>Pseudocedrela kotschy</i>	0.76	0.98	0.42	1.91	55.44	5.70	135.51
	<i>Combretum fragrans</i>	0.55	0.75	0.28	1.32	110.39	6.52	269.85
	<i>Terminalia macroptera</i>	0.54	1.24	0.35	2.64	124.87	7.33	305.25
Site 6	<i>Terminalia macroptera</i>	0.66	1.47	0.43	3.59	93.13	4.89	227.66
	<i>Crossopteryx febrifuga</i>	0.61	1.17	0.41	3.67	44.46	4.89	108.67
	<i>Combretum fragrans</i>	0.57	1.47	0.36	2.57	292.71	10.27	715.52

LAIDev = Root mean square deviation of LAI ($m^2 m^{-2}$); ELADP = Ellipsoidal Leaf Angle Distribution Parameter; DLLAI = Drip Line Leaf Area Index; GndCover = Overall fraction of ground covered by canopy (Delta-T Devices Ltd., 1999)

5.3.3 Tree density estimation from optical remote sensing derivatives

An alternative option of predicting tree density is using optical remote sensing imagery through the development of an appropriate cross-validated multivariate regression model (LAI-SEB model), which is applied to large regions within the Volta Basin.

Partial Least Squares Regression (PLSR), with robust collinearities in predictor variables, is used to predict tree density from the remote sensing image derivatives. (Figures 5.11 and 5.12).

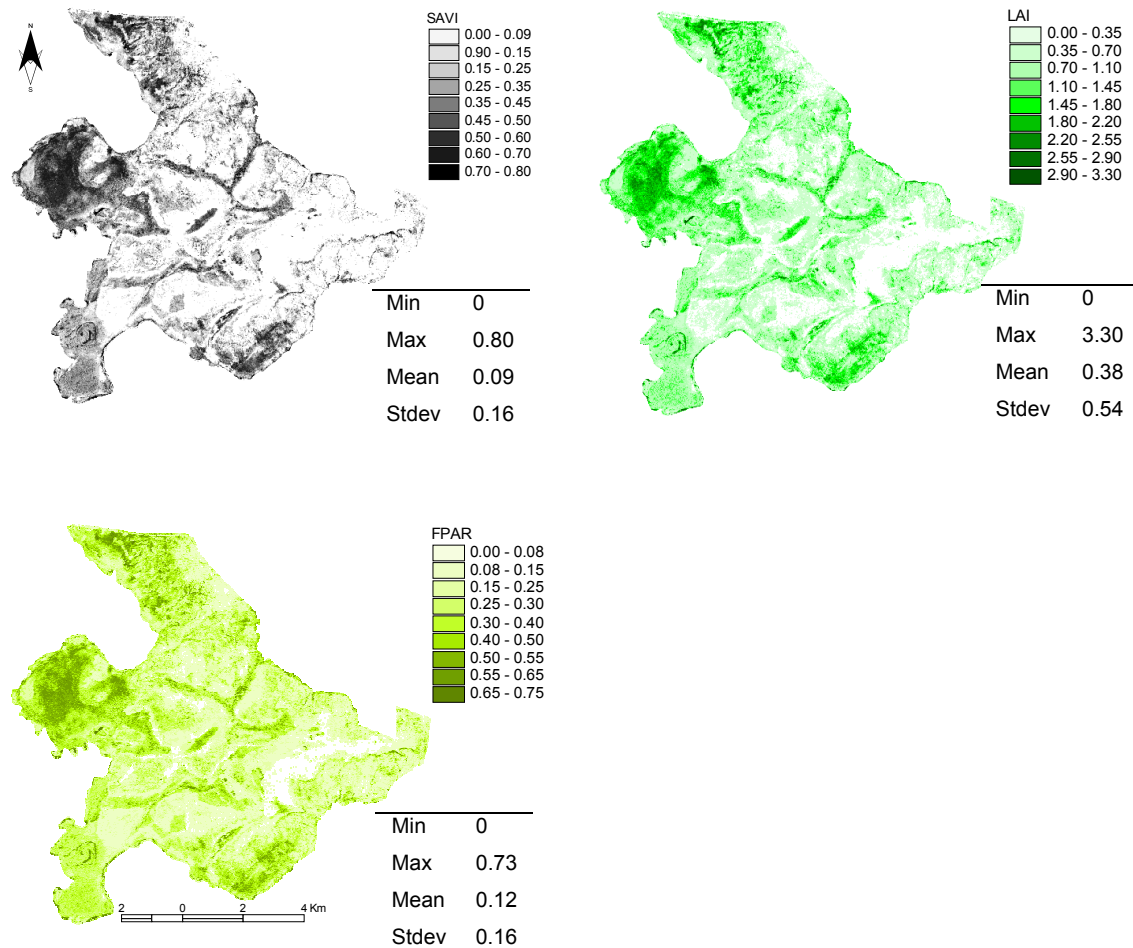


Figure 5.11: Summary maps of computed vegetation indexes

Tree density prediction by the LAI-SEB model

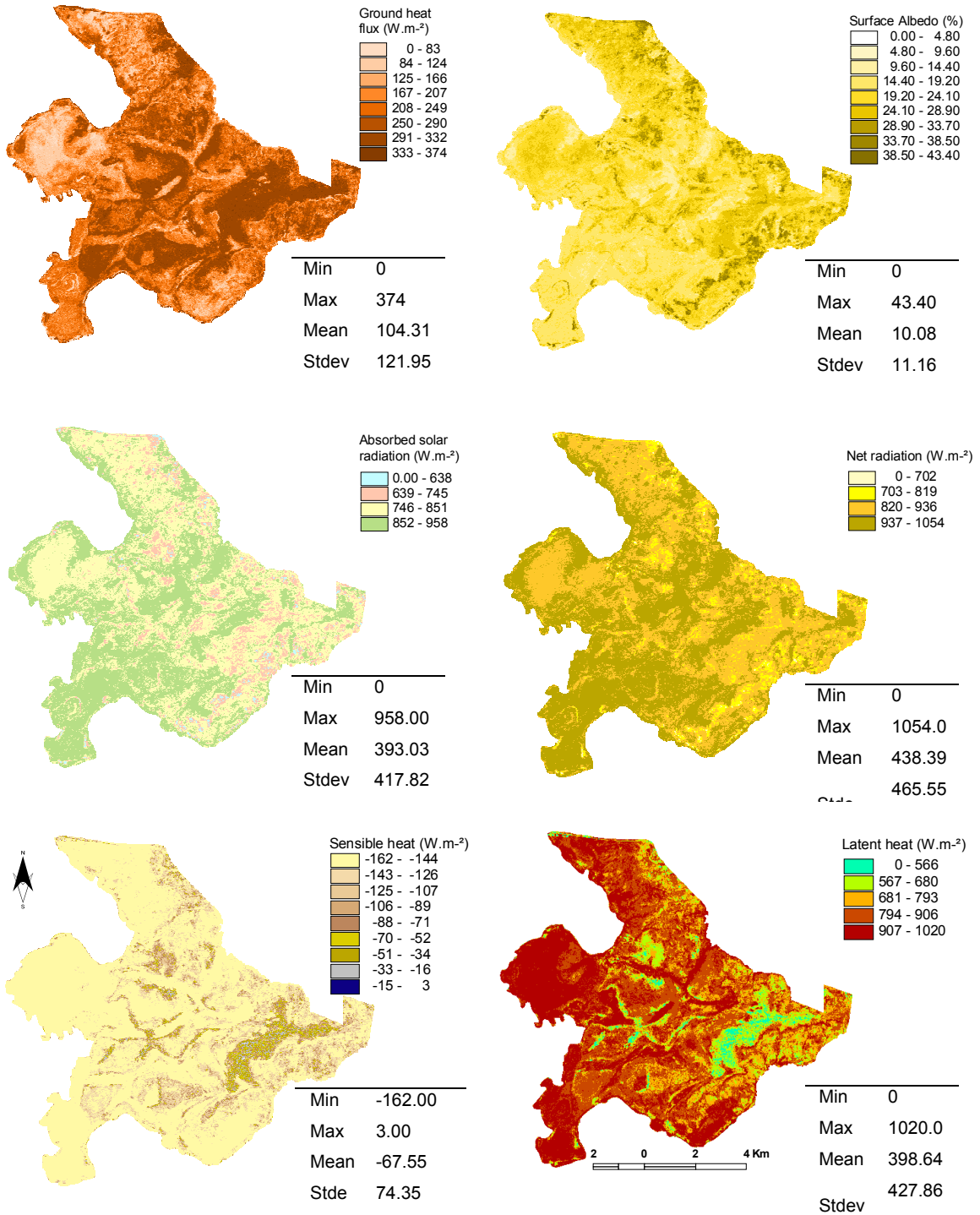


Figure 5.12: Summary maps of computed surface energy balance products (*SEB*)

Before addressing the regression itself, a validation of the remote sensing image derivatives was done by comparing them with field-based data. The computed LAI data were correlated with LAI-2000 field data, and the other computed parameters were

cross-checked with data from Eddy Covariance and microclimate stations recording continuous data in the NRB. As it turned out, although both measurement types were conducted during different flowering periods, there was a very good correlation between field-based LAI and computed LAI ($r = 0.81$, $p < 0.01$). The field-based LAI measurements were conducted on 26 April and 8 May 2006 (dry season), whereas the basis Aster image used for the computed LAI was from 17 November 2006 (wet season). In the dry season, tree crown covers are predominant in field-based LAI measurements, whereas in the wet season, both tree crown covers and high grass covers (~3 m high) are measured (Figure 5.3; section 5.3.2).

On 17 November 2006 at 10:43 hrs, the date and time of production of the basis satellite image, the microclimate and Eddy Covariance stations recorded data very close to those computed (Figures 5.11 and 5.12). In sum, the LAI-SEB model was designed using reliable data (section 5.2.3).

The LAI-SEB model development

Selection of variables for regression analysis

Based on the correlation analysis between the absolute tree density and the LAI, SEB derivates (Table 5.5), the decision was taken to run the multivariate regression model using the parameters of good correlation with absolute tree density (i.e., $r > 0.50$, $p < 0.01$). Thus, 6 parameters out of 9, namely SAVI, LAI, FPAR, G, H (Hs), and E (LE) were used for tree density estimation.

Table 5.5: Correlation between absolute tree density and computed LAI-SEB products

		Vegetation indexes (LAI)			Surface Energy Balance derivates (SEB)					
		SAVI	LAI	FPAR	Albedo	R_a	G	R_n	H	E
Tree density	Pearson Correlation	0.70**	0.70**	0.70**	-0.18*	0.18*	-0.66**	0.18*	-0.57**	0.61**
	Sig. (2-tailed)	0.000	0.000	0.000	0.048	0.046	0.000	0.045	0.000	0.000
	N	121	121	121	121	121	121	121	121	121

** Correlation is significant at the 0.01 level (2-tailed) * Correlation is significant at the 0.05 level (2-tailed)

Choice of optimal number of principal components

The choice of the optimal number of principal components (PCs) for the regression analysis was made after an inspection of the cross-validated outputs. The optimum number of PCs was taken at minimum RMSEP (Martens and Martens 2001). In practice, the regression analysis started with a 10-fold cross-validation try. At the 4-fold stage, the results showed a high correlation coefficient ($r = 0.80$) and low error of prediction (RMSEP = 87 stems ha^{-1}) with 5 PCs. The choice of 5 PCs was also guided by the significant increase in the explained variance from 51 % (2 PCs) to 63.4 % (5 PCs) (Figure 5.13).

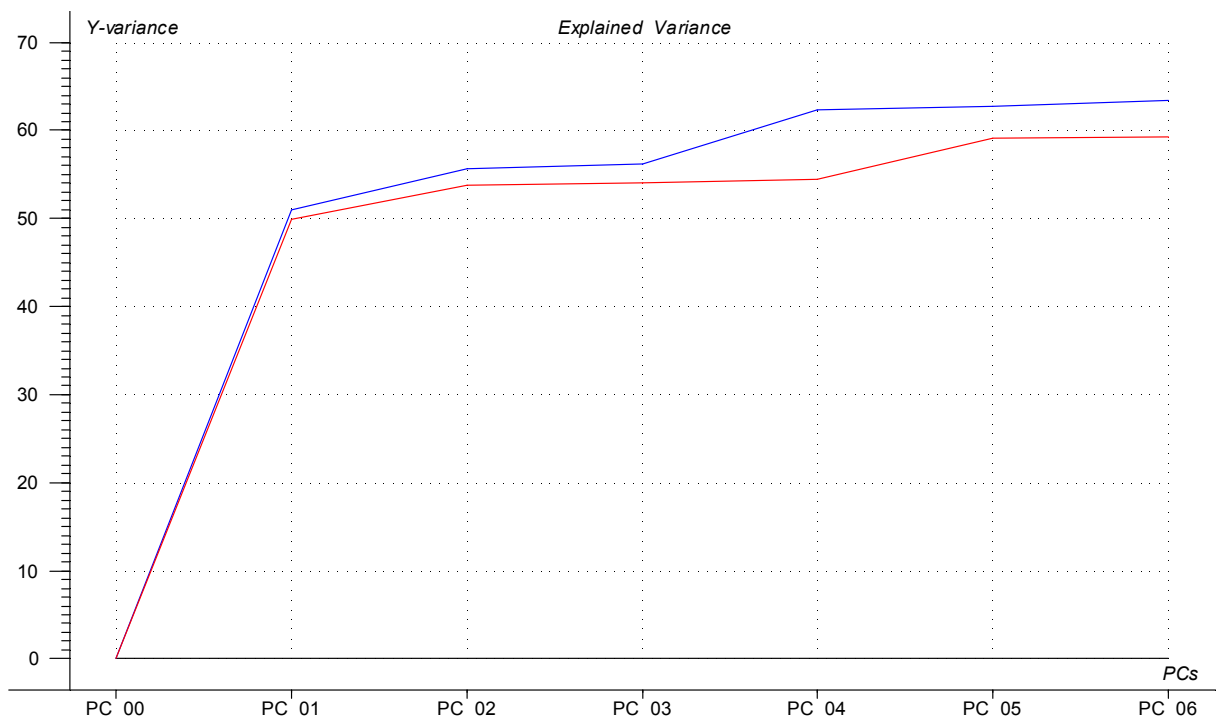


Figure 5.13: Explained calibration (blue colour) and validation (red colour) variances. The explained variance is accounted for by the regression model. (PC = Principal Component, index xx = 00, ..., 06)

Outlier identification

Outliers processing is an important issue, because these appear to deviate markedly from other members of the sample to which they belong (Kaya 2004). Several outliers were statistically identified in the data set, but not all of them were systematically rejected. They were retested one by one by re-running the regression analysis both with and without the potential outlier (De Muth 2006). In case the performance of the

model remains the same or decreases without the suspected outlier, it is definitively considered a useful value for the model, otherwise it is removed. Thus, from the list of 23 potential outliers, 14 were kept out of the calculation (12, 26, 27, 28, 38, 40, 42, 48, 71, 72, 75, 81, 82 and 119), and 9 were considered as useful values for the model (Figure 5.14). The confirmed outliers were kept in the original data set because “a potential outlier could be a legitimate observation” (De Muth 2006, p. 634) in another analysis.

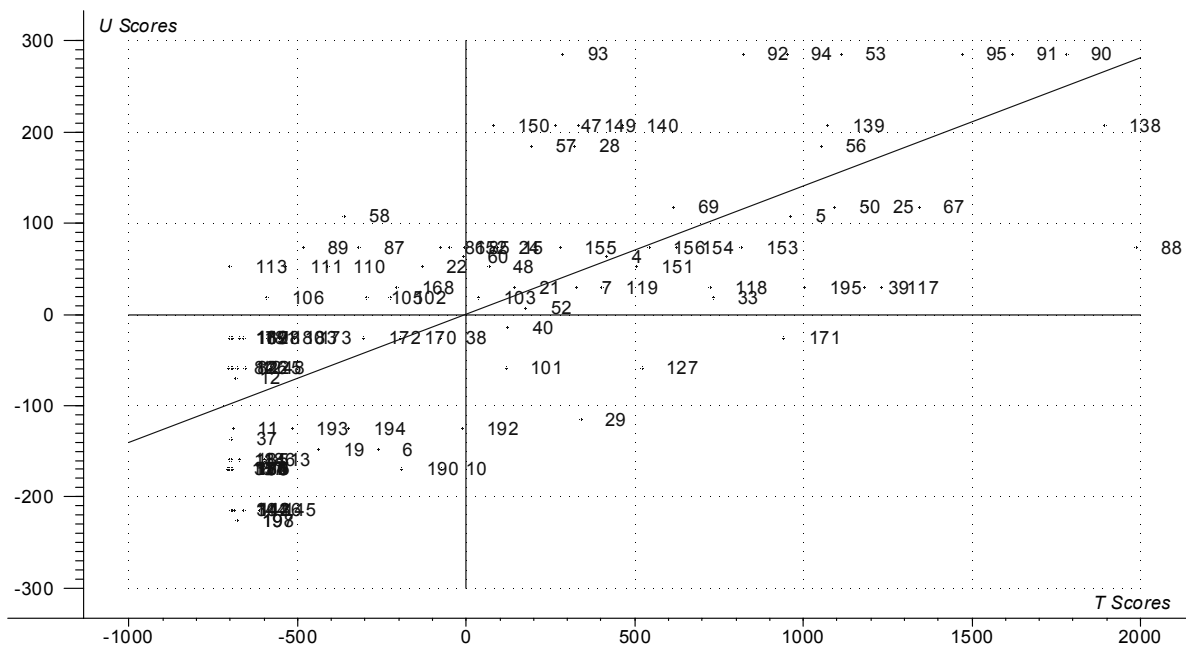


Figure 5.14: X-Y relations outliers. Optimum number of PCs = 5. Numbers are true values representing samples (tree density). Outliers significantly deviate from other members of their corresponding samples.

Y-Residuals analysis

In general, residuals measure the distance between the actual and predicted values for any estimator (Figure 5.15). They are used to assess the goodness-of-fit of the regression model (Lewis-Beck et al 2004). Analyzing Y-residuals helps to identify scores on Y that cannot be accounted for by the regression model.

There is no systematic relationship between Y-residuals and the samples. Furthermore, the bias value of -0.24, computed as the average value of the residuals, is

trivial. As such, the low level of bias close to zero attests that the predicted variables are not biased and it is proof of good fit of the model.

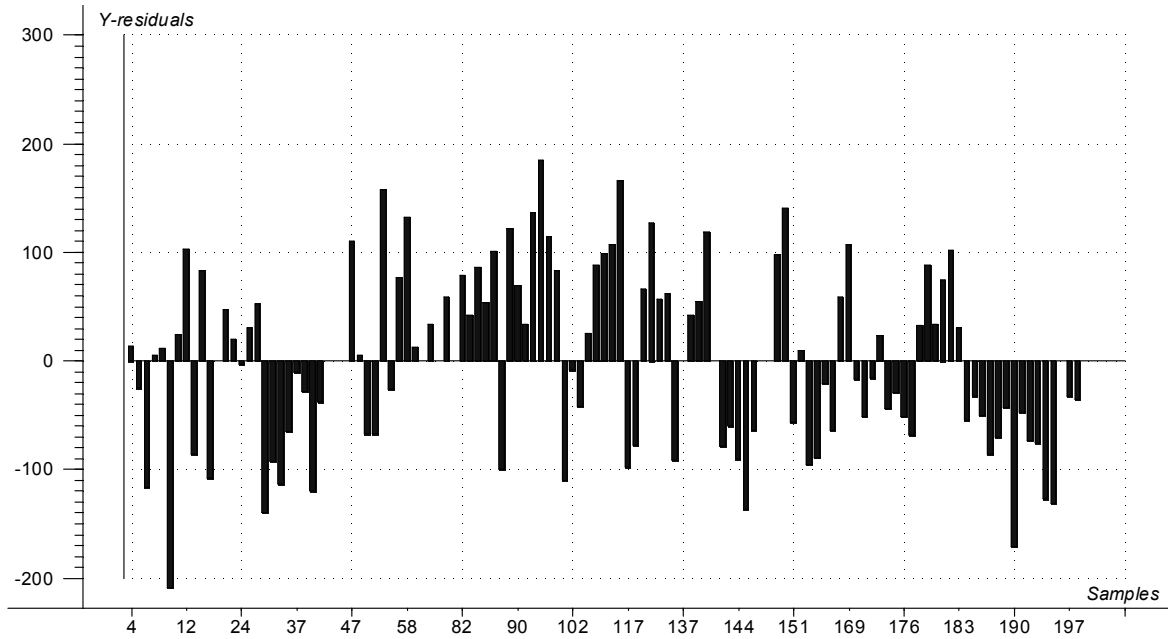


Figure 5.15: Plot of Y-residuals. Y-Bias = -0.24. 0-line corresponds to the best fit of the prediction. Residual values below the 0-line overestimate the prediction; residual values above the 0-line underestimate the prediction.

Processing the LAI-SEB model

Once the regression coefficients were determined (Figure 5.16), the straightforward tree density prediction regression LAI-SEB model (Leaf Area Index - Surface Energy Balance model) is defined as follows:

$$T_{rd} = k_0 + V_{Lai} + S_{Seb} \quad (5.9)$$

with

$$V_{Lai} = k_1 * LAI + k_2 * SAVI + k_3 * FPAR \quad (5.10)$$

$$V_{Lai} = 0.322 * LAI - 0.565 * SAVI - 2.453 * FPAR \quad (5.11)$$

$$S_{Seb} = k_4 * H + k_5 * E + k_6 * G \quad (5.12)$$

$$S_{Seb} = 2.447 * H + 2.713 * E - 4.996 * G \quad (5.13)$$

and $k_0 = 288.205$ (weighted coefficient)

where T_{rd} = Relative (predicted) tree density (*stems/ha*)

H (Hs) = Sensible Heat Flux ($W m^{-2}$)

E (LE) = Latent Heat Flux ($W m^{-2}$)

G = Ground Heat Flux ($W m^{-2}$)

SAVI = Soil Adjusted Vegetation Index

LAI = Leaf Area Index

FPAR = Fraction of Absorbed Photosynthetically Active Radiation

$k_{(0,1,...,n)}$ = Regression coefficients

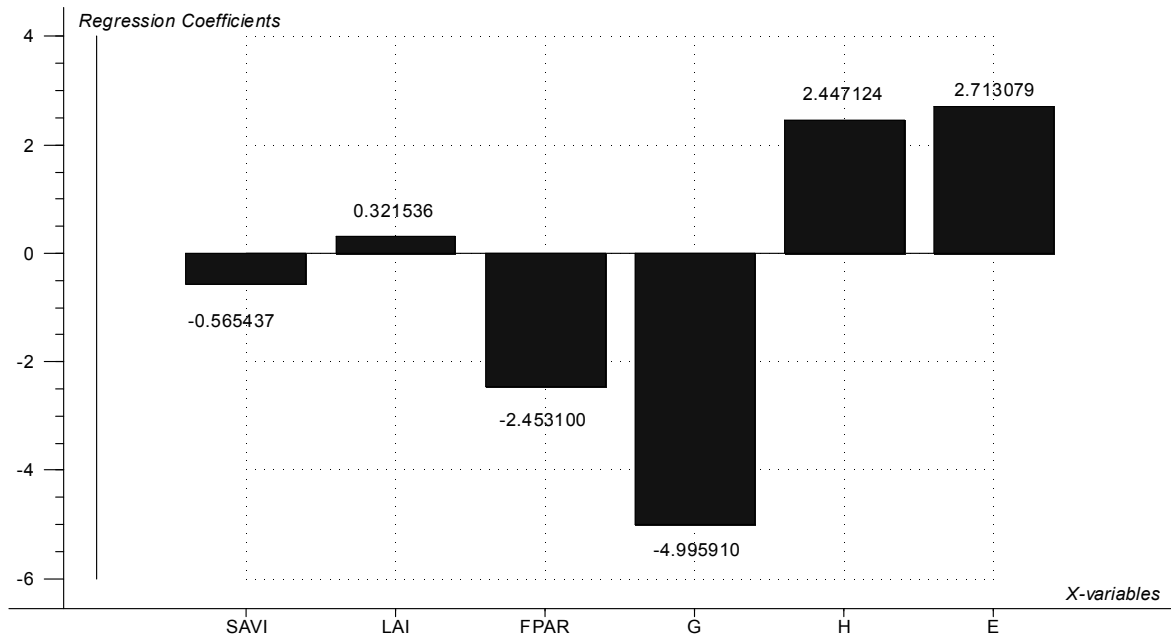


Figure 5.16: Regression coefficients of the LAI-SEB model. Optimal number of PCs = 5; weighted coefficient = 288.204468

Accuracy and reliability of the LAI-SEB model

Accuracy analysis

The calibration ($r = 0.80$) and validation ($r = 0.78$) correlations between measured and predicted tree density (Figure 5.17) confirm the good performance of the model. As a whole, the model fits well to the training data sets and works well for tree density prediction. The very low value of bias (-0.24) in the validation set gives a measure of the accuracy of the model in a certain range of prediction.

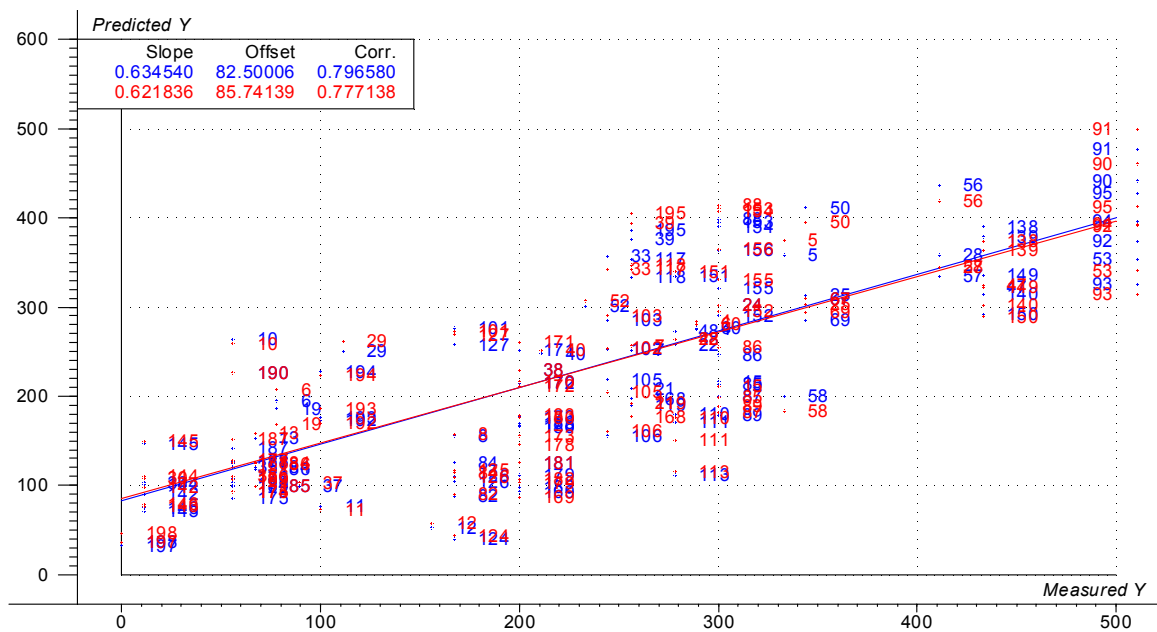


Figure 5.17: Regression analysis. Blue numbers mean tree density samples used for calibration, red numbers mean tree density samples used for validation; observation is X and prediction is Y .

However, the Root Mean Square Error of Calibration ($RMSEC = 83.60$) and the Root Mean Square Error of Prediction ($RMSEP = 87.09$) values theoretically reveal that the model has some limits in estimating tree densities (Figure 5.18), which might be due to error sources as follows:

- *GPS accuracy*: the Global Positioning System (GPS) used in the field to record the spatial position of individual trees has an accuracy of 6 m or more according to sky condition. In the open, the accuracy is between 6 and 8 m and under tree covers it varies between 9 and 11 m.

- *Sampling quadrat*: In the field, the plots were not always perfectly square 30 m x 30 m (900 m²). Every so often, there was a chance to overestimate or underestimate delimitation of plots, leading to bias, be it slight.
- *Satellite image resolution*: The Aster image used for computing the different vegetation indexes and surface energy balance products has three different pixel sizes: 15 m for the Visible Near Infra Red bands (VNIR), 30 m for the Short Wave Infra Red (SWIR) bands and 90 m for the Thermal Infra Red (TIR) bands. Despite all kinds of corrections and resampling that was undertaken, the image derivatives still contain inevitable noise.
- *Modeling errors*: The performance of the calibration model can be appreciated through the RMSEP. As explained by Van Espen (2002), the RMSEP “is calculated using PLS models with different numbers of latent variables A . The RMSEP values are plotted against A and the value where a minimum or a plateau is reached is taken”. Therefore, RMSEP is estimated using reference values which themselves are also error-prone (Esbensen 2002).
- *SAVI saturation effect*: As highlighted by Liang (2004, p. 253), for very dense vegetation canopy, $L = 0$, then SAVI = NDVI. In this case, SAVI saturates because red reflectance does not change much, but Near-IR reflectance still increases when the canopy becomes denser (Liang 2004). The saturation effect inhibits the performance of the LAI-SEB model, which cannot predict tree density beyond the level of saturation.

The sources of errors make the model very strong in the prediction of tree density in the 0 - 525 (± 87 stems ha⁻¹) range, but weak at higher values, with an error of prediction twice the RMSEP (i.e., ± 174 stems ha⁻¹). The question then arises which RMSEP should be applied to the model. The statistics reveal that 61.1 % of the predicted tree density samples have errors of prediction which vary between 1 and 87 stems ha⁻¹, whereas 37 % of the samples have errors of prediction varying between 87 and 175 stems ha⁻¹, and finally, 1.9 % of samples have errors of prediction varying from 175 to 203 stems ha⁻¹ (Figure 5.19). Based on these results, the most reliable overall error of prediction applicable to the LAI-SEB model is ± 87 stems ha⁻¹, i.e., ± 8 tree stems per pixel.

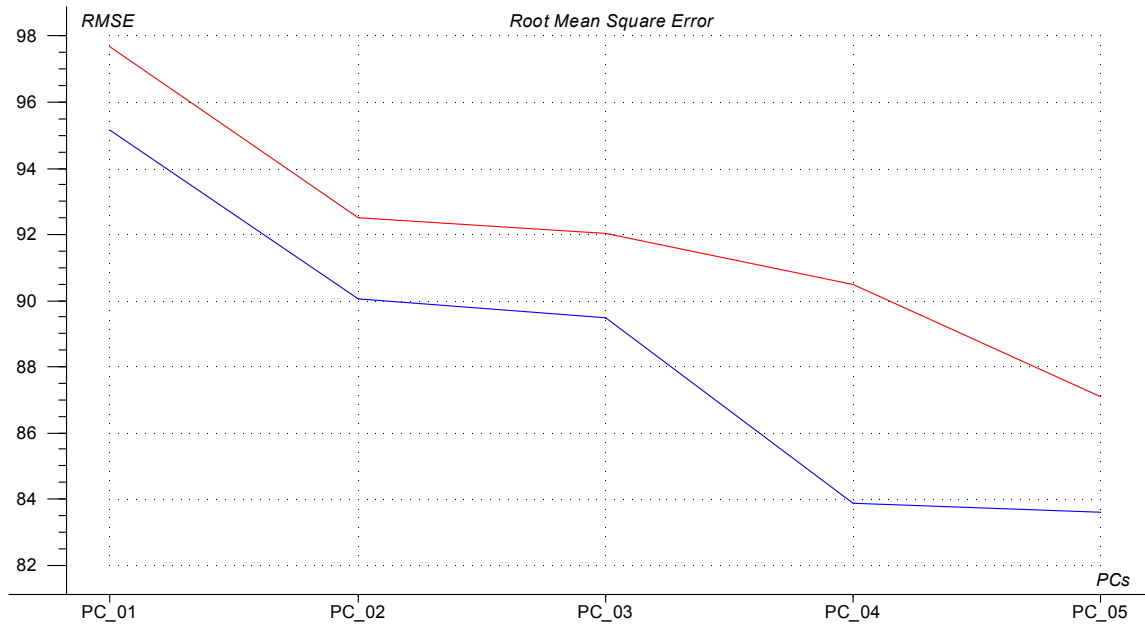


Figure 5.18: Root Mean Square Error (RMSE) as a function of Principal Components (5 PCs). Calibration RMSE (blue colour) = ± 83.60 stems ha^{-1} ; validation RMSE (red colour) = ± 87.09 stems ha^{-1}

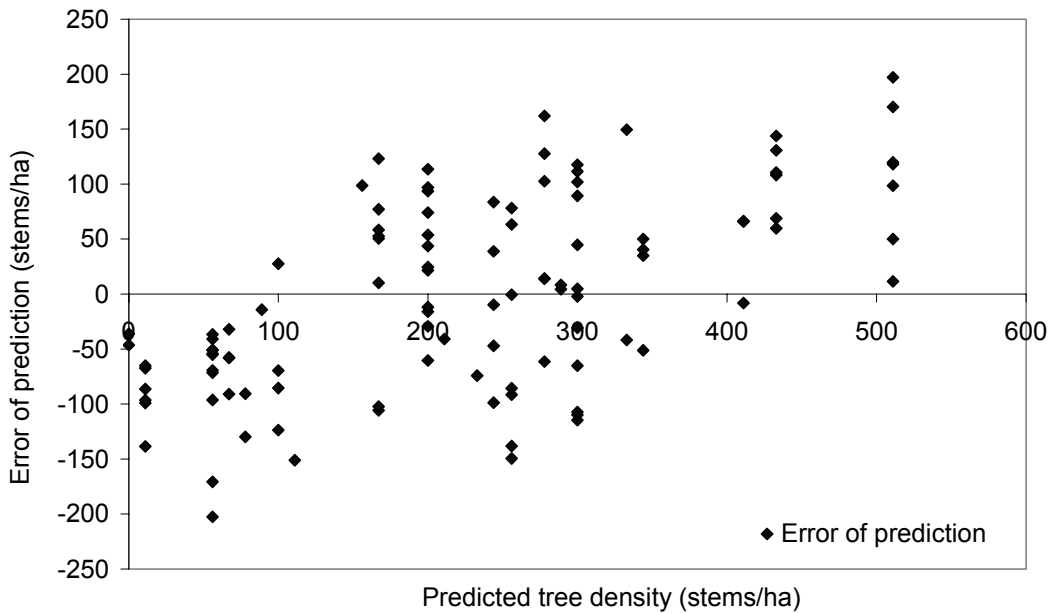


Figure 5.19: Distribution of the error of prediction as a function of the predicted tree density. Overall RMSEP of the LAI-SEB model = ± 87 stem ha^{-1} . Overestimation trend of the model in the 0-150 stem ha^{-1} range; mixed estimation trend in the 150 - 350 stem ha^{-1} range; underestimation trend beyond the limit 350 stem ha^{-1} .

In practice, the RMSEP value should be less than ± 87 stems ha^{-1} for three reasons:

- *Sampling thresholds*: According to the sampling technique (Chapter 3, section 3.3.2), trees with Diameter at breast-height (DBH) smaller than 5 cm and/or height smaller than 1.30 m were not taken into account in the process of tree stem counting in the field. Thus, the resulting field-based tree density is underestimated.
- *Aster image*: The optical remote sensing images are recorded taking into account all types of tree covers as well as grass cover. Therefore, the resulting computed vegetation indices overestimate the tree density.
- *Model calibration*: The calibration and validation of the LAI-SEB model is based on both extreme tree density variables, namely the underestimated tree density (UT) and the overestimated tree density (OT). At the end of the modeling process, the data are calibrated and adjusted to reflect at a high level the UT data. Finally, the predicted tree density is closer to the UT than to the OT.

In sum, the LAI-SEB model is an accurate and appropriate model for the prediction (estimation) of tree densities and the scaling up to the surrounding areas, because ground-truthing revealed that most of the savanna vegetation landscapes in that part of the Volta Basin of Burkina Faso are similar to the NRB.

Upscaling tree density within the Volta Basin

The spatial modeling of tree density is based on the straightforward tree density multivariate regression model LAI-SEB (Figure 5.20). The fitness and accuracy of the final map (Figure 5.21) are commented on in the next section.

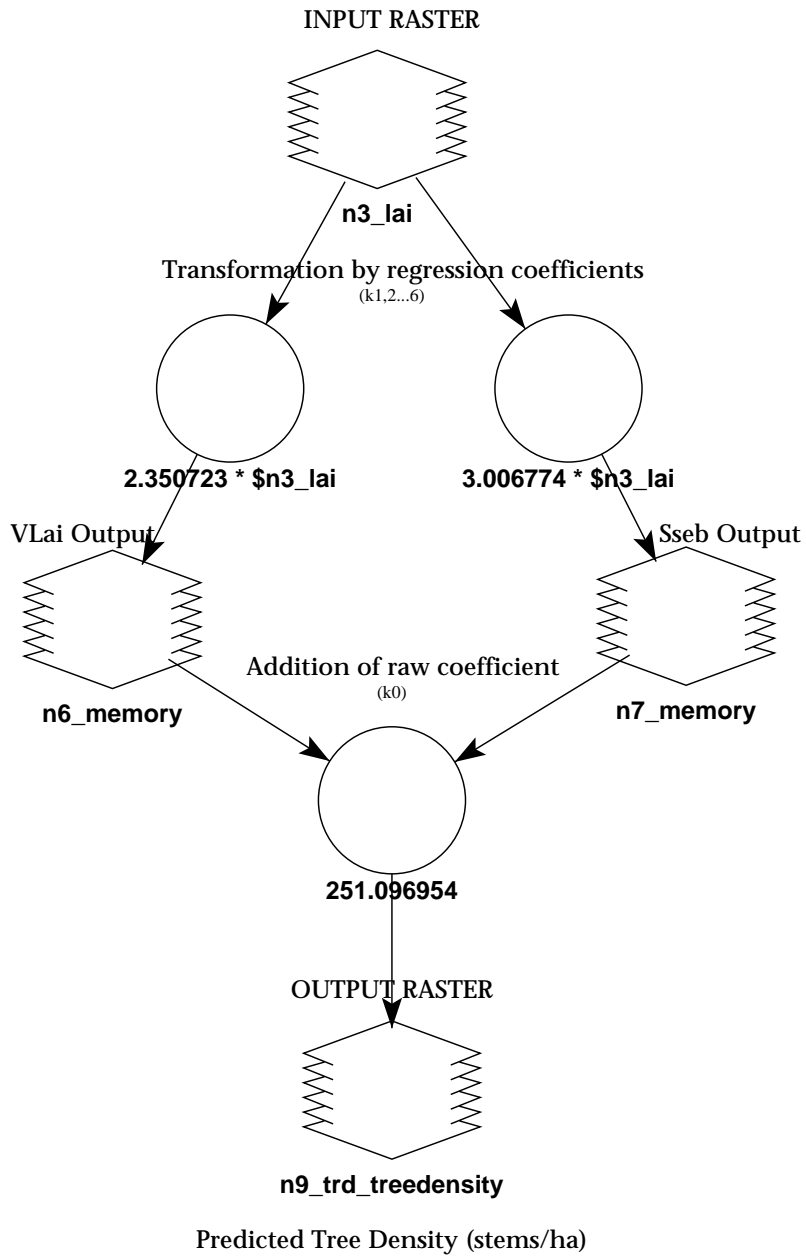


Figure 5.20: LAI-SEB model chart as designed in Erdas Imagine - Spatial Modeler

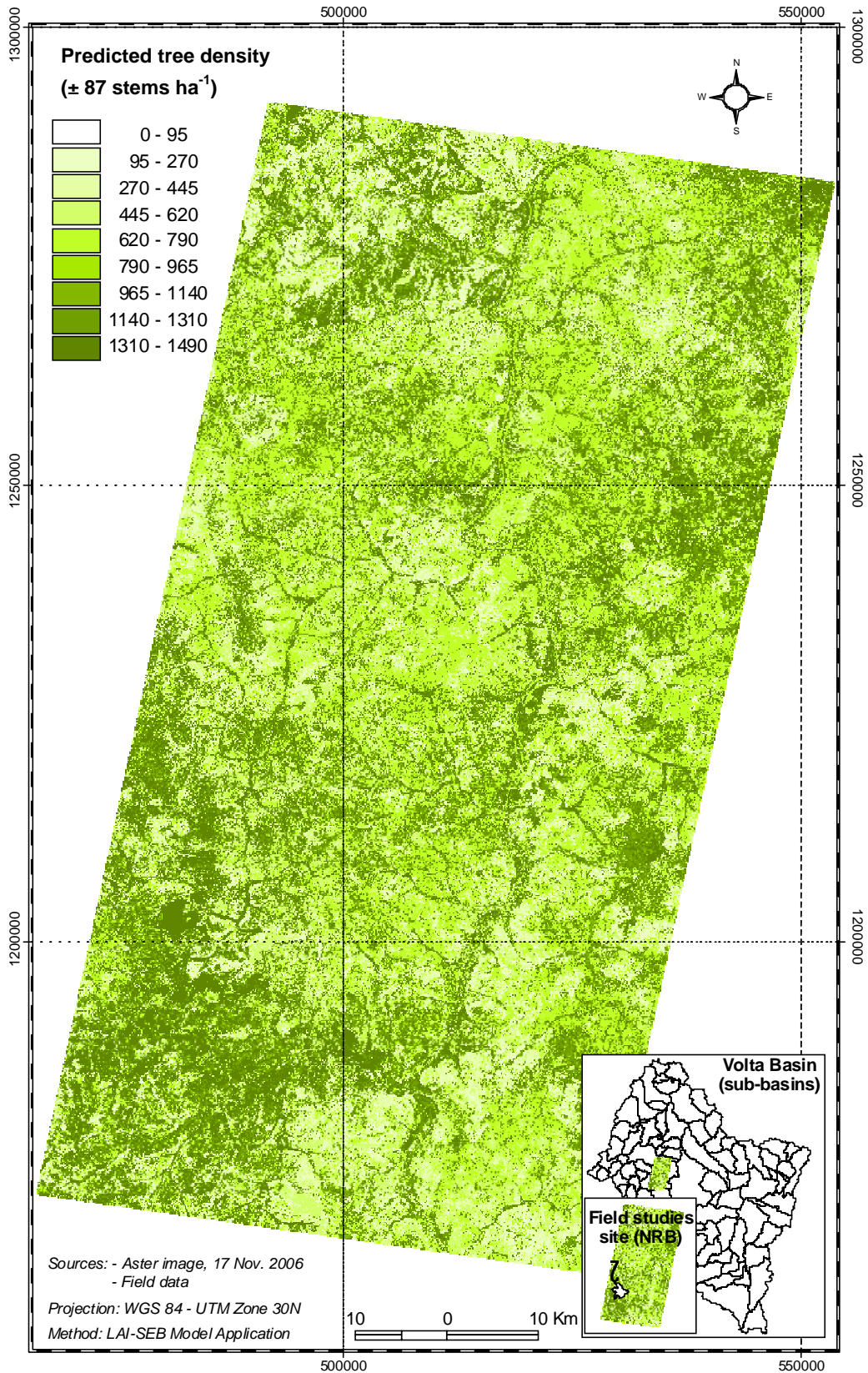


Figure 5.21: Predicted tree density map. Min.-Max. = 0 - 1486, Mean = 325; Stdev. = 259.5

Predicted (estimated) tree density map

A detailed verification of the predicted tree density map confirms the accuracy of the LAI-SEB model (Figure 5.22). A zoom to the course of the Mouhoun river (A) helps to make a clear differentiation between the open river course with 0 stem ha^{-1} and parts of the same river course covered by gallery forests with 1,400 stem ha^{-1} . The insert B shows weak or zero tree density values at human settlements (e.g., DF and DT) and on cuirass surfaces. Insert C confirms that the spatial distribution of tree density in the NRB is close to the absolute tree density presented in the respective map (Figure 5.5). But all tree density values higher than 1,490 stem ha^{-1} are also represented by this class [1310 - 1490 stem ha^{-1}] of the legend of Figure 5.21. The high values of tree density (> 1300 stem ha^{-1}) are exclusively located along the Bourgouriba River, around its oxbow lakes and in the surroundings of wet intermittent rivers.

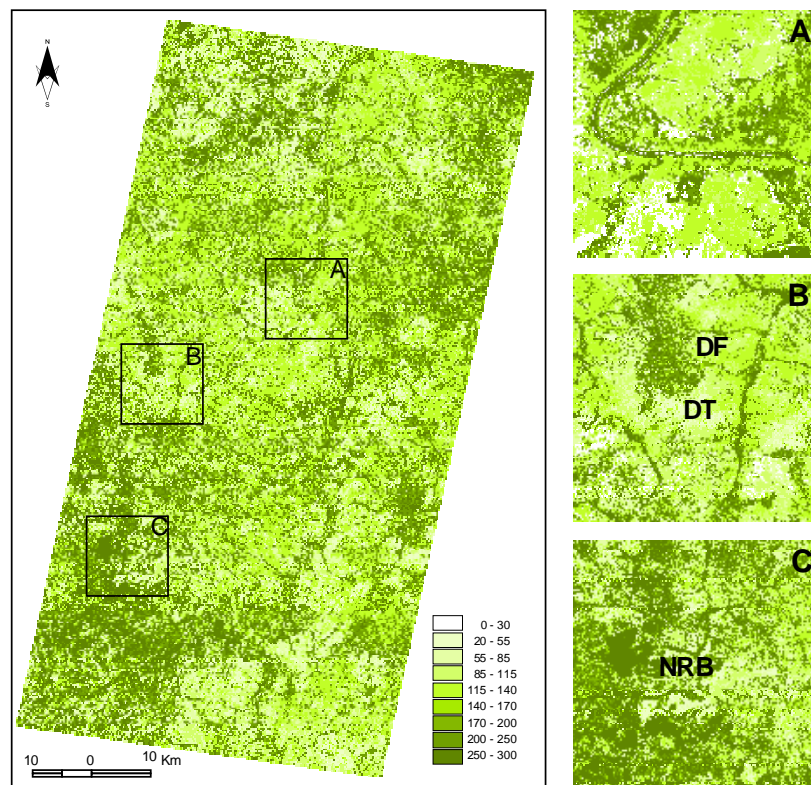


Figure 5.22: Confirmation of fitness of the predicted tree density output to ground-truthing. Insert A shows the clear course of Mouhoun River; B shows two settlements (DF = Dreyer Foundation, DT = Dano Town) and C covers the NRB.

The overall relative tree density map (Figure 5.22) presents a general view of the sparse tree density, which is prevailing in that semi-arid area, with some dense spots distributed according to environmental parameters, such as wet river beds, dams, and clay or litter soils.

Testing the LAI-SEB model

The test of the LAI-SEB model consisted of predicting the spatial distribution by tree DBH and tree crown cover densities. These two products can be useful inputs for the estimation and upscaling for whole-tree water use. The accuracy of the spatial distribution outputs of the tree water use will closely depend on one of these inputs, the one which will be chosen for its high correlation with tree sap flow data. Predicted total DBH and crown cover outputs are computed by means of the modified LAI-SEB model (Figure 5.26).

Tree DBH spatial distribution

The scaling up of tree DBH is based on the predicted tree density outputs (Figure 5.21) because of the high correlation between both variables ($r = 0.91$). The results of the regression analysis (Figure 5.23) show good accuracy of the predicted tree DBH spatial distribution map. The error of prediction, which is $\pm 68.9 \text{ cm} / 900 \text{ m}^2$ (i.e., ± 3 tree stems/quadrat), can be deemed trivial, even when it is increased by the RMSEP (= 8 stems/pixel) of the relative tree density.

Tree crown cover spatial distribution

The correlation between tree density and crown cover ($r = 0.56$) is lower than the correlation between total DBH and crown cover ($r = 0.78$) (Figure 5.24). Therefore, the predicted crown cover outputs are processed on the basis of the total DBH outputs (Figure 5.27). Similar to its reference input map (Total DBH), the crown cover map has good accuracy with an error of prediction of 7 % (i.e., ± 3 tree stems/quadrat) increased by RMSEP of both relative tree density and DBH.

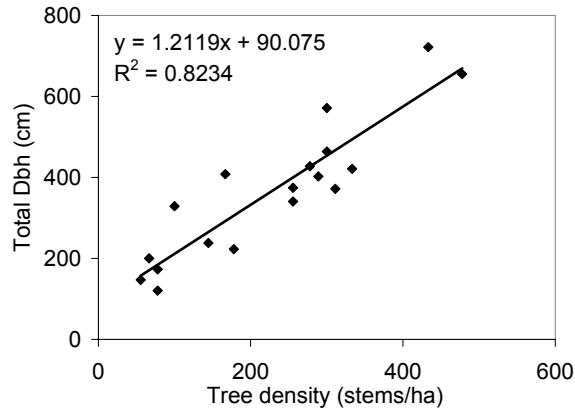


Figure 5.23: Total DBH prediction. Regression analysis variables = X-Tree density and Y-Total DBH; error of prediction ± 68.90 cm (i.e., ± 3.28 tree stems/quadrat).

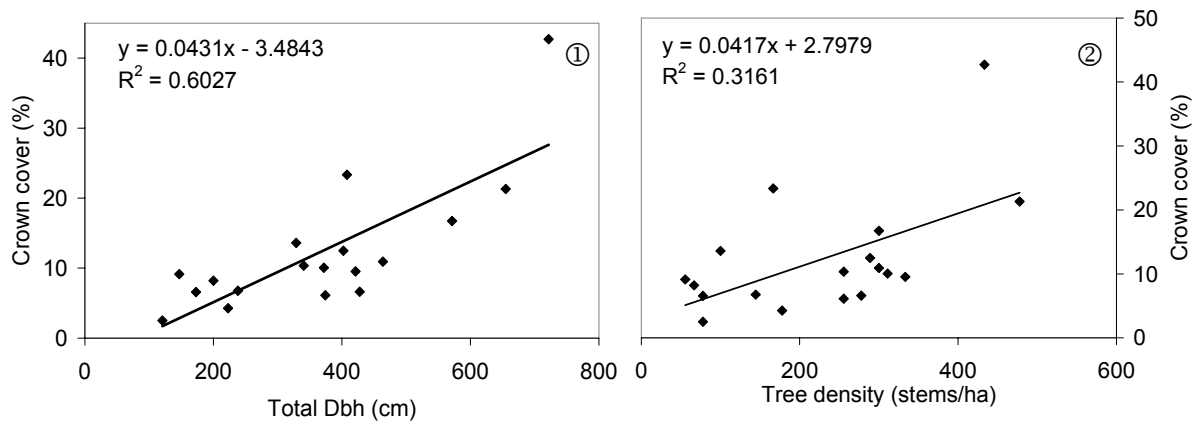


Figure 5.24: Crown cover prediction. Regression analysis variables = Tree density, Total DBH and Crown cover. Insert 1: X-Tree density and Y-Crown cover; insert 2: X-Total DBH and Y-Crown cover.

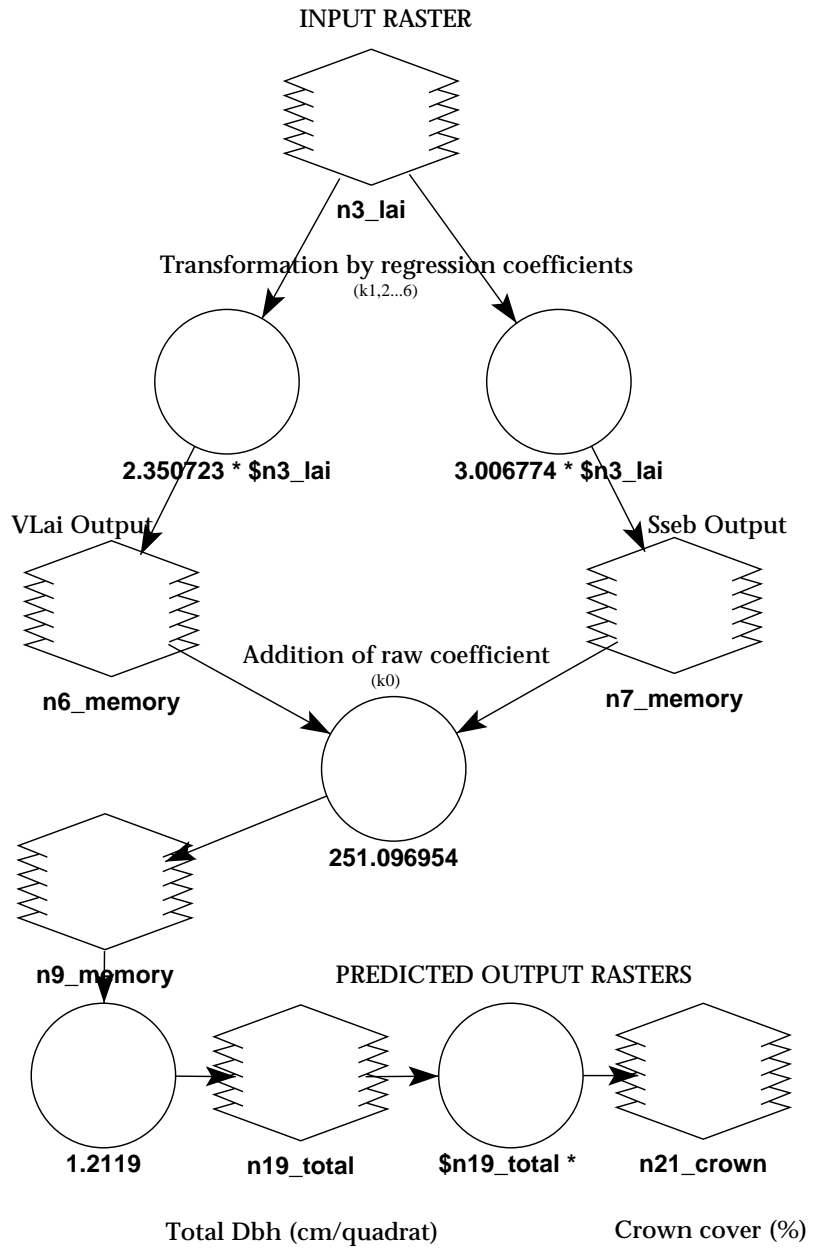


Figure 5.26: Modified LAI-SEB model chart for total DBH and crown cover prediction

Tree density prediction by the LAI-SEB model

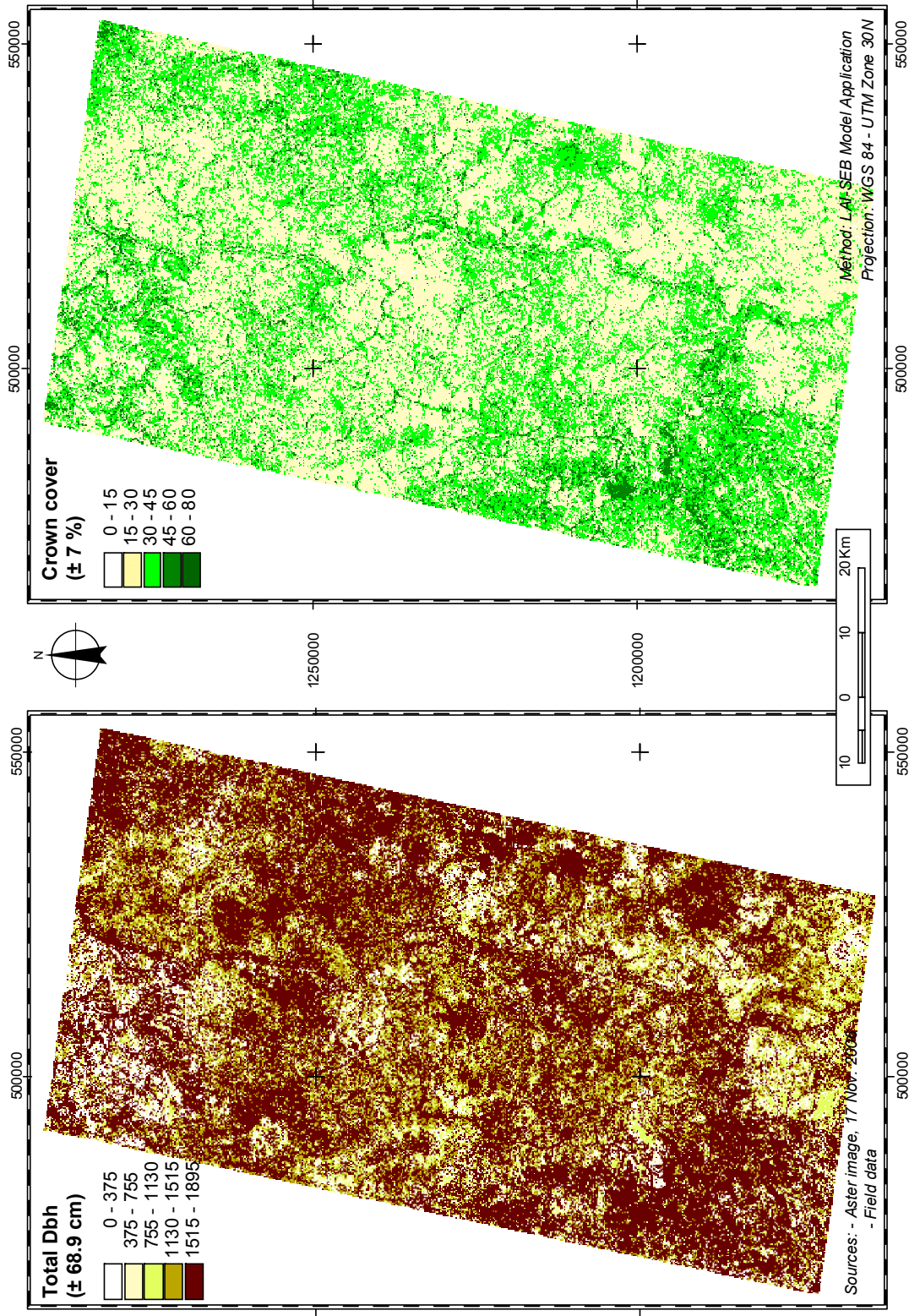


Figure 5.27: Comparison between crown cover and total DBH outputs. Crown cover: Min.-Max. = 0-77; Mean = 16.9; Stdev. = 13.5. Total DBH: Min.-Max. = 0-1891.16; Mean = 460.3; Stdev. = 344.5

5.4 Conclusions

The estimate of the mean tree density in the nature reserve of Bontioli is 331 (± 4) stem ha^{-1} , which is to some extent the same according to the savanna physiognomy and phytosociology. Additional tree density estimate methods, namely LAI-2000 and hemispherical photography, confirm the tree density level of the reserve. Furthermore, these reveal the importance of grass covers in tree density estimates from optical remote sensing imagery. In the rainy season, relative tree density is strongly influenced by high grass cover.

As a whole, trees of the NRB are not very high. Large proportions of tree heights (42.2 %) are in the 3.5 m - 6.5 m range. Few trees (2.8 %) are higher than 16 m but not more than 22 m, because tree heights are leveled down by anthropogenic disturbances: bushfires, woodcutting, previous human settlements in the reserve. The results concerning vegetation density and tree height confirm those of Fontès and Guinko (1995), who mapped the dynamics of the entire vegetation cover of the country.

The comparison between the absolute and relative mean tree densities confirms the reliability of the multivariate regression model LAI-SEB in scaling up tree density over semi-arid regions of West Africa, in conjunction with powerful optical remote sensing techniques (Figure 6.20). Even though the Aster image of 30 m resolution (Nov. 2006) was from the wrong season, which might be seen at first sight as handicap, the LAI-SEB model shows good performance. It yields good fitness to the training data sets ($r = 0.80$), very low bias (-0.24) in the validation set, a good estimation of the tree density ($r = 0.78$) (though a slight overestimation or underestimation may exist), and relative low error of prediction of ± 87 stem ha^{-1} , i.e., ± 8 trees per pixel.

Despite some limitations, the straightforward LAI-SEB model appears to be a useful adapted tool for estimating tree density in semi-arid lands of West Africa. Contributions based on high resolution spatial imagery supplied by providers like Ikonos and QuickBird, and on appropriate adjusted vegetation indexes may improve the performance of the model in the future for highly dense savannas and forest landscapes.

Finally, the model can be used to map validated large-scale (1) tree density by stem count (Figure 5.5), (2) tree density by DBH estimates, and (3) tree density by crown cover estimates (Figure 5.27). One of those outputs will be used in the final

chapter of this thesis, in conjunction with the final products of the next chapter, to estimate the dynamics and the contribution of vegetation cover to water balance, and to analyze the local climate variation as a contribution to the understanding of global change.

6 LAND USE AND LAND COVER CHANGE DETECTION

6.1 Introduction

The terms “land use” and “land cover”, which are not synonymous, are often improperly used (Briassoulis 2000; FAO 1998; Michener et al. 1994; Young 1998). Therefore, it is necessary to define them for a common understanding of their use in this study. “Land use” is understood to be “the arrangements, activities and inputs people undertake in a certain land cover type to produce, change or maintain it (FAO 1998, p. 34). Several definitions converge on that sense (Skole 1994; Turner et al. 1995, etc.). On the other hand, the term “land cover” is defined by FAO (1998, p. 31) as being “the observed (bio)physical cover on the earth’s surface”, which thus excludes the concept of “human structure” advocated by Moser (1996) in his definition of “land cover”. In the context of this study, “land cover” is more related to “vegetation cover”. Thus, “land cover change detection” should be similar to “vegetation cover conversion detection” (e.g., detection of change from tree cover to grass cover or bare soil), where “change detection” is defined by Singh (1989) as the process of identifying differences in the state of an object or phenomenon by observing it at different times.

In practice, the importance of land use and land cover knowledge resides in its usefulness for planning and management activities, and in its use for modeling and understanding the earth as a system (Lillesand et al. 2004). Several authors have referred to remote sensing techniques to assess land use and land cover changes (Haertel et al. 2004; Lambin and Strahler 1994; Laneve and Castronuovo 2005; Mas 1999; Petit et al. 2001; Salami et al. 1999; Schmidt and Gitelson 2000; Serra et al. 2003; Townshend and Justice 1995; Woodcock et al. 2001; Xiuwan 2002)

The main concern of this part of the study is to obtain quantitative rates on vegetation cover conversion, which are needed to analyze climate change at local and regional scale. This is because changes in land cover are one of the most important sources of global environment change and have profound implications for ecosystems, biogeochemical fluxes and climate (Townshend et al. 1993; Pontius and Malizia 2004). Hence, to achieve this goal, two major points are addressed, namely LULC assessment by SVM techniques and change detection processing through image differencing method.

6.2 Materials and methods

6.2.1 Choice of multi-temporal and multi-sensor images

Four satellite scenes covering the period from October 1986 to November 2006 were processed (Table 6.1). Two of them produced by the platforms Landsat 7 and Aster were from the dry season (November - April), the others were from the rainy season (September - November).

Table 6.1: Satellite images used for vegetation cover dynamics analysis. The time series varies between 1 and 13 years.

Platform sensor	Scene	Date Time	Description
Landsat-5 TM	P196-R52	08 Oct. 1986 09:52:28	7 bands; Pixel size = 28.5m; Sun elevation = 54.53; Sun azimuth = 116.92
Landsat-7 ETM+	P196-R52	20 Oct. 1999 09:52:28	7 bands, 1 panchro; Pixel sizes = 28.5, 57, 14.5m; Sun elevation = 58.20; Sun azimuth = 132.46
Landsat-7 ETM+	P196-R52	07 Nov. 2000	7 bands, 1 panchro; Pixel sizes = 28.5, 57, 14.5m; Sun elevation = 53.61; Sun azimuth = 139.66
ASTER	AST_L1B_00311 242006104945_2 0061221134014_ 14047	17 Nov. 2006 10:43:25	13 bands, 1 panchro; Pixel sizes = 28.5, 57, 14.5m; Sun elevation = 54.67; Sun azimuth = 148.88

6.2.2 Satellite image pre-processing

The satellite images were processed according to remote sensing standard methods and techniques, namely geometric corrections (for inherent system effects like satellite location and orientation), image enhancement (histogram equalization, tasseled cap, and noise reduction), transformation and interpretation. (Chapter 4, section 4.2.4).

6.2.3 Mapping LULC using the SVM technique

The SVM (Support Vector Machine) algorithm was used to map LULC. The SVM was introduced by Boser et al. (1992) and developed by Vapnik (1995, 1998). This is a new generation of methods for classification and regression problems (Arora and Varshney 2004), and is widely used for its performance. Its Structural Risk Minimization (SRM) principle (aiming at minimizing the upper bound on the expected error over the whole dataset) is superior to the Empirical Risk Minimization (ERM) principle (aiming at

minimizing the training error) employed by conventional neural networks (Gunn et al.1997).

As Canty (2006) elaborated, the SVM is used in remote sensing classification to solve the problem of two classes that are both linearly and non-linearly inseparable by choosing appropriate non-linear kernel functions (Figure 6.1). The main focus of SVM is to find an optimal hyperplane to separate two classes with a maximal margin (Luo et al. 2006). Though the SVM has the disadvantage that it is designed for two-class problems and is not able to model posterior class membership probabilities, it has been demonstrated that it delivers good results in pattern recognition (Canty 2006; Luo et al. 2006).

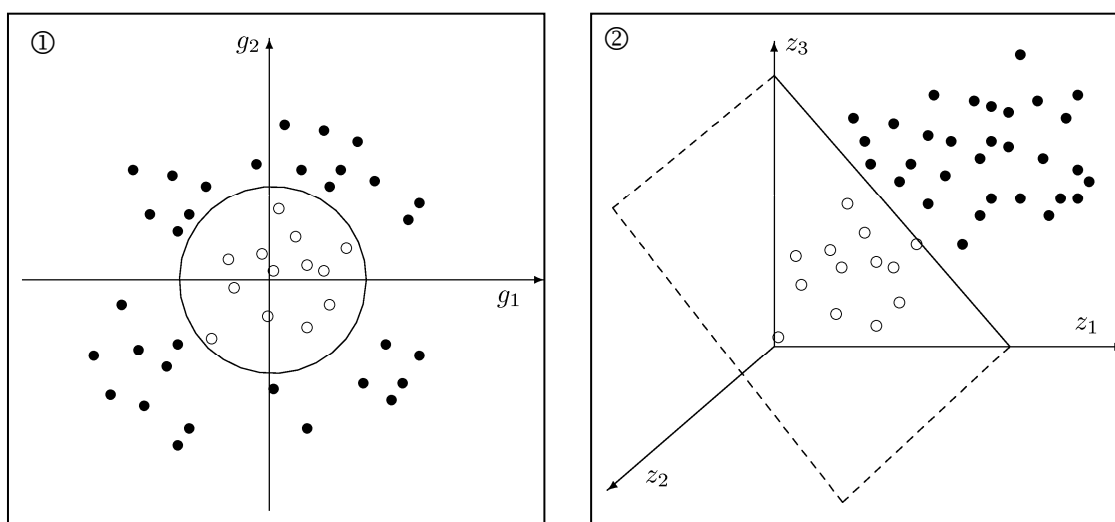


Figure 6.1: SVM Technique. Insert 1 shows two classes which are not linearly separable classes in the two-dimensional space of observations. In insert 2, the classes of insert 1 become linearly separable in a three-dimensional, non-linear feature space (Canty 2006, p. 187).

6.2.4 Change detection method

So far, several methods have been developed to address change detection, namely post-classification comparison, image differencing, radiometric normalization and multivariate alteration detection methods. The image differencing was used in this section in view of its good performance.

Multi-temporal and multi-sensor satellite scenes were used to quantitatively detect changes in the NRB vegetation cover from 1986 to 2006. The image differencing

technique was applied because it is the most widely used change detection method in the algebra-based category (Lu et al. 2004). It consists of creating an image by subtracting the first-date image from the second-date image of the same area, pixel by pixel. This operation results in an either positive or negative pixel value where change has occurred. Zero values indicate parcels where no change has occurred. The method is relatively simple, straightforward, easy to implement and interpret, but cannot provide complete matrices of change information and has the disadvantage of selection of suitable thresholds and image bands or vegetation indices to identify the changed areas (Lu et al. 2004).

In resolution of the constraints mentioned above, the current vegetation cover change detection is based on visible red band image differencing, referring to the experiences of Pilon et al. (1988) and Chavez and Mackinnon (1994), who concluded that red band image differencing provides good and accurate vegetation change detection outputs in arid and semi-arid areas in northwestern Nigeria (West Africa) and southwestern United States of America. The suitable threshold was iteratively chosen between 10 and 20 % to detect pixel brightness change and no-change. Finally, a change detection error matrix was generated to assess the overall accuracy assessment of the change detection maps. In practice, that error matrix is simplified into an increase/decrease error matrix (Congalton and Green 1999).

6.3 Results and discussions

6.3.1 Accuracy assessment of the change detection products

It is difficult to establish accuracy of change detection maps derived from satellite images taken in the past. How can increases or decreases in past land cover be confirmed when reference ground-truth data are not available? In consideration of this situation, the decision was taken only to establish the accuracy of the change detection map only over the period 2000 - 2006, for which reference ground-truth data exist. As the change detection technique is the same for the three maps of figure 6.2, we assume that the overall accuracy value of the most recent map (Figure 6.2, insert 3) is applicable to the other maps.

The overall accuracy of the change detection classification map (2000 - 2006) was 60.2 %. This accuracy is acceptable to the extent that the land cover change is

processed on the basis of the remotely sensed visible red band (band 3) which places limits on change detection. In this band it is easy to recognize land cover decrease patterns related to clearcutting, farms and bushfires. In contrast, it is complicated to detect change due to increase in spectral values of vegetation cover related to chlorophyll content fluctuation or plant activities. To substantiate this point, Tables 6.2 and 6.3 report the error matrix and the accuracy totals showing high accuracy values for decrease classes (82.6 and 100 %), whereas the accuracy values for increase classes are low (40.6 and 60.6 %), affecting the overall accuracy value.

Table 6.2: Error matrix of the change detection. The letters are defined in table 6.3

Classified Data	A	B	C	D	E	F	Total
A	56	0	0	0	0	0	56
B	0	1	0	0	0	0	1
C	0	1	19	0	2	1	23
D	0	0	0	0	0	0	0
E	1	7	31	0	58	46	143
F	1	1	1	0	10	20	33
Total	58	10	51	0	70	67	256

Table 6.3: Accuracy totals. Overall classification accuracy = 60.16 %

Class name	Reference totals	Classified totals	Number correct	Producer accuracy	User accuracy
A = Background	58	56	56	---	---
B = High decrease	10	1	1	10.0 %	100.0 %
C = Medium decrease	51	23	19	37.3 %	82.6 %
D = Unchanged	0	0	0	---	---
E = Medium Increase	70	143	58	82.9 %	40.6 %
F = High Increase	67	33	20	29.9 %	60.6 %
Totals	256	256	154		

6.3.2 Analyzing land cover change outputs

From 1986 to 1990, land cover change occurred mostly due to vegetation cover decrease over the entire satellite image (mean pixel value = -1.11). High changes occurred in the south of the scene, particularly in the surroundings of the NRB where hotspots of decrease can be observed (Figure 6.2). In a one-year period (1999 - 2000), the decrease in vegetation cover was more significant (mean pixel value = -15.4 %). Particular zones of high decrease can be observed along river beds and in densely

vegetated areas, whereas the center and eastern parts of the scene show increases in vegetation cover.

Vegetation cover highly increased between the years 2000 and 2006, as the mean pixel value increases to 18.2. Remarkable spots of increase occur in densely vegetated areas and in wetlands. As a whole, landscapes are greener in the southern and eastern parts of the area of investigation (Figure 6.2).

6.3.3 Interpreting the changes

The remotely sensed visible red band used for change detection processing highlights changes in vegetation spectral values. In principle, negative and positive pixel values of the outputs account for vegetation cover conversion and its regeneration. But in reality, the ground-truth yields different results from one year to another or from one season to the next. Thus, the three remotely sensed change bands present three different situations of vegetation dynamics linked to anthropogenic disturbances, seasonal change, annual rainfall variation and governmental surveillance measures.

Anthropogenic disturbances

In the 13-year period 1986 - 1999 (Figure 6.2, insert 1), population size increased, increasing demands for land for settlements and farming. Moreover, the woodcutting rate increased in response to population demand for firewood, charcoal, timber, etc. At first, open lands belonging to autochthons were used. But the more the population faced land-deficit pressure, the more farmers infiltrated the protected areas, namely the partial and total reserves of Bontoli where environmental conditions are more favorable (Figure 6.3). One of the most destructive habits of farmers is the setting of bushfires. Over the 13-year period, substantial parts of the vegetation cover were converted to villages, hamlets, farmlands, fallows and bare soils. The change in vegetation cover over that period was also due to erosion, which transforms fragile grasslands to bare soils.

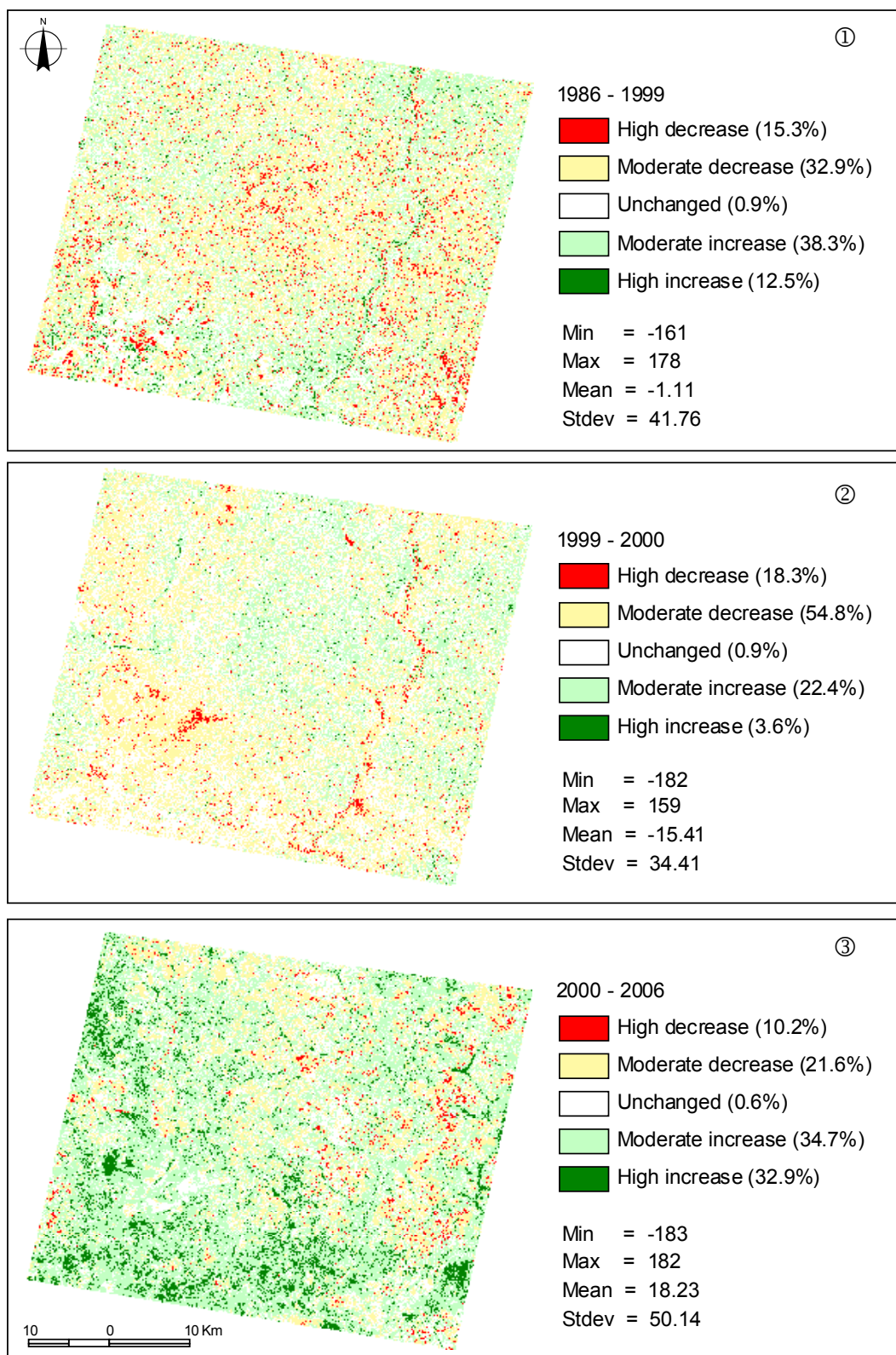


Figure 6.2: Vegetation cover change: 1986 - 2006. Negative and positive pixel values, respectively account for decrease and increase in brightness over time. Overall accuracy = 60.2 %

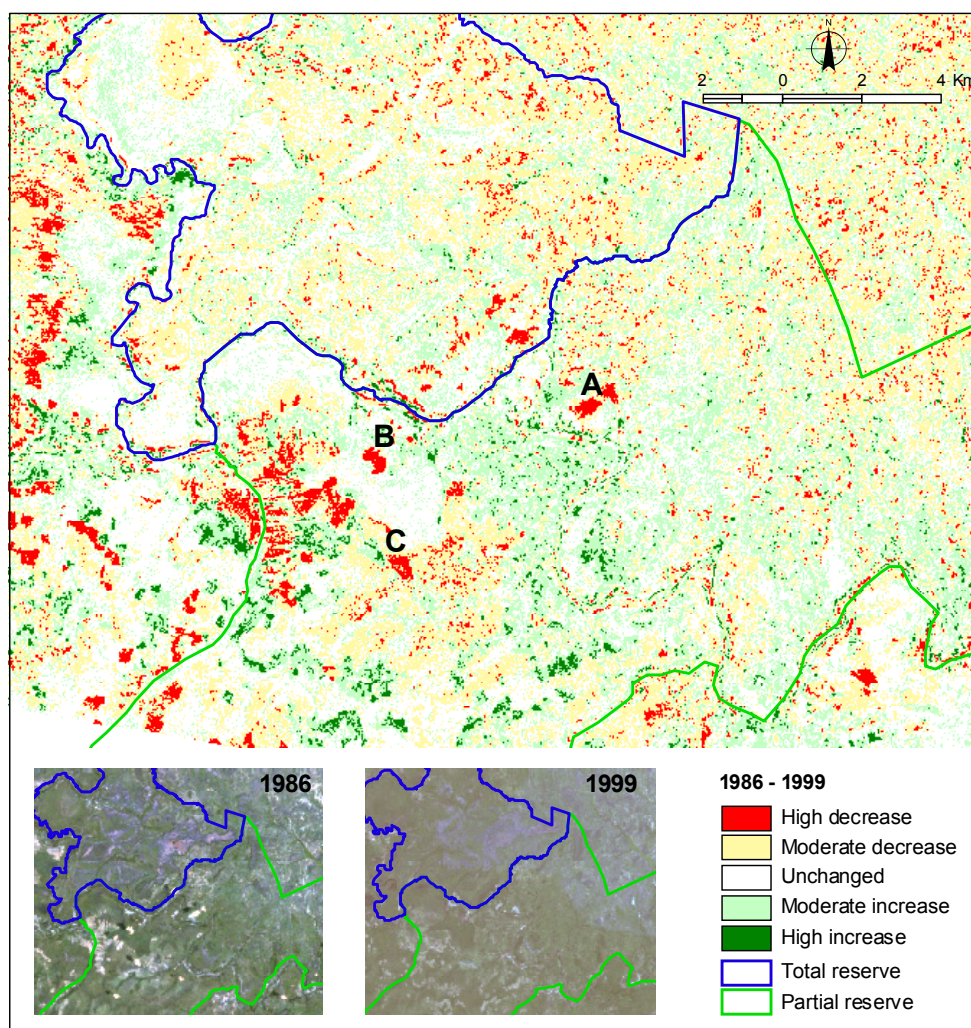


Figure 6.3: Detailed vegetation cover conversion map. This is a zoom to the southern part of Insert 1, Figure 6.2. The true-colour images below present land cover situation, respectively in 1986 and 1999. The image above is the direct result of subtraction of the 1986-image from the 1999-image. A, B and C are changes due to cloud covers.

Seasonal fluctuation of chlorophyll

The one-year (1999 - 2000) change detection output (Figure 6.2, insert 2) illustrates the seasonal variation in the spectral response of the vegetation cover due to chlorophyll content fluctuation. The earlier October 1999 image (wet period) shows the situation when vegetation is healthy and grows vigorously because of availability of sufficient water, whereas the later November 2000 image (dry period) shows a decreasing vegetation activity reflected in decreasing chlorophyll content due to increasing water-deficit in the fall dry season. At that time, trees loose their leaves and reduce their

flowering activities, and grass covers dry out completely, significantly changing landscapes (Chapter 5, section 5.3.2). This is why the decrease is high in wet areas covered by dense grass. Therefore, the high rate of decrease (mean = -15.4) observed over that period of time is more due to plant activity dynamics than to vegetation cover conversion.

Tree regeneration and surveillance activities

The change analysis period 2000-2006 (Figure 6.2, insert 3), is characterized by a general increase in vegetation cover. The ground-truth campaigns undertaken in April-June and October 2005, and in April-June 2006 confirm that tree regeneration was intensive, particularly throughout the NRB, and densities of saplings and seedlings were high. Moreover, the Burkinabe government decided to intensify monitoring of protected areas. Hence, farmers and poachers were informed and sensitized to vacate protected areas and help the authorities to protect these lands.

In addition, in 2006 annual rainfall increases compared to the previous year. The increase in spectral response of the vegetation in the dry seasons (Nov. 2000 and Nov. 2006) is likely due to an increase in vegetative growth. Unfortunately, vegetation regeneration is slowed down by bushfires, which are still one of the farmers' practices.

6.3.4 LULC output

The results of the LULC map achieved by means of the SVM technique are not different from the one achieved so far. Therefore, the map of the vegetation cover classification (Figure 4.9, Chapter 4, section 4.3.4) is kept as a reference for LULC classification of the sub-basin covering the NRB and similar areas.

The LULC classes of the vegetation classification map can be used as a basis Area Of Interest (AOI) or Region Of Interest (ROI) to derive large-scale (Landsat image coverage or sub-basin scale) LULC classification products using the SVM method. This can be achieved by means of the software imageSVM available at <ftp://geo.hu-berlin.de> (Janz et al. 2007).

6.5 Conclusions

The results of the land cover change processing based on the remotely sensed visible red band allow recognition of vegetation cover changes in terms of increase or decrease. In reality, it is easy to detect woodcutting, farms and bushfires patterns, whereas it is very difficult to determine change due to an increase in spectral values of vegetation cover related to chlorophyll content or fluctuation of plant activities. The consequence of this is the relatively low but acceptable overall accuracy of the change detection classification (60.2 %).

Three land cover changes can be observed:

- Decrease in land cover from 1986 to 1999 due to anthropogenic disturbances;
- Decrease in vegetation cover from 1999 to 2000 because of the seasonal variation in the spectral responses of vegetation cover due to chlorophyll content fluctuation.
- Increase in vegetation cover over six years (2000 - 2006), related to intense tree regeneration due to the increasing governmental protection of the reserve areas.

As such, the land use and land cover analysis cannot generate quantitative vegetation conversion rates useful to quantify the effects of vegetation cover conversion or regeneration in relation to local climate variation. However, the next chapter provides results which help assess the importance of vegetation cover dynamics in climate change.

7 CONTRIBUTION OF TREES TO WATER BALANCE

7.1 Introduction

Water is essential to life, be it biotic or abiotic. Unfortunately, the water cycle in nature is becoming seriously disturbed by increasing anthropogenic activities, which are endangering water availability, livelihood, and food security that are closely linked to rainfall. In dry areas, over one billion people are threatened by water scarcity (Oweis 2006). Furthermore, in the coming fifty years, the downward trend in rainfall and increasing rainfall variability in drylands will be aggravated by the global climate change.

The general concern of environmental research is to understand the whole change process and assess and predict its likely impacts on changes in the water balance, and develop appropriate responses. Analyzing the role of vegetation in the water balance is important because “the decrease in rainfall may at least partly be attributed to the change of surface water balance induced by a change in the surface vegetation condition” (Yasunari 2002b, p.129). The methods available for a quantitative measurement of each term of the water balance have proved extremely difficult and challenging due to the complex and sophisticated instrumentation involved (Beaumont 1989; Beven and O’Connell 1983; Kane and Yang 2004; Walker and Smith 1997).

This chapter focuses on three aspects: (1) analysis of the influence of weather conditions on the whole-tree water use during the course of a day and a season, (2) estimation at site-scale of the contribution of tree stands to the dynamics of the water balance on the basis of individual tree water use and actual evapotranspiration, and (3) determination of the effect of vegetation cover change on the water balance of the ecosystem in terms of tree transpiration flux variation.

7.2 Materials and methods

7.2.1 Surface water balance

It is necessary to understand the water balance to forecast weather with greater certainty for longer periods, and realistically predict future climate change with the associated droughts and floods in order to minimize the loss of life and property (Kane and Yang 2004).

Definition and equation

Based on the law of conservation of mass, “the water balance equation for any natural area or water body considers the relative values of inflow, outflow and change in water storage for the area or body. Generally, the inflow comprises precipitation (P) as rainfall and snow actually received at the ground surface. The outflow refers to evaporation (E) from the surface of the water body or soil” (UNESCO 1974, p.17). Detailed explanations of inflow and outflow components are given by Beven and O’Connell (1983), Oyediran (1983), and UNESCO (1974).

The surface water balance equation is given as follows (Beven and O’Connell 1983; UNESCO 1974):

$$P = Q + ET_a + L + \Delta S \quad (7.1)$$

where P is precipitation, Q is discharge, ET_a is actual evapotranspiration, L is loss to deep groundwater and ΔS is change in storage.

The components of that equation may be expressed as a mean depth of water over the basin or water body (mm), or as a volume of water (m^3), or in the form of flow rates ($m^3 s^{-1}$) (UNESCO 1974).

Evapotranspiration is the major component of the surface water balance. It indicates the importance of biological control by plants on water release into the atmosphere and provides the linkage between water balance and energy balance (Zhang et al. 2002). Evapotranspiration forms the major losses of water from the land surface in drylands (Beaumont 1989).

Estimation of actual evapotranspiration (ET_a)

“Evapotranspiration (ET) represents the loss of water from the Earth’s surface through the combined process of evaporation (from soil and plant surfaces) and plant transpiration” (Allen et al. 2005, p. 2).

Preference is sometimes given to estimation of ET due to the difficulties related to measurement requirements. Several measurement techniques, such as the Heat Pulse technique, the xylem Heat-Balance technique (i.e., Sap flow measurement

technique), the Bowen (1926) ratio approach, the Lysimeter technique, the Ventilated chambers (Alternative approach to lysimeter), the Evaporation domes, and the Complementary relationship approaches are experimented with satisfaction for direct measurement, but “the Eddy Correlation (*EC*) approach is scientifically the most satisfying method for measuring *ET*” (Zhang et al. 2002, p.8) because of its direct micrometeorological flux measurement method. In all of these approaches, *ET* can be calculated based on theoretical and empirical formulae.

The *EC* technique measures turbulent motions to determine the net difference in material moving between the canopy and the atmosphere (Kutzbach 2004). Its direct measurement of *ET_a* consists of measuring the fluctuations of vertical wind speed and water vapour density and then computing the correlation over a short period of time.

The latent heat flux (*LE*) data provided by the *EC* station - 200 m away from the sap flow measurement sites - is used to derive *ET_a*, because *LE* can be expressed by the product of the latent heat of evaporation *L* and the rate of evaporation *E* (Peixoto and Oort 1992). *LE* is converted to *ET_a* as follows (Monteith and Unsworth 1990):

$$ET_a = 3600 \times \frac{LE}{\lambda} \quad (mm \ h^{-1}) \quad (7.2)$$

$$\lambda = 2500300 - 2359 \times t \quad (7.3)$$

where λ is the latent heat of evaporation, and t ($^{\circ}C$) is the mean hourly air temperature.

7.2.2 Sap flow measurement by xylem Heat-Balance method

Principle and technique

The estimation of individual tree water use is based on the principle of sap flow measurement. Six sap flow measurement sites were installed in the NRB so as to cover a large number of dominant tree species according to the savanna physiognomy (Figure 3.2, Chapter 3, section 3.2.1). The choice of the dominant tree species is highlighted in Chapter 5, section 5.3.1 (Tables 5.1 and 5.2). In total, sap flow rates were measured on 17 tree species on a continuous basis from April 2005 to December 2006, with some gaps mainly due to broken-down sensors and power supply interruptions.

The description of equipment installation and sap flow measurement principles and techniques are detailed in Chapter 3, section 3.2.

Below is a listing of the tree species distribution for the different sap flow measurement sites:

- Site 1 (Loc3): *Detarium microcarpum*, *Vitellaria paradoxa*, *Terminalia laxiflora*, *Pterocarpus erinaceus*;
- Site 2 (Loc4): *Burkea africana*, *Anogeissus leiocarpus*, *Daniellia oliveri*, *Lannea microcarpa*, *Pterocarpus erinaceus*;
- Site 3 (Loc5): *Pseudoceudrela Kostchii*, *Combretum fragrans*, *Terminalia macroptera*;
- Site 4 (Loc6): *Acacia dudgeoni*, *Combretum glutinosum*, *Entada africana*, *Pterocarpus erinaceus*, *Parkia biglobosa*, *Lannea microcarpa*, *Anogeissus leiocarpus*, *Lannea acida*.
- Site 5 (Loc7): *Pseudoceudrela Kostchii*, *Combretum fragrans*, *Terminalia macroptera*,
- Site 6 (Loc8): *Combretum fragrans*, *Terminalia macroptera*, *Crossopteryx febrifuga*.

Estimation of whole-tree water uptake

Sapwood samples collected from the 17 trees species were conserved in a bottle of alcohol (ethanol, 70 %) to avoid bias in the analysis results due to drying of the samples. They were transported from the field to the laboratory for visual analysis with a microscope. The whole-tree water use rate was calculated using the equations 3.2 and 3.3. For details on sapwood sampling, sapwood area determination and sap flow calculation, refer to Chapter 3, section 3.2.3.

The analysis of sap flow patterns was done in conjunction with data provided by both the microclimate and Eddy Correlation stations (10°51'55''N, 3°04'21''W) installed 370 m from the sap flow measurement sites (10°51'54''N, 3°04'37''W). The distance between the weather stations was 80m. Parameters of concern are air temperature, air pressure, relative humidity, soil heat flux, soil temperature, wind speed, rainfall, latent heat flux, and sensible heat flux.

Tree stands contribution to water balance

As only 24 % (17/71) of the tree species of the NRB were considered for sap flow measurements, sap flow rates of other trees were estimated from the correlation between DBH and sap flow, using the linear regression as follows:

$$sf_e = a_1 + b_1 \times Dbh_m \quad (7.4)$$

where a_1 is a constant, b_1 is a regression coefficient (slop), sf_e is sap flow rate extrapolated, and Dbh_m is tree DBH measured in the field.

Then the estimation of tree stand transpiration (T_p) in a given plot is obtained by dividing the total sap flow values of tree stands in that plot by the plot surface as follows:

$$T_p = \frac{\sum sf + \sum sf_e}{900 \text{ m}^2} \quad (7.5)$$

Once the transpiration rate is known at the plot level, a correlation is established between plot transpiration and plot total DBH as follows:

$$T_p = a_2 + b_2 \times Dbh_p \quad (7.6)$$

where a_2 is a constant, b_2 is a regression coefficient (slop), T_p is the transpiration rate at plot level, and Dbh_p is the total DBH of the same plot.

Finally, the predicted transpiration map is obtained by applying equation 7.6 to the remotely sensed image products, i.e., the predicted DBH band resulted from the multivariate regression analysis in Chapter 5, section 5.3.3 (Figure 5.27), in the spatial modeler of the software Erdas (or Envi).

7.2.3 Impacts of vegetation cover change on water balance

In principle, once tree stand transpiration is estimated, the determination of the potential impacts of vegetation cover change on the water balance can be done using the LULCC products of Chapter 6. These data are coupled with *in-situ* Eddy Correlation and microclimatic data.

7.3 Results and discussion

7.3.1 Whole-tree water use

Quantitative estimation of whole-tree water use

Contrary to initial plans, whole-tree sap flow rates could not be estimated over the entire period from 15 April 2005 to 30 December 2006 because of gaps in the data records. Instead, the time periods April-June (2005 and 2006) were chosen for the calculation of sap flow rates for two reasons: (1) this period covers the dry and rainy seasons, and (2) the sap flow measurement sensors operated all together without anomalies and interruption during those periods in 2005 and 2006.

The estimated water use rates on a one-minute basis of the dominant tree species indicate that average daily tree water use ranged from 10.1 kg day⁻¹ for *Crossopteryx febrifuga* to 492.1 kg day⁻¹ for *Pterocarpus erinaceus* (Table 7.1). A comparison of the species water use, on the basis of the normalized mean tree water use per centimeter DBH, reveals in descending order 10 species as the major consumer of water (in kg day⁻¹ cm⁻¹): *Detarium microcarpum* (4.3), *Pterocarpus erinaceus* (4.1), *Parkia biglobosa* (3.1), *Lannea microcarpa* (2.4), *Daniellia oliveri* (2.2), *Burkea africana* (2.2), *Lanea acida* (1.9), *Terminalia laxiflora* (1.8), *Terminalia macroptera* (1.8), and *Combretum fragrans* (1.7).

As these tree species have been previously described (Chapter 4, section 4.3.1), the emphasis here is on their relationship with sap flow rates. It appears that large trees with DBH varying between the 20.3 – 119 cm range (75.9 %), have high rates of water use (22.5 – 492 kg day⁻¹). The correlation coefficient indicates that a very strong relationship exists between tree water use rates and DBH ($r = 0.95$), whereas the correlations between tree water use and crown cover ($r = 0.74$) and tree height ($r = 0.70$) are substantially weaker. These results confirm reports by Granier et al. (2003), who suggest that “sap flow is higher in large trees than in small trees”. They state that

maximum sap flow rates vary between 10 kg day⁻¹ for trees of 12 cm DBH and 400 kg day⁻¹ for trees of 60 cm DBH, whereas in young stands, the daily sap flow rates were in the 2 – 25 kg day⁻¹ range.

Overview of other tree water use rates

A comparison was made between the present results with those derived from 52 studies compiled in the review of whole-tree water use of Wullschleger et al. (1998, p. 501). It becomes clear that trees in the NRB, which are not high (max. height = 19 m; average height = 9 m), use high rates of water when compared with those in other studies, where trees average 21 m in height and have water use rates between 10 and 200 kg day⁻¹. The authors also reported high rates of water use for certain trees species, namely *Ocotea sp.* (396 kg day⁻¹), *Quercus petraea* (400 kg day⁻¹), *Pseudotsuga menziesii* (530 kg day⁻¹), and *Eperua purpurea* (1,180 kg day⁻¹).

The scope of these comparisons is neither to review the methods of estimations nor to analyze the environmental locations or conditions of the trees, but to have an idea of existing whole-tree water use rates worldwide. Further details on authors and techniques of those studies can be found in the paper of Wullschleger et al. (1998).

Table 7.1: Average daily whole-tree water use rates. Mean water use = 86.94 kg day⁻¹ per tree. Mean error of estimation is ± 9.81 %. Estimations based on the time periods April-June 2005 and 2006.

Species name	Height (m)	Crown cover (m ²)	DBH (cm)	Sapwood area (cm ²)	Water use (kg day ⁻¹)			
					Min	Max	Mean	Stdev
Site 1								
<i>Detarium microcarpum</i>	8.5	96.4	66.0	1395.7	65.0	417.5	285.4	55.7
<i>Vitellaria paradoxa</i>	4.5	39.8	37.0	156.2	3.2	19.6	13.4	2.9
<i>Terminalia laxiflora</i>	8.0	87.9	35.0	668.4	20.7	162.9	62.7	31.2
<i>Pterocarpus erinaceus</i>	13.0	241.6	55.0	769.8	58.1	280.5	139.9	62.4
<i>Terminalia laxiflora</i>	9.0	106.0	45.0	373.1	9.4	63.0	40.9	7.7
Site 2								
<i>Burkea africana</i>	13.8	197.7	53.8	399.5	65.5	154.7	116.5	22.3
<i>Anogeissus leiocarpus</i>	18.8	215.8	67.9	947.7	77.3	281.3	206.3	42.1
<i>Daniellia oliveri</i>	12.9	111.6	33.5	1320.6	18.9	96.6	73.7	19.1
<i>Pterocarpus erinaceus</i>	19.0	246.4	119.1	1318.2	103.9	783.5	492.3	172.2
<i>Lannea microcarpa</i>	6.0	17.9	43.0	173.3	27.0	113.8	85.4	22.5

Table 7.1 (Continued)

Species name	Height (m)	Crown cover (m ²)	DBH (cm)	Sapwood area (cm ²)	Water use (kg day ⁻¹)			
					Min	Max	Mean	Stdev
Site 3								
<i>Pseudocedrela kotschyi</i>	12.0	80.9	22.4	371.9	3.3	77.7	26.3	19.6
<i>Combretum fragrans</i>	7.5	8.9	11.1	93.4	5.0	71.7	14.7	19.2
<i>Terminalia macroptera</i>	11.0	124.2	29.3	577.4	13.5	106.8	52.0	31.8
Site 4								
<i>Entada africana</i>	9.0	52.1	23.3	176.6	0.6	49.1	29.4	12.8
<i>Combretum glutinosum</i>	4.3	18.6	12.7	124.8	8.6	31.2	19.8	5.5
<i>Acacia dudgeoni</i>	4.8	23.0	12.1	92.0	1.0	26.1	12.2	5.6
<i>Pterocarpus erinaceus</i>	7.0	23.9	9.6	71.1	3.6	85.3	22.1	20.6
<i>Parkia biglobosa</i>	7.8	32.7	22.3	286.7	17.1	145.8	68.6	29.8
<i>Anogeissus leiocarpus</i>	7.3	36.5	12.0	112.2	8.4	85.9	29.4	15.6
<i>Lanea microcarpa</i>	6.6	18.8	14.8	171.4	5.2	115.9	35.4	22.7
<i>Combretum collinum</i>	6.0	23.1	22.6	70.8	3.9	34.3	19.9	7.8
<i>Lanea acida</i>	6.3	39.5	20.5	328.5	0.8	109.7	38.2	22.7
Site 5								
<i>Pseudocedrela kotschyi</i>	7.5	19.6	21.7	186.8	3.9	22.6	18.1	7.1
<i>Terminalia macroptera</i>	8.4	28.6	25.5	347.6	10.6	31.4	28.2	8.4
<i>Combretum fragrans</i>	8.3	29.3	20.3	303.2	7.5	32.1	22.5	8.8
Site 6								
<i>Terminalia macroptera</i>	6.8	54.1	21.5	316.2	29.3	28.1	28.4	17.0
<i>Crossopteryx febrifuga</i>	6.8	16.6	14.1	147.9	2.0	11.2	10.1	4.9
<i>Combretum fragrans</i>	10.8	52.3	24.4	467.4	24.9	42.8	42.5	12.7

7.3.2 Tree water use and weather conditions

Daily tree water use

General pattern of daily sap flow

Weather conditions play an important role in the regulation of whole-tree water use during the course of the day. Figure 7.1 illustrates daily tree water use pattern during a clear and stable day in the NRB, i.e., a day without rainfall, with little fluctuating wind speed and a normal increase and decrease in air temperature from the morning to the night. (Figure 7.1, insert 1).

The observation of insert 3 of Figure 7.1 shows that water use rates of these 5 trees evolve in five main steps: (1) from 23:30 hrs to 6:30 hrs rates are equal or close to zero, (2) from 6:30 hrs tree water use increases progressively up to maximum rates around 11:00 - 12:00 hrs, (3) from mid-day rates decrease until 13:10 hrs, (4) rates

increase again peaking a second time in the interval 15:00 - 16:00 hrs, and (5) from 16:00 hrs they decrease progressively to reach the lowest values at about 23:30 hrs. The water use patterns of *Vitellaria paradoxa* (Vp) and *Pterocarpus erinaceus* (Pe) are mono-modal whereas the other tree species have bi-modal water use curves.

The explanation of the daily whole-tree water use dynamics is linked to the weather conditions (inserts 1 and 2 of Figure 7.1. The variation following changing weather conditions clarifies that important factors, namely net radiation, air pressure, air temperature and relative humidity influence daily tree water uptake. The most important factor is net radiation (solar energy) that is necessary for photosynthesis. During the process of photosynthesis, trees make use of solar energy to synthesize their organic molecules, which results in the reduction of carbon dioxide into sugars. The photosynthesis and its mechanism of light absorption and energy transformation at the electron-level are explained in detail by several authors, among others, Archer and Barber (2004), Fogiel (2000), Leibl and Mathis (2004), Mathis (1992).

During the day time, the progressive increases in light, air temperature, air pressure and the decrease in relative humidity linked to the increase in net radiation stimulates tree leaves to open their stomata. Then, the “chloroplasts absorb light energy and use CO₂ and H₂O to synthesize carbohydrates” (Fogiel 2000, p.18). That process results in water vapour release into the atmosphere by transpiration and modifies the water column in the trunk. In order to maintain the equilibrium water gradient in the trunk, trees increase their water demand from the soil. They reach their maximum sap flow rates at 11:00 - 12:00 hrs and 15:00 - 16:00 hrs in response to the high flux of solar radiation. Photosynthetic activities decrease at mid-day around 12:00 - 13:00 hrs with the depression (Figure 7.1, insert 1).

The final decrease in tree sap flow rates from 16:00 hrs is due to the progressive decrease in net radiation (light). The daily variation of tree water use patterns observed in insert 3 is due to the fact that different species react differently to some sudden variations in the weather conditions.

The daily sap flow pattern described here is possible only when water is available in the soil and when the root system is not damaged. Otherwise, leaf stomata are closed to “prevent the columns of water in the xylem system of the tree from breaking and air entering the xylem elements” (Roberts et al. 2006, p. 184).

Contribution of trees to water balance

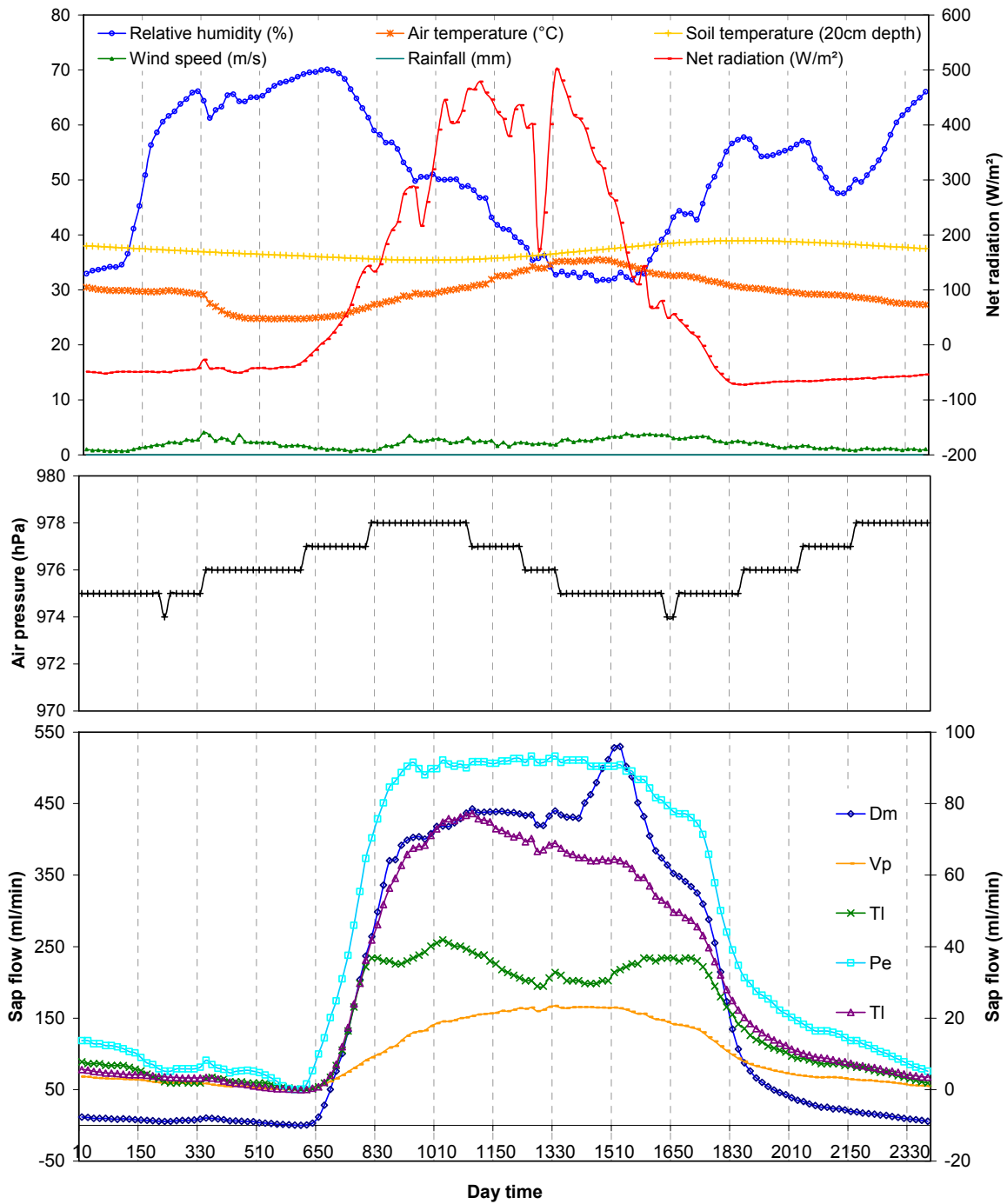


Figure 7.1: Daily whole-tree water use patterns as a function of weather conditions. Water use patterns of *Detarium microcarpum* (Dm), *Vitellaria paradoxa* (Vp), *Terminalia laxiflora* (TI) and *Pterocarpus erinaceus* (Pe) on 27 May 2005, clear and stable day. Site location: 10°51'54'' N, 3°04'37'' W. 510 means 5:10 hrs. (Climate data source: J. Szarsynski – BIOTA West Project)

Daily sap flow and seasonal rainfall

The daily sap flow rates differ depending on dry or rainy season, and on rainy or non-rainy day. Comparison of the variation in sap flow rates according to the season is done in the next section.

In general, sap flow rates are higher on non-rainy days than on rainy days. For illustration, three days in the rainy season are compared (Figure 7.3): the days 31 May and 6 June are both non-rainy days, respectively before and after the rainy day 4 June 2005. From the non-rainy day to the rainy day, the sap flow rates change significantly, decreasing from 276 kg day⁻¹ to 65 kg day⁻¹ for Dm, and from 14.2 to 3.2 kg day⁻¹ for Vp. This was due to the sudden decrease in net radiation, soil heat flux and air temperature (from 26.8 °C to 21.1 °C) as explained herein. The day after the rainfall, the sap flow rates were higher than the day before the rain, increasing to 310 kg day⁻¹ and 15.4 kg day⁻¹, respectively for Dm and Vp. This was caused by the rainfall (28.4 mm day⁻¹), which increased soil moisture and cooled down the atmosphere.

For the dry season, the pattern is similar to that of the rainy season, with the difference that the changes in sap flow rates after a rainy day (5 May 2005) are not significantly different from those before the rainy day. Sap flow rates are 306 kg day⁻¹ and 13.1 kg day⁻¹, for Dm and Vp, respectively, before the rainy day, and after the rainy day they are 290 kg day⁻¹ and 15 kg day⁻¹ for the same species (Figure 7.2). A possible interpretation is that in the dry season, soil moisture level is so low that a one-day slight rain cannot modify soil water content of the cuirass. Thus, the first rain, which is absorbed by the first centimeters of soil layers, evaporates quickly with the solar radiation of the following days. Deep-rooted trees cannot benefit significantly from such rainfall.

Contribution of trees to water balance

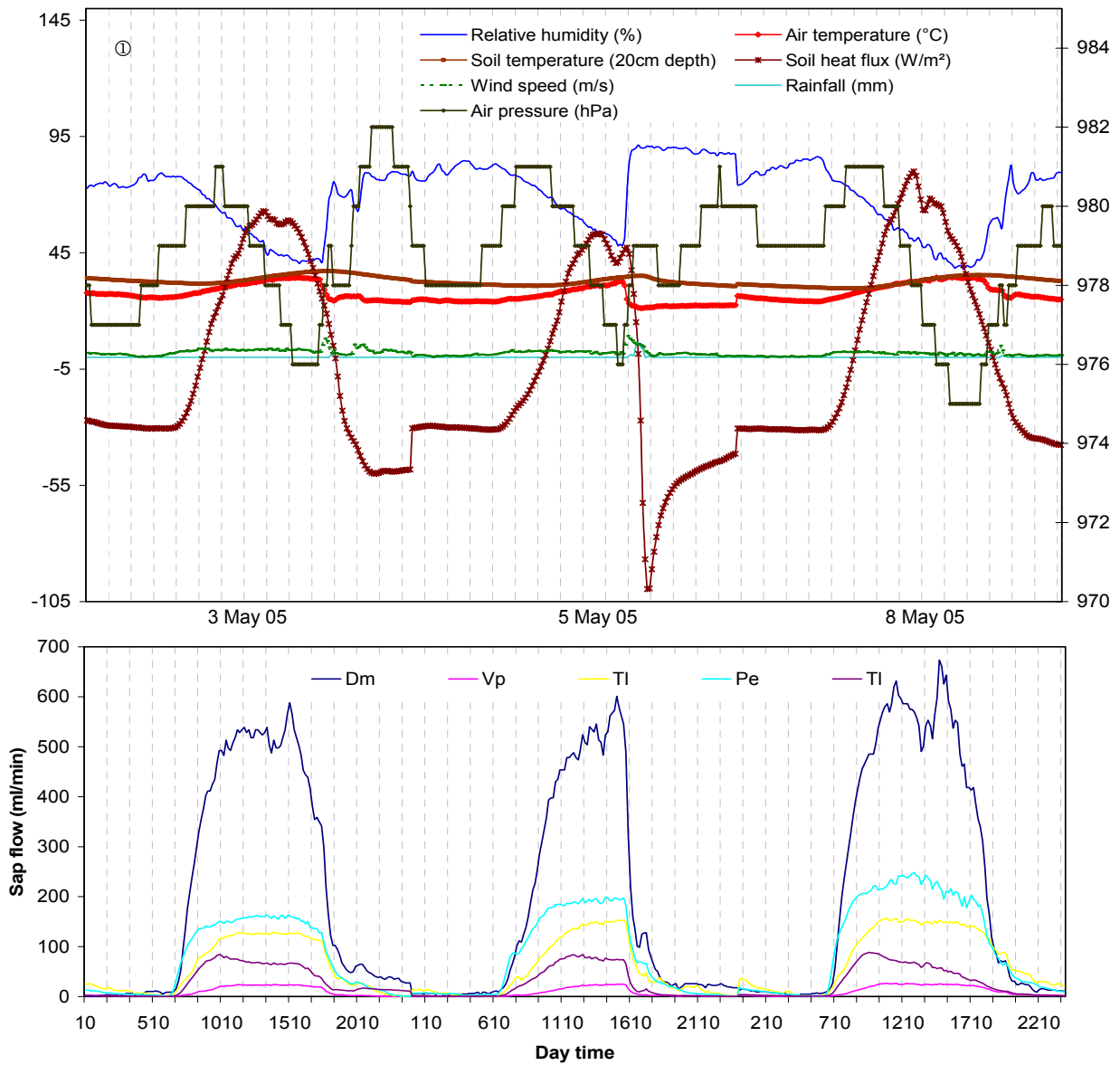


Figure 7.2: Daily whole-tree water use pattern after rainfall (23.60 mm day⁻¹) in dry season. Water use patterns of *Detarium microcarpum* (Dm), *Vitellaria paradoxa* (Vp), *Terminalia laxiflora* (Tl) and *Pterocarpus erinaceus* (Pe) on clear days and rainy day. Site location: 10°51'54'' N, 3°04'37''W. 510 means 5:10 hrs. (Climate data source: J. Szarsynski – BIOTA West)

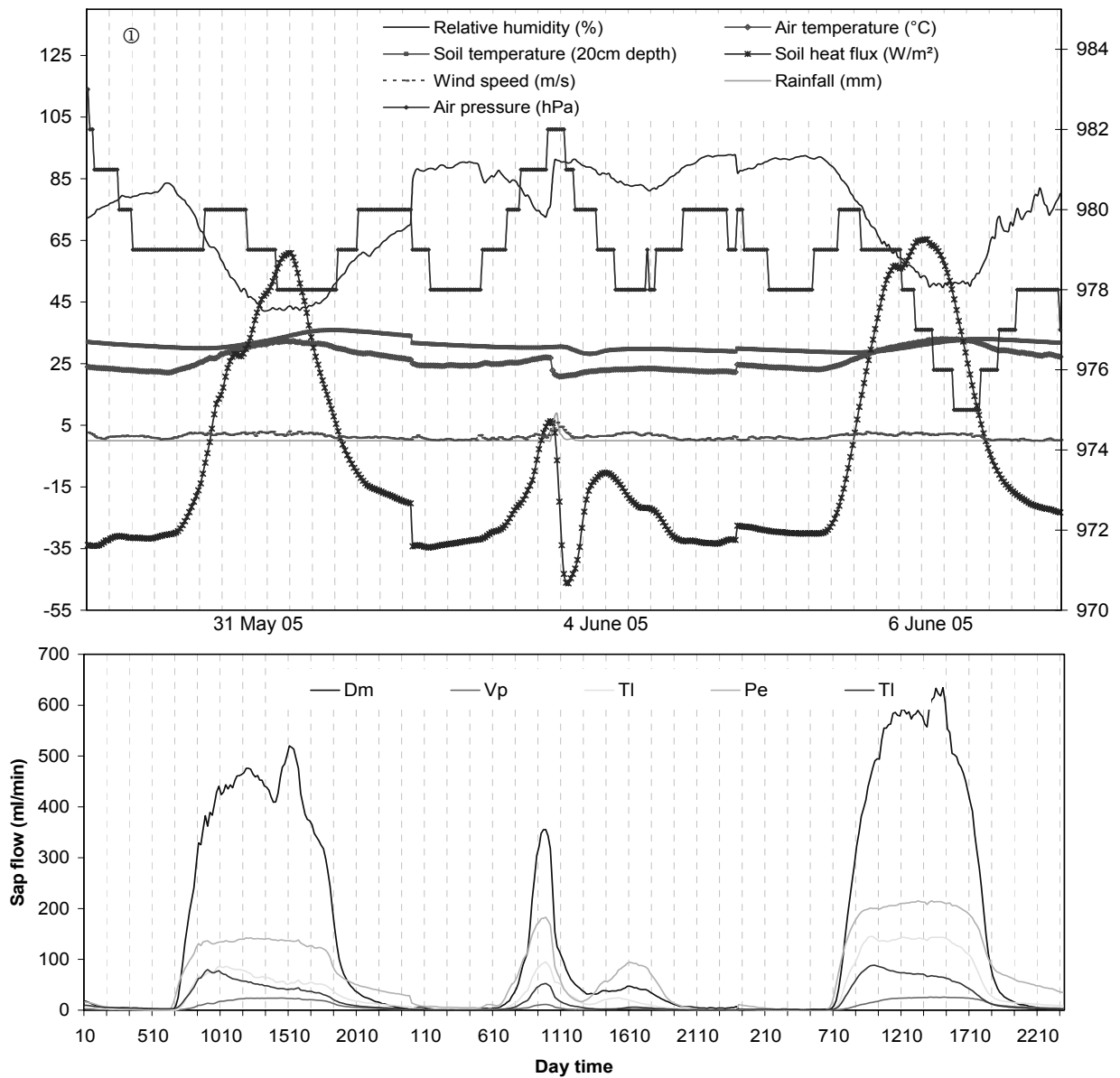


Figure 7.3: Daily whole-tree water use pattern after rainfall ($28.40 \text{ mm day}^{-1}$) in rainy season. Water use patterns of *Detarium microcarpum* (Dm), *Vitellaria paradoxa* (Vp), *Terminalia laxiflora* (TI) and *Pterocarpus erinaceus* (Pe) on clear days and rainy day. Site location: $10^{\circ}51'54'' \text{ N}$, $3^{\circ}04'37'' \text{ W}$. 510 means 5:10 hrs. (Climate data source: J. Szarsynski – BIOTA West)

Daily sap flow and actual evapotranspiration (ET_a)

In general, sap flow and ET_a evolve simultaneously whatever the season and the weather conditions. However, sap flow lags behind ET_a . In the dry season, the time lag is 2 hours with ET_a and sap flow starting to increase respectively at 4:30 hrs and 6:30 hrs. In the rainy season, the time lag is reduced to 1 hour (5:30 hrs and 6:30 hrs). Toward the end of the day at 20:30 hrs, a sudden increase in ET_a was observed in the dry season, which did not occur in the rainy season, where both parameters decreased progressively toward their low night rates (Figures 7.4 and 7.5).

The interpretations of the rising and falling curves of both sap flow and ET_a during the course of the day in conjunction with net radiation, air temperature, relative humidity and soil temperature help to explain the relationship between sap flow and ET_a . Indeed, the time lag is due to soil and air properties in reaction to net radiation. In the morning, air temperature increases faster than soil temperature. Thus, with rising air temperature, evaporation starts from the soil and the tree leaf surfaces covered with dew. Tree transpiration starts later when sun light intensity is sufficient to cause photosynthesis.

The sudden increase in ET_a in the evening (20:30 hrs) is due to a sudden and simultaneous increase in relative humidity and decrease in air temperature, while soil temperature is still high. The absence of light is a signal to the trees to stop transpiration, but the increase humidity in contact with the soil, which is still warm, reinforces evaporation. Finally, evaporation decreases when soil temperature decreases to its usual level. During rainfall, sap flow decreases significantly in favour of evaporation (Figure 7.5) until soils are cooled down and saturated with water.

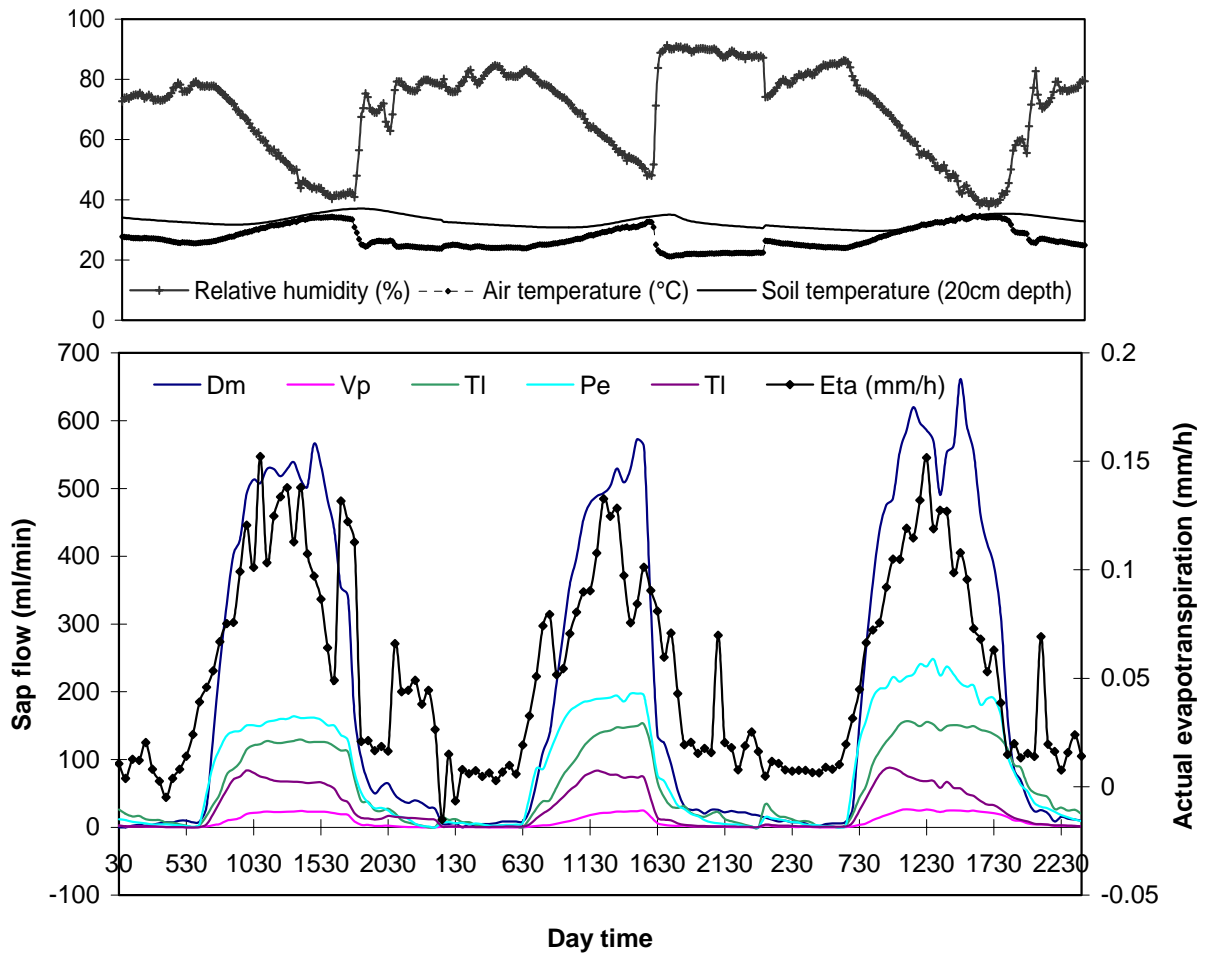


Figure 7.4: Sap flow patterns and actual evapotranspiration in the dry season. Top: weather conditions. Bottom: water use patterns of *D. microcarpum* (Dm), *V. paradoxa* (Vp), *T. laxiflora* (Tl) and *P. erinaceus* (Pe) on clear days and rainy day. 530 means 5:30 hrs. (Data sources: J Szarsynski – BIOTA West, C. Brümmer – Virtual Institute)

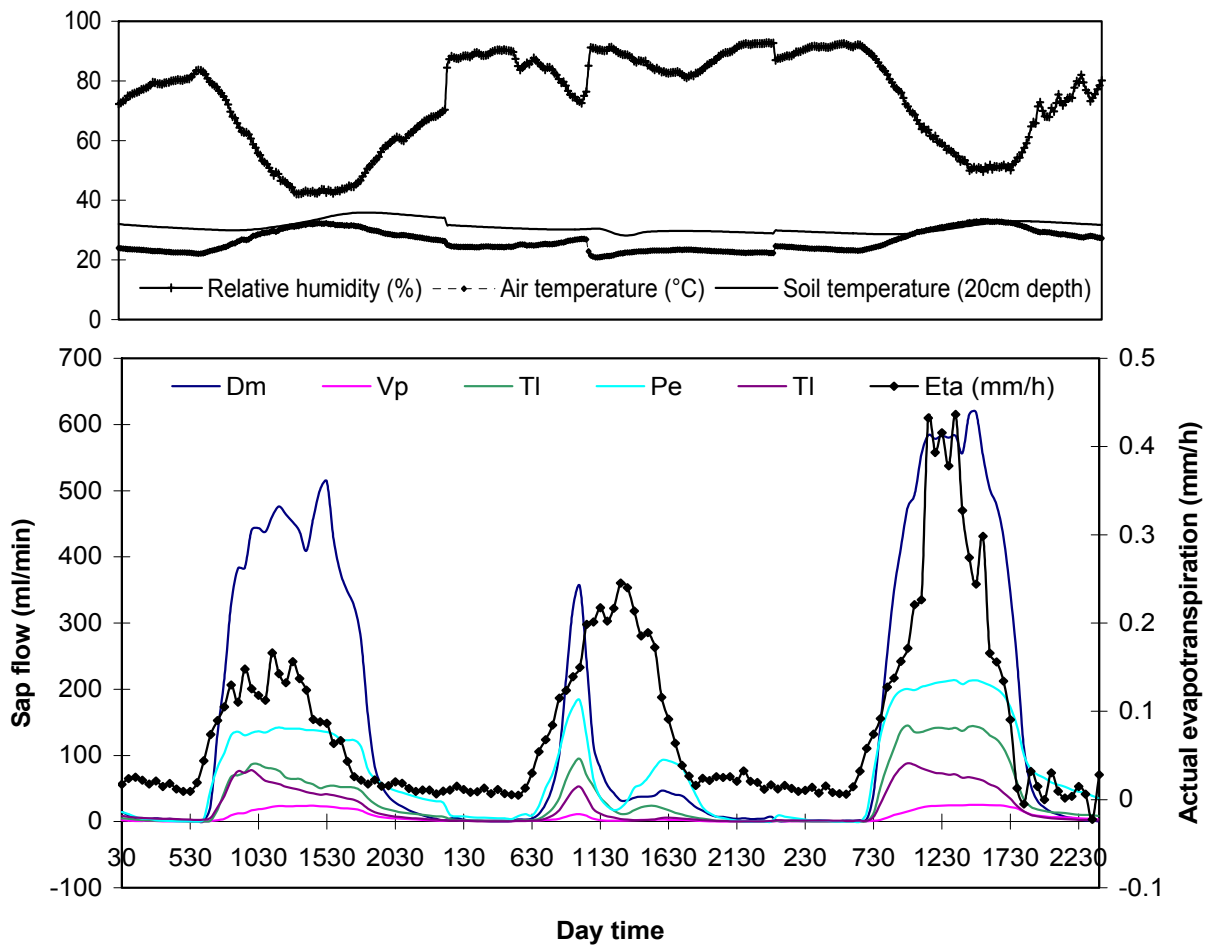


Figure 7.5: Sap flow patterns and actual evapotranspiration in the rainy season. Top: weather conditions. Bottom: water use patterns of *D. microcarpum* (Dm), *V. paradoxa* (Vp), *T. laxiflora* (Tl) and *P. erinaceus* (Pe) on clear days and rainy day. 630 means 6:30 hrs. (Data sources: J. Szarsynski – BIOTA West, C. Brümmer – Virtual Institute)

Seasonal variation of tree water use

Tree water use over repeated rainy and dry seasons confirms that during rainfall sap flow rates decrease significantly. Most of the sudden sap flow decreases (Figure 7.6) correspond to wet days, and the strong increases correspond to water-stress periods.

Considering all measurements as a whole, tree water use showed an upward trend from the dry season to the rainy season. This is the direct consequence of water-stress reduction with increasing rainfall, and the changes in tree functioning during the

case in the period from 27 April to 30 June 2005, when the total rainfall was 113.4 mm. The following year (for the same period) the total rainfall was double (213.3 mm), thus supplying the trees with more water. Consequently, the sap flow rates of all the tree species increased (Figure 7.6). Notable exceptions are observed for *Vitellaria paradoxa* and *Terminalia laxiflora* during the dry year 2005.

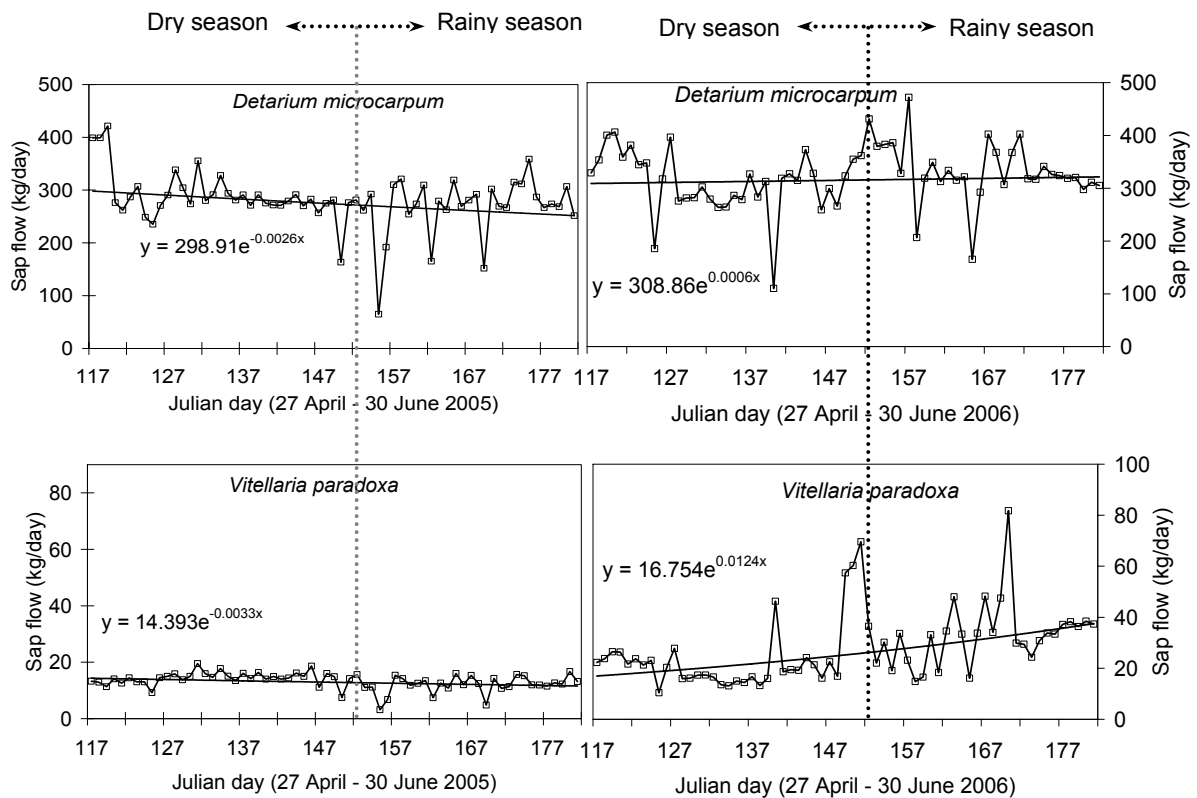


Figure 7.6: Daily and seasonal variation of sap flow rates over a two-year period (2005 and 2006). The period of 117 - 152 corresponds to dry season, and 153 - 177 corresponds to rainy season. Sequences of 25 days are taken into account for the readability of the graphs.

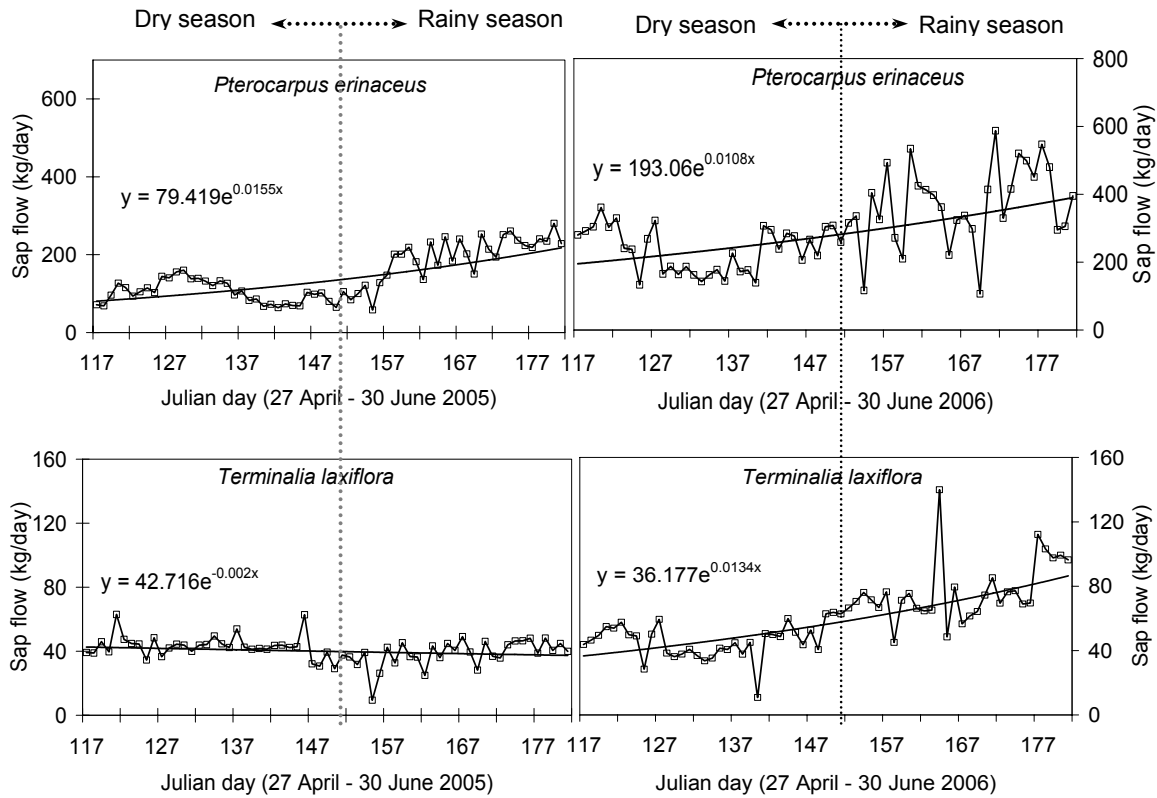


Figure 7.6: (Continued)

One of the consequences of rainfall reduction and variability could be the reduction in the productivity of commercial species, namely *Vitellaria paradoxa* (Karité, sheanut tree), *Detarium microcarpum*, *Lannea microcarpa* (Raisin, local grapes), *Parkia biglobosa* (Néré). Since “photosynthesis is the basis food-making process through which inorganic CO₂ and H₂O are transformed to organic compounds” (Fogiel 2000, p.18), water shortage will lead to lower productivity. In the context of global warming, commercial trees are likely to produce less, thus reducing farmers’ incomes. That may cause problems for livelihood and food security, and cause poverty should the predictions concerning the global warming and climate change for West Africa become true.

Summary

Trees contribute to surface water balance through ETa (Equation 7.1) as a reaction to weather conditions. The photosynthetic process plays an important role in the regulation of tree water uptake from the soil and its release into the atmosphere. In the morning, the contribution of trees is from the evaporation of leaf surface moisture. Once photosynthesis starts due to solar radiation, the maximum contribution occurs at mid-day through transpiration.

The more water is available, the more trees will contribute to the surface water balance according to the law of conservation of mass. Therefore, from the dry to rainy season, the contribution of trees to the water balance increases, peaking in the rainy season, i.e., from mid-June to mid-September (Figure 7.7).

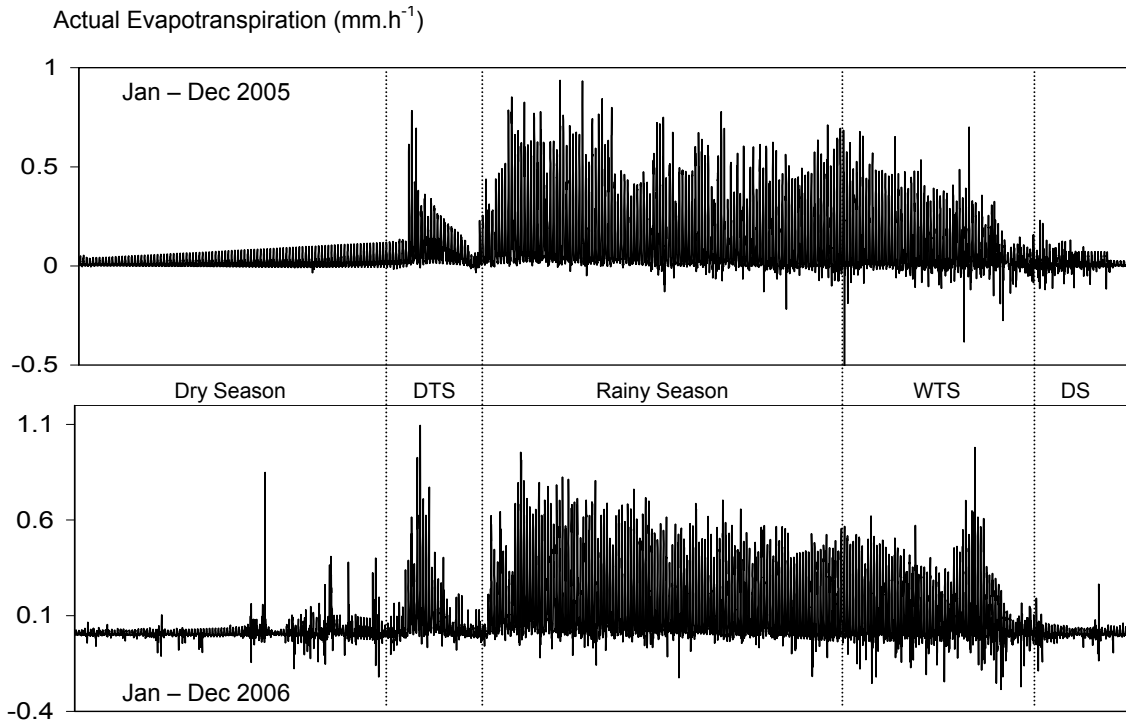


Figure 7.7: Seasonal variation of hourly ET_a in a two-year period. Latent heat flux and air temperature data (used to derive ET_a) were simultaneously recorded at Eddy Correlation and microclimate stations. Summary values for the year 2005: Mean $ET_a = 0.09$, Max. = 0.94, Min. = 0 mm day⁻¹. Year 2006: Mean $ET_a = 0.09$, Max. = 1.09, Min. = 0. Negative values on the graphs mean no ET_a occurs. Abbreviations: DTS = Dry transition season, WTS = Wet transition season, and DS = Dry season. (Data sources: J. Szarsynski – BIOTA West, and C. Brümmer – Virtual Institute)

7.3.3 Tree stand transpiration

Transpiration estimation

Stand transpiration flux

There is a very good correlation between sap flow rate and DBH, much less than crown cover (Figure 7.8). Hence, equation 7.4 is used to predict the sap flow rates of tree

species that were not covered by *in-situ* sap flow measurements. The regression coefficient and the constant of equation 7.4 are defined as follows:

$$sf_e = -57.849 + 4.179 \times Dbh_m \quad (7.7)$$

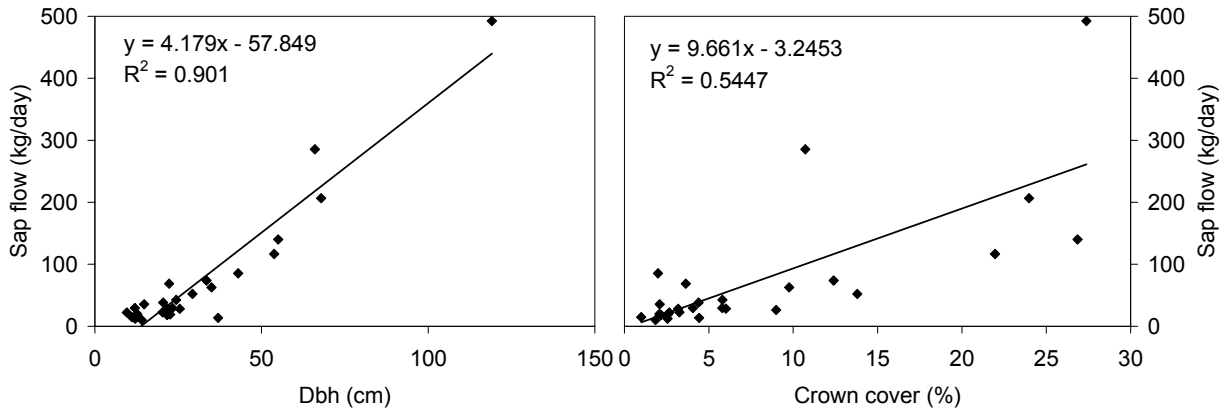


Figure 7.8: Relationship between sap flow, DBH and crown cover at tree level.

The linear regression was established between the DBH of large trees and their sap flow rates. Equation 7.4 failed to predict the sap flow rates of young trees with DBH less than 14 cm (53.3 %). As an approximation, the variables of the youngest tree that fitted equation 7.4 (DBH 14 cm and sap flow rate 0.66 kg day^{-1}) were used to calculate the sap flow rates of the other young trees as follows:

$$sf_e = \frac{Dbh_e \times 0.66}{14} \quad (7.8)$$

where sf_e is the sap flow rate of a given young tree and Dbh_e is its diameter at breast-height.

The sum of all sf_e in every plot lead to the values of all T_p as explained previously, with a mean T_p of 0.7 mm day^{-1} , maximum of 3 mm day^{-1} , minimum of 0.1 mm day^{-1} , and standard deviation of 0.4 mm day^{-1} . Individual tree transpiration and associated biometric parameters are given in appendix 5.

Stand transpiration and *ETa*

The calculation of the actual evapotranspiration (*ETa*) over the same period as the estimation of the mean T_p revealed that the mean daily *ETa* was 3.6 mm day⁻¹, the maximum 6.8 mm day⁻¹, the minimum 0.3 mm day⁻¹, and the standard deviation 1.7 mm day⁻¹. The mean hourly *ETa* over a one-year period was 0.1 mm h⁻¹, both in 2005 and 2006.

Based on the mean T_p and the mean *ETa*, over the period from 27 April - 31 June 2005, the contribution of tree stands to actual evapotranspiration in the NRB is calculated to be 20.6 %. The remaining 79.4 % of *ETa* are explained by the transpiration of young trees with DBH a less than 5 cm, shrubs, saplings, seedlings and grass covers, and by the evaporation of soil and water surfaces (ponds, dams, rivers, etc.).

Mapping large-scale tree stand transpiration

In principle, the predicted tree transpiration map should be processed on the basis of crown cover parameters to the extent that the correlation coefficient between crown cover and transpiration ($r = 0.87$) is higher than the correlation coefficient between DBH and transpiration ($r = 0.82$) (Figure 7.9). But preference is given to build the predicted tree transpiration map on the basis of DBH values, because the crown cover band (Chapter 5, section 5.3.3; Figure 5.27) is derived from the DBH band, which in turn is derived from the remotely sensed tree density band. Indeed, using the crown cover band for prediction of tree transpiration over large areas significantly increases the uncertainty of the output by addition of the uncertainties of the other bands.

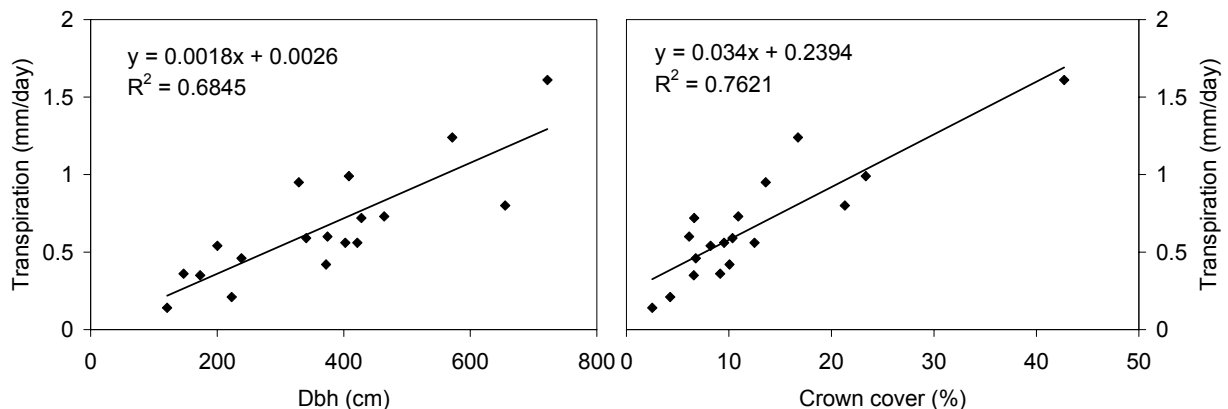


Figure 7.9: Relationships between transpiration, DBH and crown cover at plot level.

Thus, the best-fit prediction of tree transpiration map is based on equation 7.6 as follows:

$$T_p = 26 * 10^{-4} + 18 * 10^{-4} \times Dbh_p \quad (7.9)$$

Justification of RMSEP

The direct RMSEP of predicted tree stand transpiration derived from the regression analysis is $\pm 0.3 \text{ mm day}^{-1}$. But in a rigorous scientific validation, the final error of prediction of the transpiration outputs should take into account the RMSEP of the anterior products from which it is derived, namely the remotely sensed bands of tree density ($\pm 87.1 \text{ stems ha}^{-1}$) and DBH ($\pm 68.9 \text{ cm/pixel}$). Hence, the justified transpiration RMSEP is $0.25 \text{ mm day}^{-1} + 87.1 \text{ stems ha}^{-1} (0.26 \text{ mm day}^{-1}) + 68.9 \text{ cm/pixel} (0.13 \text{ mm day}^{-1})$, i.e. $\pm 0.6 \text{ mm day}^{-1}$.

Transpiration map

As much as 62.1 % of the area covered by the map are unproductive with regard to stand transpiration. The map surface is dominated by cuirass soils, bare soils, fallows, etc. The dominant mean transpiration rates (34.3 %) are in the $0 - 1 \text{ mm day}^{-1}$ range ($\pm 0.6 \text{ mm day}^{-1}$). Some hotspots of stand transpiration ($1 - 2 \pm 0.6 \text{ mm day}^{-1}$), representing 3.6 % of the total area covered by the map, can be observed mainly in wet areas, i.e., along river beds (Figure 7.10). Thus, spatial transpiration rates can be accounted for by the geographical location of the area of investigation in southwestern Burkina Faso. This is a semi-arid region (tropical dry climate of Sudano-Sahelian type), where mean annual rainfall, air temperature, relative humidity, net radiation and latent heat flux over the years 2005 - 2006 are 950 mm, 27.1 °C, 58.7 %, 97.2 W m⁻² and 56.5 W m⁻², respectively. These data were recorded by the Eddy Correlation and microclimate stations (10°51'55''N, 3°04'21''W).

A similar study, based on the xylem Heat-Balance technique and conducted in the Kalahari region of Botswana, concluded that dry season tree transpiration flux ranged from 0 to 0.15 mm day^{-1} (Lubczynski et al. 2004). These results are lower than those of the NRB in Burkina Faso in the present study, because the sap flow was measured in dry seasons. Nevertheless, they help validate the current results to the

extent that they confirm the range of 0 - 1 mm day⁻¹ as being the mean tree transpiration flux for less rainy regions of Africa. The transpiration flux is higher for rainy and densely vegetated regions. For instance, in a study conducted on a secondary-growth *Abies amabilis* forest (> 2000 trees ha⁻¹) in western Washington, USA, tree stand transpiration ranged from 0.01 to 3.52 mm day⁻¹ (Martin et al. 1997).

7.3.4 Tree stand contribution to surface water balance

Transpiration, *ETa* and rainfall

In 2005, 94.1 % of the rainfall returned to the atmosphere as *ETa*. Moreover, during the period from 27 April - 31 June 2005, rainfall satisfied the tree water demand so that the trees did not need to take water from the groundwater. The mean tree stand contribution to *ETa* was 20.6 %. From this, one can estimate the mean tree stand contribution to the water balance through transpiration to have been 19.4 % of the rainfall in the densely vegetated area (Table 7.2). In fact, this rate will vary according to the vegetation type (Huggett and Cheesmen 2002), season, weather and environmental conditions.

For illustration, in the same year for a large-scale sparsely vegetated area (Figure 7.10), the tree stand contribution to the water balance decreased to 11 % of the rainfall. The remaining 89 % were contributed by transpiration from other vegetation cover, and evaporation from soil, ponds and reservoir water surfaces. In sum, the contribution of large trees (DBH > 5 cm) to the surface water balance ranged from 11 to 19.4 % of rainfall, depending on the area was densely or sparsely vegetated.

During the wetter year (2006), the tree stand contribution to the water balance was lower than for the dryer year (2005). The rates were 16.5 % and 9.4 %, respectively, for dense and sparse vegetation areas. These proportions were thus higher in dry season than in the rainy season. Similarly, the *ETa* contribution to the water balance was higher in the dry year (94.1 %) than in the wet year (80.2 %) (Table 7.2). This last conclusion is in line with the results of Martin (2005), who worked on the water balance of Atankwidi River in Navrongo, southeastern Burkina Faso.

Table 7.2: Tree stand contribution to surface water balance. Dense vegetation area corresponds to site-scale area (Mean crown cover = 31 %); sparse vegetation area corresponds to upscaled large-scale area (Mean crown cover = 17 %). Values marked with asterisk indicate rainfall-deficit proportions.

Year	Season	Rainfall (mm)	ET_a (mm)	ET_a / Rainfall (%)	Tree stand contribution (% of rainfall)	
					Dense vegetation	Sparse vegetation
	Total	744.8	700.9	94.1	19.4	11.0
2005	Dry season	19.0	71.2	374.7*	77.2*	43.8*
	Rainy season	455.4	356.3	78.3	16.1	9.2
	Total	922.2	739.5	80.2	16.5	9.4
2006	Dry season	8.8	48.1	546.0*	112.5*	63.9*
	Rainy season	584.6	351.3	60.1	12.4	7.0

Rainfall-deficit, ET_a , transpiration and groundwater

In the dry season, the rarity of rainfall leads to frequent rainfall deficits. In order to make up for these deficits and still meet ET_a (Table 7.2), deep-rooted trees use groundwater resources to maintain transpiration as a natural process. In such periods, ET_a is equal to transpiration because evaporation of soil water is almost equal to zero. This is the natural process that regulates the ecosystems of dryland environments.

Unfortunately, natural processes are disturbed by anthropogenic activities, which threaten the survival of trees in arid and semi-arid regions. How to reconcile the existences of trees with human survival? In this context, it is not realistic to advocate local-scale cutting down of trees. On the contrary, regional and concerted efforts should be made to restore natural cycles by re-establishing tree stands.

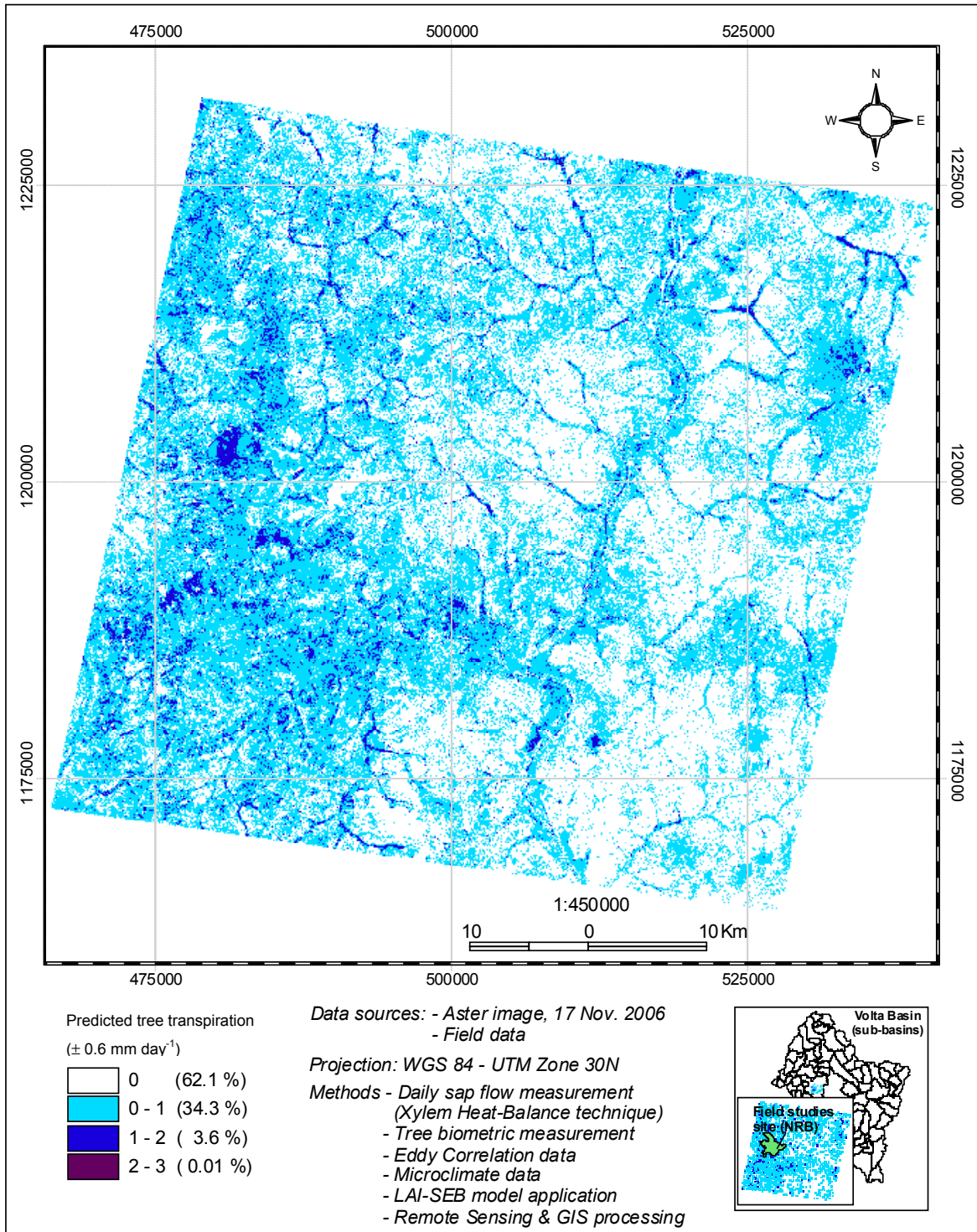


Figure 7.10: Mean daily tree transpiration. Mean = 0.4 mm day^{-1} , Min. – Max. = $0 - 3 \text{ mm day}^{-1}$, and Stdev = 0.6 mm day^{-1} ($\pm 0.6 \text{ mm day}^{-1}$). Field data: April 2005 – Dec. 2006.

7.4 Conclusions

The water use of the savanna vegetation depends on its species composition. Thus, average daily tree water use ranged from 10.1 kg day^{-1} for *Crossopteryx febrifuga* to 492 kg day^{-1} for *Pterocarpus erinaceus*. The fluctuation of tree water uptake during the course of the day is influenced and regulated by weather conditions, i.e., net radiation, relative humidity, air temperature, and air pressure. On a day scale, the water use rates are higher at mid-day and lower at mid-night. On a seasonal scale, tree water use increases from the dry season to the rainy season, when it reaches maximum rates in the period between mid-June and mid-September.

Trees contribute to the surface water balance through transpiration, which occurs in the photosynthesis process as a reaction to weather conditions. The mean daily tree transpiration at the NRB scale was 0.7 mm day^{-1} , the maximum 3 mm day^{-1} , the minimum 0.1 mm day^{-1} , and the standard deviation 0.4 mm day^{-1} . The predicted stand transpiration map obtained by means of the LAI-SEB model best fits the ground-truth information. It shows that 62.1 % of southwestern Burkina Faso were not contributing to tree transpiration, whereas 34.3 % of the region transpire in the range of $0\text{-}1 \text{ mm day}^{-1}$. The mean daily actual evapotranspiration was 3.6 mm day^{-1} , the maximum 6.8 mm day^{-1} , the minimum 0.3 mm day^{-1} , and the standard deviation 1.7 mm day^{-1} .

The analysis of both the mean tree stand transpiration and the mean actual evapotranspiration over the time period 27 April - 31 June in 2005 and 2006, indicates that the contribution of large trees ($\text{DBH} > 5 \text{ cm}$) to the surface water balance ranges from 9.4 to 19.4 % of the rainfall, depending on the vegetation density and the season.

These results demonstrate the importance of trees, and particularly of protected areas, in the surface water balance of semi-arid environments. Thus, it is easily understood that deforestation leads to changes to the surface water balance through rainfall reduction (Yasunari 2002b). Consequently, effective fights against drought, water scarcity, poverty, and threats to livelihood and food security should start by preventing destructive effects of anthropogenic activities on vegetation covers.

8 GENERAL CONCLUSION

The application of remote sensing and GIS techniques to vegetation and climatic variables to estimate tree stand contribution to the surface water balance under a changing climate has proven to be a proper choice. Reliable results representative for large regions in West Africa were produced.

8.1 General summary

8.1.1 Usefulness of biodiversity conservation

The Nature Reserve of Bontioli appears to be useful for biodiversity conservation in semi-arid regions of West Africa despite the harsh environmental conditions and constant anthropogenic disturbances. It provides a habitat for 71 (± 2) tree species representing 19 families. The tree community of the reserve is organized according to three main vegetation types, namely tree savanna (38.7 %), shrub savanna (43 %) and gallery forest (0.9 %).

The major tree species are *Terminalia macroptera* (11.7 %), *Detarium microcarpum* (9 %), *Vitellaria paradoxa* (9 %), and *Entada africana* (6.7 %). These results lead to the design of two basic maps: (1) map of the phytoecological zones, and (2) map of the vegetation cover classification.

Because of its richness in primary tree species of the relevant phytogeographical region, the NRB has proven to be useful for the present study on tree transpiration, surface water balance and climate change. This could not have been achieved if representative tree communities of the area had not existed or had been sparsely distributed.

8.1.2 The LAI-SEB model for tree density prediction

The development of the multivariate regression model - LAI-SEB model – provides a quick and simple means of predicting and upscaling tree densities over larger regions within the Volta Basin, West Africa. The LAI-SEB model is based on remotely sensed Vegetation Indexes (*VI*s) and Surface Energy Balance (*SEB*) products, and shows good performance in estimating tree density, with a low RMSE of Prediction of ± 87 stems ha⁻¹, i.e., ± 8 trees per pixel. The reliability of the model is also proven

through the comparison between the mean absolute tree density (331 ± 4 stems ha^{-1}) and the mean relative tree density (325 ± 87 stems ha^{-1}).

As a whole, the model is designed to map validated large-scale (1) tree density by stem count (Figure 5.21), (2) tree density by DBH estimates, and (3) tree density by crown cover estimates (Figure 5.27). The accuracy of the output (3) is crucial in the estimation of tree stand transpiration. The model shows low bias levels due to the influence of the reflectance of high grass covers in the rainy season and it is of great help in the analysis of the relationship between tree stands and climate through the functioning of the surface water balance.

8.1.3 Tree stand contribution to surface water balance

In southwestern Burkina Faso, average daily whole-tree water use ranged from 10.1 kg day^{-1} for *Crossopteryx febrifuga* to 492 kg day^{-1} for *Pterocarpus erinaceus*. The variation of tree water uptake during the course of the day is influenced and regulated by weather conditions, specifically solar energy, which drives photosynthesis.

The field-specific mean daily tree stand transpiration was 0.7 mm day^{-1} , the maximum 3 mm day^{-1} , the minimum 0.1 mm day^{-1} , and the standard deviation 0.4 mm day^{-1} . Transpiration rates were higher at mid-day and lower at mid-night, and increased from the dry season to the rainy season with peaks during the period between mid-June and mid-September. The estimated stand transpiration map obtained by means of the LAI-SEB model shows that 62.1 % of the map surface (in southwestern Burkina Faso) do not contribute to tree transpiration, whereas 34.3 % of that area transpire between 0 and 1 mm day^{-1} .

Trees contribute to the surface water balance through transpiration, which occurs according to photosynthesis as a reaction to weather conditions. The mean daily actual evapotranspiration was 3.6 mm day^{-1} , the maximum 6.8 mm day^{-1} , the minimum 0.3 mm day^{-1} , and the standard deviation 1.7 mm day^{-1} . The results confirm that the contribution of large trees (DBH > 5 cm) to the surface water balance ranged from 9.4 to 19.4 % of the rainfall, depending on the vegetation density and the season.

These results demonstrate the importance of trees, particularly in protected areas, in the equilibrium of the surface water balance of semi-arid environments. Thus,

it is easily understood that deforestation induces changes to the surface water balance through rainfall reduction (Yasunari 2002b).

8.1.4 LULC and climate change

The main land use and land cover (LULC) classes of the area of investigation are farm, fallow, dwelling, bare soil, tree savanna, shrub savanna, gallery forest, cuirass soil, and river course. The results of the land cover change processing based on remotely sensed visible red band emphasizes the recognition of vegetation cover patterns in terms of increase or decrease.

Two periods of decreasing land cover can be observed in the NRB in the periods of 1986 - 1999 and 1999 - 2000, due to anthropogenic disturbances, whereas in the period 2000 - 2006, the vegetation covers significantly increased due to the regeneration strength and improved governmental surveillance of the reserve.

The final land use land cover change outputs cannot be used to quantify the effects of vegetation cover conversion or regeneration on local climate variation. They are only useful for qualitative analysis.

8.2 Conclusions and recommendations

Trees play important roles in the functioning of the surface water balance and climate regulation. In semi-arid regions, this is especially so, particularly in the dry seasons when trees are the major actors in evapotranspiration maintenance. Only recently trees have been recognized in drylands as being responsible for the reduction of groundwater volume and availability. Trees never fail to play the role of maintaining the hydrological cycle through rainfall capture and transpiration. Therefore, advocating tree cutting to maintain groundwater levels in drylands has the opposite consequence of a reduction of rainfall sooner or later, which may eventually lead to a lowering of groundwater levels.

Disturbances in natural cycles, namely deforestation, water scarcity, drought, and food security, are due to humans and not trees. Global warming, global climate change are the direct effects of economic growth. Consequently, effective fights against drought, water scarcity, poverty, threats to livelihood and food security should start by preventing destructive effects of anthropogenic activities on vegetation covers. In this

context, it is realistic to advocate regional and concerted efforts to restore natural vegetation through reforestation campaigns. This is how decision-makers can reconcile existence of trees with human survival.

To strengthen the scientific conclusions about tree-groundwater relations, further studies should be undertaken on the relationships between tree root systems and groundwater in order to determine specific tree species as indicators of groundwater presence and level. From those results, tree communities can be classified and mapped according to their root depth system, and according to their degree of use of groundwater resources.

The modeling approach for the management of large-scale natural resources is an effective strategy. Despite some limits, the straightforward LAI-SEB model appears to be a useful and adapted tool for the estimation of tree density and tree stand transpiration in the semi-arid lands of West Africa. To improve the model, the following recommendations are formulated:

- *Need of high-resolution imagery*

Contributions based on high-resolution images supplied by providers like Ikonos and QuickBird may improve the performance of the model.

- *Use of LAI field data to adjust inputs*

An approach consists of collecting exhaustive LAI field-data to be used as basis to compute spatial LAI coverage. The predicted LAI data will then be used to recalibrate the other *VIs* products and also to adjust the surface energy balance derivatives. Finally, the adjusted data will be used to determine the regression coefficients of the model. That approach can also lead to the possibility of predicting tree density using field-based LAI-2000 data.

- *Experimentation with other sensors*

Experimenting with different optical sensors (SPOT, QuickBird and Ikonos), hyperspectral sensors (CASI and MEIS), digital cameras (Tetracam), and radar sensors (RADARSAT-2 and LIDAR) can be helpful to determine which sensor fits best to the prediction of tree density applying the LAI- SEB model. Thus, the generalization of the model's method can be based on the identified sensor.

The LAI-SEB model can be applied over large regions in West Africa to map large-scale tree density and LULC, and to derive tree stand transpiration transects from drylands to wetlands (e.g., Burkina Faso - Ghana). The methods applied throughout this study can also be used to establish phytoecological zones of West Africa in order to establish biodiversity conservation priorities. In sum, the results of this work are valuable inputs for regional vegetation dynamics analysis and climate change modeling.

REFERENCES

- Allen RG, Walter IA, Elliott R, Howell T, Itenfisu D and Jensen M (eds) (2005) The Asce Standardized Reference Evapotranspiration Equation. ASCE Publications, US
- Arbonnier M (2002) Arbres, arbustes et lianes des zones sèches d'Afrique de l'Ouest. 2nd edn. CIRAD-MNHN, Paris
- Archer MD and Barber J (eds) (2004) Molecular to global photosynthesis. Imperial College Press, UK
- Arora MK and Varshney PK (2004) Advanced image processing techniques for remotely sensed hyperspectral data. Springer, Berlin
- Asrar G, Fuchs M, Kanemasu ET and Hatfield JL (1984) Estimating absorbed photosynthetically active radiation and leaf area index from spectral reflectance in wheat. *Agron. Journal* 76:300-306
- Austin MP (2005) Vegetation and environment: discontinuities and continuities. In: van der Maarel E (ed) *Vegetation Ecology*. Blackwell Publishing, London, pp52-84
- AVV (ed) (1988) Etude d'agropastoralisme, de la faune et de la couverture forestière de la Bougouriba. S.A. AGRER NV, Bruxelles
- Bagayoko F (2006) Impact of land-use intensity on evaporation and surface runoff: Processes and parameters for eastern Burkina Faso, West Africa. PhD Thesis, University of Bonn, Bonn
- Baret F and Guyot G (1991) Potentials and limits of vegetation indices for LAI and APAR assessment. *Remote Sensing of Environment*. 35:161-173
- Baret F, Weiss M, Allard D and al. (no date) Valeri: a network of sites and a methodology for the validation of medium spatial resolution land satellite products. *Remote Sensing of Environment* (submitted). <http://www.avignon.inra.fr/valeri/>. Cited 5 February 2008
- Baskent EZ and Misir M (2002) The role of GIS in multi-objective forest planning. International symposium on GIS. Sept. 23-26, 2002, Istanbul-Turkey
- Beaumont P (1989) Drylands environmental management and development. Routledge, London New York
- Beven KJ and O'Connell PE (1983) General report on water balance computation techniques. In: Van der Beken A and Herrmann A (eds) *New approaches in water balance computations*. Proceedings of the Hamburg Workshop, August 1983. Vol. IAHS Publ. No 148. http://www.cig.ensmp.fr/~iahs/redbooks/a148/iahs_148_0041.pdf. Cited 15 July 2007
- Bian L (1997) Multiscale nature of spatial data in scaling up environmental models. In: Quattrochi AD and Goodchild MF (eds) *Scaling in remote sensing and GIS*. Lewis Publishers, Boca Raton USA, p432
- BIOTA (2007) The project: Biota West Africa. http://www.biota-africa.org/1024o/biota_west_english/structure_west.htm. Cited 2 February 2008
- Boser B, Guyon I and Vapnik V (1992) A training algorithm for optimal margin classifiers. In: Haussler D (ed) *Proceedings of the 5th Annual ACM Workshop on Computational Learning Theory*. ACM Press, New York, pp144-152.
- Bounoua L, Defries R, Collatz GJ, Sellers P and Khan H (2002) Effects of land cover conversion on surface climate. *Climatic Change* 52:29-64

- Bowen IS (1926) The ratio of heat losses by conduction and by evaporation from any water surface. *Physics Review* 27:779-787
- Briassoulis H (2000) Analysis of land use change: Theoretical and modeling approaches. Available via The Web Book of Regional Science, ed., Scott Loveridge. Morgantown, WV: Regional Research Institute, West Virginia University. <http://www.rri.wvu.edu/regscweb.htm>. Cited 17 June 2007
- Budyko MI (1956) The heat balance of the Earth's surface. (English translation Stepanova NA, 1958, Office of Technical Services, Washington). In: Yair A and Berkowicz SM (eds) *Arid and semi-arid environments: Geomorphological and pedological aspects*, Vol 14. Catena Verlag, Cremlingen-Destedt
- Canty MJ (2006) *Image analysis, classification and change detection in remote sensing: with algorithms for ENVI/IDL*. Taylor & Francis, London
- Chao A and Shen T-S (2003) Nonparametric estimation of Shannon's index of diversity when there are unseen species in sample. *Environmental and Ecological Statistics* 10:429-443
- Chase TN, Pielke RAS, Kittel TGF et al (2000) Simulated impacts of historical land cover changes on global climate in Northern winter. *Climate Dynamics* 16:93-105
- Chavez PS JR and Mackinnon DJ (1994) Automatic detection of vegetation changes in the southwestern United States using remotely sensed images. *Photogrammetric Engineering and Remote Sensing* 60:571-583
- Choudhury BJ (1994) Synergism of multispectral satellite observations for estimating regional land surface evaporation. *Remote Sensing of Environment* 49:264-274
- CIA (2007) *The World Factbook*. Central Intelligence Agency. <https://www.cia.gov/library/publications/the-world-factbook/rankorder/2004rank.html>. Cited 18 October 2007
- CIESIN (2006) The importance of satellite remote sensing for global change research. Via CIESIN. www.ciesin.org/TG/RS/satremot.html. Cited 18 Decembre 2006
- Congalton RG and Green K (1999) *Assessing the accuracy of remotely sensed data: Principles and practices*. Lewis Publishers, Boca Raton USA
- De Muth JE (2006) *Basic statistics and pharmaceutical statistical applications*, 2nd edn. Chapman and Hall, London
- Digby PGN and RA Kempton (1987) *Population and Community Biology Series: Multivariate analysis of ecological communities*. Chapman and Hall, London
- Dolédec S and Chessel D (1991) Recent developments in ordination methods for environmental sciences. *Journal of Advances in Ecology* 1:133-155
- Dregne HE (1992) *Degradation and restoration of arid lands*. Lubbock: International Center for Arid and Semi arid Land Studies. Texas Tech University
- Erdas (1999) *Erdas imagine version 8.4: Tour guides*. Erdas Inc, Atlanta Georgia USA
- Esbensen KH (2002) *Multivariate data analysis in practice. An introduction to multivariate data analysis and experimental design*, 5th edn. CAMO Process AS, Oslo
- FAO (1996) *Burkina Faso: Rapport de pays pour la conférence technique internationale de la FAO sur les ressources phytogénétiques*. Conférence, Leipzig 17-23 Juin 1996. <http://www.fao.org/ag/AGP/agps/Pgrfa/pdf/burkinaf.pdf>. Cited 20 February 2007

- FAO (1998) Terminology for integrated planning and management. Choudhury K and Jansen LJM (eds). FAO, Rome
- Fleming JR (1998) Historical perspectives on climate change. Oxford University Press, New York
- Fogiel M (2000) Essentials of biology I. REA, Canada
- Fontès J and Guinko S (1995) Cartographie de la végétation et de l'occupation du sol du Burkina Faso. Note explicative. Projet Campus 88 313 101, Ministère de la Coopération Française
- Fontès J, Diallo A and Compaoré JA (1994) Carte de la végétation naturelle et de l'Occupation du Sol – Burkina Faso. SIG-BF
- Freeman PH and Fox R (1994) Satellite mapping of tropical forest cover and deforestation: A review with recommendations for USAID. Available via CIESEN. <http://www.ciesin.org/docs/005-325/005-325.html>. Cited 5 August 2004
- Freitas AA (2002) Data mining and knowledge discovery with evolutionary algorithms. Springer, Berlin
- Friend AD (2003) Modeling dynamic vegetation for decadal to century climate change studies. Available via SciDAC Alumni Project. http://www.scidac.gov/BER/BER_veg/reports/. Cited 25 January 2007
- Geosystems (2006) Atcor for Imagine 9.1. Haze reduction, atmospheric and topographic correction. User manual Atcor 2 and Atcor 3. Germering, Germany
- GLOWA (2000) Sustainable water use under changing land use, rainfall reliability and water demands in the Volta Basin. GLOWA Project Proposal 1. ZEF, Bonn
- GLOWA (2002) GLOWA Volta Phase II: From concepts to application. GLOWA Project Proposal 2. ZEF, Bonn
- Granier A (1987) Mesure du flux de sève brute dans le tronc du Douglas par une nouvelle méthode thermique. *Annales des Sciences Forestières*. 44(1):1-14
- Granier A, Aubinet M, Epron D et al (2003) Deciduous Forests (Beech): Carbon and water fluxes, balances, ecological and ecophysiological determinants. In: Valentini R (ed) Flux of carbon, water and energy of European forests. *Ecological Studies* 163. Springer, Berlin, p274
- Guinko S (1984) Végétation de la Haute-Volta. Thèse de doctorat es Sciences Naturelles, Université de Bordeaux III, Bordeaux
- Gunn SR, Brown M and Bossley KM (1997) Network performance assessment for neurofuzzy data modelling. In: Liu X, Cohen P and Berthold M (eds) *Advances in Intelligent Data Analysis. Lecture Notes in Computer Science*, Vol 1280. Springer, New York, pp313–323
- Haertel V, Shimabukuro YE and Almeida-Filho R (2004) Fraction images in multitemporal change detection. *International Journal of Remote Sensing* 25(23):5473-5489
- Heirtzler JR (1993) Topography. In: Gurney RJ, Foster JL and Parkinson CL *Atlas of satellite observations related to global change*. Cambridge University Press, Cambridge, p484
- Hill T and Lewicki P (2006) *Statistics: Methods and applications. A comprehensive reference for science, industry, and data mining*. StatSoft, USA
- Hoekstra AY (1998) *Perspective on water. An integrated model-based exploration of the future*. International Books, Utrecht

- Holland SM (2003) Analytic Rarefaction 1.3. Available via University of Georgia. <http://www.uga.edu/~strata/software/Software.html>. Cited 25 January 2007
- Huang C, Yang L, Wylie B and Homer C (2001) A strategy for estimating tree canopy density using Landsat 7 ETM+ and high resolution images over larger areas. Proceeding of the 3rd International Conference on Geospatial Information in Agriculture and Forestry. Denver, Colorado, 5-7 Nov. 2001
- Huete AR (1988) A soil adjusted vegetation index (SAVI). *Remote Sensing of Environment* 6:295-309
- Huggett R and Cheesmen J (2002) *Topography and the environment*. Prentice Hall - Pearson Education, London, New York, England
- IFAD (2004) Community investment program for agricultural fertility. Executive Board Document: EB 2003/79/R.19/Rev.1. <http://www.ifad.org/operations/projects/regions/PA/des/BF.htm#1220>. Cited 17 July 2004
- IUCN (2004) Protected areas and world heritage program. Available via UNEP. http://www.unep-wcmc.org/protected_areas/index.html. Cited 27 June 2004
- Janz AS, van der Linden B, Waske and Hostert P (2007) imageSVM - A user-oriented tool for advanced classification of hyperspectral data using Support Vector Machines. In: Proceedings of the 5th EARSeL workshop on imaging spectroscopy, Bruges, Belgium, 23-25 April, 2007, CD-Rom
- Jonckheere I, Fleck S, Nackaerts K et al (2004) Review of methods for in situ leaf area index determination. Part I. Theories, sensors and hemispherical photography. *Agricultural and Forest Meteorology* 121:19-35
- Kabat P, Claussen M, Dirmeyer PA, Gash JH, de Guenni LB, Meybeck M, Pielke Sr RA, Vörösmarty CJ, Hutjes RWA and Lütke-meier S (eds) (2004) *Vegetation, water, humans and the climate: A new perspective on an interactive system*. The IGBP series. Springer-Verlag, Berlin Heidelberg New York
- Kane DL and Yang D (2004) Overview of water balance determinations for high latitude watersheds. In: Northern research basins water balance. Proceeding workshop, Victoria, Canada, March 2004. IAHS Publ. 290, pp1-12
- Kassas M (1992) Desertification. In: Dregne HE *Degradation and restoration of arid lands*. International Center for Arid and Semi arid Land Studies, Texas Tech University, pp11-25
- Kaya A (2004) Outlier effects on databases. In: Yakhno T (ed) *Advances in information systems*. Proceedings 3rd International Conference, ADVIS 2004, Izmir, Turkey, Oct. 2004. Springer-Verlag, Berlin, Heidelberg, pp88-95
- Kersten GE, Mikolajuk Z and Yeh AG (eds) (2000) *Decision support systems for sustainable development: a resource book of methods and applications*. IDRC, Ottawa
- Kim JW, Kim JH, Lee JB and Heo J (2006) Correlation analysis between forest volume, ETM+ bands, and height estimated from C-Band SRTM product. *Korean Journal of Remote Sensing* 22(5):427-431
- Konecny G (2002) *Geoinformation: Remote Sensing, Photogrammetry and Geographical Information Systems*. Taylor & Francis, London
- Kovar K and Nachtnebel HP (1996) *Application of geographic information systems in hydrology and water resources management*. International Association of Hydrological Sciences N° 235, The Netherlands
- Krebs CJ (1989) *Ecological methodology*. Harper Collins Publishers, University of British Columbia

- Kutzbach L (2004) Carbon, water and energy flux measurements by the Eddy Covariance method. <http://www.awi-potsdam.de/www-pot/geo/eddy.html>. Cited 7 September 2007
- Lambert JDH, Ryden P.A and Esikuri EE (2005) Capitalizing on the bio-economic value of multi-purpose medicinal plants for the rehabilitation of drylands in Sub-Saharan Africa. Global Environment Facility Program. The World Bank, Washington
- Lambin EF and Strahler AH (1994) Change-vector analysis in multitemporal space: A tool to detect and categorize land-cover change processes using high temporal-resolution satellite data. *Remote Sen. Environ.* 48:231-244
- Laneve G and Castronuovo M.M (2005) Comparison between vegetation change analysis in Kenya based on AVHRR and SeaWiFS images. *International Journal of Remote Sensing* 26(12):2549-2559
- Lehouérou HN (1992) An overview of vegetation and land degradation in world arid lands. In: Dregne HE Degradation and restoration of arid lands. International Center for Arid and Semi arid Land Studies. Texas Tech University, pp99-126
- Leibl W and Mathis P (2004) Electron transfer in photosynthesis. In: Archer MD and Barber J (eds) *Molecular to global photosynthesis*. Imperial College Press, UK, pp117-163
- Lepš J and Šmilauer P (2003) *Multivariate analysis of ecological data using CANOCO*. Cambridge University Press, UK
- Lewis-Beck MS, Bryman A and Liao TF (eds) (2004) *The sage encyclopedia of social science research methods*. Vol. 3. Sage Publications, Thousand Oaks, London, New Delhi
- Liang SS (2004) *Quantitative remote sensing of land surfaces*. John Wiley & Sons, New York
- Li-cor Inc (1992) LAI-2000 plant canopy analyzer. Instruction manual. Li-cor Inc, Nebraska
- Lillesand TM, Kieffer RW and Chipman JW (2004) *Remote sensing and image interpretation*. 5th edn. John Wiley & Sons, New York
- Longley P and Batty M (1996) Analysis, modelling, forecasting, and GIS technology. In: Longley P and Batty M *Spatial analysis: modelling in a GIS environment*. John Wiley & Sons, New York
- Lu D, Mausel P, Brondizio E and Moran E (2004) Change detection technique. *International Journal of Remote Sensing* 25(12):2365-2407
- Lubczynski M, Fregoso A, Mapanda W, Ziwa C, Keeletsang M, Chavarro DC and Obakeng O (2004) Dry season Kalahari sap flow measurements for tree transpiration mapping - Serowe study case, Botswana. In: Stephenson D, Shemang EM, Chaoka TR (eds) *Water resources of arid areas*. Taylor & Francis, London, pp541-545
- Ludwig JA and Reynolds JF (1988) *Statistical ecology: a primer on methods and computing*. John Wiley & Sons, New York
- Luo J, Ming D, Shen Z, Wang M and Sheng H (2006) Multi-scale information extraction from high resolution remote sensing imagery and region partition methods based on GMRF-SVM. *Int. J. Remote Sensing* pp1-18. PrEview article. <http://www.informaworld.com>. Cited 27 July 2007
- Madani M (2001) Importance of digital photogrammetry for a complete GIS, 5th global spatial data infrastructure conference, Cartagena, Columbia, May 21-25, 2001

- Malczewski J (1999) GIS and Multicriteria Decision Analysis. John Wiley & Sons, New York
- Martens H and Martens M (2001) Multivariate analysis of quality: An introduction. John Wiley & Sons, New York
- Martin N (2006) Development of a water balance for the Atankwidi catchment, West Africa – A case study of groundwater recharge in a semi-arid climate. PhD Thesis, Ecology and Development Series No 41. Cuvillier Verlag, Göttingen
- Martin TA, Brown KJ, Cermák J, Ceulemans R, Kucera J, Meinzer FC, Rombold JS, Sprugel DG and Hinckley TM (1997) Crown conductance and tree and stand transpiration in a second-growth *Abies amabilis* forest. Can. J. For. Res. 27:797-808
- Mas J-F (1999) Monitoring land-cover changes: a comparison of change detection techniques. International Journal of Remote Sensing 20(1):139-152
- Mather PL (1999) Computer processing of remotely-sensed images: An introduction. 2nd edn. John Wiley & Sons, England
- Mathis P (1992) Photosynthesis: biological conversion of light into chemical energy. In: Kochanski E Photoprocesses in transition metal complexes, biosystems and other molecules. Experiment and theory. Proceedings of the NATO Advances Study Institute, September 1-13, Aussois, France. Kluwer Academic Publishers, Dordrecht, The Netherlands, pp333-348
- McCarthy JJ (ed) (2001) Climate change 2001: Impacts, adaptation, and vulnerability. IPCC Working Group II. Cambridge University Press, Cambridge
- McCloy KR (1995) Resource management information systems: Process and practice. Taylor & Francis, London
- McCloy KR (2005) Resource management information systems: remote sensing, GIS and modeling, 2nd edn. Taylor & Francis, London
- MET (1994) Rapport spécifique d'activités dans la zone pilote de Bontioli. MET, Burkina Faso
- Michener WK, Brunt JW and Stafford SG (eds) (1994) Environmental information management and analysis: Ecosystem to global scales. Taylor & Francis, London
- Moniod F, Pouyau B and Sechet P (1977) Le bassin du fleuve Volta. Monographies hydrologiques ORSTOM n°5. ORSTOM, Paris
- Monteith JL and Unsworth MH (1990) Principles of environmental physics. 2nd edn. Edward Arnold, London
- Moore DS and McCabe GP (1998) Introduction to the practice of statistics 3rd edn. WH Freeman and Company, USA
- Moser SC (1996) A partial instructional module on global and regional land use/cover change: Assessing the data and searching for general relationships. Geojournal 39(3):241-283
- Naff T (1999) Data sharing for international water resource management: Eastern Europe, Russia, and the CIS. NATO ASI. Series. Environment Vol 61. Kluwer Academic Publishers, Dordrecht
- NASA (2002) Global warming. NASA Facts, The Earth Science Enterprise Series, June 2002 - NF 222, Maryland,
- NLR (2003) Objective-Introduction remote sensing. <http://remotesensing.nlr.nl/objectives/>. Cited 25 May 2004

- Orloci L (1978) Multivariate analysis in vegetation research. Vegetation. 2nd edn. W. Junk, The Hague
- Oweis T (2006) Improving access to water in deserts and drylands. Science and Development Network. <http://www.scidev.net/dossiers/>. Cited 18 Oct 2006
- Oyediran O (1983) Water balance computation in West Africa: problems and prospects. In: Van der Beken A and Herrmann A (eds) New approaches in water balance computations. Proceedings of the Hamburg Workshop, August 1983. Vol. IAHS Publ. No 148
- Peixoto JP and Oort AH (1992) Physics of climate. Springer, New York
- Petit C, Scudder T and Lambin E (2001) Quantifying processes of land-cover change by remote sensing: resettlement and rapid land-cover changes in south-eastern Zambia. *International Journal of Remote Sensing* 22(17) :3435-3456
- Pigeonnière AL and Ménager MT (2001) Les atlas de l'Afrique - Atlas du Burkina Faso. 4^{ème} éd. Les éditions JA, Paris
- Pilon PG, Howarth PJ, Bullock RA and Adeniyi PO (1988) An enhanced classification approach to change detection in semi-arid environments. *Photogrammetric Engineering and Remote Sensing* 54:1709-1716
- PISCES (2001) Community Analysis Package. A program to search for structure in ecological community data. Vers. 2.0, Lymington, England
- Poisson SD (1837) Recherches sur la probabilité des jugements en matière criminelle et en matière civile, précédées des règles générales du calcul des probabilités. Bachelier, Imprimeur-Libraire pour les Mathématiques, Paris
- Pontius Jr RG and Malizia NR (2004) Effects of category aggregation on map comparison. In: Egenhofer MJ, Freksa C and Miller HJ (eds) *GIScience 2004*, LNCS 3234. Springer, Berlin, pp251-268
- Quenouille MH (1949) Approximative tests of correlation in time-series. *Journal of Royal Statistical Society, Series B*, 11, 18-84
- Rich PM (1990) Characterizing plant canopies with hemispherical photographs. *Remote Sens. Rev.* 5:13-29
- Roberts J, Jackson N and Smith M (2006) Tree roots in the built environment. Research for Amenity Trees No 8. CEH, The Stationery Office, UK
- Rondeux J (1999) La mesure des arbres et des peuplements forestiers. Les Presses Agronomiques de Gembloux, Gembloux
- Rouse JW, Haas RH, Deering DW and Schell JA (1974) Monitoring the vernal advancement and retrogradation (Green wave effect) of natural vegetation. Final Report RSC 1978-4. Remote Sensing Center, Texas A&M Univ., College Station.
- Sala OE, Jackson RB, Mooney HA and Howarth (eds) (2000). *Methods in ecosystem science*. Springer, Berlin
- Salami AT, Ekanade O and Oyinloye RO (1999) Detection of forest reserve incursion in south-western Nigeria from a combination of multi-date aerial photographs and high resolution satellite imagery. *International Journal of Remote Sensing* 20:1487-1497
- Sanders HL (1968) Marine benthic diversity: a comparative study. *Am. Natur.* 102:243-282
- Saunders C, Haroon DR and John S-T (2004) Using string kernels to identify famous performers from their playing style. In: Boulicaut J-F, Esposito F, Giannotti F

- and Pedreschi (eds) Machine learning: ECML 2004. Springer-Verlag, Berlin, Heidelberg, pp384-395
- Sawadogo H, Hien F, Sohero A and Kambou F (2001) Pits for trees: How farmers in semi-arid Burkina Faso increase and diversify plant biomass. In: Reij C and Waters-Bayer A, (eds), Farmer innovation in Africa: A Source of inspiration for agricultural development. Earthscan, London
- Sawadogo K (1997) La pauvreté au Burkina Faso: une analyse critique des politiques et des stratégies d'intervention locales. Document de travail ECDPM No 51. Maastricht: ECDPM
- Schmidt H and Gitelson A (2000) Temporal and spatial vegetation cover changes in Israeli transition zone: AVHRR-based assessment of rainfall impact. *International Journal of Remote Sensing* 21(5):997-1010
- Serra P, Pons X and Saurí D (2003) Post-classification change detection with data from different sensors: some accuracy considerations. *International Journal of Remote Sensing* 24(16):3311-3340
- Shamsi UM (2002) GIS tools for water, wastewater, and stormwater systems. American Society of Civil Engineers Press, Virginia
- Shannon CE (1948) A mathematical theory of communication. *Bell System Technical Journal* 27:379-423
- Simberloff DS (1972) Properties of the rarefaction diversity measurement. *Am. Natur.* 106:414-418
- Simpson EH (1949) Measurement of diversity. *Nature* 163:688
- Singh A (1989) Digital change detection techniques using remotely sensed data. *International Journal of Remote Sensing* 10:989-1003
- Skole DL (1994) Data on global land-cover change: Acquisition, assessment, and analysis. In: Meyer W.B. and Turner II B.L. (eds). *Changes in land use and land cover: A global perspective*. Cambridge University Press, Cambridge, pp437-471
- ter Braak C.J.F. and Šmilauer P (2002) CANOCO Reference manual and CanoDraw for Windows user's guide: Software for Canonical Community Ordination (Vers. 4.5). Microcomputer Power, Ithaca, NY
- Townshend JRG and Justice CO (1995) Spatial variability of images and the monitoring of changes in the normalized difference vegetation index. *International Journal of Remote Sensing* 16:2187-2195
- Townshend JRG, Tucker CJ, Goward SN (1993) Global vegetation mapping. In: Gurney RJ, Foster JL and Parkinson CL *Atlas of satellite observations related to global change*. Cambridge University Press, Cambridge
- Tucker CJ (1979) Red and photographic infrared linear combinations for monitoring vegetation. *Remote Sensing of Environment*, 8(2)127-150
- Tukey JW (1958) Bias and confidence in not quite large samples (abstract). *Annals of Mathematical Statistics*, 29, p614
- Turner II BL, Skole D, Sanderson S, Fischer G, Fresco L and Leemans R (1995) Land-use and land-cover change. Science/Reserach Plan. IGBP Report No. 35, HDP Report No. 7, Stockholm
- UN (1970) *Integrated river basin development*. 2nd edn. New York
- UN (2006) *Coping with water scarcity: a strategic issue and priority for system-wide action*. UN-Water Thematic Initiatives. www.unwater.org. Cited 19 December 2006

- UNEP (1997) World Atlas of Desertification. UNEP, Nairobi
- UNESCO (1974) Methods for water balance computations: An international guide for research and practice. A contribution to the International Hydrological Decade. Sokolov AA and Chapman TG (eds). Unesco Press, Paris
- UNU (2004) Natural resource management, Environment and sustainable development programme. <http://www.unu.edu/env/index.htm>. Cited 9 July 2004
- UP (2001) UP sap flow system. User manual version 2.6. Umweltanalytische Produkte GmbH, Ibbenbüren
- Van Espen P (2002) Spectrum evaluation. In: Van Grieken R.E. and Markowicz A.A. (Eds.). Handbook of X-Ray spectrometry, 2nd edn. Marcel Dekker, New York, Basel, pp239-340
- Van Huffel S (ed) (1997) Recent advances in total least squares techniques and errors-in-variables modeling. SIAM, Proceedings of the second international workshop on total least squares and errors-in-variables modeling. Leuven, Belgium, August 21-24, 1996
- Vance VD, Eisenberg R and Walsh D (2000) Inside AutoCAD Map 2000. OnWord Press series, Canada
- Vandana S (1991) Ecology and the politics of survival. Conflicts over natural resources in India. UNU. Sage Publications. Available via UNU <http://www.unu.edu/unupress/unupbooks/80a03e/80A03E00.htm>. Cited 26 January 2006
- Vapnik VN (1995) The nature of statistical learning theory. Springer-Verlag, New York
- Vapnik VN (1998) Statistical learning theory. John Wiley & Sons, New York
- Vlek PLG and van de Giesen N (2002) Integration in the Glowa Volta Project: from concept to feasibility. In: GSF, German Programme on Global Change in the Hydrological Cycle (GLOWA). Status Report 2002, München
- Walker LR and Smith SD (1997) Impacts of invasive plants on community and ecosystem properties. In: Luken JO and Thieret (eds) Assessment and management of plant invasions. Springer, 324p
- Walter B, Steffen W (eds) (1996) Global change and terrestrial ecosystems. IGBP, Cambridge University Press, Cambridge
- Watson RT, Zinyowera MC and Moss RH (eds) (1998) The regional impacts of climate change: An assessment of vulnerability. IPCC Report, Cambridge University Press, Cambridge
- Weiss M (2001) Valeri LAI-2000 data processing. INRA, Avignon. <http://www.avignon.inra.fr/valeri/>. Cited 25 August 2006
- West PW (2004) Tree and forest measurement. Springer-Verlag, Berlin
- Wickens GE (1998) Ecophysiology of economic plants in arid and semi-arid lands. Springer-Verlag, New York
- Wilson EB and Hilferty MM (1931) The distribution of chi-square. Proceedings of the National Academy of Sciences, USA, No 17, pp684-688
- Wold H (1966) Estimation of principal components and related models by iterative least squares. In: Krishnaiah PR (ed) Multivariate Analysis. Proceedings of the international symposium, Dayton, 1965. New York, Academic Press, pp391-420
- Woodcock CE, Macomber SA, Pax-Lenney M and Cohen WB (2001) Monitoring large areas for forest change using Landsat: generalization across space, time and Landsat sensors. Remote Sensing of Environment 78:194–203

References

- Wullschleger SD, Meinzer FC and Vertessy RA (1998) A review of whole-plant water use studies in trees. *Tree Physiology* 18:499-512
- Yasunari T (2002a) How will the global hydrological cycle change with "global warming"? *Frontier Newsletter* n° 19 – Jul. 2002. Joint Promotion Office, Frontier Research System for Global Change
- Yasunari T (2002b) The role of large-scale vegetation and land use in the water cycle and climate in Monsoon Asia. In: Steffen W, Jäger J, Carson DJ and Bradshaw C (eds) *Challenges of a changing Earth. Proceedings of the global change open science conference, Amsterdam, The Netherlands, 10-13 July 2001.* Springer, Berlin, p 216
- Young A (1998) *Land resources. Now and for the future.* Cambridge University Press, Cambridge
- Zhang L, Walker GR and Fleming M (2002) Surface water balance for recharge estimation. Part 9 of *The basics for recharge and discharge.* CSIRO Publishing, Victoria, Australia

APPENDICES

Appendix 1: Ecological modeling

(1) Jackknife estimate model (\hat{S})

The variance of the equation (5.3) is given by

$$\text{var}(\hat{S}) = \left(\frac{r-1}{r} \right) \left[\sum_{j=1}^s (j^2 f_j) - \frac{k^2}{r} \right] \quad (\text{a1})$$

where s = Observed total number of species present in r plots; r = Total number of plots sampled; k = Number of unique species and f_j = Number of plots containing j unique species.

The confidence limits for equation (a1) can be deduced from equation a2 as follows:

$$\hat{S} \pm t_{\alpha} \sqrt{\text{var}(\hat{S})} \quad (\text{a2})$$

where \hat{S} = Jackknife model (equation a1); t_{α} = Student's value for $r-1$ degree of freedom for the appropriate value of α ; $\text{var}(\hat{S})$ = Variance of equation a1

(2) Poisson distribution

The Poisson distribution is a discrete probability distribution (Poisson 1837). The model is described by:

$$p_{(x,\mu)} = e^{-\mu} \left(\frac{\mu^x}{x!} \right) \quad (\text{a3})$$

where $p_{(x,\mu)}$ = Proportion of observing x individuals in a plot; e = Base of the natural logarithm ($e = 2.71828\dots$); x = Non-negative integer counter; μ = Observed mean of the distribution ($\mu = \bar{x}$); $x!$ = Factorial of x

The Poisson distribution assumes that the expected number of trees is the same in all plots and is equal to μ . After calculating the proportions of trees per plot in the expected Poisson distribution (a3), the final expected number of trees is obtained by multiplying each proportion by the number of plots sampled. Finally, tests for Goodness of Fit are used to test the null hypothesis that the Poisson distribution provides an adequate fit to the observed data (i.e., the spatial pattern of tree is a random one). Two methods are used to test the goodness of fit of the Poisson distribution: The Index of Dispersion Test and the Chi-Square Goodness-of-Fit Test.

- Index of Dispersion Test (I)

$$I = \frac{s^2}{\bar{x}} \quad (\text{a4})$$

- The statistic test of equation (a4) is the chi-square:

$$x^2 = I(n-1) \quad (\text{a5})$$

where s^2 = Observed variance of the distribution; \bar{x} = Observed mean of the distribution; n = Number of plots counted; x^2 = Value of chi-square with n-1 degree of freedom

If $x_{0.975}^2 < \text{Observed chi-square} < x_{0.025}^2$ the null hypothesis is accepted i.e. the spatial pattern of tree is a random one. For large value of n the rule to accept the null hypothesis (Wilson and Hilferty 1931)

$$\left(\frac{x^2}{n}\right)^{1/3} - \left(1 - \frac{2}{9n}\right) \text{ shall exceed } 1.65\sqrt{\frac{2}{9n}} \quad (\text{for } \sigma = 0.05) \quad (\text{a6})$$

Chi-Square Goodness-of-Fit Test (Krebs 1989)

$$X^2 = \sum \frac{\left(\text{Observed frequency} - \text{Expected frequency}\right)^2}{\text{Expected frequency}} \quad (\text{a7})$$

The null hypothesis is accepted if the observed chi-square is larger than the computed test statistic for $\alpha = 0.05$.

(3) Negative binomial distribution

The negative binomial distribution is a discrete probability distribution. By convention, it is reserved for the case of an integer-valued parameter x

The probability $P(x)$ (Ludwig and Reynolds 1988) of finding x individuals in a sample unit, where $x = 0, 1, 2, \dots, r$ individuals, μ is the number of individuals per sample unit ($\mu = \bar{x}$) and k is a parameter related to the degree of clumping, is given by:

$$P(x) = \left[\frac{\mu}{(\mu + k)} \right]^x \left\{ \frac{(k + x - 1)!}{[x!(k - 1)!]} \right\} \left[1 + \frac{\mu}{k} \right]^{-k} \quad (\text{a8})$$

The variance of equation (a8) is:

$$s^2 = \mu + \frac{\mu^2}{k} \quad (\text{a9})$$

The parameter k tends toward zero at maximum clumping. Its estimate (i.e., \hat{k}) is obtained using the following iterative equation:

$$\log_{10} \left(\frac{N}{N_0} \right) = \hat{k} \log_{10} \left(1 + \frac{\bar{x}}{\hat{k}} \right) \quad (\text{a10})$$

A straightforward and good initial estimate of \hat{k} for the first iteration is obtained from

$$\hat{k} = \frac{\bar{x}^2}{s^2 - \bar{x}} \quad (\text{a11})$$

where N = Total number of quadrat; N_0 = Number of quadrat containing zero individual, s^2 , k^2 and \bar{x} are defined above.

In the iteration process, values of \hat{k} are found until both side of the equation (a10) converge to the same value.

(4) General confidence interval for a population mean

Most confidence intervals have the form “*Estimate ± Margin of Error*”. In practice, given a sample of size n from a population having unknown mean μ and known standard deviation σ . A level C confidence interval for μ is

$$\left[\bar{x} - z \frac{\sigma}{\sqrt{n}}, \bar{x} + z \frac{\sigma}{\sqrt{n}} \right] \tag{a12}$$

where z = Value on the standard normal curve with area C between $-z$ and z . This interval is exact when the population distribution is normal and is approximately correct for large n as margin of error of a confidence decreases with the increasing sample size n . Refer to Moore and McCabe (1998) for details.

Appendix 2: Field survey form

TREE BIOMETRIC MEASUREMENT

Date:...../ 05 / 2006 Location:..... Investigator name:..... Height:..... (m)

Dm: Detarium microcarpum *Tl: Terminalia laxiflora* *Pe: Pterocarpus erinaceus* *Vp: Vitelaria paradoxa* *Do: Danielia oliveri*

Al: Anogeissus leiocarpus *Lm: Lanea microcarpa* *Pk: Pseudocedrela kotschyi* *Cf: Combretum fragrans* *Ea: Entada africana*

Tm: Terminalia macroptera *Sp. 11:..... Sp. 12:.....*

ID	Species Code	GCP	DBH (cm)	Tree Height (m)	Crown Radius (m)		Crown Height (m)	Observations
					Long	Short		
1					/	/		
2					/	/		
§					/	/		
4					/	/		
5					/	/		
6					/	/		
7					/	/		
8					/	/		
...

Appendices

Appendix 3: Distribution of tree species as a function of vegetation type

ID	Common tree species	Count	ID	Common tree species	Count
Tree savanna			Shrub savanna (cont.)		
1	<i>Terminalia macroptera</i>	183	6	<i>Terminalia laxiflora</i>	44
2	<i>Vitellaria paradoxa</i>	61	7	<i>Acacia dudgeoni</i>	36
3	<i>Pseudocedrela kotschyi</i>	54	8	<i>Combretum collinum</i>	33
4	<i>Detarium microcarpum</i>	45	9	<i>Lannea microcarpa</i>	32
5	<i>Entada africana</i>	37	10	<i>Combretum molle</i>	28
6	<i>Combretum fragrans</i>	36	11	<i>Pterocarpus erinaceus</i>	27
7	<i>Crossopteryx febrifuga</i>	28	12	<i>Pericopsis laxiflora</i>	20
8	<i>Piliostigma thonningii</i>	28	13	<i>Anogeissus leiocarpus</i>	19
9	<i>Daniellia oliveri</i>	19	14	<i>Bombax costatum</i>	17
10	<i>Terminalia laxiflora</i>	19	15	<i>Daniellia oliveri</i>	13
11	<i>Lannea acida</i>	17	16	<i>Diospyros mespiliformis</i>	12
12	<i>Acacia sieberiana</i>	11	17	<i>Lannea acida</i>	11
13	<i>Pterocarpus santalinoides</i>	11	18	<i>Terminalia Glaucescens</i>	11
14	<i>Burkea africana</i>	9	19	<i>Lonchocarpus laxiflorus</i>	10
15	<i>Bombax costatum</i>	6	20	<i>Combretum fragrans</i>	9
16	<i>Stereospermum kunthianum</i>	6	21	<i>Terminalia avicennioides</i>	9
17	<i>Pterocarpus erinaceus</i>	5	22	<i>Vitex doniana</i>	9
18	<i>Acacia dudgeoni</i>	4	23	<i>Acacia sieberiana</i>	8
19	<i>Gardenia erubescens</i>	4	24	<i>Parkia biglobosa</i>	8
20	<i>Isobertia doka</i>	4	25	<i>Pterocarpus santalinoides</i>	8
21	<i>Combretum glutinosum</i>	3	26	<i>Combretum nigricans</i>	7
22	<i>Combretum molle</i>	2	27	<i>Hexalobus monopetalus</i>	7
23	<i>Ximenia americana</i>	2	28	<i>Khaya senegalensis</i>	7
24	<i>Anogeissus leiocarpus</i>	1	29	<i>Stereospermum kunthianum</i>	5
25	<i>Cassia sieberiana</i>	1	30	<i>Piliostigma thonningii</i>	4
26	<i>Diospyros mespiliformis</i>	1	31	<i>Lannea velutina</i>	3
27	<i>Gardenia ternifolia</i>	1	32	<i>Xeroderris stuhlmannii</i>	3
28	<i>Maytenus senegalensis</i>	1	33	<i>Acacia macrostachya</i>	2
29	<i>Pericopsis laxiflora</i>	1	34	<i>Strychnos innocua</i>	2
30	<i>Terminalia Glaucescens</i>	1	35	<i>Burkea africana</i>	1
31	<i>Xeroderris stuhlmannii</i>	1	36	<i>Feretia apodanthera</i>	1
			37	<i>Grewia bicolor</i>	1
			38	<i>Garcinia livingstonei</i>	1
			39	<i>Hymenocardia acida</i>	1
			40	<i>Saba senegalensis</i>	1
			41	<i>Tamarindus indica</i>	1
			42	<i>Terminalia macroptera</i>	1
Shrub savanna					
1	<i>Detarium microcarpum</i>	84			
2	<i>Vitellaria paradoxa</i>	72			
3	<i>Entada africana</i>	65			
4	<i>Combretum glutinosum</i>	49			
5	<i>Crossopteryx febrifuga</i>	46			

Appendices

ID	Common tree species	Count	ID	Common tree species	Count
Galery Forest			Wood savanna		
1	<i>Syzygium guineense</i>	4	1	<i>Pterocarpus santalinoides</i>	34
2	<i>Cola laurifolia</i>	1	2	<i>Pericopsis laxiflora</i>	20
3	<i>Garcinia livingstonei</i>	1	3	<i>Combretum glutinosum</i>	16
4	<i>Keetia cornelia</i>	1	4	<i>Piliostigma thonningii</i>	13
5	<i>Lannea acida</i>	1	5	<i>Detarium microcarpum</i>	12
6	<i>Maytenus senegalensis</i>	1	6	<i>Crossopteryx febrifuga</i>	9
7	<i>Paullinia pinnata</i>	1	7	<i>Diospyros mespiliformis</i>	9
8	<i>Vitex chrysocarpa</i>	1	8	<i>Isoberlinea doka</i>	8
			9	<i>Combretum collinum</i>	7
Sparse forest			10	<i>Daniellia oliveri</i>	7
1	<i>Daniellia oliveri</i>	16	11	<i>Lonchocarpus laxiflorus</i>	7
2	<i>Terminalia laxiflora</i>	10	12	<i>Terminalia laxiflora</i>	6
3	<i>Isoberlinea doka</i>	4	13	<i>Vitellaria paradoxa</i>	6
4	<i>Bridelia scleroneura</i>	3	14	<i>Combretum fragrans</i>	5
5	<i>Lannea acida</i>	3	15	<i>Entada africana</i>	4
6	<i>Pterocarpus erinaceus</i>	3	16	<i>Pterocarpus erinaceus</i>	4
7	<i>Crossopteryx febrifuga</i>	1	17	<i>Lannea acida</i>	3
8	<i>Gardenia ternifolia</i>	1	18	<i>Parkia biglobosa</i>	3
9	<i>Lonchocarpus laxiflorus</i>	1	19	<i>Hexalobus monopetalus</i>	2
10	<i>Lannea microcarpa</i>	1	20	<i>Lannea microcarpa</i>	2
11	<i>Piliostigma thonningii</i>	1	21	<i>Terminalia glaucescens</i>	2
12	<i>Sarcocephalus latifolius</i>	1	22	<i>Combretum molle</i>	1
13	<i>Vitellaria paradoxa</i>	1	23	<i>Gardenia ternifolia</i>	1
			24	<i>Khaya senegalensis</i>	1
			25	<i>Terminalia avicennioides</i>	1
			26	<i>Vitex doniana</i>	1

Appendix 4: Frequencies of tree species families of the NRB

ID	Family	Count	ID	Family	Count
1	Combretaceae	569	11	Bignoniaceae	11
2	Cesalpiniaceae	277	12	Verbenaceae	11
3	Mimosaceae	188	13	Annonaceae	9
4	Sapotaceae	141	14	Apocynaceae	6
5	Fabaceae, Papilionaceae	105	15	Myrtaceae	4
6	Rubiaceae	96	16	Euphorbiaceae	3
7	Anacardiaceae	74	17	Loganiaceae	2
8	Meliaceae	64	18	Olacaceae	2
9	Bombacaceae	23	19	Tiliaceae	2
10	Ebenaceae	22			

Appendix 5: Overview of individual tree sap flow rate and biometric parameters

ID	Plot	Species name	DBH	sf	Th	Cc	ID	Plot	Species name	DBH	sf	Th	Cc
1	2	<i>Pterocarpus erinaceus</i>	119.1	439.9	19.0	246.4	31	24	<i>Crossopteryx febrifuga</i>	45.7	133.1	8.0	32.7
2	12	<i>Pterocarpus erinaceus</i>	88.6	312.4	19.0	153.7	32	23	<i>Daniellia oliveri</i>	45.4	131.9	13.4	94.0
3	24	<i>Isobertia doka</i>	85.6	299.9	16.0	167.2	33	7	<i>Terminalia laxiflora</i>	45.1	130.4	9.0	120.8
4	23	<i>Daniellia oliveri</i>	69.1	230.9	20.0	117.1	34	1	<i>Lannea microcarpa</i>	44.7	129.0	5.0	35.5
5	2	<i>Anogeissus leiocarpus</i>	67.9	225.9	18.8	215.8	35	2	<i>Lannea microcarpa</i>	44.5	128.1	7.8	50.9
6	11	<i>Vitellaria paradoxa</i>	67.3	223.4	13.0	62.9	36	20	<i>Daniellia oliveri</i>	44.5	128.1	14.5	168.6
7	11	<i>Lannea microcarpa</i>	65.9	217.6	11.0	189.3	37	24	<i>Isobertia doka</i>	44.3	127.3	16.5	74.2
8	3	<i>Lannea microcarpa</i>	64.4	211.3	10.0	55.4	38	14	<i>Combretum fragrans</i>	43.5	123.9	9.8	69.1
9	23	<i>Daniellia oliveri</i>	64.2	210.4	16.8	212.2	39	2	<i>Lannea microcarpa</i>	43.0	121.9	6.0	17.9
10	20	<i>Terminalia laxiflora</i>	63.2	206.3	17.8	1.0	40	7	<i>Vitellaria paradoxa</i>	42.8	121.0	7.0	34.7
11	2	<i>Lannea microcarpa</i>	62.5	203.3	4.0	63.6	41	9	<i>Terminalia macroptera</i>	40.9	113.1	10.0	121.3
12	20	<i>Isobertia doka</i>	61.4	198.7	21.8	296.1	42	20	<i>Daniellia oliveri</i>	40.8	112.6	19.8	148.9
13	15	<i>Vitellaria paradoxa</i>	59.9	192.3	10.0	59.9	43	2	<i>Terminalia laxiflora</i>	40.4	111.0	7.0	33.5
14	8	<i>Pterocarpus erinaceus</i>	58.5	186.6	15.8	281.7	44	7	<i>Terminalia laxiflora</i>	39.5	107.3	6.8	63.7
15	8	<i>Parkia biglobosa</i>	56.7	179.1	14.8	322.4	45	7	<i>Pterocarpus erinaceus</i>	39.5	107.3	12.5	111.7
16	24	<i>Burkea africana</i>	54.5	169.9	11.8	90.9	46	23	<i>Daniellia oliveri</i>	39.5	107.2	12.8	101.7
17	2	<i>Burkea africana</i>	53.8	167.0	13.8	197.7	47	20	<i>Daniellia oliveri</i>	39.3	106.4	17.0	163.6
18	23	<i>Daniellia oliveri</i>	53.0	163.6	17.0	178.4	48	10	<i>Parkia biglobosa</i>	38.7	103.9	13.0	203.3
19	20	<i>Daniellia oliveri</i>	52.9	163.2	21.8	82.8	49	12	<i>Pterocarpus erinaceus</i>	38.5	103.0	16.0	102.0
20	20	<i>Daniellia oliveri</i>	52.3	160.7	16.9	275.2	50	4	<i>Terminalia macroptera</i>	36.5	94.7	10.8	108.4
21	13	<i>Pterocarpus erinaceus</i>	52.1	159.9	12.5	63.2	51	17	<i>Entada africana</i>	36.5	94.7	7.5	26.6
22	11	<i>Lannea microcarpa</i>	51.1	155.7	14.0	161.6	52	22	<i>Lanea acida</i>	36.5	94.7	8.0	62.1
23	14	<i>Terminalia laxiflora</i>	50.5	153.0	6.0	37.4	53	15	<i>Vitellaria paradoxa</i>	36.4	94.3	7.0	39.5
24	8	<i>Lannea microcarpa</i>	50.1	151.3	7.0	83.7	54	10	<i>Vitellaria paradoxa</i>	36.2	93.4	13.0	101.2
25	4	<i>Terminalia macroptera</i>	48.9	146.5	11.0	159.3	55	8	<i>sp1</i>	36.1	93.0	14.0	162.3
26	20	<i>Daniellia oliveri</i>	47.7	141.5	18.0	251.6	56	1	<i>Tamarindus indica</i>	36.0	92.6	7.5	92.4
27	22	<i>Combretum glutinosum</i>	46.9	138.2	4.2	35.3	57	15	<i>Combretum fragrans</i>	35.9	92.2	6.3	40.3
28	21	<i>Terminalia laxiflora</i>	46.5	136.5	6.5	58.6	58	12	<i>Lanea acida</i>	35.5	90.3	7.0	49.4
29	12	<i>Lannea microcarpa</i>	46.3	135.6	8.0	68.4	59	8	<i>sp1</i>	35.3	89.7	11.0	79.3
30	21	<i>Terminalia laxiflora</i>	46.2	135.2	7.0	52.1	60	13	<i>Vitellaria paradoxa</i>	35.0	88.6	7.5	42.1

Appendices

Appendix 5: (continued) Abbreviations: *DBH* = Diameter at breast-height (cm), *sf* = Sap flow (kg day⁻¹), *Th* = Tree height (m), *Cc* = Crown cover (m²)

ID	Plot	Species name	<i>DBH</i>	<i>sf</i>	<i>Th</i>	<i>Cc</i>	ID	Plot	Species name	<i>DBH</i>	<i>sf</i>	<i>Th</i>	<i>Cc</i>
61	22	<i>Combretum glutinosum</i>	34.9	88.0	5.5	28.7	90	22	<i>Detarium microcarpum</i>	28.8	62.5	6.0	17.3
62	1	<i>Anogeissus leiocarpus</i>	34.8	87.6	15.0	71.8	91	22	<i>Detarium microcarpum</i>	28.7	62.1	5.0	35.3
63	5	<i>Entada africana</i>	33.8	83.4	7.0	35.2	92	10	<i>sp2</i>	28.5	61.3	9.0	76.5
64	9	<i>Daniellia oliveri</i>	33.8	83.4	10.0	45.5	93	9	<i>Terminalia macroptera</i>	28.4	60.8	10.0	70.0
65	24	<i>Burkea africana</i>	33.8	83.4	16.0	138.2	94	20	<i>Daniellia oliveri</i>	28.3	60.4	19.0	57.9
66	2	<i>Daniellia oliveri</i>	33.5	82.2	12.8	111.6	97	1	<i>Lannea microcarpa</i>	28.0	59.2	7.5	26.0
67	17	<i>Entada africana</i>	33.5	82.2	7.0	43.2	98	6	<i>Terminalia macroptera</i>	27.9	58.8	8.5	53.9
68	2	<i>Burkea africana</i>	33.3	81.3	4.0	201.6	99	5	<i>Daniellia oliveri</i>	27.8	58.3	11.5	55.5
69	9	<i>Terminalia macroptera</i>	33.1	80.5	8.0	87.4	100	9	<i>Pseudocedrela kotschyi</i>	27.7	57.9	10.0	9.8
70	18	<i>Entada africana</i>	32.9	79.6	5.0	31.9	101	21	<i>Terminalia macroptera</i>	27.7	57.9	2.0	62.5
71	13	<i>Parkia biglobosa</i>	32.7	78.8	9.0	126.2	102	3	<i>Xeroderris stuhlmannii</i>	27.6	57.5	9.0	47.7
72	12	<i>Hexalobus monopetalus</i>	32.5	78.0	6.0	9.6	103	9	<i>Terminalia macroptera</i>	27.5	57.1	10.0	75.5
73	20	<i>Daniellia oliveri</i>	32.3	77.1	15.7	78.6	104	10	<i>Vitellaria paradoxa</i>	27.2	55.8	10.0	63.2
74	8	<i>Anogeissus leiocarpus</i>	31.9	75.5	11.8	59.9	105	22	<i>Combretum glutinosum</i>	27.2	55.8	3.0	3.9
75	21	<i>Terminalia laxiflora</i>	31.8	75.0	8.0	24.2	106	11	<i>Vitellaria paradoxa</i>	27.0	55.0	9.5	68.3
76	6	<i>Terminalia macroptera</i>	31.7	74.6	11.0	69.7	107	24	<i>Crossopteryx febrifuga</i>	26.7	53.7	8.0	39.5
77	12	<i>Lannea microcarpa</i>	31.7	74.6	6.5	53.8	108	14	<i>Vitellaria paradoxa</i>	26.6	53.3	8.2	83.0
78	5	<i>Daniellia oliveri</i>	31.1	72.1	11.5	45.1	109	1	<i>Anogeissus leiocarpus</i>	26.5	53.0	13.0	99.5
79	9	<i>Pseudocedrela kotschyi</i>	30.8	70.9	9.0	1.0	110	11	<i>Vitellaria paradoxa</i>	26.3	52.1	10.0	55.1
80	19	<i>Vitellaria paradoxa</i>	30.8	70.9	7.8	39.6	111	12	<i>Lannea microcarpa</i>	26.2	51.6	5.0	29.7
81	1	<i>Hexalobus monopetalus</i>	30.2	68.4	5.0	41.9	112	9	<i>Pseudocedrela kotschyi</i>	25.7	49.6	11.0	20.3
82	17	<i>Combretum glutinosum</i>	30.1	67.9	6.0	24.0	113	11	<i>Vitellaria paradoxa</i>	25.6	49.1	10.0	30.3
83	23	<i>Daniellia oliveri</i>	30.1	67.9	12.0	39.2	114	16	<i>Detarium microcarpum</i>	25.2	47.5	4.5	4.4
84	15	<i>Entada africana</i>	30.0	67.5	5.5	27.8	115	4	<i>Terminalia macroptera</i>	25.1	47.0	11.0	42.5
85	6	<i>Terminalia macroptera</i>	29.9	67.1	8.5	84.4	119	17	<i>Vitellaria paradoxa</i>	25.1	47.0	7.0	25.0
86	20	<i>Vitellaria paradoxa</i>	29.9	67.1	14.8	60.1
87	21	<i>Gardenia erubescens</i>	29.6	65.9	2.3	9.9	555	22	<i>Lanea acida</i>	5.0	0.2	2.0	0.6
88	13	<i>Vitellaria paradoxa</i>	29.5	65.4	8.5	29.9	556	22	<i>Detarium microcarpum</i>	5.0	0.2	3.0	0.4
89	23	<i>Daniellia oliveri</i>	29.2	64.2	12.0	32.8	557	24	<i>Detarium microcarpum</i>	5.0	0.2	3.5	3.1

ACKNOWLEDGEMENTS

I would like to extend my warmest thanks to a number of organizations and people who made it possible for me to carry out the present studies. I would like to start with Dr Hans-Ulrich Caspary and Prof. Dr. Dieter Anhuf who arranged and backed my first visit to Germany.

I am also indebted to all those who contributed scientifically to the success of this study, especially Prof. Dr. Paul L.G. Vlek for his enormous support and for his general supervision of the workflows. I thank Dr. Jörg Szarzynski and Dr. Toshiya Okuro for their introduction to the technical set-up of sap flow and microclimatic data recording, and to tree biometric measurement. I am also grateful to my second supervisor Prof. Dr. Sebastian Schmidlein, who introduced me to multivariate regression modeling; also to P.D. Dr. Jürgen Burkhardt for his great help in the analysis of sapwood samples; and to Dr. Manfred Denich for his constructive inputs to the ecological modeling.

I am grateful to the Biota team of the German Aerospace Center (DLR) for providing me with Aster images, to Mr. Christian Brümmer from the Atmospheric Environmental Research Division of the Institute of Meteorology and Climate Research (IMK-IFU), who provided me with Eddy Correlation data, and also to Prof. Dr. Gunter Menz and his staff members from the Geographical Institute for their collaboration. My thanks also go to the team of Prof. Dr. Thiombiano Adjima from the University of Ouagadougou, especially to Dr. Amadé Ouédraogo who helped me identify the tree species on ground. I also thank Dr. Bagayoko Fafré for his advice and field assistance.

Many thanks go to the German government through the German Academic Exchange Services (DAAD) and the Ministry of Education, Science and Technology (BMBF) for providing me with a stipend and funds for the field campaigns. I would like to name, among others, Mrs Marie-Renée Leistriz and Dr. Roland Weiss both from DAAD for their very helpful and constructive advice.

I strongly appreciate the financial support of the Glowa Volta and Biota West Africa Projects, and the Virtual Institute, and also the staff members of ZEF, especially Dr Günther Manske, for their technical and administrative assistance.

My sincere gratitude goes to my wife Vieira Colette and my sons Franck Candide and Hans-Himmel, who helped me through casual stressing situations.

Finally I would like to thank all those people, too numerous to mention here, who have contributed their support and the benefit of their knowledge to the fulfilment of this study.